Substituted Indenyl Complexes for Ethylene Polymerisation

by

Phakpoom Angpanitcharoen



This thesis is submitted in partial fulfilment of the requirement for the degree of Doctor of Philosophy at the University of Oxford

St John's College

October 2018

The work described in this thesis was carried out in the Chemistry Research Laboratory, Mansfield Road, Oxford between October 2013 and October 2018 under the supervision of Professor Dermot O'Hare. All the work is my own unless stated to the contrary, and has not been previously submitted for any degree at this or any other university.

Phakpoom Angpanitcharoen
St John's College
October 2018

Abstract

Substituted Indenyl Complexes for Ethylene Polymerisation

Phakpoom Angpanitcharoen **D.Phil Thesis**

St John's College **Trinity Term 2018**

The principle aims of this thesis have been to synthesise novel substituted indenyl complexes inspired by the very active ^{Me2}SBI*$ZrCl_2$. By looking to improve on the ethylene polymerisation activity and the racemo-selectivity, the ^{Me2}SBI* ligand framework has been modified. The synthesised complexes have been tested for homogeneous and heterogeneous ethylene polymerisation activity and evaluated for their potential industrial applications.

Chapter One provides a background to the chemistry of cyclopentadienyl and indenyl ligands, group 4 *ansa*-metallocenes and their ethylene polymerisation activity. The mechanism of ethylene polymerisation is reviewed. A summary of the development of homogeneous and heterogeneous ethylene polymerisation is discussed including the use of solid supports; silica, solid polymethylaluminoxane (sMAO) and layered double hydroxides.

Chapter Two describes modification of the ^{Me2}SBI* ligand by introducing different alkyl and aryl groups on the silyl bridge and at the 3- position of the indenyl rings. ^{Et2}SBI*H_2, $^{n\text{Pr,Me}}$SBI*H_2, ^{All,Me}SBI*H_2 and ^{Me2}SB($^{3\text{-Et}}$I*)H_2 pro-ligands have been synthesised. All pro-ligands and their synthetic intermediates have been fully characterised by NMR spectroscopy.

Chapter Three details the synthesis of substituted indenyl group 4 complexes. All complexes have been fully characterised by single crystal X-ray diffraction and NMR spectroscopy. Comparisons of the crystal structure metrical parameters are made.

Chapter Four investigates the homogeneous and heterogeneous ethylene polymerisation activity of the synthesised substituted indenyl complexes. The complexes have been immobilised onto sMAO and characterised by solid state NMR spectroscopy and SEM. The resulting polyethylenes have been characterised by GPC, XRD and SEM.

Chapter Five studies the solid support comparison between sMAO, SSMAO and LDHMAO. The optimisation of polymerisation conditions for the sMAO-[^{Me2}SB($^{3\text{-Et}}$I*)$ZrCl_2$] catalyst has been carried out. Potential industrial applications including polyethylene waxes and LLDPE have been explored.

Chapter Six provides experimental details and characterising data for the preceding chapters. **Electronic appendix** contains the CIF, CheckCIF and PLATON files of all single crystal structures.

Acknowledgements

Firstly, I would like to thank Professor Dermot O'Hare for accepting me into his group as a Part II student and letting me stay on to complete my DPhil degree. I am very grateful for his help and advice throughout my time as a chemist.

I also would like to thank JC and Zoë for their guidance and friendship. A big special thank you is reserved for JC for his unending patience and unwavering support during my darkest hours. I would have been lost without his extended hand.

I must thank people who have helped me with my chemistry; Nick for running SSNMR, Zoë and Tom for sorting out my single crystal structures and Kate for her help with solid state techniques.

O'Hare group members past and present will always hold a special place in my heart as the most fun and enjoyable collection of people to have spent time with. A special mention for Chris who has journeyed with me throughout my time in the lab and taught me how to play football properly!

I am also grateful to the Thai community in Oxford for accepting me as part of the family. I will always cherish the memories I made with those people and how much fun we have had!

I have the deepest gratitude for my parents who have taken care of me all my life. I am looking forward to spending more time with them back in Thailand in the future.

Last but definitely not least, Nat, words cannot describe how much your support means to me. I love you very much.

List of abbreviations

°C	degrees Celsius
Å	ångström, 10^{-10} m
α	ring tilt angle
All	allyl, $CH_2CH{=}CH_2$
AMO-LDH	high surface area LDH synthesised using AMOST
AMOST	aqueous miscible organic solvent treatment
b	broad
*i*Bu	iso-butyl, CH_2CHMe_2
*n*Bu	n-butyl, $CH_2CH_2CH_2CH_3$
cent	centroid
CEF	crystallisation elution fractionation
COSY	correlation spectroscopy
Cp	cyclopentadienyl, C_5H_5
Cp*	pentamethylcyclopentadienyl, C_5Me_5
Cp′	methylcyclopentadienyl, C_5H_4Me
CPMAS	cross-polarisation magic-angle spinning
δ	chemical shift
$\Delta_{M\text{-}C}$	slip parameter
d	doublet
DCM	dichloromethane, CH_2Cl_2
DFT	density functional theory
DMF	N,N-dimethylformamide
η	hapticity
EBI	ethylenebis(1-indenyl), $IndCH_2CH_2Ind$
EBI*	ethylenebis(hexamethyl-1-indenyl), $Ind^{\#}CH_2CH_2Ind^{\#}$
EDS	energy dispersive X-ray spectroscopy
EI	electron ionisation
ESI	electrospray ionisation
ESD	estimated standard deviation
Et	ethyl, CH_2CH_3
FT	Fourier transform

GPC	gel permeation chromatography
h	hour
HA	hinge angle
HDPE	high-density polyethylene
HMBC	heteronuclear multiple-bond correlation spectroscopy
HRMS	high-resolution mass spectrometry
HSQC	heteronuclear single-quantum correlation spectroscopy
ICP	inductively coupled plasma
Ind	indenyl, C_9H_7
Ind*	heptamethylindenyl, C_9Me_7
Ind$^{\#}$	hexamethylindenyl, C_9HMe_6
IR	infrared
K	Kelvin
LDH	layered double hydroxide
LDHMAO	LDH supported MAO
LLDPE	linear low-density polyethylene
μ	bridging
m	multiplet
M_n	number-average molecular weight
M_w	weight-average molecular weight
MAO	methylaluminoxane
MAS	magic-angle spinning
Me	methyl, CH_3
MWD	molecular weight distribution
NMR	nuclear magnetic resonance
PDI	polydispersity index
PES	photoelectron spectroscopy
Ph	phenyl, C_6H_5
ppm	parts per million
*i*Pr	iso-propyl, $CHMe_2$
*n*Pr	n-propyl, $CH_2CH_2CH_3$
psi	pounds per square inch
q	quartet
ROESY	rotating-frame nuclear Overhauser effect spectroscopy

s	singlet
^{Me2}SB($^{3\text{-}Et}$I*)	dimethylsilylbis(3-ethyl-2,4,5,6,7-pentamethyl-1-indenyl), $^{3\text{-}Et}$Ind$^{\#}{}_2$SiMe$_2$
^{Me2}SB($^{3\text{-}Ph}$I*)	dimethylsilylbis(2,4,5,6,7-pentamethyl-3-phenyl-1-indenyl), $^{3\text{-}Ph}$Ind$^{\#}{}_2$SiMe$_2$
^{Me2}SBI	dimethylsilylbis(1-indenyl), Ind$_2$SiMe$_2$
^{All,Me}SBI*	allyl(methyl)silylbis(hexamethyl-1-indenyl), Ind$^{\#}{}_2$SiAllMe
^{Et2}SBI*	diethylsilylbis(hexamethyl-1-indenyl), Ind$^{\#}{}_2$SiEt$_2$
^{Me2}SBI*	dimethylsilylbis(hexamethyl-1-indenyl), Ind$^{\#}{}_2$SiMe$_2$
^{Ph2}SBI*	diphenylsilylbis(hexamethyl-1-indenyl), Ind$^{\#}{}_2$SiPh$_2$
^{iPr2}SBI*	diisopropylsilylbis(hexamethyl-1-indenyl), Ind$^{\#}{}_2$Si*i*Pr$_2$
^{nPr,Me}SBI*	methyl(propyl)silylbis(hexamethyl-1-indenyl), Ind$^{\#}{}_2$Si*n*PrMe
SEM	scanning electron microscopy
sMAO	solid polymethylaluminoxane
SSMAO	silica supported MAO
SSNMR	solid state NMR spectroscopy
t	triplet
TA	torsion angle
TEA	triethylaluminium, AlEt$_3$
THF	tetrahydrofuran, C$_4$H$_8$O
TIBA	triisobutylaluminium, Al*i*Bu$_3$
TMA	trimethylaluminium, AlMe$_3$
XRD	powder X-ray diffraction

Table of Contents

Chapter One – Introduction

1.1 Cyclopentadienyl chemistry 1
1.2 Indenyl chemistry 1
1.3 Group 4 *ansa*-metallocenes 2
1.4 Mechanism of ethylene polymerisation 4
1.5 Homogeneous α-olefin polymerisation 6
1.6 Heterogeneous supported metallocene catalysts 6
1.7 Scope of thesis 8
1.8 References 8

Chapter Two – Ligand synthesis

2.1 Introduction 11
2.2 Variations of alkyl groups on silyl bridge 12
2.2.1 Synthesis of ^{Et2}SBI*H$_2$ 12
2.2.2 Attempted synthesis of ^{R2}SBI*H$_2$ (R = *i*Pr, Ph) 15
2.2.3 Synthesis of ^{R,Me}SBI*H$_2$ (R = *n*Pr, All) 16
2.3 Variations of alkyl groups at 3- position of indenyl rings 19
2.3.1 Synthesis of RCH=CMeCOCl (R = Et, Ph) 20
2.3.2 Synthesis of $^{3\text{-}R}$Ind$^{\#}$=O (R = Et, Ph) 23
2.3.3 Synthesis of $^{3\text{-}R}$Ind$^{\#}$H (R = Et, Ph) 26
2.3.4 Synthesis of $^{3\text{-}R}$Ind$^{\#}$Li (R = Et, Ph) 30
2.3.5 Synthesis of ^{Me2}SB($^{3\text{-}R}$I*)H$_2$ (R = Et, Ph) 32
2.4 Conclusions 35
2.5 References 35

Chapter Three – Complex synthesis

3.1 Introduction 37
3.2 Unbridged substituted indenyl complexes 38

3.2.1 Synthesis of ($^{3\text{-R}}$Ind$^{\#}$)$_2$MCl$_2$ (R = Et, Ph; M = Zr, Hf) 38
3.2.2 Synthesis of ($^{3\text{-R}}$Ind$^{\#}$)$_2$ZrBr$_2$ (R = Me, Et) 45
3.2.3 Synthesis of (Ind$^{\#}$)(PhN(CH$_2$)$_3$NPh)ZrCl 49
3.3 Silyl bridged substituted indenyl complexes 52
3.3.1 Synthesis of ^{Et2}SBI*ZrCl$_2$ 52
3.3.2 Attempted synthesis of ^{R,Me}SBI*ZrCl$_2$ (R = *n*Pr, All) 56
3.3.3 Synthesis of ^{Me2}SB($^{3\text{-Et}}$I*)ZrX$_2$ (X = Cl, Br) 57
3.4 Dibenzyl substituted indenyl complexes 65
3.4.1 Synthesis of *rac*-($^{3\text{-Et}}$Ind$^{\#}$)$_2$Zr(CH$_2$Ph)$_2$ 65
3.4.2 Synthesis of *meso*-($^{3\text{-R}}$Ind$^{\#}$)$_2$Zr(CH$_2$Ph)$_2$ (R = Me, Et) 67
3.4.3 Synthesis of *rac*-^{Me2}SBI*Zr(CH$_2$Ph)$_2$ 72
3.4.4 Synthesis of ^{Me2}SB($^{3\text{-Et}}$I*)Zr(CH$_2$Ph)$_2$ 73
3.5 Conclusions 77
3.6 References 77

Chapter Four – Ethylene polymerisation studies

4.1 Introduction 79
4.2 Homogeneous ethylene polymerisation 79
4.3 Complex immobilisation 82
4.3.1 Synthesis of sMAO supported metallocene catalysts 82
4.3.2 Characterisation of sMAO-[^{Me2}SB($^{3\text{-Et}}$I*)ZrCl$_2$] catalyst 83
4.4 Heterogeneous ethylene polymerisation 85
4.5 Polymer characterisation 91
4.6 Conclusions 92
4.7 References 92

Chapter Five – ^{Me2}SB($^{3\text{-Et}}$I*)ZrCl$_2$ polymerisation studies

5.1 Introduction 94
5.2 Heterogeneous supports 94
5.2.1 Synthesis of SSMAO- and LDHMAO-[^{Me2}SB($^{3\text{-Et}}$I*)ZrCl$_2$] catalysts 94

5.2.2 Support comparisons 96
5.3 Polymerisation condition optimisation 98
5.3.1 Impurity scavenger 98
5.3.2 Complex loading 101
5.3.3 Catalyst loading and reaction volume 102
5.4 Hydrogen as chain transfer agent 103
5.5 1-Hexene copolymerisation 105
5.6 Conclusions 106
5.7 References 106

Chapter Six – Experimental details

6.1 Characterisation techniques 108
6.1.1 Solution phase NMR spectroscopy 108
6.1.2 Solid state NMR spectroscopy 108
6.1.3 Infrared spectroscopy 108
6.1.4 Mass spectrometry 109
6.1.5 Elemental analysis 109
6.1.6 Single crystal X-ray diffraction 109
6.1.7 Powder X-ray diffraction 110
6.1.8 Gel permeation chromatography 110
6.1.9 Scanning electron microscopy 110
6.2 General procedures 110
6.3 Starting materials 111
6.3.1 Commercially supplied reagents 111
6.3.2 Literature preparations 111
6.4 Experimental details for Chapter Two 112
6.4.1 Synthesis of ^{Et_2}SBI*H$_2$ 112
6.4.2 Synthesis of $^{n\text{Pr,Me}}$SBI*H$_2$ 113
6.4.3 Synthesis of $^{\text{All,Me}}$SBI*H$_2$ 114
6.4.4 Synthesis of EtCH=CMeCOCl 115
6.4.5 Synthesis of PhCH=CMeCOCl 115

6.4.6 Synthesis of $^{3\text{-Et}}Ind^{\#}$=O 116
6.4.7 Synthesis of $^{3\text{-Ph}}Ind^{\#}$=O 117
6.4.8 Synthesis of $^{3\text{-Et}}Ind^{\#}H$ 118
6.4.9 Synthesis of $^{3\text{-Ph}}Ind^{\#}H$ 119
6.4.10 Synthesis of $^{3\text{-Et}}Ind^{\#}Li$ 120
6.4.11 Synthesis of $^{3\text{-Ph}}Ind^{\#}Li$ 121
6.4.12 Synthesis of $^{Me2}SB(^{3\text{-Et}}I^{*})H_2$ 122
6.4.13 Synthesis of $^{Me2}SB(^{3\text{-Ph}}I^{*})H_2$ 123
6.5 Experimental details for Chapter Three 124
6.5.1 Synthesis of $(^{3\text{-Et}}Ind^{\#})_2ZrCl_2$ 124
6.5.2 Synthesis of $(^{3\text{-Et}}Ind^{\#})_2HfCl_2$ 125
6.5.3 Synthesis of $(^{3\text{-Ph}}Ind^{\#})_2ZrCl_2$ 126
6.5.4 Synthesis of $(Ind^{\#})_2ZrBr_2$ 127
6.5.5 Synthesis of $(^{3\text{-Et}}Ind^{\#})_2ZrBr_2$ 128
6.5.6 Synthesis of $(Ind^{\#})(PhN(CH_2)_3NPh)ZrCl$ 129
6.5.7 Synthesis of $^{Et2}SBI^{*}ZrCl_2$ 130
6.5.8 Synthesis of $^{Me2}SB(^{3\text{-Et}}I^{*})ZrCl_2$ 131
6.5.9 Synthesis of $^{Me2}SB(^{3\text{-Et}}I^{*})ZrBr_2$ 133
6.5.10 Synthesis of *rac*-$(^{3\text{-Et}}Ind^{\#})_2Zr(CH_2Ph)_2$ 134
6.5.11 Synthesis of *meso*-$(Ind^{\#})_2Zr(CH_2Ph)_2$ 135
6.5.12 Synthesis of *meso*-$(^{3\text{-Et}}Ind^{\#})_2Zr(CH_2Ph)_2$ 136
6.5.13 Synthesis of *rac*-$^{Me2}SBI^{*}Zr(CH_2Ph)_2$ 137
6.5.14 Synthesis of $^{Me2}SB(^{3\text{-Et}}I^{*})Zr(CH_2Ph)_2$ 138
6.6 Experimental details for Chapter Four 139
6.6.1 Synthesis of sMAO supported metallocene catalysts 139
6.6.2 50 mL ethylene polymerisation 140
6.6.3 Polymerisation data 141
6.7 Experimental details for Chapter Five 144
6.7.1 Synthesis of silica supported methylaluminoxane (SSMAO) 144
6.7.2 Synthesis of layered double hydroxide supported methylaluminoxane (LDHMAO) 145
6.7.3 Synthesis of SSMAO-[$^{Me2}SB(^{3\text{-Et}}I^{*})ZrCl_2$] catalyst 145

6.7.4 Synthesis of LDHMAO-[^{Me_2}SB($^{3\text{-}Et}$I*)$ZrCl_2$] catalyst 145
6.7.5 250 mL ethylene polymerisation 146
6.7.6 1 L ethylene polymerisation 146
6.7.7 High throughput ethylene polymerisation 146
6.7.8 Polymerisation data 146
6.8 References 148

Conclusions

Conclusions 149

Chapter One – Introduction

1.1 Cyclopentadienyl chemistry

The cyclopentadienyl ligand ($C_5H_5^-$; Cp) was first reported in ferrocene in 1951,[1] with its connectivity determined in 1952 by Wilkinson and Fischer.[2,3] Ever since, the Cp ligand has been at the forefront of organometallic chemistry with complexes featuring elements from the main group, d block, lanthanides and actinides.[3–8] Group 4 metallocenes were discovered soon after ferrocene, with Cp_2TiCl_2 and Cp_2ZrCl_2 reported by Wilkinson in 1954.[3] This provided the platform for research into its uses; most relevantly as a catalyst in ethylene polymerisation.[9]

The properties of Cp as a ligand are dominated by its ability to coordinate to metals in an η^5-fashion where the delocalised electrons in the π system of the carbocycle interact with the empty d- and/or f- orbitals on the metal.[10] The less commonly found η^1- and η^3- bonding modes are reviewed elsewhere in the literature.[11,12]

The significance of the cyclopentadienyl ligand prompted interest in the study of other closely related ligands with the synthesis of Cp'_2Fe published in 1959 ($C_5H_4Me^-$; Cp′).[13] The most notable of these developments was the eventual synthesis of complexes containing the pentamethylcyclopentadienyl ligand ($C_5Me_5^-$; Cp*). These complexes are more stable than their non-methylated counterparts which can be attributed to both electronic and steric effects.[14] The Cp* ligand possesses greater steric bulk than Cp and has a greater donor strength due to the inductive effect of the methyl groups. In general, this increased donor ability leads to an increase in the strength of the metal-carbon bond. Other complexes, such as Jutzi's Cp^*_2Si, are kinetically stabilised by the steric bulk of the ligand rather than its electron donating ability.[15]

1.2 Indenyl chemistry

The ring carbons of the Cp ligands can bear numerous substituents. This results in a high degree of steric and electronic versatility depending on the specific chosen ligand. The benzannulated version of Cp, indenyl ($C_9H_7^-$; Ind), has also been the subject of much research,[16,17] most notably for exhibiting the indenyl effect; a more facile η^5 to η^3 rearrangement (Figure 1.1).[12]

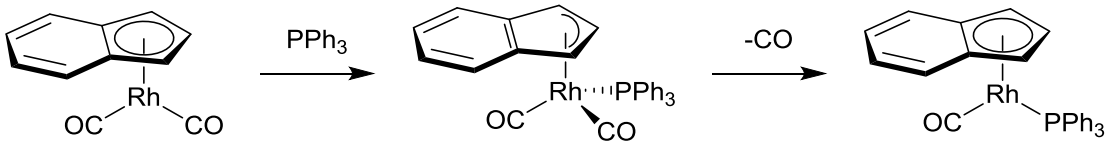


Figure 1.1. Illustration of the indenyl effect, as reported by Basolo and co-workers.[18]

This ring slippage allows the rhodium centre in $IndRh(CO)_2$ to maintain 18 electrons over the course of the ligand substitution reaction while still maintaining aromaticity in one of the rings thus lowering the activation energy of the reaction relative to the corresponding Cp complex.[19] However, this ring slippage also leads to increased lability of the indenyl ligand.[20]

The permethylindenyl ligand ($C_9Me_7^-$; Ind*) was first described by Miyamoto *et al.* in the ferrocene derivative, Ind^*_2Fe.[21] Soon after, the synthesis of many permethylindenyl lanthanide complexes was reported, including Ind^*LnCl_2 and Ind^*_3Ln, where the steric bulk and electronic character of the ligand were seen to encourage strong covalent bonding with the largely ionic rare earth metals.[22] It should be noted that at the time the synthesis of Cp analogues of these complexes had proved elusive. In an attempt to quantify these electronic characteristics, Marder and co-workers studied a variety of substituted indenyl rhodium complexes, including $Ind^*Rh(C_2H_4)_2$, using photoelectron spectroscopy (PES) combined with density functional theory (DFT) studies.[23,24] From this, it was concluded that Ind ligands were more effective electron donors to d^8 ML_2 fragments than their Cp counterparts, as evidenced by the ionisation energies of the metal based non-bonding orbitals. It was also found that permethylated ligands increased this ability to donate electrons.

1.3 Group 4 *ansa*-metallocenes

Group 4 metallocenes are generally defined as d^0, pseudo-tetrahedral organometallic compounds in which the transition metal atom bears two η^5-cyclopentadienyl-based ligands and two σ-ligands.[25] Upon the activation of group 4 metallocenes by co-catalysts (e.g. MAO), the resulting highly electrophilic alkyl metallocene cations, stabilised by non-nucleophilic, very weakly coordinating anions, are known to be the active species for α-olefin polymerisation.[26–28] The stability of the cationic intermediate and the electron density, accessibility and geometry of the active site, all of which are influenced by ligand structure, are believed to be the main influencing factors towards reactivity and stereospecificity of the corresponding metallocene.[29]

Derived from the Latin prefix *ansa* meaning "bent handle, attached at both ends", *ansa*- bridges provide a method of linking two cyclopentadienyl-type units in metallocene complexes. The bridge can vary considerably, from a single sp^3-hybridised carbon to multiple atoms including heteroatoms.[29,30] Depending on the nature of the bridge, it can impart significant control over the geometry and structure of the metallocene such as introducing potential additional stereochemistry, exemplified in the *rac*- and *meso*- isomers of bridged indenyl complexes (Figure 1.2).[25]

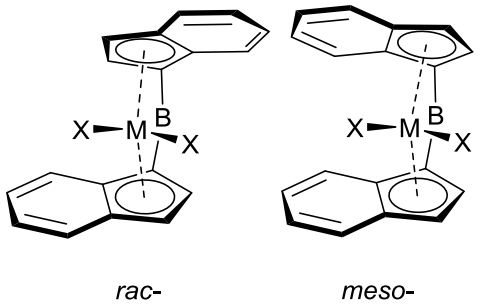
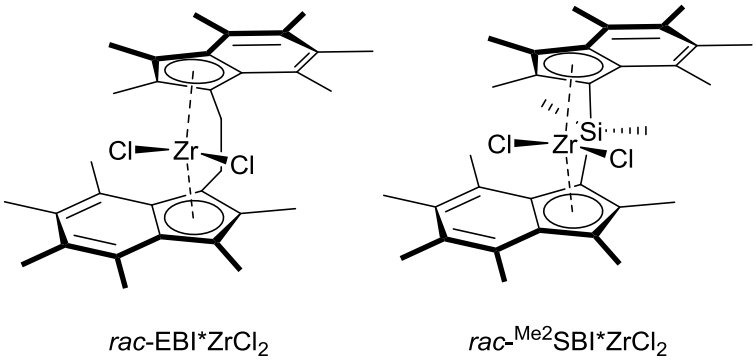


Figure 1.2. *rac* and *meso* isomers of bridged indenyl complexes (B being a desired bridging atom).

As previously stated, introducing a bridge can lead to some difficulties in isolating the desired isomer. While *rac*- and *meso*- isomers are diastereomers and often separable by fractional crystallisation, there are several methodologies which allow one isomer to stereoselectively being synthesised over the other. One such method, developed by Diamond *et al.*, is to use amide ligands for selective formation of the *rac*- isomer.[31–33] By moving away from an irreversible salt metathesis reaction to a reversible amine elimination, the thermodynamic product is formed. Jordan and co-workers were able to extend this idea to a silyl-bridged indenyl zirconocene,[34] before the use of chelating diamide ancillary ligand resulted in even better control of the stereochemistry.[35–40]

A new substituted indenyl family, including ethylenebis(hexamethyl-1-indenyl) zirconium dichloride, EBI*$ZrCl_2$, recently reported by O'Hare and co-workers, have shown very high activity towards solution-phase polymerisation of ethylene (Figure 1.3, left).[41,42] O'Hare *et al.* have recently reported the synthesis of dimethylsilylbis(hexamethyl-1-indenyl) zirconium dichloride, ^{Me2}SBI*$ZrCl_2$, and its use in homogeneous and heterogeneous ethylene polymerisation (Figure 1.3, right).[43]



rac-EBI*$ZrCl_2$ *rac*-^{Me2}SBI*$ZrCl_2$

Figure 1.3. *rac*-EBI*$ZrCl_2$ and *rac*-^{Me2}SBI*$ZrCl_2$.

1.4 Mechanism of ethylene polymerisation

With a global production volume of 150 million tonnes per annum,[44] which accounts for more than 70% of the polymer market,[45] polyolefins have become an essential material for the modern world. The increasing variety of polyolefins available in the market leads to new applications ranging from food packaging to electrical insulators, replacing more expensive natural materials.[46] With the sheer scale of the polyethylene production (80 million tonnes per annum),[47] research in this area remains very important.

Due to their high activity and relatively low cost, a very large portion of the global polyethylene production is still achieved using heterogeneous Ziegler-Natta catalysts.[45] Despite their higher cost, metallocene catalysts with their remarkable control over the polymer properties can find their places in a more niche market.[48]

For metallocenes, the mechanism for the polymerisation of ethylene is composed of three general steps: initiation, propagation and termination.[49] Initiation involves the generation of a 14 electron active species by alkylation and subsequent anion abstraction by the co-catalyst, to form a highly electrophilic group 4 metallocene cation which is weakly coordinated to a non-nucleophilic anion (Figure 1.4).[50]

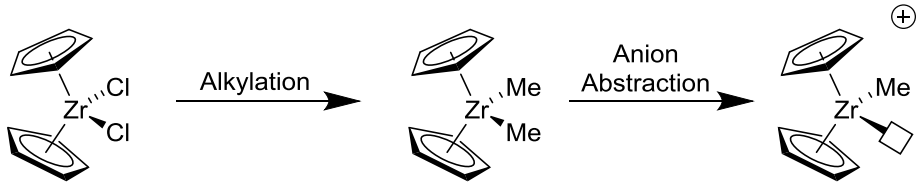


Figure 1.4. Generation of the active species using MAO as a co-catalyst.

Once the non-nucleophilic anion is dissociated, the vacant site is quickly replaced by the ethylene which bonds to the metal in an η^2-fashion. The alkyl substituent then undergoes a

1,2-insertion onto the ethylene double bond. The vacant site is again replaced by an ethylene molecule and the process of chain growth repeats itself until a chain transfer step occurs (Figure 1.5).[26]

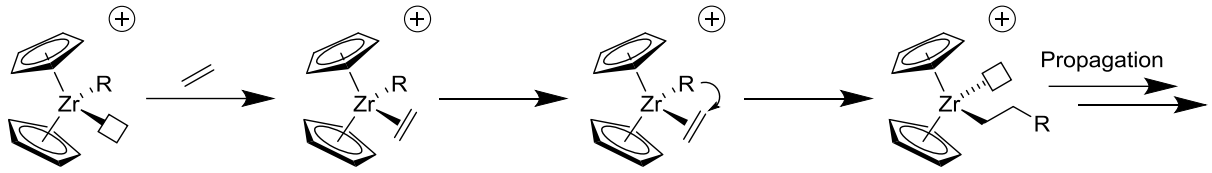


Figure 1.5. Propagation steps in ethylene polymerisation.

There are several chain transfer processes which can result in termination. These include: chain transfer to aluminium, β-H transfer to monomer and σ-bond metathesis with H_2.

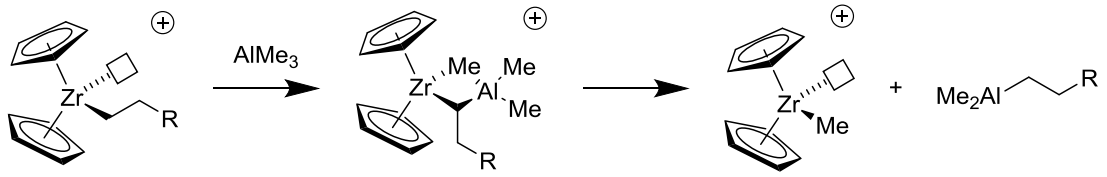


Figure 1.6. Mechanism of chain transfer to aluminium.

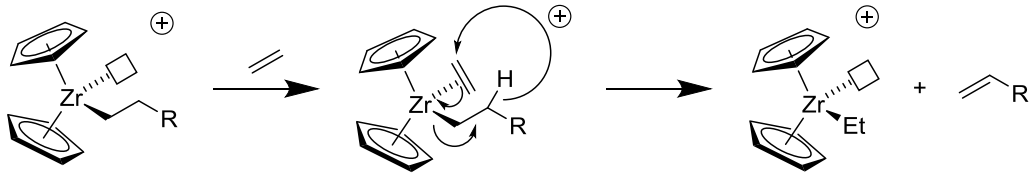


Figure 1.7. Mechanism of β-H transfer to monomer.

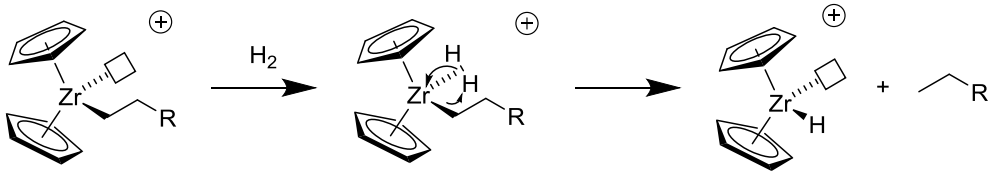


Figure 1.8. Mechanism of σ-bond metathesis with H_2.

Chain transfer to aluminium is a bimolecular process which involves a bridging intermediate shown in Figure 1.6. The chain transfer takes place via a three-centre two-electron bridge. In the case of β-H transfer to monomer, the transition metal alkyl complex, containing a β-hydrogen atom, undergoes a hydrogen shift onto the coordinated monomer and eliminate an alkene (Figure 1.7). σ-bond metathesis, or hydrogenolysis, can be used to control

the molecular weight of the polymer by adding small amounts of H_2 into the polymerisation reactor to increase termination rate (Figure 1.8).

The molecular weight of the polyethylene produced is dependent on the ratio of the rates of propagation and elimination. These rates are influenced differently by changing variables, including: ligand structure, transition metal centre, co-catalyst, co-catalyst concentration, temperature, time, and H_2 concentration. Therefore, to a certain extent, the molecular weight of the polymer formed can be controlled by optimising these conditions.[51]

1.5 Homogeneous α-olefin polymerisation

A few years after the discovery of heterogeneous polyolefin catalysts by Ziegler and Natta in the 1950s, the first homogeneous metallocene α-olefin polymerisation catalyst, consisting of Cp_2TiCl_2 and $AlEt_2Cl$, was reported.[52,53] The discovery of oligomeric methylaluminoxane (MAO) and its ability to activate metallocenes marked the beginning of an era of metallocene-mediated α-olefin polymerisation.[54]

In 1980, Sinn and co-workers reported the discovery and application of MAO, synthesised by the controlled hydrolysis of trimethylaluminium (TMA), to significantly augment the metallocene catalyst activity.[55] MAO is a generic term, used to describe a cocktail of oligomeric and polymeric species containing Al-O-Al and Al-CH_3 bonds that coexist in multiple equilibria. The steric bulk of MAO is a key factor for the high activity of metallocene catalysis. Following an initial activation step, the weak coordination of MAO to the activated metallocene cation allows the monomer to have easier access the active site.[56]

Since this landmark discovery, numerous group 4 complexes were shown to be effective in the production of polyolefins.[57] In contrast to the heterogeneous Ziegler-Natta systems, metallocene catalysts produce polyolefins with a much narrower molecular weight distribution (PDI ~ 2). The 'single-site' nature of metallocene systems has also enabled an unprecedented ability to fine-tune polymer microstructure by ligand design.[48]

1.6 Heterogeneous supported metallocene catalysts

The discovery of 'single-site' metallocene-based catalysts has revived α-olefin polymerisation chemistry as these catalyst systems enable the production of (co)polyolefins with tuneable molecular structures, stereochemistries and molecular weight distributions (MWD). Yet these catalysts are rarely used for industrial processes, with a few exceptions

including Dowlex (Dow) and Sclairtech (Nova Chem. Corp.); due to the incompatibility with the existing gas or slurry phase olefin polymerisation processes.[45] By immobilising metallocene catalysts onto support materials, the processability problem is solved and the advantages of metallocene catalysts, including narrow MWD, high activity, and precise control over polymer microstructure, are preserved to a great extent.[58]

A major factor controlling the resultant polymer and limiting the activity of supported 'single-site' catalysts is the fragmentation of catalyst particle during polymer particle growth. As polymerisation proceeds, the fragmentation of the initial catalyst particle occurs, due to the hydraulic forces of the growing polymer, and the fragmented catalyst sub-particles are left scattered within the growing polymer matrix (Figure 1.9).[59] Uniform polymer particle growth, as a result of widespread fragmentation of the initial catalyst particle, is essential to efficiently control over the resulting polymer morphology.[60] Physical properties of the support, including porosity and friability, can play an important role in the fragmentation process.[58] With low friability, polymer formation in the pores of unfragmented catalyst particles can lead to diffusion-limitation of the monomer to all the active sites, inhibiting further polymerisation.[61] To prevent disintegration of the catalyst particle and allow controlled progressive growth of the polymer particle during polymerisation, the mechanical strength of the catalyst support needs to be optimised.[45]

Many materials were tested as olefin polymerisation supports including inorganic solids such as silicate clays,[62] zirconia[63] and $MgCl_2$.[64] Various functionalised polymers have also been investigated as supports.[46,65,66]

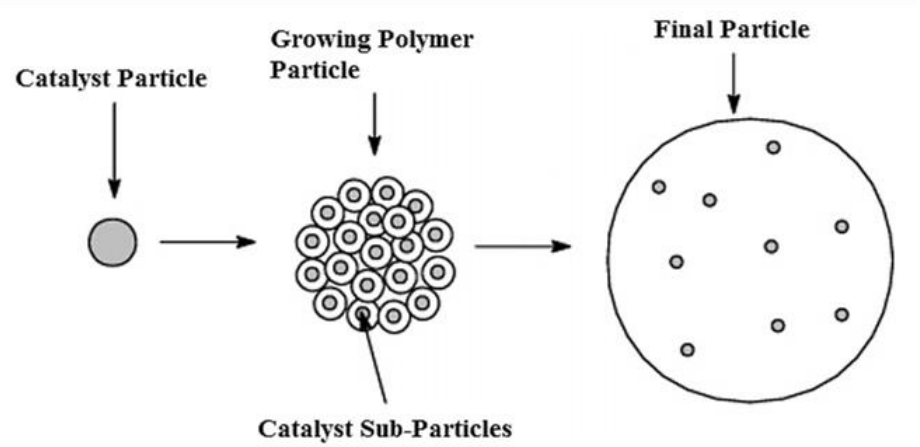


Figure 1.9. Schematic of polymer particle growth mechanism.[45]

Silica is the most commonly used support for heterogeneous metallocene catalysts. Calcination temperature, which determines the type and concentration of silanol groups on the

silica surface, and its effects on polymerisation activities have been extensively studied.[67,68] The silanol groups allow silica to be functionalised but high concentration of the silanol groups can lead to the decomposition of metallocenes upon immobilisation.[69] Impregnation of MAO onto silica, to form silica supported MAO (SSMAO), followed by the simultaneous adsorption and activation of metallocene pre-catalyst, was reported as the best immobilisation method because of increased homogeneity of the resulting catalyst, yielding polyethylene with narrow molecular weight distribution. Precontacting the silica surface with MAO was reported to increase catalyst loadings.[70,71]

The use of layered double hydroxides (LDHs), a class of anionic clays consisting of positively charged Brucite-like layers with weakly bound anions intercalated between them, as catalyst supports for olefin polymerisation has been recently reported by the O'Hare group.[72]

Heat treatment of MAO for a prolonged period was reported to increase polymerisation activity of up to 25%. This is believed to be caused by the aggregation of MAO to form larger particles which are insoluble in hydrocarbon solvents. This insoluble 'solid MAO' can act simultaneously as both co-catalyst and support in slurry phase ethylene polymerisation.[73,74]

1.7 Scope of thesis

The aim of the thesis is to synthesise novel substituted indenyl complexes inspired by the very active ^{Me2}SBI*$ZrCl_2$. By looking to improve on the ethylene polymerisation activity and the racemo-selectivity, different alkyl and aryl groups are introduced on the silyl bridge and at the 3- position of the indenyl rings. The synthesised complexes are then tested for homogeneous and heterogeneous ethylene polymerisation activity and evaluated for their potential industrial applications, including polyethylene waxes by using hydrogen as a chain transfer agent, and linear low-density polyethylene (LLDPE) by copolymerisation of ethylene and 1-hexene.

1.8 References

1 T. J. Kealy and P. L. Pauson, *Nature*, 1951, **168**, 1039–1040.
2 E. O. Fischer and W. Pfab, *Zeitschrift fuer Naturforsch.*, 1952, **7b**, 377–379.
3 G. Wilkinson and J. M. Birmingham, *J. Am. Chem. Soc.*, 1954, **76**, 4281–4284.
4 T. S. Piper and G. Wilkinson, *J. Inorg. Nucl. Chem.*, 1956, **3**, 104–124.
5 L. T. Reynolds and G. Wilkinson, *J. Inorg. Nucl. Chem.*, 1956, **2**, 246–253.
6 P. Jutzi, *Chem. Rev.*, 1986, **86**, 983–996.
7 S. Harder, *Coord. Chem. Rev.*, 2000, **199**, 331–334.

8 S. Arndt and J. Okuda, *Chem. Rev.*, 2002, **102**, 1953–1976.
9 A. L. McKnight and R. M. Waymouth, *Chem. Rev.*, 1998, **98**, 2587–2598.
10 J. C. Green, *Chem. Soc. Rev.*, 1998, **27**, 263–272.
11 C. P. Casey, J. M. O'Connor, W. D. Jones and K. J. Haller, *Organometallics*, 1983, **2**, 535–538.
12 J. M. O'Connor and C. P. Casey, *Chem. Rev.*, 1987, **87**, 307–318.
13 M. L. H. Green, L. Pratt and G. Wilkinson, *J. Chem. Soc.*, 1958, 3753–3767.
14 R. B. King, *Coord. Chem. Rev.*, 1976, **20**, 155–169.
15 V. P. Jutzi, D. Kanne and C. Krüger, *Angew. Chemie*, 1986, **98**, 163–164.
16 V. Cadierno, J. Díez, M. P. Gamasa, J. Gimeno and E. Lastra, *Coord. Chem. Rev.*, 1999, **193–195**, 147–205.
17 P. J. Chirik, *Organometallics*, 2010, **29**, 1500–1517.
18 M. E. Rerek, L.-N. Ji and F. Basolo, *J. Chem. Soc. Chem. Commun.*, 1983, 1208–1209.
19 M. J. Calhorda, C. C. Romão and L. F. Veiros, *Chem. - A Eur. J.*, 2002, **8**, 868–875.
20 E. Samuel and R. Setton, *J. Organomet. Chem.*, 1965, **4**, 156–158.
21 T. K. Miyamoto, M. Tsutsui and L.-B. Chen, *Chem. Lett.*, 1981, **10**, 729–730.
22 M. Tsutsui, L.-B. Chen, D. E. Bergbreiter and T. K. Miyamoto, *J. Am. Chem. Soc.*, 1982, **104**, 855–856.
23 A. K. Kakkar, S. F. Jones, N. J. Taylor, S. Collins and T. B. Marder, *J. Chem. Soc. Chem. Commun.*, 1989, 1454–1456.
24 T. M. Frankcom, J. C. Green, A. Nagy, A. K. Kakkar and T. B. Marder, *Organometallics*, 1993, **12**, 3688–3697.
25 L. Resconi, L. Cavallo, A. Fait and F. Piemontesi, *Chem. Rev.*, 2000, **100**, 1253–1345.
26 H. H. Brintzinger, D. Fischer, R. Mülhaupt, B. Rieger and R. M. Waymouth, *Angew. Chemie, Int. Ed. English*, 1995, **34**, 1143–1170.
27 D. Braga, F. Grepioni, E. Tedesco and M. J. Calhorda, *Zeitschrift für Anorg. und Allg. Chemie*, 2000, **626**, 462–470.
28 M. Bochmann, R. D. Cannon and F. Song, *Kinet. Catal.*, 2006, **47**, 160–169.
29 B. Wang, *Coord. Chem. Rev.*, 2006, **250**, 242–258.
30 G. G. Hlatky, *Chem. Rev.*, 2000, **100**, 1347–1376.
31 G. M. Diamond, S. Rodewald and R. F. Jordan, *Organometallics*, 1995, **14**, 5–7.
32 G. M. Diamond, R. F. Jordan and J. L. Petersen, *J. Am. Chem. Soc.*, 1996, **118**, 8024–8033.
33 G. M. Diamond, R. F. Jordan and J. L. Petersen, *Organometallics*, 1996, **15**, 4030–4037.
34 J. N. Christopher, G. M. Diamond, R. F. Jordan and J. L. Petersen, *Organometallics*, 1996, **15**, 4038–4044.
35 X. Zhang, Q. Zhu, I. A. Guzei and R. F. Jordan, *J. Am. Chem. Soc.*, 2000, **122**, 8093–8094.
36 M. D. LoCoco and R. F. Jordan, *Organometallics*, 2003, **22**, 5498–5503.
37 A. R. Dunn, L. E. Sweet, D. C. Wiser, M. D. LoCoco and R. F. Jordan, *Organometallics*, 2004, **23**, 5671–5680.
38 M. D. LoCoco and R. F. Jordan, *J. Am. Chem. Soc.*, 2004, **126**, 13918–13919.
39 M. D. LoCoco, X. Zhang and R. F. Jordan, *J. Am. Chem. Soc.*, 2004, **126**, 15231–15244.
40 R. M. Buck, N. Vinayavekhin and R. F. Jordan, *J. Am. Chem. Soc.*, 2007, **129**, 3468–3469.
41 P. Ransom, A. E. Ashley, N. D. Brown, A. L. Thompson and D. O'Hare, *Organometallics*, 2011, **30**, 800–814.
42 T. A. Q. Arnold, J.-C. Buffet, Z. R. Turner and D. O'Hare, *J. Organomet. Chem.*, 2015, **792**, 55–65.
43 J.-C. Buffet, T. A. Q. Arnold, Z. R. Turner, P. Angpanitcharoen and D. O'Hare, *RSC Adv.*, 2015, **5**, 87456–87464.
44 M. Gahleitner, L. Resconi and P. Doshev, *MRS Bull.*, 2013, **38**, 229–233.
45 J. R. Severn, J. C. Chadwick, R. Duchateau and N. Friederichs, *Chem. Rev.*, 2005, **105**, 4073–4147.
46 B. Heurtefeu, C. Bouilhac, É. Cloutet, D. Taton, A. Deffieux and H. Cramail, *Prog. Polym. Sci.*, 2011, **36**, 89–126.
47 O. G. Piringer and A. L. Baner, *Plastic Packaging: Interactions with Food and Pharmaceuticals*, Wiley, 2nd edn., 2008.

48 W. Kaminsky, A. Funck and H. Hähnsen, *Dalt. Trans.*, 2009, 8803–8810.
49 S. Ahmadjo, H. Arabi, M. Nekoomanesh, S. M. M. Mortazavi, G. Zohuri, M. Ahmadi and S. Bolandi, *Chem. Eng. Technol.*, 2011, **34**, 249–256.
50 W. Kaminsky, *Macromol. Chem. Phys.*, 1996, **197**, 3907–3945.
51 S. S. Reddy and S. Sivaram, *Prog. Polym. Sci.*, 1995, **20**, 309–367.
52 G. Natta, P. Pino, G. Mazzanti and U. Giannini, *J. Am. Chem. Soc.*, 1957, **79**, 2975–2976.
53 D. S. Breslow and N. R. Newburg, *J. Am. Chem. Soc.*, 1957, **79**, 5072–5073.
54 W. Kaminsky, *J. Chem. Soc. Dalt. Trans.*, 1998, 1413–1418.
55 H. Sinn, W. Kaminsky, H.-J. Vollmer and R. Woldt, *Angew. Chemie*, 1980, **92**, 396–402.
56 V. Busico, *Dalt. Trans.*, 2009, 8794–8802.
57 W. Kaminsky and A. Laban, *Appl. Catal. A Gen.*, 2001, **222**, 47–61.
58 J. R. Severn and J. C. Chadwick, *Dalt. Trans.*, 2013, **42**, 8979–87.
59 G. Fink, B. Tesche, F. Korber and S. Knoke, *Macromol. Symp.*, 2001, **173**, 77–87.
60 T. F. McKenna and J. B. P. Soares, *Chem. Eng. Sci.*, 2001, **56**, 3931–3949.
61 H. Hammawa and S. E. Wanke, *J. Appl. Polym. Sci.*, 2007, **104**, 514–527.
62 P. A. Zapata, C. Belver, R. Quijada, P. Aranda and E. Ruiz-Hitzky, *Appl. Catal. A Gen.*, 2013, **453**, 142–150.
63 T. Pothirat, B. Jongsomjit and P. Praserthdam, *Catal. Commun.*, 2008, **9**, 1426–1431.
64 K. Soga, T. Arai and T. Uozumi, *Polymer (Guildf).*, 1997, **38**, 4993–4995.
65 A. S. Shearer, Y. R. de Miguel, E. A. Minich, D. Pochan and C. Jenny, *Inorg. Chem. Commun.*, 2007, **10**, 262–264.
66 J. Lei, D. Li, H. Wang, Z. Wang and G. Zhou, *J. Polym. Sci. Part A Polym. Chem.*, 2011, **49**, 1503–1507.
67 J. H. Z. dos Santos, S. Dorneles, F. C. Stedile, J. Dupont, M. M. de Camargo Forte and I. J. R. Baumvol, *Macromol. Chem. Phys.*, 1997, **198**, 3529–3537.
68 J. H. Z. dos Santos, C. Krug, M. B. da Rosa, F. C. Stedile, J. Dupont and M. de C. Forte, *J. Mol. Catal. A Chem.*, 1999, **139**, 199–207.
69 D. Bianchini, F. C. Stedile and J. H. Z. dos Santos, *Appl. Catal. A Gen.*, 2004, **261**, 57–67.
70 G. B. Galland, M. Seferin, R. Guimarães, J. A. Rohrmann, F. C. Stedile and J. H. Z. dos Santos, *J. Mol. Catal. A Chem.*, 2002, **189**, 233–240.
71 R. Guimarães, F. C. Stedile and J. H. Z. dos Santos, *J. Mol. Catal. A Chem.*, 2003, **206**, 353–362.
72 J.-C. Buffet, N. Wanna, T. A. Q. Arnold, E. K. Gibson, P. P. Wells, Q. Wang, J. Tantirungrotechai and D. O'Hare, *Chem. Mater.*, 2015, **27**, 1495–1501.
73 A. F. R. Kilpatrick, J.-C. Buffet, P. Nørby, N. H. Rees, N. P. Funnell, S. Sripothongnak and D. O'Hare, *Chem. Mater.*, 2016, **28**, 7444–7450.
74 A. F. R. Kilpatrick, N. H. Rees, S. Sripothongnak, J.-C. Buffet and D. O'Hare, *Organometallics*, 2018, **37**, 156–164.

Chapter Two – Ligand synthesis

2.1 Introduction

The synthesis of permethylated indenyl ligand (C_9Me_7, Ind*, I*) was first reported by Miyamoto *et al.* in 1981.[1] O'Hare and co-workers later extended its transition metal chemistry to include Fe, Co, Cr, Ti and Zr.[2–5]

Dichloro(ethylenebis(1-indenyl))zirconium(IV) ($EBIZrCl_2$) and dichloro(dimethylsilylbis(1-indenyl))zirconium(IV) ($^{Me2}SBIZrCl_2$) have been shown by Kaminsky *et al.*[6] and Herrmann *et al.*,[7] respectively, to be very active for ethylene polymerisation. The permethylated analogues, dichloro(ethylenebis(hexamethyl-1-indenyl))zirconium(IV) ($EBI*ZrCl_2$) and dichloro(dimethylsilylbis(hexamethyl-1-indenyl))zirconium(IV) ($^{Me2}SBI*ZrCl_2$), were also synthesised and shown to be very active for ethylene polymerisation.[8,9]

Möhring *et al.* have shown that steric and electronic effects of ring substituents on cyclopentadienyl (Cp) rings have strong influence on ethylene polymerisation activity of the corresponding group 4 complexes.[10–14] Wang has also demonstrated that the bridge has a large influence on the reaction cavity around the metal centres and on the stability of the catalysts by altering the molecular frameworks and electronic densities.[15]

Otero and co-workers have shown that introducing alkyl groups at the 3- positions of $^{Me2}SBIZrCl_2$ can increase the stability and ethylene polymerisation activity of the corresponding complexes.[16–18] Alt *et al.* suggested that alkyl substituents, which are in direct contact with the active catalyst centre, increase the distance between the cationic metal centre and the anionic MAO co-catalyst, thus making the active site more accessible by ethylene, increasing the activity.[19]

The aims of this research are to modify the very active $^{Me2}SBI*ZrCl_2$ system to further increase the activity. By taking inspirations from the work mentioned above, different alkyl groups were introduced on the silyl bridge (R) and at the 3- position of the indenyl rings (R′) shown in Figure 2.1.

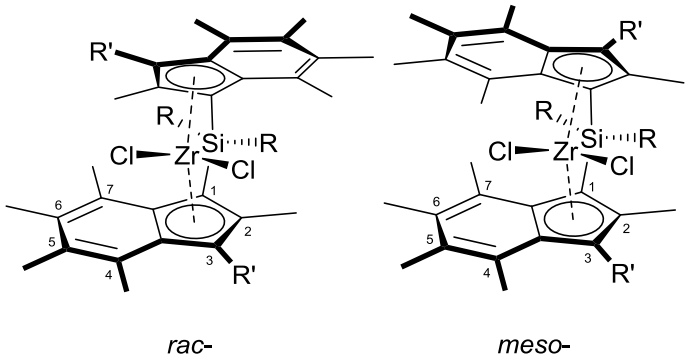
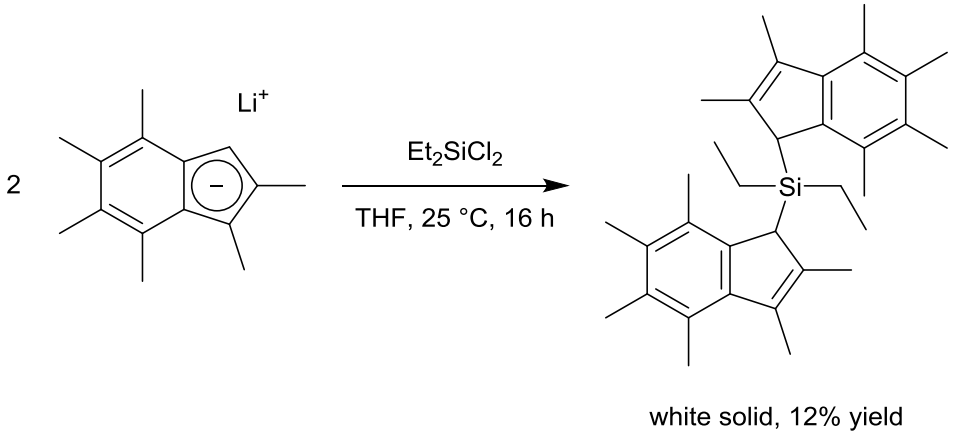


Figure 2.1. Alkyl group variations on the silyl bridge (R) and at the 3- position of the indenyl rings (R′) of ^{Me2}SBI*ZrCl$_2$.

2.2 Variations of alkyl groups on silyl bridge

2.2.1 Synthesis of ^{Et2}SBI*H$_2$



Scheme 2.1. Synthesis of ^{Et2}SBI*H$_2$.

The first alteration was to introduce various alkyl groups on the silyl bridge. The aim is to induce a change in the molecular framework with minimal steric disruption on the active site of the subsequent complex. Symmetric dialkyldichlorosilanes were chosen in order to simplify the stereochemistry and, hence, purification of the resulting complexes.

The synthesis of diethylsilylbis(hexamethyl-1-indene) (^{Et2}SBI*H$_2$) was modified from the synthesis of dimethylsilylbis(hexamethyl-1-indene) (^{Me2}SBI*H$_2$) reported by O'Hare and co-workers.[9,20] Double nucleophilic substitution of hexamethylindenyl lithium (Ind$^{\#}$Li) on dichlorodiethylsilane (Et_2SiCl_2) was attempted (Scheme 2.1).

One equivalent of Et_2SiCl_2 was reacted with two equivalents of Ind$^{\#}$Li in THF at 0 °C, then slowly warmed up to room temperature and left stirring for 16 hours. The resulting

brown solution was dried *in vacuo* to remove all volatiles and an extraction using DCM was carried out. The DCM filtrate was analysed by ^{1}H NMR spectroscopy showing a mixture of the desirable product, *rac*- and *meso*-^{Et_2}SBI*H$_2$, and the protonated starting material, hexamethylindene (Ind$^{\#}$H). The formation of the Ind$^{\#}$H side-product has not been observed before in the ^{Me_2}SBI*H$_2$ synthesis and can be attributed to the slower substitution reaction due to the bulkier ethyl groups. *rac*-^{Et_2}SBI*H$_2$ was isolated as a white solid (12% yield) by a pentane extraction of the dried DCM filtrate.

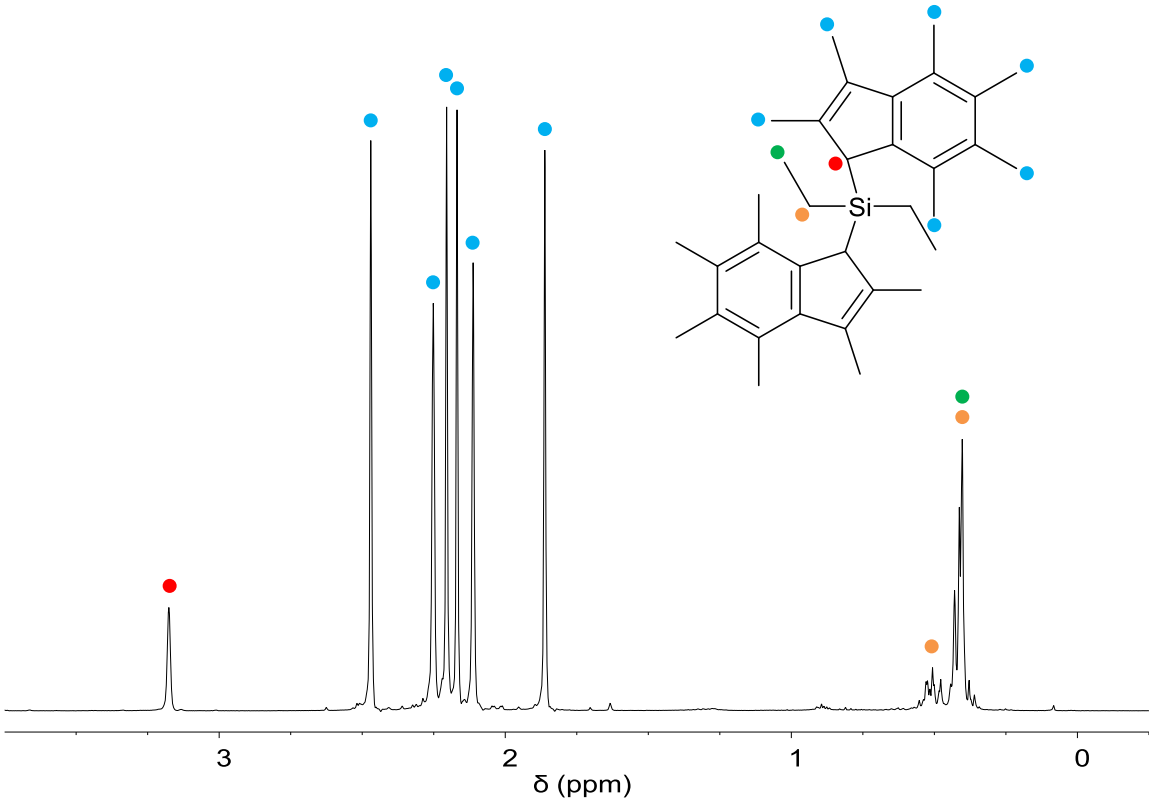


Figure 2.2. ^{1}H NMR spectrum (400 MHz, 298 K, chloroform-d_1) of *rac*-^{Et_2}SBI*H$_2$.

The ^{1}H NMR spectrum of *rac*-^{Et_2}SBI*H$_2$ shows a singlet resonance at 3.18 ppm corresponding to the protons on the 5-membered rings (Figure 2.2). Six singlet resonances between 1.80 and 2.50 ppm correspond to the methyl groups on the indenyl rings. The methyl signal for the two ethyl groups on the silyl bridge is observed at 0.41 ppm as a triplet resonance. The methylene protons are diastereotopic and are assigned to two multiplet resonances at 0.40 and 0.51 ppm.

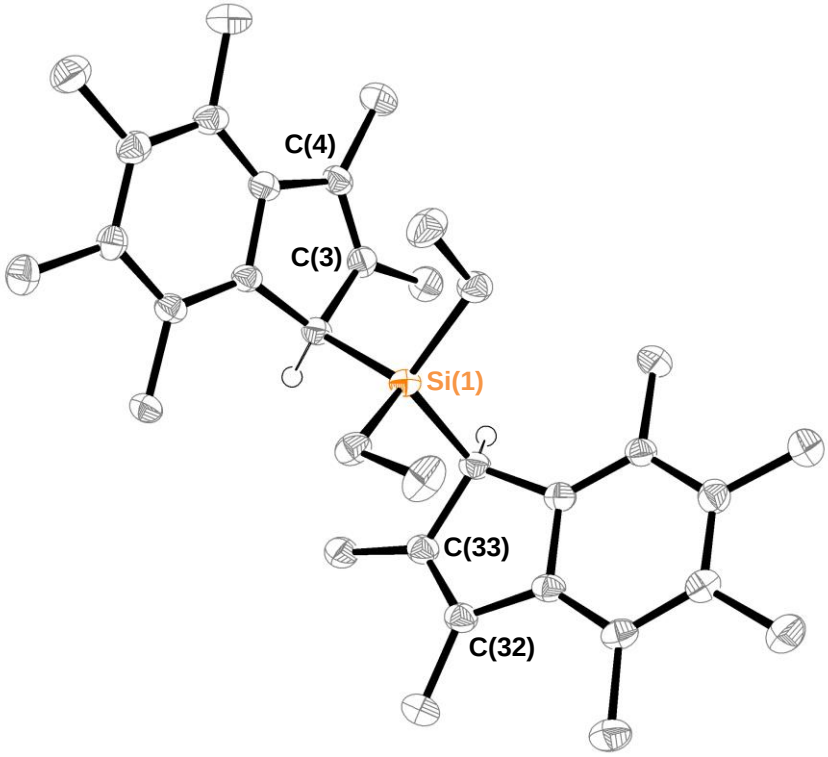
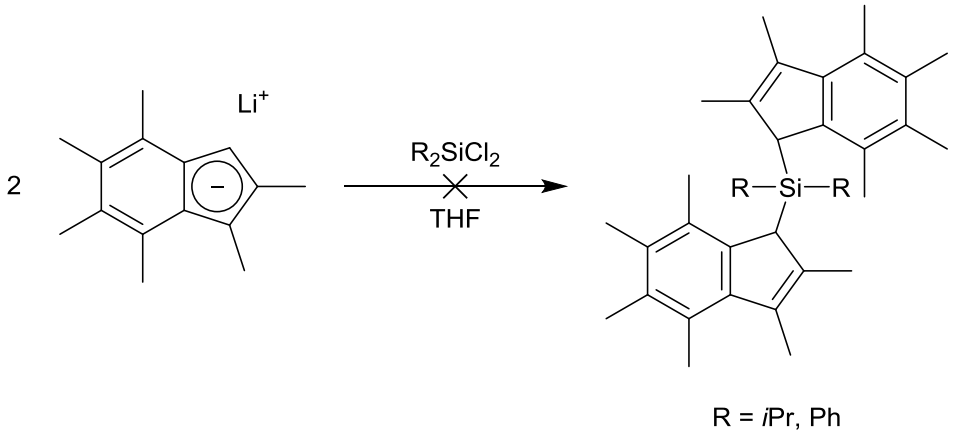


Figure 2.3. Molecular structure of *rac*-^{Et2}SBI*H_2. Hydrogen atoms omitted for clarity (except for stereocentres), ellipsoids drawn at 50% probability.

Colourless crystals of *rac*-^{Et2}SBI*H_2 suitable for single crystal X-ray diffraction were grown in pentane at 0 °C. The molecular structure is shown in Figure 2.3. The stereochemistry of the two chiral centres and the monoclinic space group $P2_1/c$ show that the pro-ligand crystallised as a racemic mixture. The crystal structure also confirms the position of the C(3)=C(4) and C(32)=C(33) double bonds, both with the same bond length of 1.355(4) Å. The structure displays a similar average Si-C_{Ind*} bond length (1.945(3) Å) compared to the reported value for *rac*-^{Me2}SBI*H_2 (1.939(6) Å).[9]

2.2.2 Attempted synthesis of ^{R2}SBI*H$_2$ (R = *i*Pr, Ph)



Scheme 2.2. Attempted synthesis of ^{R2}SBI*H$_2$ (R = *i*Pr, Ph).

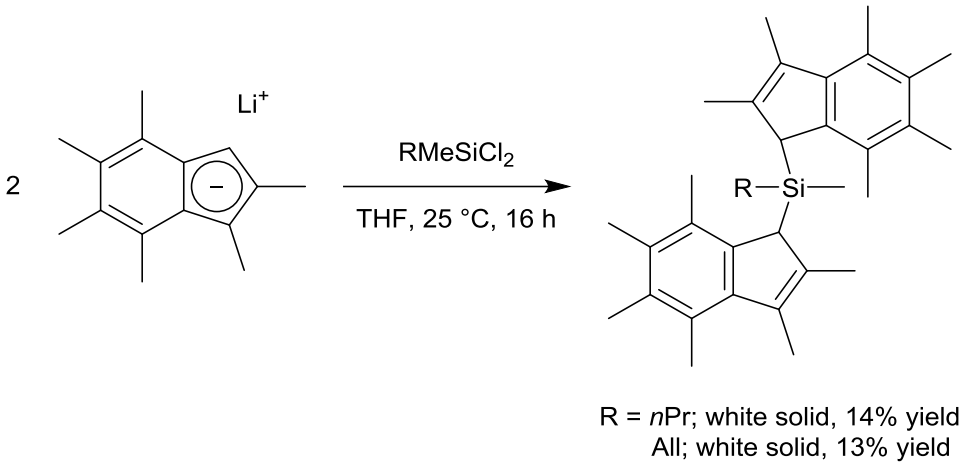
Reactions of Ind$^{\#}$Li with other symmetric dialkyldichlorosilanes have also been attempted (Scheme 2.2). Following the synthesis procedure for ^{Et2}SBI*H$_2$, one equivalent of dichlorodiisopropylsilane (*i*Pr$_2$SiCl$_2$) was reacted with two equivalents of Ind$^{\#}$Li in THF at 0 °C and then slowly warmed up to room temperature. The formation of the monosubstituted product and the Ind$^{\#}$H side-product were identified by ^{1}H NMR spectroscopy. However, the desirable disubstituted product, diisopropylsilylbis(hexamethyl-1-indene) (^{iPr2}SBI*H$_2$), was not observed. An elevated reaction temperature of 60 °C was used in an attempt to force the second substitution but only led to decomposition of the reactants. This suggests that the two isopropyl groups are too large and sterically prevent the second substitution reaction to occur.

The formation of the Ind$^{\#}$H side-product in the Et$_2$SiCl$_2$ and *i*Pr$_2$SiCl$_2$ reactions with Ind$^{\#}$Li is suspected to be the product of deprotonation of α-proton of the silane reactants by Ind$^{\#}$Li acting as a base instead of a nucleophile. The resulting carbanions are stabilised by hyperconjugation of the filled carbanion p orbital to the empty σ* orbital of the adjacent Si-C bond. As a consequence, the Ind$^{\#}$Li reactant is consumed by the side-reaction before it can undergo the sterically hindered second substitution.

Thus, to prevent the possible deprotonation side-reaction, dichlorodiphenylsilane (Ph$_2$SiCl$_2$), with no α-protons, was chosen for a reaction with Ind$^{\#}$Li. However, using the same synthesis procedure, the reaction of Ph$_2$SiCl$_2$ with Ind$^{\#}$Li yielded an intractable mixture of products. Neither mono- nor disubstituted product, diphenylsilylbis(hexamethyl-1-indene) (^{Ph2}SBI*H$_2$), was observed in the ^{1}H NMR spectrum and the reaction mixture slowly decomposed over time. Forced reaction conditions were also used to no avail. In contrast to

Et_2SiCl_2 and iPr_2SiCl_2, it can be concluded that Ph_2SiCl_2 is too sterically hindered to undergo the substitution reaction with bulky Ind#Li.

2.2.3 Synthesis of ^{R,Me}SBI*H_2 (R = *n*Pr, All)



Scheme 2.3. Synthesis of ^{R,Me}SBI*H_2 (R = *n*Pr, All).

Based on the high steric demand of the unfruitful syntheses of ^{iPr_2}SBI*H_2 and ^{Ph_2}SBI*H_2, asymmetric alkyl(dichloro)methylsilanes were reacted with Ind#Li in order to reduce the steric requirement of the double nucleophilic substitution reaction. Additionally, introducing an allyl group on the silyl bridge of group 4 *ansa*-metallocenes has been shown to provide useful post-synthesis functionalities to the complexes such as self-immobilisation capability during ethylene polymerisation.[21] O'Hare *et al.* have further functionalised the allyl group to a pendant Si-Cl anchor for grafting on silica supports to produce heterogeneous catalysts for the polymerisation of ethylene and propylene.[22]

Inspired by these previous works, methyl(propyl)silylbis(hexamethyl-1-indene) and allyl(methyl)silylbis(hexamethyl-1-indene) (^{R,Me}SBI*H_2; R = *n*Pr, All) were synthesised following the same procedure as for the ^{Et_2}SBI*H_2 synthesis (Scheme 2.3). One equivalent of dichloro(methyl)propylsilane (*n*PrMeSiCl_2) or allyl(dichloro)methylsilane (AllMeSiCl_2) was added dropwise to two equivalents of Ind#Li in THF at 0 °C. The reaction was then allowed to slowly warm up to room temperature and left stirring for 16 hours. After work-up, *rac*-^{R,Me}SBI*H_2 was isolated as a white solid in 14 or 13% yield (R = *n*Pr or All, respectively).

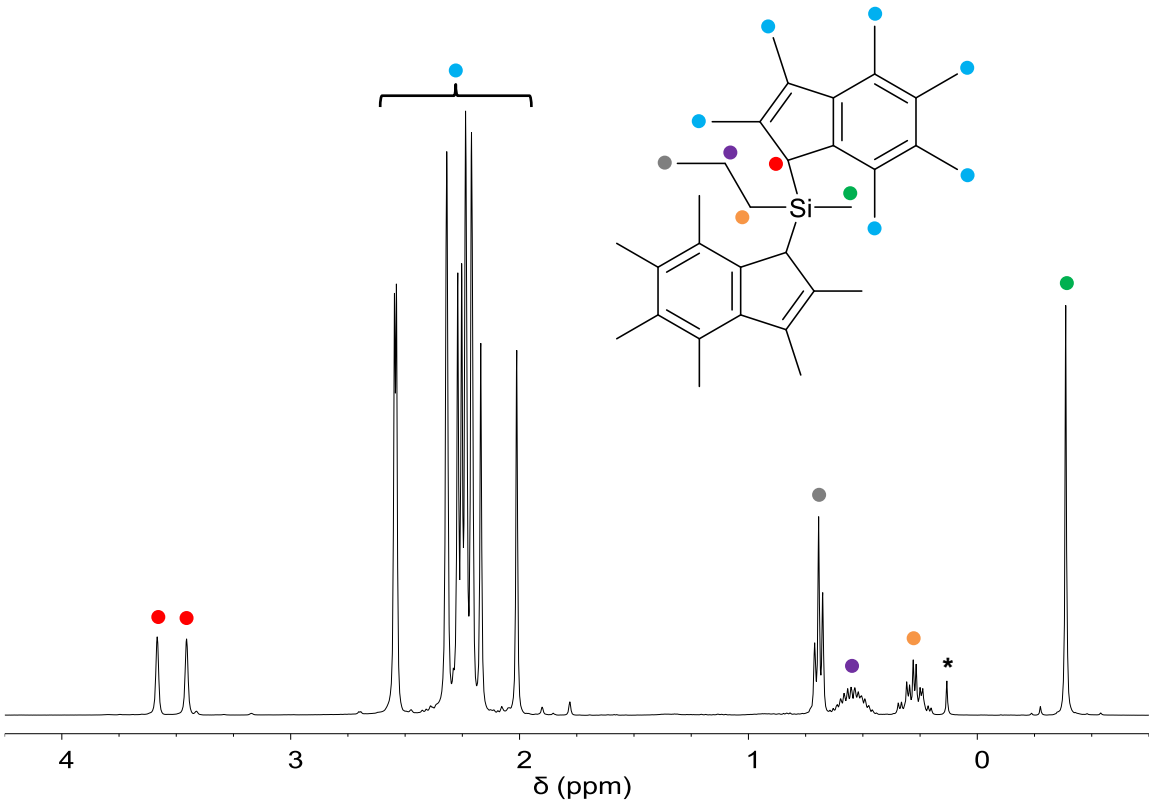


Figure 2.4. ^{1}H NMR spectrum (400 MHz, 298 K, chloroform-d_1) of *rac*-$^{n\text{Pr,Me}}$SBI*H_2. *: silicone grease.

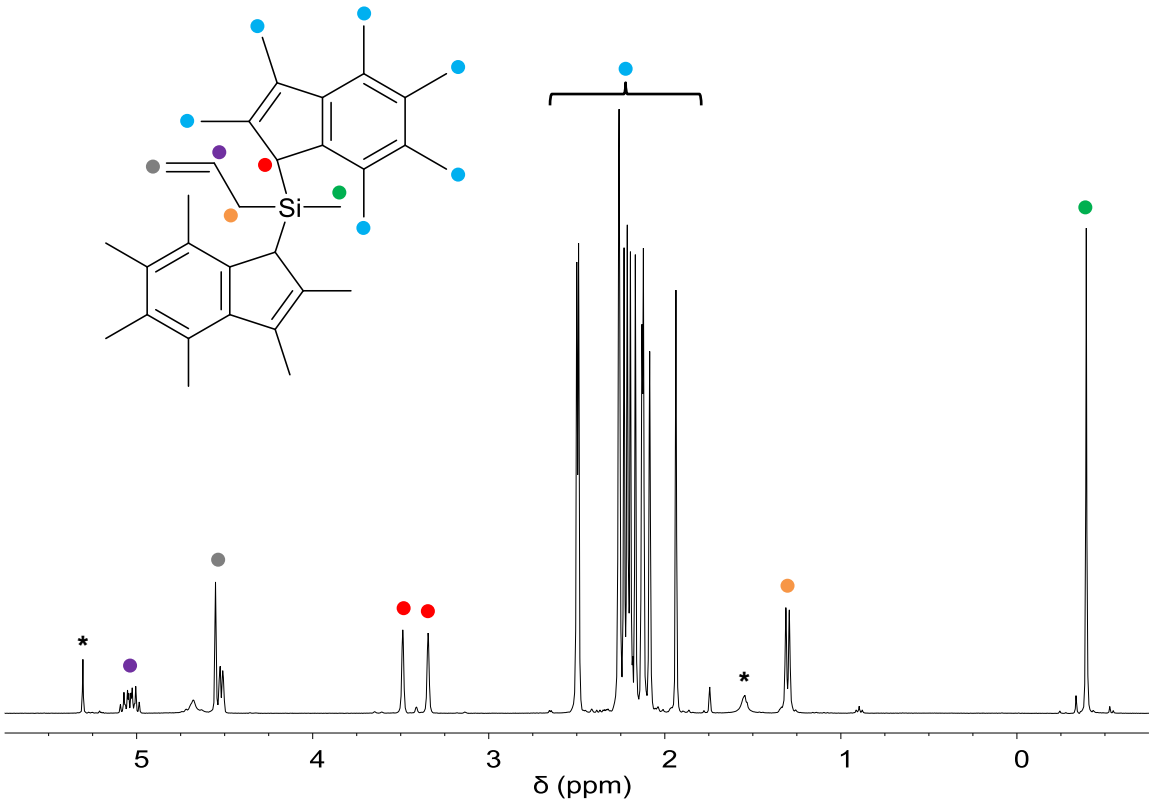
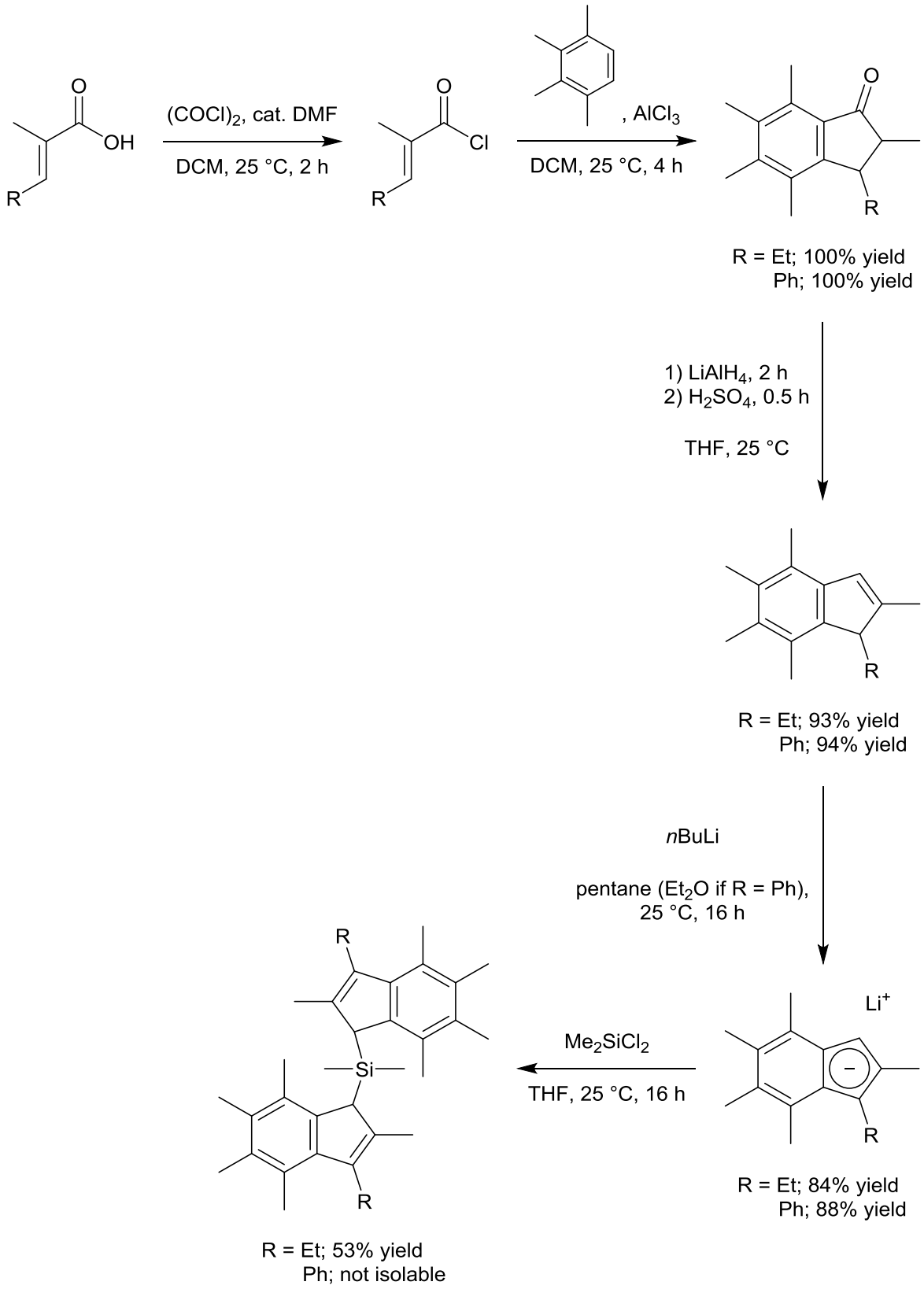


Figure 2.5. ^{1}H NMR spectrum (400 MHz, 298 K, chloroform-d_1) of *rac*-$^{\text{All,Me}}$SBI*H_2. *: DCM, water.

The ^{1}H NMR spectrum of *rac*-$^{n\text{Pr,Me}}$SBI*H_2 shows that the two indenyl rings are not magnetically equivalent and are observed as two sets of resonances (Figure 2.4). Two singlet resonances at 3.45 and 3.58 ppm correspond to the protons on each of the 5-membered ring. There are 12 singlet resonances between 2.00 and 2.60 ppm, with some overlapping, corresponding to the methyl groups on both indenyl rings. The propyl group resonances are observed, in the order from the methyl group to the methylene group attached to the silicon atom, at 0.69 (triplet), 0.54 (multiplet) and 0.27 ppm (multiplet), respectively. Lastly, a singlet resonance at -0.39 ppm corresponds to the methyl group on the silyl bridge.

The ^{1}H NMR spectrum of *rac*-$^{\text{All,Me}}$SBI*H_2 is shown in Figure 2.5. Similar to *rac*-$^{n\text{Pr,Me}}$SBI*H_2, the two indenyl rings are not magnetically equivalent and are observed as two sets of resonances. Two singlet resonances at 3.34 and 3.49 ppm correspond to the protons on each of the 5-membered ring. There are 12 singlet resonances between 1.90 and 2.50 ppm, with some overlapping, corresponding to the methyl groups on both indenyl rings. A doublet resonance is recorded at 1.30 ppm corresponding to the allylic protons. The internal vinylic proton signal is observed as a multiplet resonance at 5.04 ppm. Doublet and singlet resonances at 4.52 and 4.55 ppm, respectively, both correspond to the terminal vinylic protons. Another singlet resonance at -0.39 ppm corresponds to the methyl group on the silyl bridge.

2.3 Variations of alkyl groups at 3- position of indenyl rings

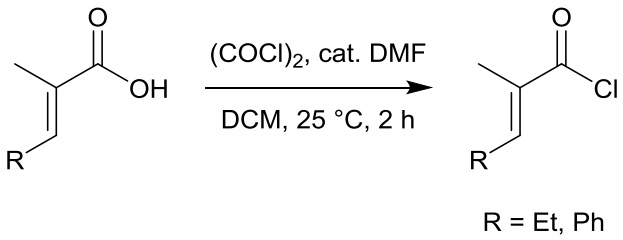


Scheme 2.4. Overall synthesis of $^{Me2}SB(^{3\text{-}R}I^{*})H_2$ (R = Et, Ph).

Another targeted change was the substitution of the methyl group at the 3- position of the permethylated indenyl rings. Otero and co-workers have demonstrated that, for ^{Me2}SBIZrCl$_2$, this modification increases the stability of the active species generated after combining the modified complexes with MAO co-catalyst.[16–18] It has also been shown that introducing methyl or ethyl group, in particular, increases the ethylene polymerisation activity of the corresponding complexes while producing polyethylenes with lower molecular weights. This effect is desirable because it has been shown that, by adding hydrogen gas to the polymerisation reaction, indenyl metallocene catalysts can produce polyethylenes with very low molecular weights, which are commonly known as polyethylene waxes and widely used industrially.[23]

The overall synthesis of dimethylsilylbis(3-ethyl-2,4,5,6,7-pentamethyl-1-indene) and dimethylsilylbis(2,4,5,6,7-pentamethyl-3-phenyl-1-indene) pro-ligands (^{Me2}SB($^{3\text{-}R}$I*)H$_2$; R = Et, Ph) is shown in Scheme 2.4.[24] The synthesis was based on previous works on the dimethylsilyl analogous ligand carried out by O'Hare and co-workers.[2,9,20,25] The ethyl or phenyl group was introduced by substituting the original starting material, tiglic acid (R = Me), with (*E*)-2-methylpent-2-enoic acid (R = Et) or (*E*)-α-methylcinnamic acid (R = Ph), respectively. The acid was chlorinated using oxalyl chloride and then reacted with 1,2,3,4-tetramethylbenzene, in the presence of $AlCl_3$, to form 3-alkyl-2,4,5,6,7-pentamethylindan-1-one ($^{3\text{-}R}$Ind$^{\#}$=O), which was subsequently reduced by $LiAlH_4$ and dehydrated using concentrated H_2SO_4 to obtain 3-alkyl-2,4,5,6,7-pentamethylind-1-ene ($^{3\text{-}R}$Ind$^{\#}$H). The indene was later lithiated by *n*BuLi and reacted with dichlorodimethylsilane (Me_2SiCl_2) to yield the desirable pro-ligand, ^{Me2}SB($^{3\text{-}R}$I*)H$_2$.

2.3.1 Synthesis of RCH=CMeCOCl (R = Et, Ph)



Scheme 2.5. Synthesis of RCH=CMeCOCl (R = Et, Ph).

(*E*)-2-methylpent-2-enoic acid (R = Et) and (*E*)-α-methylcinnamic acid (R = Ph) were reacted with oxalyl chloride in DCM to obtain (*E*)-2-methylpent-2-enoyl chloride and (*E*)-α-methylcinnamoyl chloride (RCH=CMeCOCl), respectively. A catalytic amount of N,N-dimethylformamide (DMF) was added creating effervescence (Scheme 2.5). The reaction was stirred for 2 hours after which an aliquot was analysed showing that the reaction had gone to completion. The resulting pale yellow solution was immediately used in the next step of the synthesis.

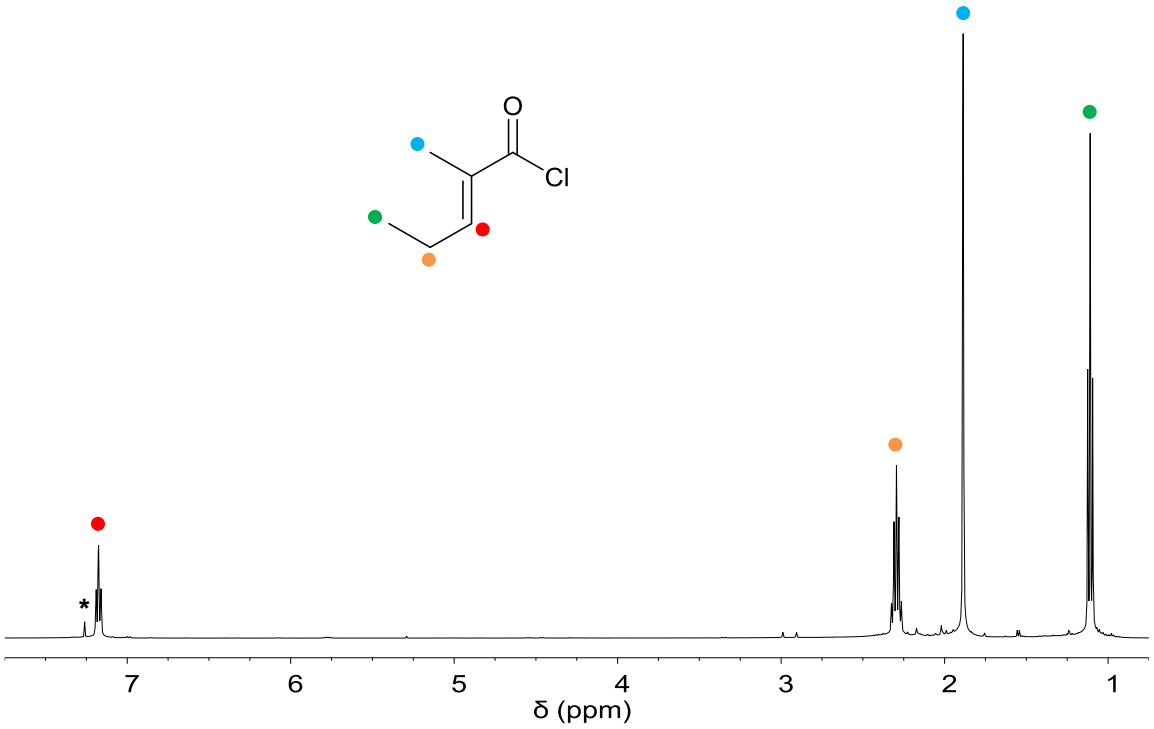


Figure 2.6. ^{1}H NMR spectrum (500 MHz, 298 K, chloroform-d_1) of EtCH=CMeCOCl. *: chloroform.

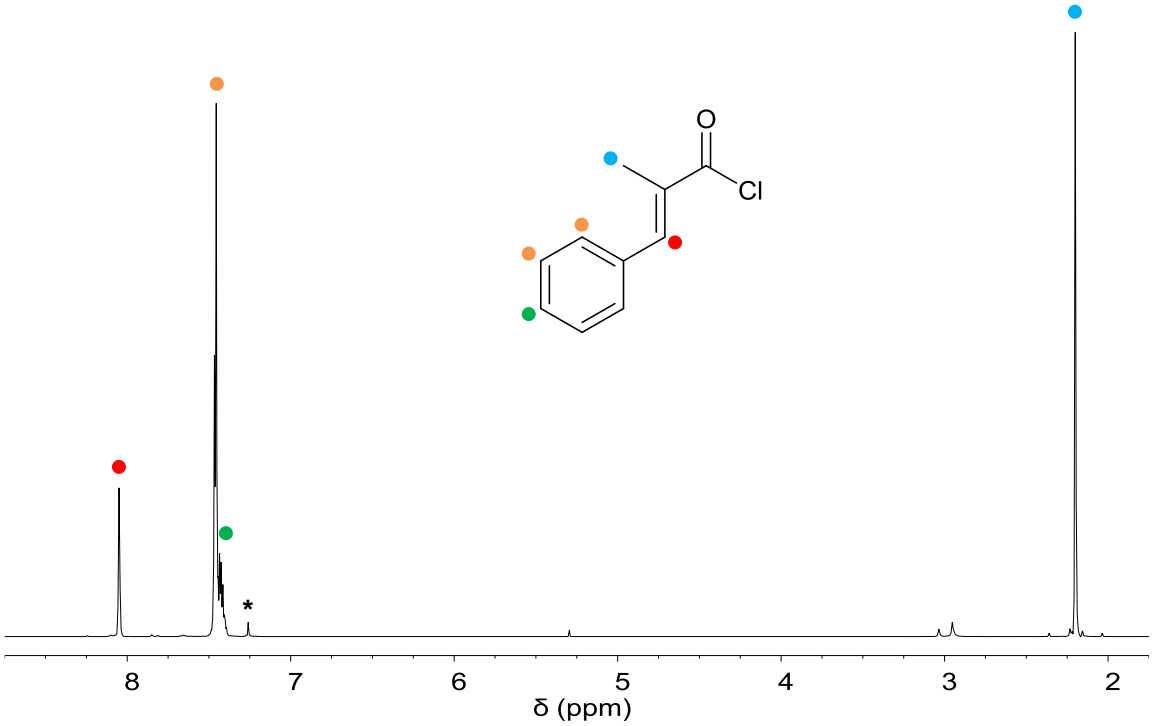
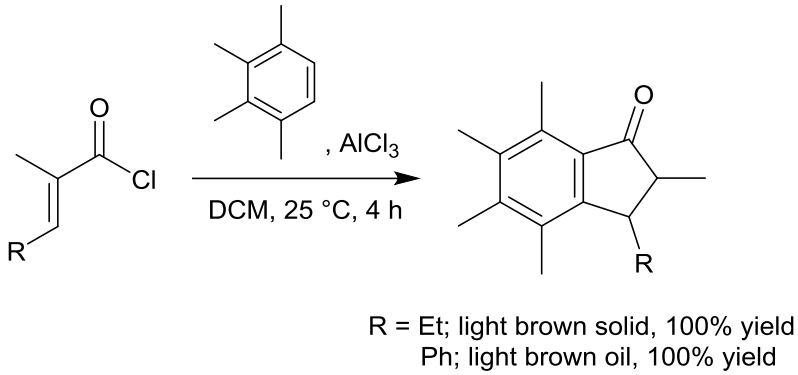


Figure 2.7. ^{1}H NMR spectrum (400 MHz, 298 K, chloroform-d_1) of PhCH=CMeCOCl. *: chloroform.

The ^{1}H NMR spectrum of EtCH=CMeCOCl shows a triplet resonance at 7.17 ppm corresponding to the vinylic proton (Figure 2.6). The methyl and methylene signals of the ethyl group are observed at 1.11 (triplet) and 2.29 ppm (doublet of quartets), respectively. A singlet resonance at 1.89 ppm corresponds to the vinylic methyl group.

The ^{1}H NMR spectrum of PhCH=CMeCOCl shows a singlet resonance at 8.05 ppm corresponding to the vinylic proton (Figure 2.7). A broad doublet resonance at 7.46 ppm is assigned to the *ortho* and *meta* protons on the phenyl group. The *para* proton is observed as a multiplet resonance at 7.43 ppm. The vinylic methyl group is corresponded to a singlet resonance at 2.20 ppm.

2.3.2 Synthesis of $^{3\text{-R}}$Ind$^{\#}$=O (R = Et, Ph)



R = Et; light brown solid, 100% yield
Ph; light brown oil, 100% yield

Scheme 2.6. Synthesis of $^{3\text{-R}}$Ind$^{\#}$=O (R = Et, Ph).

The synthesis of $^{3\text{-R}}$Ind$^{\#}$=O (R = Et, Ph) utilised Friedel-Crafts acylation and concomitant Nazarov cyclisation reactions, both catalysed by a Lewis acid ($AlCl_3$). $AlCl_3$ was slowly added to the RCH=CMeCOCl solution to yield an orange solution. 1,2,3,4-tetramethylbenzene was diluted in DCM and then added dropwise to the reaction mixture over 30 minutes where a colour change from orange to blood red was observed (Scheme 2.6). The reaction was then stirred for 4 hours after which a 1:1 mixture of concentrated HCl and ice was added slowly to quench the reaction. The reaction mixture changed colour from blood red to light orange during the work-up. The product was extracted with DCM and the combined organic layer was washed with saturated $NaHCO_3$ solution and deionised water before being dried using anhydrous $MgSO_4$. The mixture was filtered and the resulting filtrate was dried *in vacuo* to afford $^{3\text{-R}}$Ind$^{\#}$=O as a light brown solid (R = Et; 100% yield) or a light brown oil (R = Ph; 100% yield). In both cases, the crude product contained several diastereomers most of which can be extracted by pentane leaving only the *cis* isomer as a white solid.

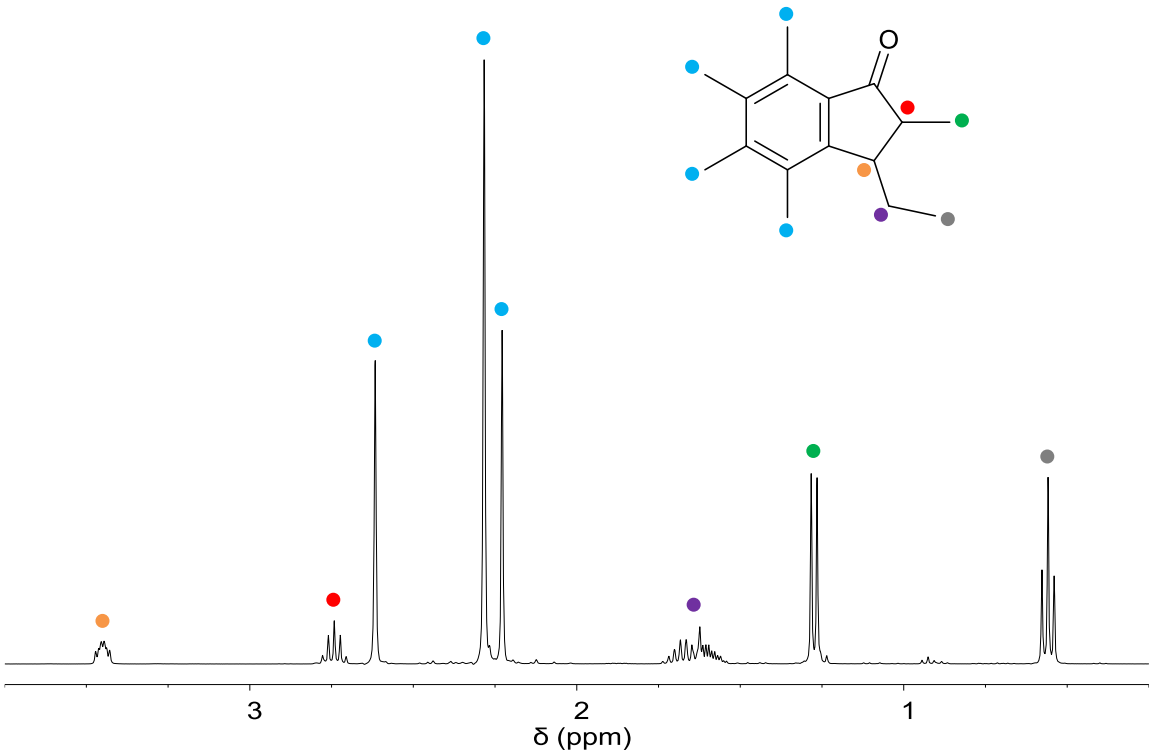


Figure 2.8. ^{1}H NMR spectrum (400 MHz, 298 K, chloroform-d_1) of *cis*-$^{3\text{-Et}}$Ind$^{\#}$=O.

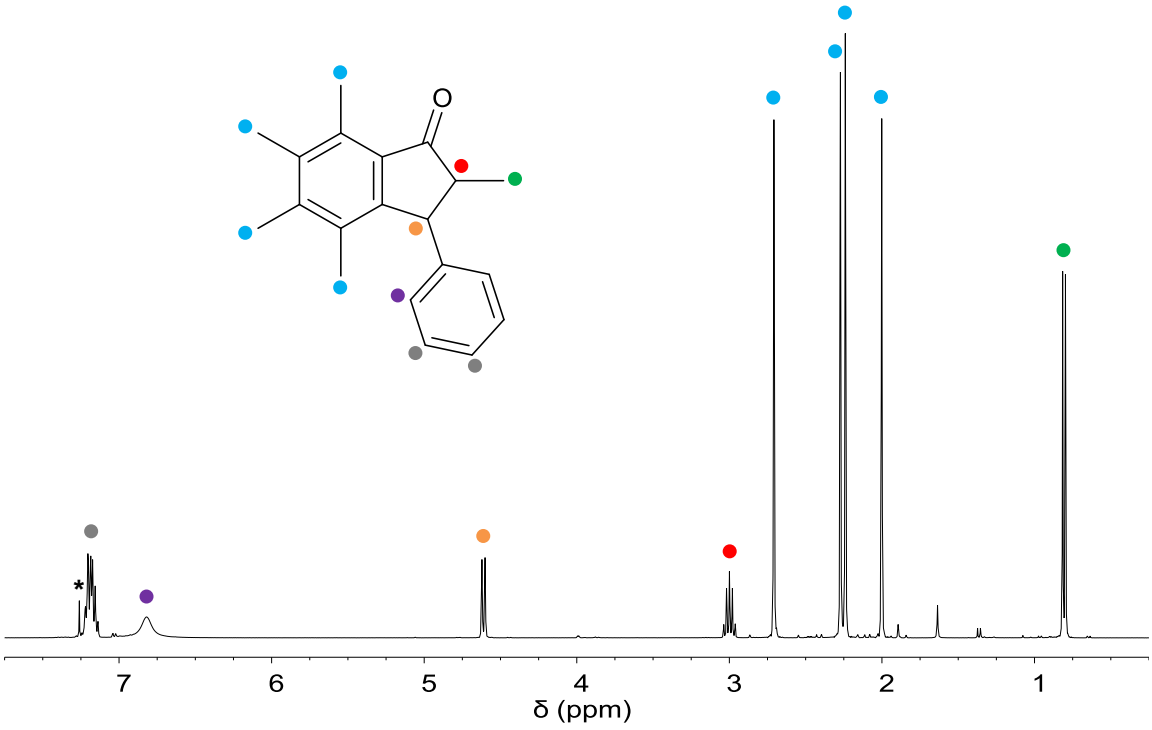


Figure 2.9. ^{1}H NMR spectrum (400 MHz, 298 K, chloroform-d_1) of *cis*-$^{3\text{-Ph}}$Ind$^{\#}$=O. *: chloroform.

The ^{1}H NMR spectrum of *cis*-$^{3\text{-Et}}$Ind$^{\#}$=O shows two resonances at 2.74 (doublet of quartets) and 3.45 ppm (multiplet) corresponding to the two -CH groups of the 5-membered ring with the latter connected to the ethyl group (Figure 2.8). Four aromatic methyl groups are observed between 2.20 and 2.70 ppm as singlet resonances. Resonances assigned to the methyl and methylene protons of the ethyl group are seen at 0.56 (triplet) and 1.63 ppm (multiplet), respectively. A doublet resonance at 1.27 ppm is assigned to the methyl group on the 5-membered ring.

The ^{1}H NMR spectrum of *cis*-$^{3\text{-Ph}}$Ind$^{\#}$=O shows a multiplet resonance at 7.18 ppm corresponding to the *meta* and *para* protons of the phenyl group (Figure 2.9). The *ortho* protons are observed as a broad singlet resonance at 6.82 ppm. A doublet of quartets resonance at 3.00 ppm and a doublet resonance at 4.61 ppm correspond to the two -CH groups of the 5-membered ring with the latter connected to the phenyl group. Singlet resonances between 2.00 and 2.80 ppm are assigned to the four aromatic methyl groups. A doublet resonance at 0.81 ppm corresponds to the methyl group on the 5-membered ring.

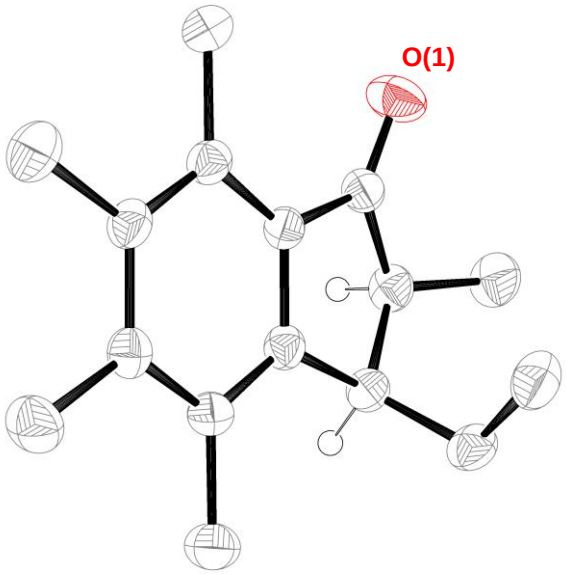


Figure 2.10. Molecular structure of *cis*-$^{3\text{-Et}}$Ind$^{\#}$=O. Hydrogen atoms omitted for clarity (except for stereocentres), ellipsoids drawn at 50% probability.

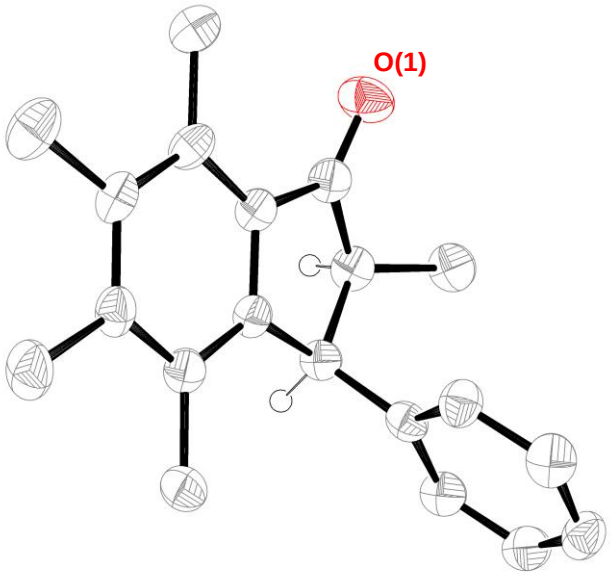
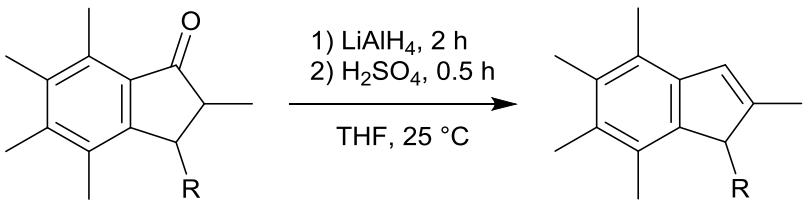


Figure 2.11. Molecular structure of *cis*-$^{3\text{-Ph}}$Ind$^{\#}$=O. Hydrogen atoms omitted for clarity (except for stereocentres), ellipsoids drawn at 50% probability.

Colourless crystals of $^{3\text{-R}}$Ind$^{\#}$=O (R = Et, Ph) suitable for single crystal X-ray diffraction were grown in hexane at 0 °C. The molecular structures are shown in Figure 2.10 and Figure 2.11, respectively. $^{3\text{-Et}}$Ind$^{\#}$=O crystallised in the triclinic space group $P\bar{1}$ while $^{3\text{-Ph}}$Ind$^{\#}$=O crystallised in the orthorhombic space group $Pna2_1$ both as a racemic mixture. Both crystal structures correspond to the *cis* isomers as previously reported for hexamethylindan-1-one (Ind$^{\#}$=O).[26] The C=O bond lengths of 1.219(2) and 1.222(6) Å, respectively, are almost identical to that of the Ind$^{\#}$=O (1.218(3) Å). All other bond lengths and bond angles are consistent with the characteristics of an aromatic benzene ring and the 5-membered ring in an envelope conformation.

2.3.3 Synthesis of $^{3\text{-R}}$Ind$^{\#}$H (R = Et, Ph)



R = Et; light brown solid, 93% yield
Ph; light brown solid, 94% yield

Scheme 2.7. Synthesis of $^{3\text{-R}}$Ind$^{\#}$H (R = Et, Ph).

The synthesis of $^{3\text{-R}}\text{Ind}^{\#}\text{H}$ (R = Et, Ph) involved two synthetic steps; reduction of $^{3\text{-R}}\text{Ind}^{\#}\text{=O}$ by $LiAlH_4$ followed by dehydration of the resulting alcohol by concentrated H_2SO_4 (Scheme 2.7). $LiAlH_4$ was added dropwise to a THF solution of $^{3\text{-R}}\text{Ind}^{\#}\text{=O}$ over 30 minutes and the resulting yellow solution was stirred for 2 hours. The reaction was cooled to 0 °C and then slowly quenched by the addition of deionised water. Concentrated H_2SO_4 was added dropwise to the reaction mixture over 30 minutes after which the reaction mixture turned dark brown. The reaction was then quenched with deionised water and extracted with DCM. The combined organic layer was washed with saturated $NaHCO_3$ solution and deionised water, dried over anhydrous $MgSO_4$ and filtered. The resulting yellow solution was dried *in vacuo* to afford $^{3\text{-R}}\text{Ind}^{\#}\text{H}$ as a light brown solid in 93 or 94% yield (R = Et or Ph, respectively).

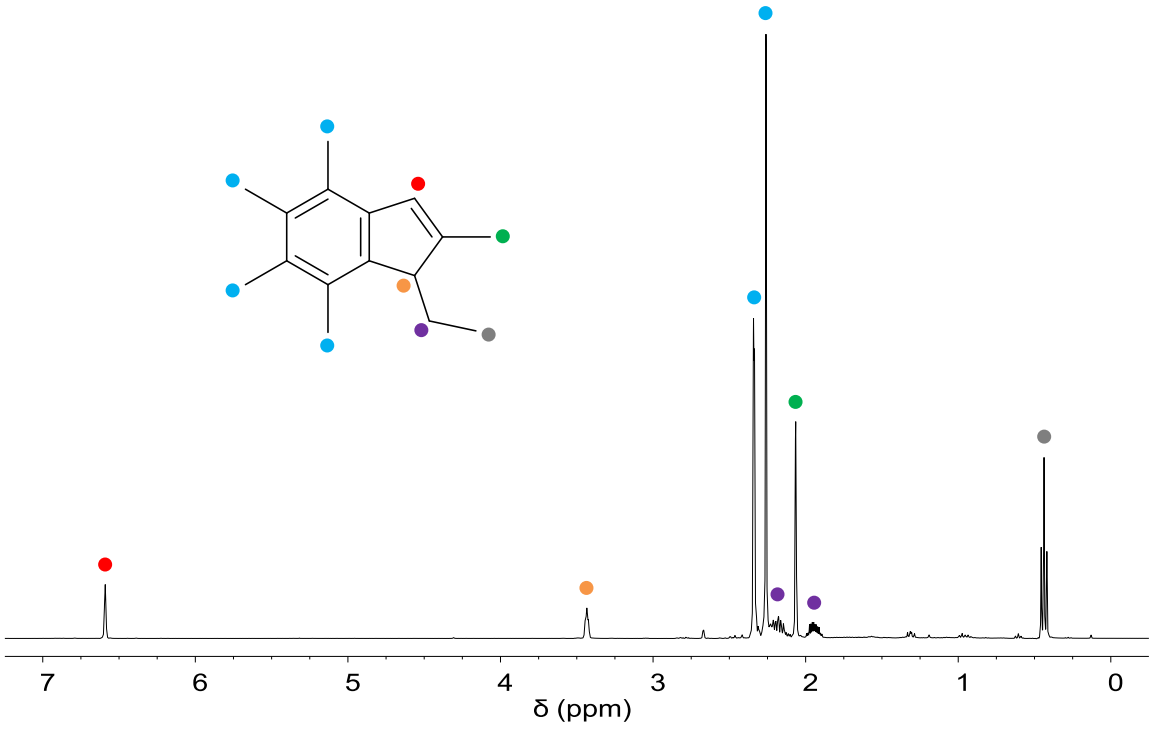


Figure 2.12. ^{1}H NMR spectrum (400 MHz, 298 K, chloroform-d_1) of $^{3\text{-Et}}\text{Ind}^{\#}\text{H}$.

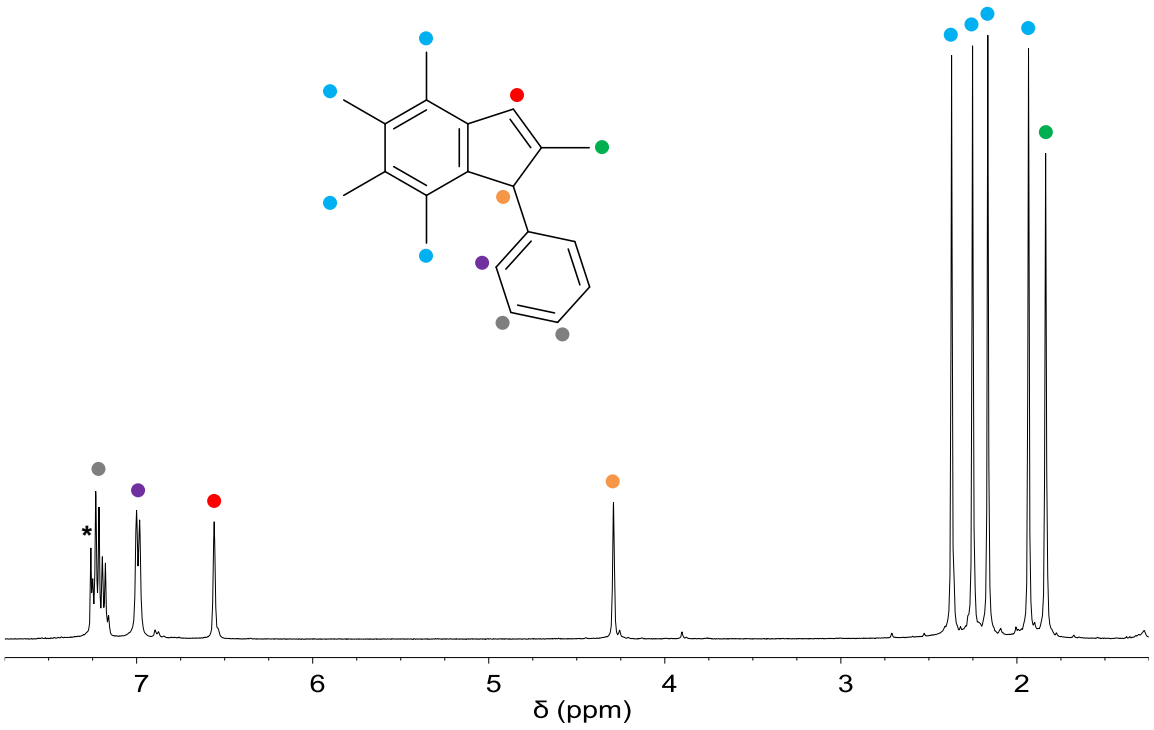


Figure 2.13. ^{1}H NMR spectrum (400 MHz, 298 K, chloroform-d_1) of $^{3\text{-Ph}}$Ind$^{\#}$H. *: chloroform.

The ^{1}H NMR spectrum of $^{3\text{-Et}}$Ind$^{\#}$H confirms the formation of the less substituted double bond product (Figure 2.12). The vinylic proton is observed as a singlet resonance at 6.59 ppm. A triplet resonance at 3.43 ppm corresponds to the other -CH group of the 5-membered ring. Four aromatic methyl groups are seen between 2.20 and 2.40 ppm as singlet resonances. The methyl group on the 5-membered ring is observed as a singlet resonance at 2.07 ppm. A triplet resonance at 0.44 ppm is assigned to the methyl protons of the ethyl group. Interestingly, the methylene protons are diastereotopic and observed as two multiplet resonances at 1.94 and 2.18 ppm.

The ^{1}H NMR spectrum of $^{3\text{-Ph}}$Ind$^{\#}$H shows a vinylic proton signal as a singlet resonance at 6.56 ppm confirming the formation of the less substituted double bond product (Figure 2.13). A singlet resonance at 4.29 ppm corresponds to the other -CH group of the 5-membered ring. The *ortho* protons of the phenyl group are observed as a doublet resonance at 6.99 ppm. A multiplet resonance at 7.20 ppm is assigned to the *meta* and *para* protons. Four singlet resonances between 1.90 and 2.40 ppm correspond to the aromatic methyl groups. The methyl group on the 5-membered ring is seen as a singlet resonance at 1.84 ppm.

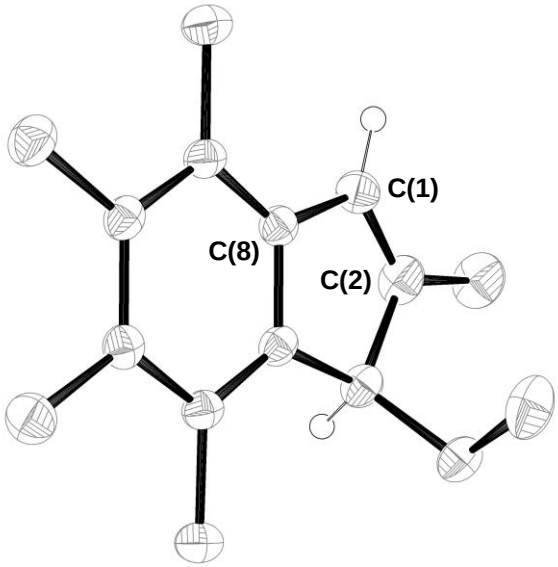


Figure 2.14. Molecular structure of $^{3\text{-Et}}$Ind$^{\#}$H. Hydrogen atoms omitted for clarity (except for stereocentres), ellipsoids drawn at 50% probability.

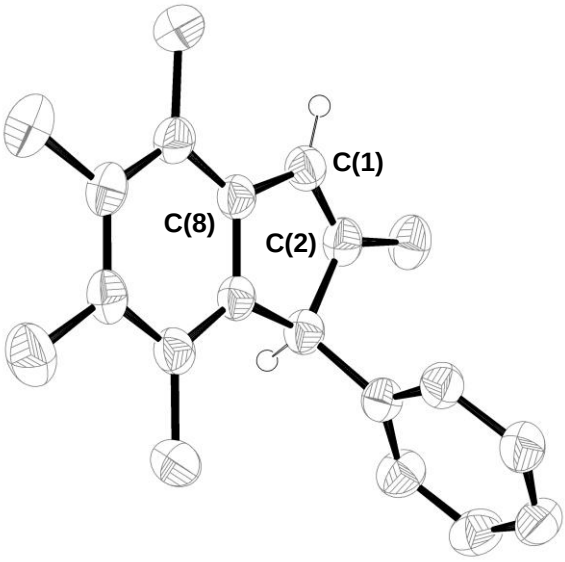
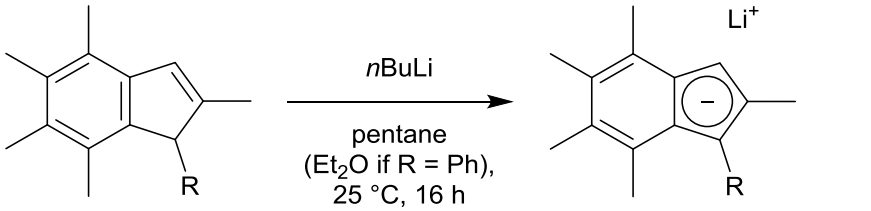


Figure 2.15. Molecular structure of $^{3\text{-Ph}}$Ind$^{\#}$H. Hydrogen atoms omitted for clarity (except for stereocentres), ellipsoids drawn at 50% probability.

Colourless crystals of $^{3\text{-R}}$Ind$^{\#}$H suitable for single crystal X-ray diffraction were grown in toluene (R = Et) or hexane (R = Ph) at 0 °C. The molecular structures are shown in Figure 2.14 and Figure 2.15, respectively. $^{3\text{-Et}}$Ind$^{\#}$H crystallised in the monoclinic space group *C*2/*c* while $^{3\text{-Ph}}$Ind$^{\#}$H crystallised in the monoclinic space group $P2_1/c$ both as a racemic mixture. Both crystal structures confirm the formation of the less substituted C(1)=C(2) double bonds

with the bond lengths of 1.343(2) and 1.330(3) Å, respectively. The C(1)-C(8) bond lengths of 1.473(2) and 1.465(2) Å, respectively, show some negative deviation from typical C-C single bond length values suggesting that there is some π conjugation between the C=C double bond and the benzene ring.

2.3.4 Synthesis of $^{3\text{-R}}$Ind$^{\#}$Li (R = Et, Ph)



R = Et; off-white solid, 84% yield
Ph; off-white solid, 88% yield

Scheme 2.8. Synthesis of $^{3\text{-R}}$Ind$^{\#}$Li (R = Et, Ph).

$^{3\text{-R}}$Ind$^{\#}$H was dissolved in pentane (R = Et) or Et_2O (R = Ph) to form a yellow solution. *n*BuLi was added dropwise to the solution at 0 °C (Scheme 2.8). The reaction was allowed to warm up to room temperature and left stirring for 16 hours. The resulting yellow suspension was filtered to yield a solid, which was washed with pentane and then dried *in vacuo* to afford 3-alkyl-2,4,5,6,7-pentamethylindenyl lithium ($^{3\text{-R}}$Ind$^{\#}$Li) as an off-white solid in 84 or 88% yield (R = Et or Ph, respectively).

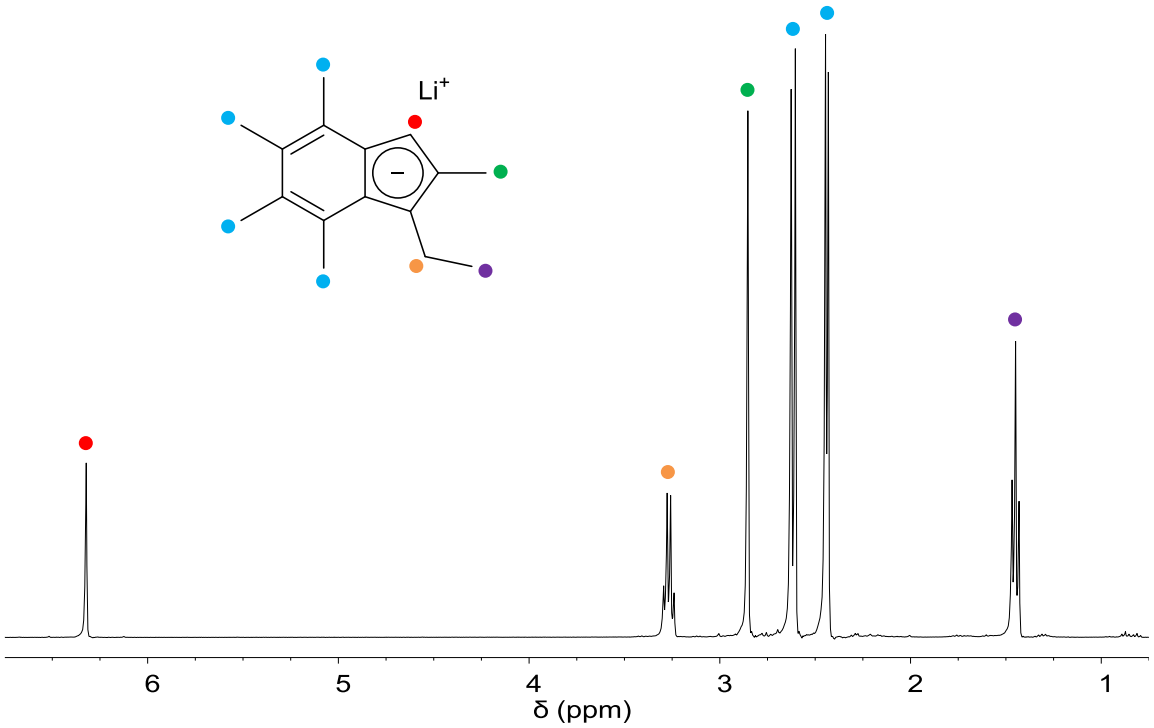


Figure 2.16. ^{1}H NMR spectrum (400 MHz, 298 K, pyridine-d_5) of $^{3\text{-Et}}$Ind$^{\#}$Li.

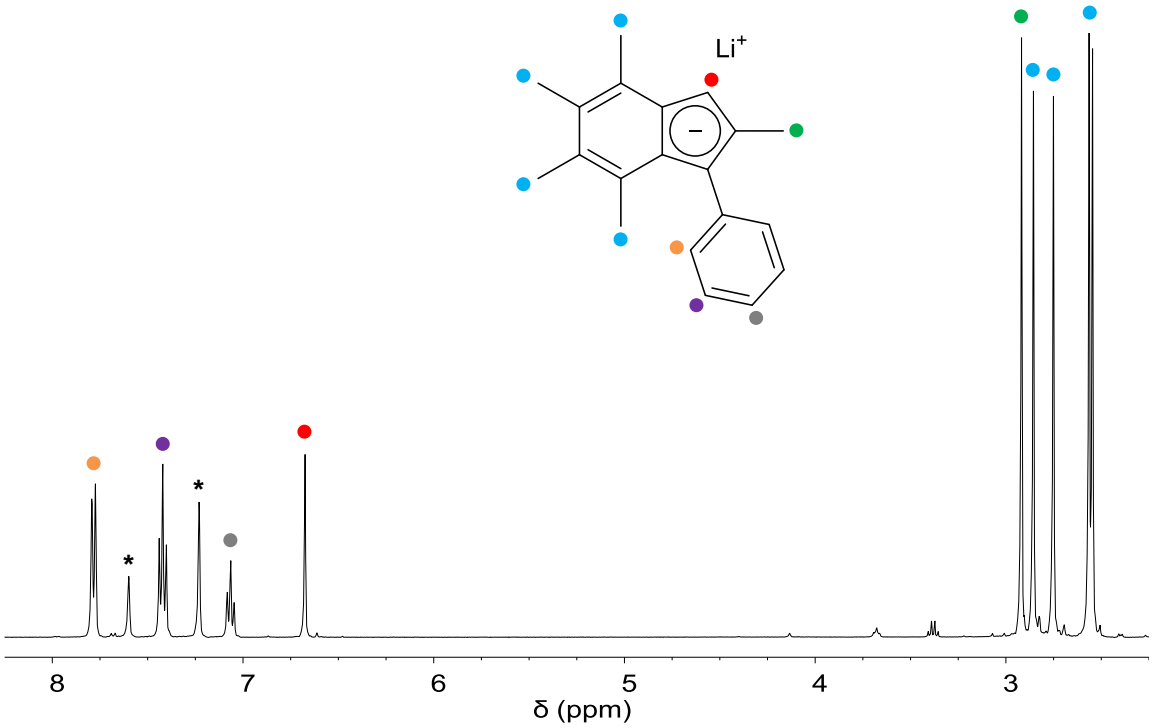
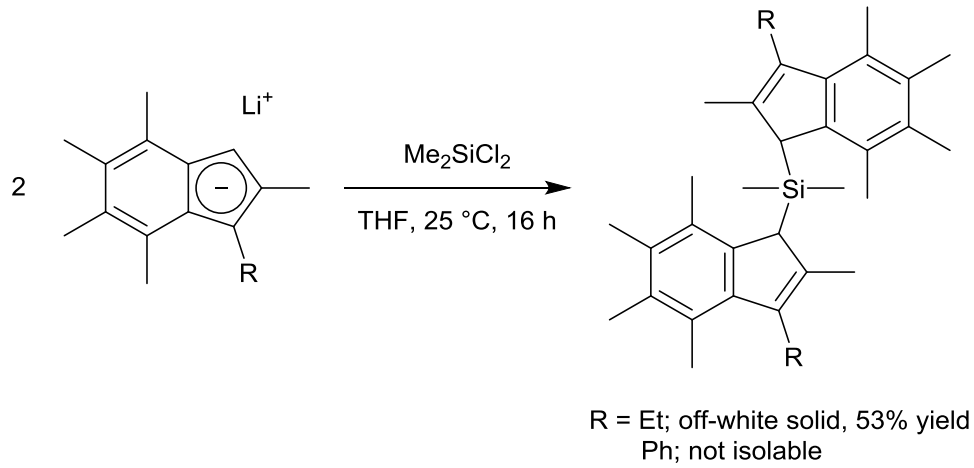


Figure 2.17. ^{1}H NMR spectrum (400 MHz, 298 K, pyridine-d_5) of $^{3\text{-Ph}}$Ind$^{\#}$Li. *: pyridine.

The ^{1}H NMR spectrum of $^{3\text{-Et}}$Ind$^{\#}$Li is shown in Figure 2.16. A singlet resonance at 6.32 ppm corresponds to the Cp proton. The methyl group on the Cp ring can be distinguished from other methyl resonances as a singlet resonance at 2.85 ppm by 2D NMR spectroscopy correlation. Singlet resonances between 2.40 and 2.70 ppm are assigned to the other four methyl groups on the benzene ring. The methyl and methylene signals of the ethyl group are observed as a triplet resonance at 1.45 ppm and a quartet resonance at 3.27 ppm, respectively.

The ^{1}H NMR spectrum of $^{3\text{-Ph}}$Ind$^{\#}$Li was recorded (Figure 2.17). A doublet resonance at 7.78 ppm, a doublet of doublets resonance at 7.42 ppm and a triplet resonance at 7.06 ppm correspond to the *ortho*, *meta* and *para* protons of the phenyl group, respectively. The Cp proton is observed as a singlet resonance at 6.67 ppm. The methyl group on the Cp ring can be distinguished from other methyl resonances as a singlet resonance at 2.92 ppm by 2D NMR spectroscopy correlation. Four singlet resonances between 2.50 and 2.90 ppm correspond to the other four aromatic methyl groups.

2.3.5 Synthesis of ^{Me2}SB($^{3\text{-R}}$I*)H$_2$ (R = Et, Ph)



Scheme 2.9. Synthesis of ^{Me2}SB($^{3\text{-R}}$I*)H$_2$ (R = Et, Ph).

One equivalent of Me_2SiCl_2 diluted in THF was added dropwise to a THF solution of two equivalents of $^{3\text{-R}}$Ind$^{\#}$Li (R = Et, Ph) at 0 °C (Scheme 2.9). The reaction was allowed to warm up to room temperature and left stirring for 16 hours. For R = Et, the resulting pale yellow solution was dried *in vacuo* to remove all volatiles. Extraction using DCM was carried out and the resulting pale yellow filtrate was dried *in vacuo* to yield a 50:50 mixture of *rac*- and *meso*-^{Me2}SB($^{3\text{-Et}}$I*)H$_2$ as an off-white solid (53% yield).

For R = Ph, the resulting brown solution was dried *in vacuo* to remove all volatiles. DCM extraction was carried out and the resulting yellow filtrate was dried *in vacuo* to yield a yellow viscous oil containing *rac*-^{Me_2}SB($^{3\text{-}Ph}$I*)H$_2$, *meso*-^{Me_2}SB($^{3\text{-}Ph}$I*)H$_2$ and $^{3\text{-}Ph}$Ind$^{\#}$H. Similar to the ^{Et_2}SBI*H$_2$ synthesis, the formation of the $^{3\text{-}Ph}$Ind$^{\#}$H side-product can be attributed to the slower substitution reaction due to steric hindrance of the phenyl group. The desirable product was not separable from $^{3\text{-}Ph}$Ind$^{\#}$H.

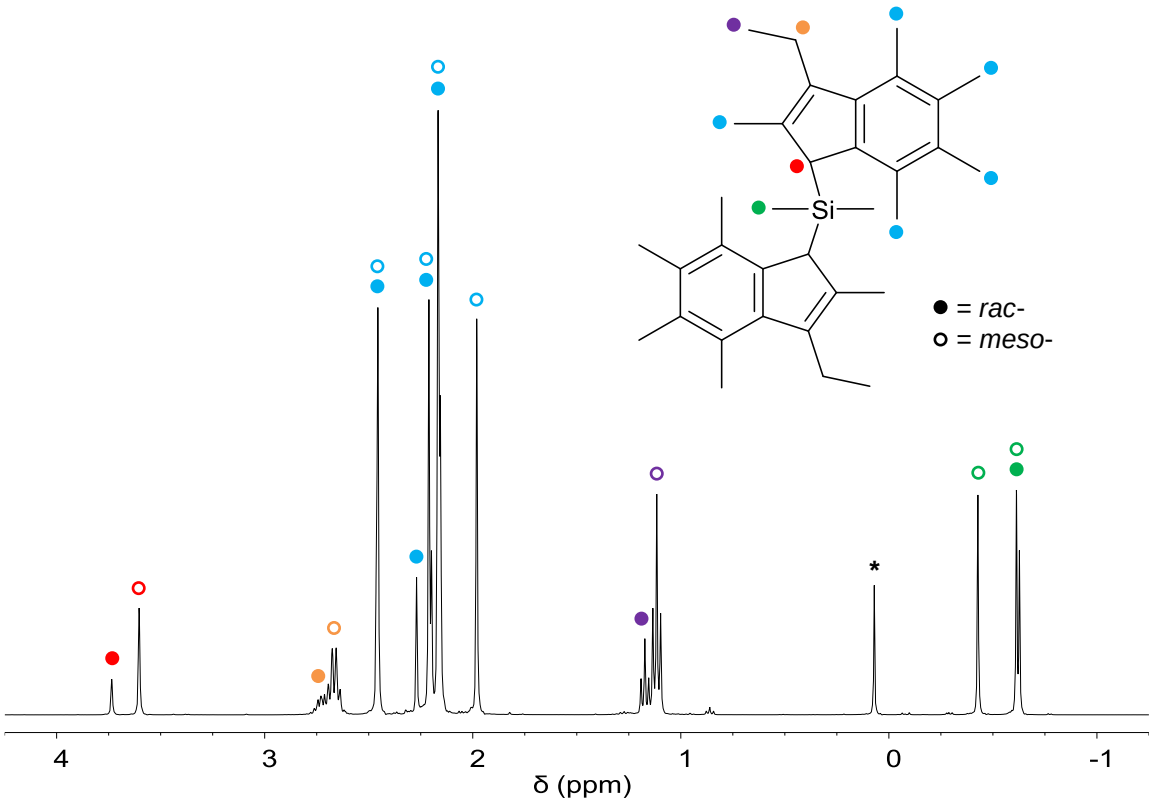


Figure 2.18. ^{1}H NMR spectrum (400 MHz, 298 K, chloroform-d_1) of a 25:75 mixture of *rac*- and *meso*-^{Me_2}SB($^{3\text{-}Et}$I*)H$_2$. *: silicone grease.

The ^{1}H NMR spectrum of a mixture of *rac*- and *meso*-^{Me_2}SB($^{3\text{-}Et}$I*)H$_2$ is shown in Figure 2.18. Two sets of resonances can be distinguished from each other by the difference in integration and 2D NMR spectroscopy correlations. For both isomers, the two indenyl rings are magnetically equivalent.

For *rac*-^{Me_2}SB($^{3\text{-}Et}$I*)H$_2$, a singlet resonance at 3.74 ppm corresponds to the protons on the indenyl rings and confirms the position of the C=C double bonds. Singlet resonances at 2.16 (two coincident resonances), 2.20, 2.27 and 2.46 ppm correspond to the five methyl groups on each indenyl ring. The methyl and methylene signals of the ethyl groups can be observed as a triplet resonance at 1.17 ppm and a quartet resonance at 2.74 ppm, respectively. The methyl

groups on the silyl bridge are observed as a singlet resonance at -0.63 ppm indicating that they are enantiotopic and, hence, the isomer is racemic.

On the other hand, for *meso*-^{Me2}SB($^{3\text{-}Et}$I*)H$_2$, the methyl groups on the silyl bridge are assigned to two singlet resonances at -0.61 and -0.43 ppm and, thus, are diastereotopic. The other resonances, however, match the same pattern as the racemic isomer. A singlet resonance at 3.60 ppm corresponds to the protons on the indenyl rings confirming the position of the C=C double bonds. Singlet resonances at 1.98, 2.17 (two coincident resonances), 2.21 and 2.46 ppm correspond to the five methyl groups on each indenyl ring. The methyl and methylene signals of the ethyl groups can be observed as a triplet resonance at 1.12 ppm and a quartet resonance at 2.67 ppm, respectively.

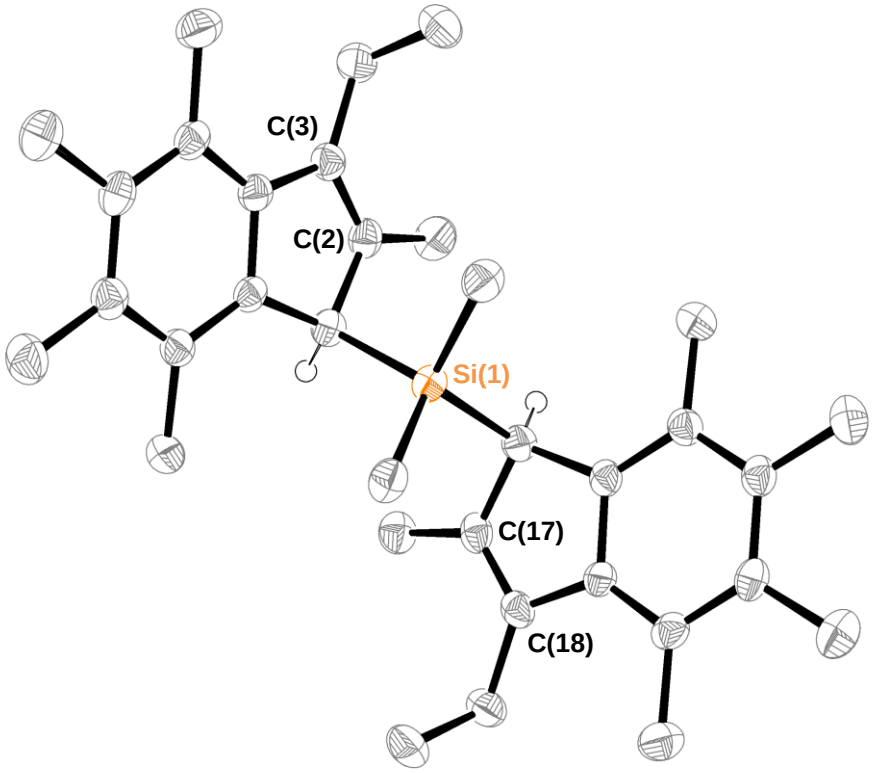


Figure 2.19. Molecular structure of *rac*-^{Me2}SB($^{3\text{-}Et}$I*)H$_2$. Hydrogen atoms omitted for clarity (except for stereocentres), ellipsoids drawn at 50% probability.

Colourless crystals of *rac*-^{Me2}SB($^{3\text{-}Et}$I*)H$_2$ suitable for single crystal X-ray diffraction were grown in Et$_2$O at -30 °C. The molecular structure is shown in Figure 2.19. Unlike *rac*-^{Et2}SBI*H$_2$, the pro-ligand crystallised in the monoclinic space group $P2_1$. However, with the Flack parameter value of 0.38(16) (near 0.5), the crystals are most likely racemic. The

crystal structure also confirms the position of the C(2)=C(3) and C(17)=C(18) double bonds with the average bond length of 1.351(6) Å, which is very similar to that of the *rac*-^{Et_2}SBI*H_2 (1.355(4) Å). The structure displays a similar average Si-C_{Ind*} bond length (1.934(4) Å) compared to the reported value for *rac*-^{Me_2}SBI*H_2 (1.939(6) Å).[9]

2.4 Conclusions

Chapter Two describes the modifications of ^{Me_2}SBI* ligand by introducing various alkyl groups on the silyl bridge and at the 3- position of the indenyl rings. ^{Et_2}SBI*H_2, $^{n\text{Pr,Me}}$SBI*H_2 and $^{\text{All,Me}}$SBI*H_2 pro-ligands were successfully synthesised and fully characterised. However, attempts to introduce larger alkyl groups, including isopropyl and phenyl groups, were unsuccessful due to high steric demand.

Ethyl and phenyl groups were successfully introduced at the 3- position of the indenyl rings of the ligand. The synthesis of ^{Me_2}SB($^{3\text{-Et}}$I*)H_2 pro-ligand was accomplished. The pro-ligand and its synthetic intermediates were fully characterised. However, ^{Me_2}SB($^{3\text{-Ph}}$I*)H_2 pro-ligand, despite being successfully synthesised, was unable to be isolated for further use.

2.5 References

1 T. K. Miyamoto, M. Tsutsui and L.-B. Chen, *Chem. Lett.*, 1981, **10**, 729–730.
2 D. O'Hare, J. C. Green, T. Marder, S. Collins, G. Stringer, A. K. Kakkar, N. Kaltsoyannis, A. Kuhn, R. Lewis, C. Mehnert, P. Scott, M. Kurmoo and S. Pugh, *Organometallics*, 1992, **11**, 48–55.
3 D. O'Hare, V. J. Murphy and N. Kaltsoyannis, *J. Chem. Soc. Dalt. Trans.*, 1993, 383–392.
4 D. O'Hare, V. J. Murphy, G. M. Diamond, P. L. Arnold and P. Mountford, *Organometallics*, 1994, **13**, 4689–4694.
5 V. J. Murphy and D. O'Hare, *Inorg. Chem.*, 1994, **33**, 1833–1841.
6 A. Ahlers and W. Kaminsky, *Die Makromol. Chemie, Rapid Commun.*, 1988, **9**, 457–461.
7 W. A. Herrmann, J. Rohrmann, E. Herdtweck, W. Spaleck and A. Winter, *Angew. Chemie, Int. Ed. English*, 1989, **28**, 1511–1512.
8 P. Ransom, A. E. Ashley, N. D. Brown, A. L. Thompson and D. O'Hare, *Organometallics*, 2011, **30**, 800–814.
9 J.-C. Buffet, T. A. Q. Arnold, Z. R. Turner, P. Angpanitcharoen and D. O'Hare, *RSC Adv.*, 2015, **5**, 87456–87464.
10 P. C. Möhring and N. J. Coville, *J. Mol. Catal.*, 1992, **77**, 41–50.
11 P. C. Möhring, N. Vlachakis, N. E. Grimmer and N. J. Coville, *J. Organomet. Chem.*, 1994, **483**, 159–166.
12 P. C. Möhring and N. J. Coville, *J. Organomet. Chem.*, 1994, **479**, 1–29.
13 P. C. Möhring and N. J. Coville, *J. Mol. Catal. A Chem.*, 1995, **96**, 181–195.
14 P. C. Möhring and N. J. Coville, *Coord. Chem. Rev.*, 2006, **250**, 18–35.
15 B. Wang, *Coord. Chem. Rev.*, 2006, **250**, 242–258.
16 C. Alonso-Moreno, A. Antiñolo, F. Carrillo-Hermosilla, A. Otero, A. M. Rodríguez, J. Sancho, V. Volkis and M. Eisen, *Eur. J. Inorg. Chem.*, 2006, 972–979.

17 C. Alonso-Moreno, A. Antiñolo, F. Carrillo-Hermosilla, P. Carrión, A. M. Rodríguez, A. Otero and J. Sancho, *J. Mol. Catal. A Chem.*, 2007, **261**, 53–63.
18 C. Alonso-Moreno, J. Sancho, F. Carrillo-Hermosilla, A. Otero, A. Antiñolo and I. López-Solera, *Inorg. Chem. Commun.*, 2009, **12**, 184–186.
19 H. G. Alt and A. Köppl, *Chem. Rev.*, 2000, **100**, 1205–1221.
20 F. M. Alías, S. Barlow, J. S. Tudor, D. O'Hare, R. T. Perry, J. M. Nelson and I. Manners, *J. Organomet. Chem.*, 1997, **528**, 47–58.
21 G. Tang, G.-X. Jin and L. Weng, *J. Organomet. Chem.*, 2004, **689**, 678–684.
22 C. J. Miller and D. O'Hare, *Chem. Commun.*, 2004, **44**, 1710–1711.
23 M. Napoli, R. De Vita, I. Immediata, P. Longo and G. Guerra, *Polym. Adv. Technol.*, 2011, **22**, 458–462.
24 P. Angpanitcharoen, G. Hay, J.-C. Buffet, Z. R. Turner, T. A. Q. Arnold and D. O'Hare, *Polyhedron*, 2016, **116**, 216–222.
25 T. A. Q. Arnold, J.-C. Buffet, Z. R. Turner and D. O'Hare, *J. Organomet. Chem.*, 2015, **792**, 55–65.
26 T. A. Q. Arnold, *D.Phil. Thesis*, University of Oxford, 2015.

Chapter Three – Complex synthesis

3.1 Introduction

Group 4 indenyl complexes have been widely used in ethylene polymerisation.[1,2] Several reviews reported that the *rac* isomer of indenyl complexes is generally more active in ethylene polymerisation compared to the *meso* isomer.[3] As a result, in-depth research on the racemo-selective synthesis of indenyl complexes has been conducted. Diamond and co-workers took advantage of the reversibility of amine elimination reaction to selectively synthesise *rac*-EBIZr$(NMe_2)_2$ and *rac*-^{Me2}SBIZr$(NMe_2)_2$.[4–7] Jordan and co-workers used bidentate amine ligands to perform chelate-controlled synthesis of racemic *ansa*-zirconocenes.[8–13] A similar approach using biphenolate ligands has also been successfully carried out.[14] Transmetalation reactions using diastereotopic disilylated and distannylated bisindenyl ligands have been used to selectively synthesise *rac* or *meso* isomer of *ansa*-zirconocenes.[15,16] $ZrCl_3NHtBu$ reagent was used to achieve racemo-selectivity in the synthesis of *ansa*-zirconocenes.[17,18]

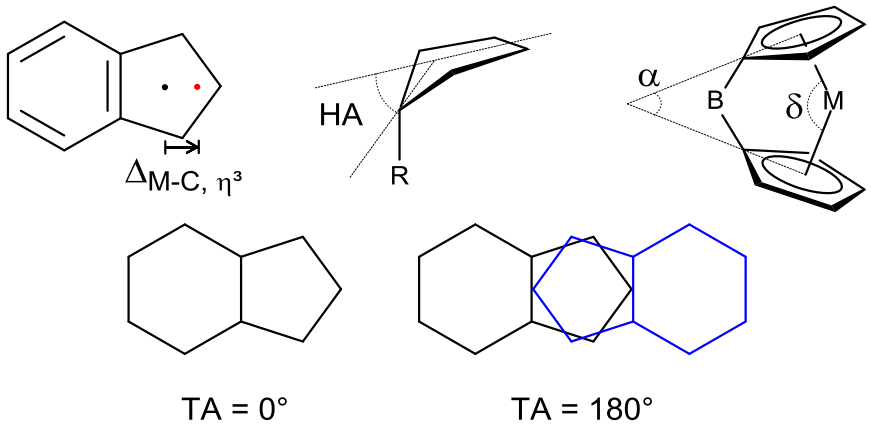


Figure 3.1. Visual representations of structural parameters.

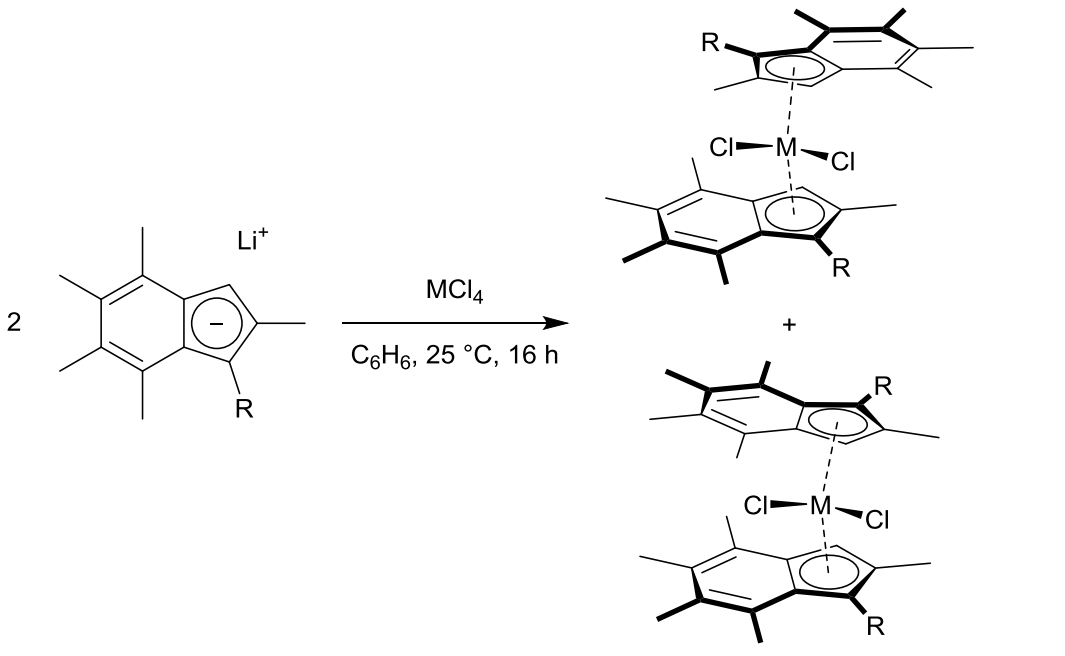
To help with general comparisons between the molecular structures of indenyl complexes, a number of structural parameters have been introduced (Figure 3.1). The slip parameter (Δ_{M-C}) is traditionally defined as the difference in the average bond lengths of the metal to bridgehead carbons and the metal to the adjacent carbons of the five-membered ring.[19] Although the Δ_{M-C} parameter is useful for relative comparisons, its value does not match the actual slip distance. The true slip parameter ($\Delta_{M-C,\ max}$) is defined as the distance between the centroid of the five-membered ring and the projection of the metal on the ring plane. The

$\Delta_{M\text{-}C,\ max}$ parameter does not specify the direction of the slip and, hence, $\Delta_{M\text{-}C,\ \eta^3}$ parameter is defined as the projected distance of the $\Delta_{M\text{-}C,\ max}$ vector in the η^3-coordination direction. The hinge angle (HA) represents the bending at the carbon of the five-membered ring adjacent to the ring junction. A larger HA parameter is associated with a distortion away from η^5 geometry. The ring tilt angle (α) is defined as the angle between the planes of the five-membered ring.[20] The δ angle is the angle between the vectors from the metal to the ring centroids.[21] The torsion angle (TA) is defined as the dihedral angle between the [C(2), Cp_{cent}, Cp'_{cent}] and [C(2)′, Cp_{cent}, Cp'_{cent}] planes; where Cp_{cent} and Cp'_{cent} are, respectively, the centroids of the five-membered rings of the two indenyl ligands.[22]

The aims of this research are to improve the selectivity towards *rac* isomer in the synthesis of substituted indenyl group 4 complexes. Several methods have been tested including using various metal halide starting materials, Jordan's reagent and ligand tuning by introducing the bulkier diethylsilyl bridge.

3.2 Unbridged substituted indenyl complexes

3.2.1 Synthesis of $(^{3\text{-}R}Ind^{\#})_2MCl_2$ (R = Et, Ph; M = Zr, Hf)



R = Et, M = Zr; orange yellow solid, 31% yield
R = Et, M = Hf; yellow solid, 47% yield
R = Ph, M = Zr; orange yellow solid, 45% yield

Scheme 3.1. Synthesis of $(^{3\text{-}R}Ind^{\#})_2MCl_2$ (R = Et, Ph; M = Zr, Hf).

For R = Et, two equivalents of $^{3\text{-Et}}$Ind$^{\#}$Li and one equivalent of MCl_4 (M = Zr, Hf) were mixed in benzene and left stirring for 16 hours at room temperature (Scheme 3.1). The reaction mixture was allowed to settle before being filtered. The orange filtrate (M = Zr) or yellow filtrate (M = Hf) was dried *in vacuo* to afford a 50:50 mixture of *rac*- and *meso*-($^{3\text{-Et}}$Ind$^{\#}$)$_2$MCl_2 as an orange yellow solid (M = Zr; 31% yield) or a yellow solid (M = Hf; 47% yield). Recrystallisation of the isomeric mixture of both complexes in toluene at -30 °C yielded *rac*-($^{3\text{-Et}}$Ind$^{\#}$)$_2$MCl_2 as yellow crystals. Fractional crystallisation from the toluene filtrate at -30 °C yielded *meso*-($^{3\text{-Et}}$Ind$^{\#}$)$_2$ZrCl_2 as orange yellow crystals. Attempts to isolate *meso*-($^{3\text{-Et}}$Ind$^{\#}$)$_2$HfCl_2 were unsuccessful.

For R = Ph, two equivalents of $^{3\text{-Ph}}$Ind$^{\#}$Li and one equivalent of $ZrCl_4$ were mixed in benzene and left stirring for 16 hours at room temperature (Scheme 3.1). The reaction mixture was allowed to settle before being filtered. The orange filtrate was dried *in vacuo* to afford a 50:50 mixture of *rac*- and *meso*-($^{3\text{-Ph}}$Ind$^{\#}$)$_2$ZrCl_2 as an orange yellow solid (45% yield).

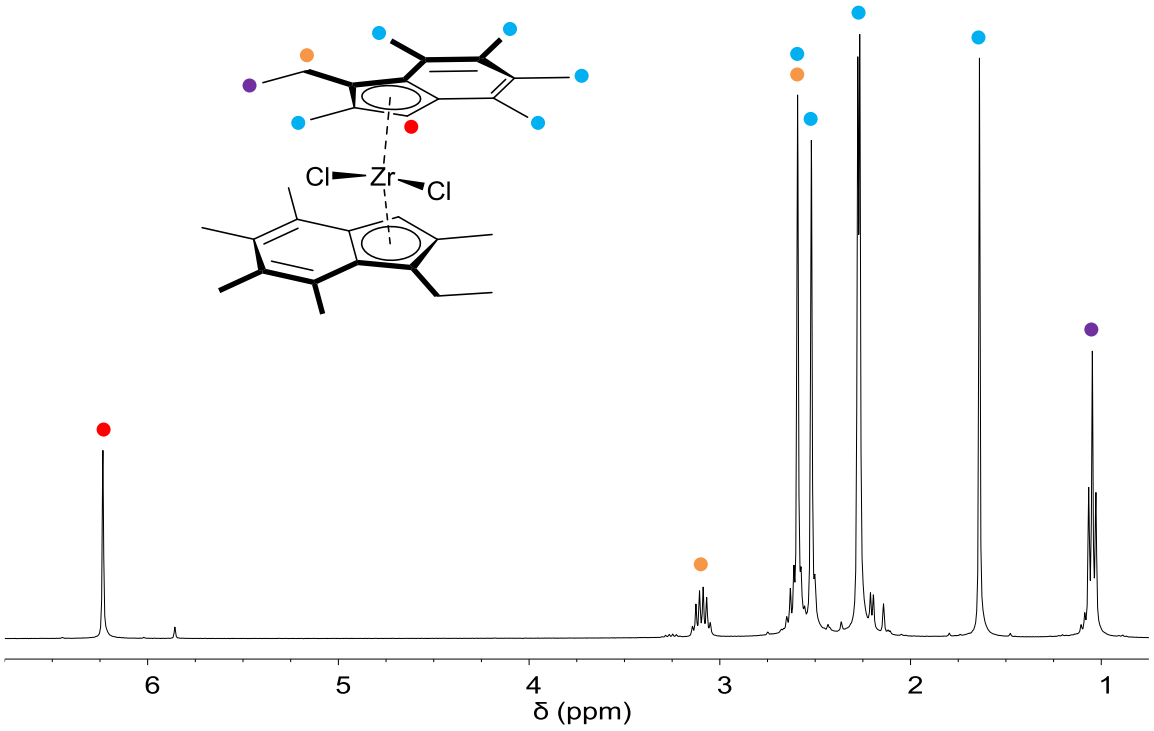


Figure 3.2. ^{1}H NMR spectrum (400 MHz, 298 K, chloroform-d_1) of *rac*-($^{3\text{-Et}}$Ind$^{\#}$)$_2$ZrCl_2.

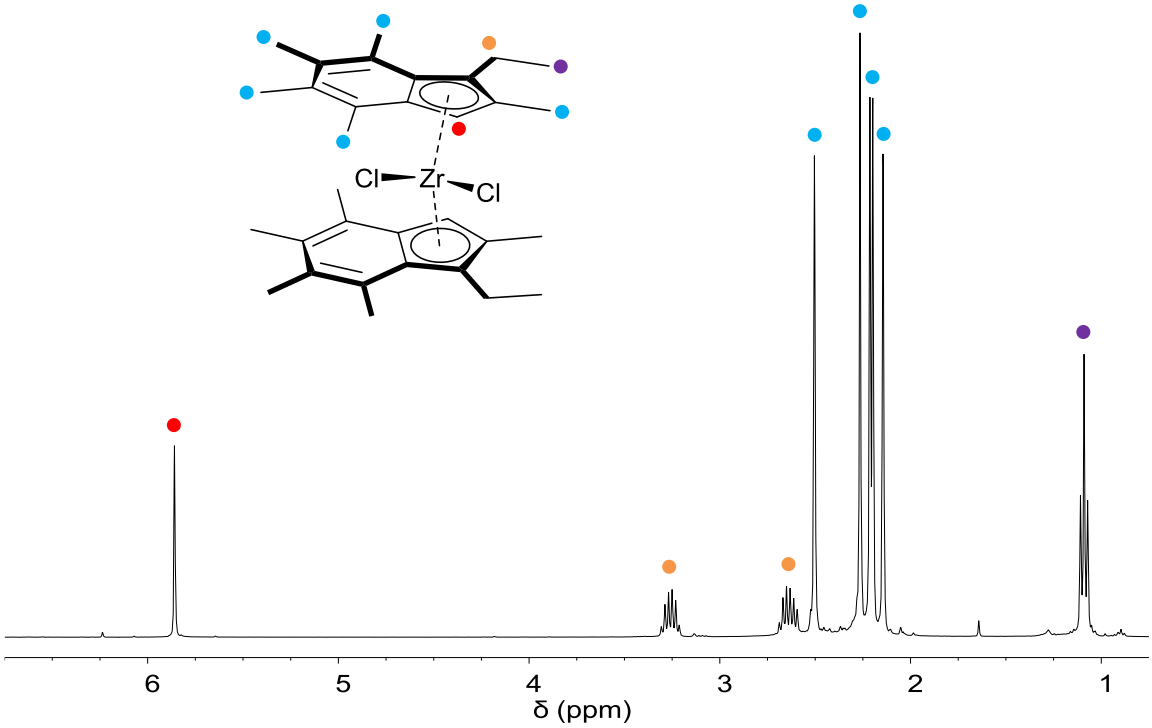


Figure 3.3. ^{1}H NMR spectrum (400 MHz, 298 K, chloroform-d_1) of *meso*-($^{3\text{-Et}}$Ind$^{\#}$)$_2$ZrCl$_2$.

The ^{1}H NMR spectrum of *rac*-($^{3\text{-Et}}$Ind$^{\#}$)$_2$ZrCl$_2$ is shown in Figure 3.2. The two indenyl rings are magnetically equivalent, hence, displaying as one set of resonances. A singlet resonance at 6.23 ppm corresponds to the Cp protons. Two doublet of quartets resonances at 2.60 and 3.10 ppm are assigned to the diastereotopic methylene protons of the ethyl groups. The methyl groups on the indenyl rings are observed as five singlet resonances between 1.60 and 2.60 ppm. A triplet resonance at 1.05 ppm is assigned to the methyl protons of the ethyl groups.

The ^{1}H NMR spectrum of *meso*-($^{3\text{-Et}}$Ind$^{\#}$)$_2$ZrCl$_2$ (Figure 3.3) shows the same pattern as that of the *rac* isomer. The Cp protons are seen at 5.86 ppm as a singlet resonance. Two doublet of quartets resonances at 2.64 and 3.26 ppm correspond to the diastereotopic methylene protons of the ethyl groups. Five singlet resonances between 2.10 and 2.50 ppm are assigned to the methyl groups on the indenyl rings. The methyl signal of the ethyl groups is observed as a triplet resonance at 1.09 ppm.

Interestingly, for *rac*-($^{3\text{-Et}}$Ind$^{\#}$)$_2$ZrCl$_2$, the singlet resonance corresponded to the methyl groups on the Cp rings has a relatively low chemical shift (1.64 ppm) compared to those of the other methyl groups, possibly due to the ring current effect of the opposite indenyl ring. The same effect is not observed for the *meso* isomer.

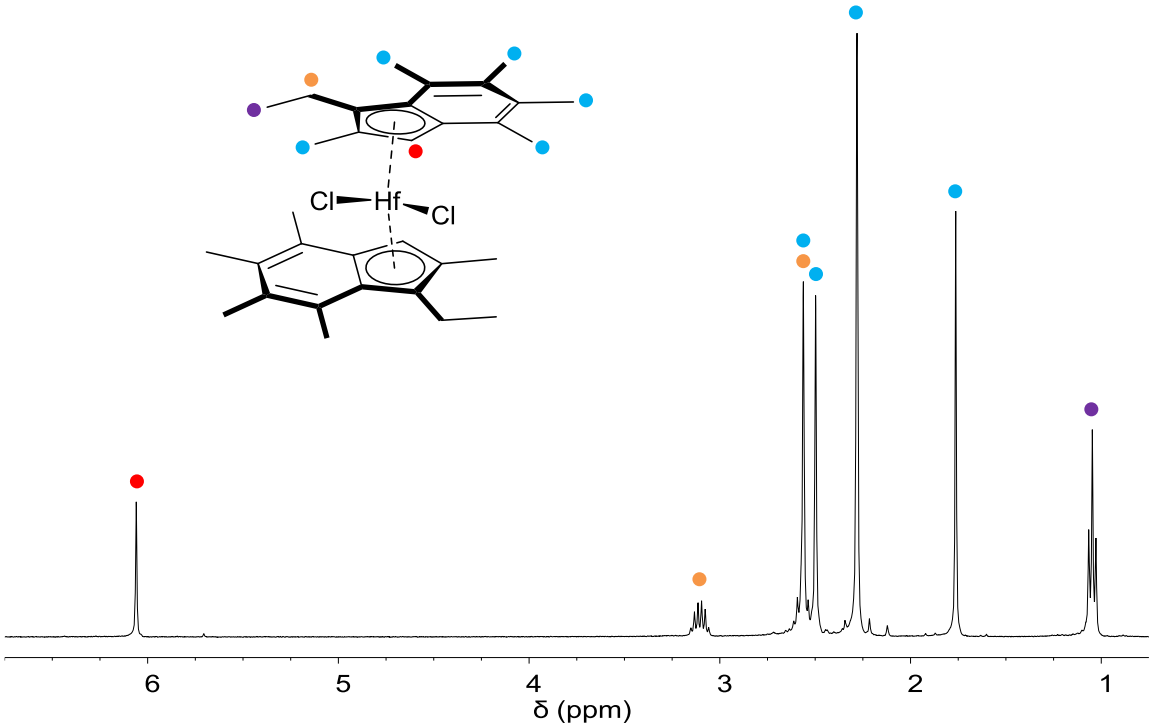


Figure 3.4. ^{1}H NMR spectrum (400 MHz, 298 K, chloroform-d_1) of *rac*-($^{3\text{-Et}}$Ind$^{\#}$)$_2$HfCl$_2$.

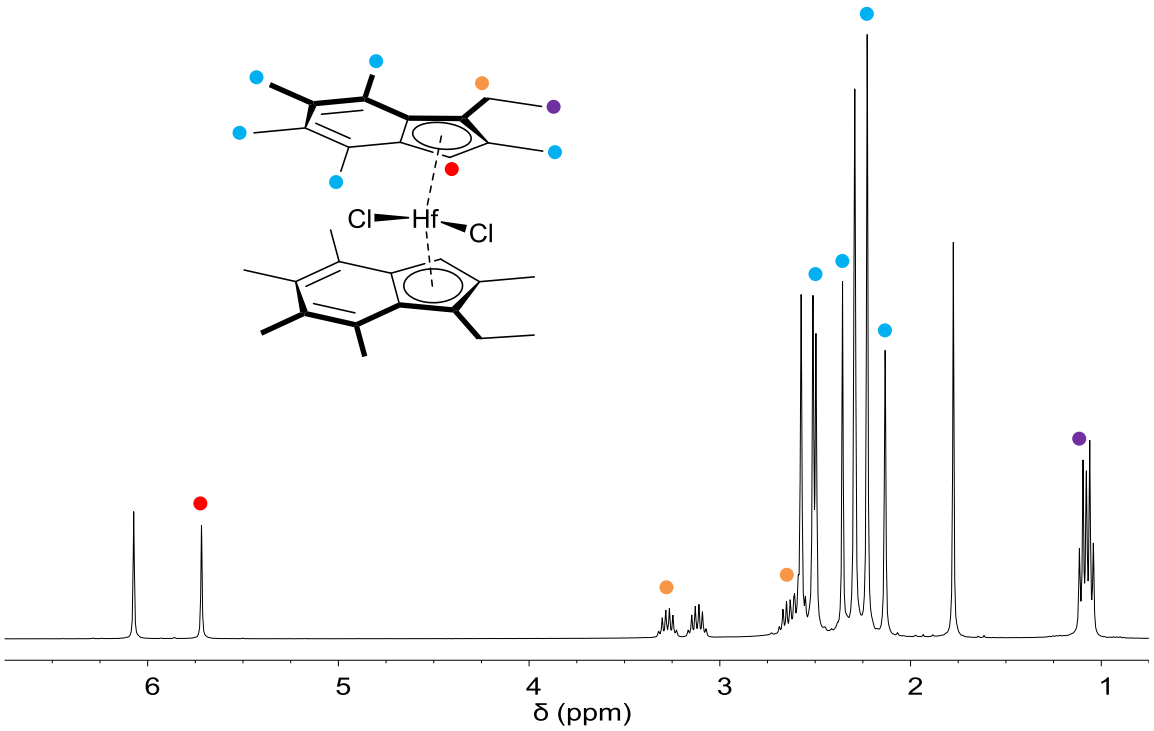


Figure 3.5. ^{1}H NMR spectrum (400 MHz, 298 K, chloroform-d_1) of a mixture of *rac*- and *meso*-($^{3\text{-Et}}$Ind$^{\#}$)$_2$HfCl$_2$.

The ^{1}H NMR spectrum of *rac*-($^{3\text{-Et}}$Ind$^{\#}$)$_2$HfCl$_2$ (Figure 3.4) is nearly identical to that of the analogous zirconocene. A singlet resonance at 6.06 ppm is assigned to the Cp protons. Two doublet of quartets resonances at 2.56 and 3.11 ppm correspond to the diastereotopic methylene protons of the ethyl groups. The methyl groups on the indenyl rings are observed as five singlet resonances between 1.70 and 2.60 ppm, two of which are coincident at 2.28 ppm. The methyl signal of the ethyl groups is seen at 1.05 ppm as a triplet resonance.

The ^{1}H NMR spectrum of a mixture of *rac*- and *meso*-($^{3\text{-Et}}$Ind$^{\#}$)$_2$HfCl$_2$ is shown in Figure 3.5. By accounting for the signals of the *rac* isomer from the spectrum, resonances corresponding to the *meso* isomer can be assigned. The Cp protons are observed as a singlet resonance at 5.70 ppm. Two doublet of quartets resonances at 2.63 and 3.26 ppm are assigned to the diastereotopic methylene protons of the ethyl groups. Five singlet resonances at 2.12, 2.21 (two coincident resonances), 2.34 and 2.48 ppm correspond to the methyl groups on the indenyl rings. A triplet resonance at 1.08 ppm is assigned to the methyl protons of the ethyl groups.

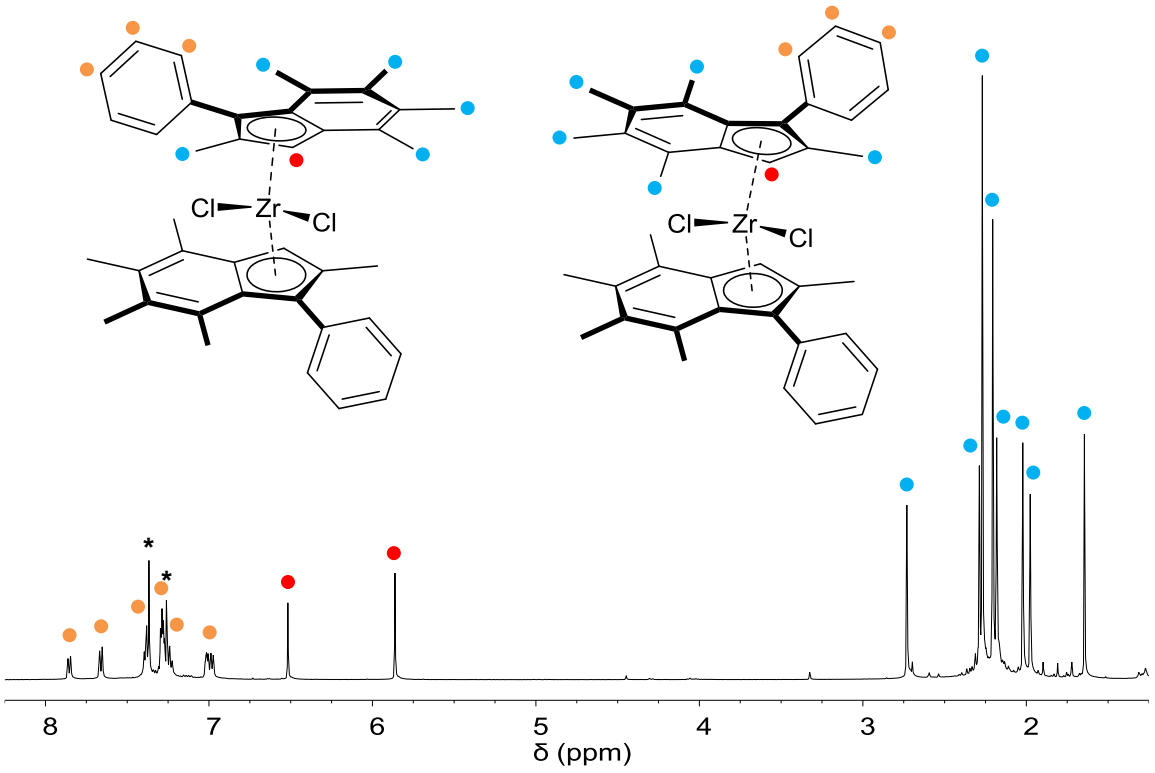


Figure 3.6. ^{1}H NMR spectrum (500 MHz, 298 K, chloroform-d_1) of a mixture of *rac*- and *meso*-($^{3\text{-Ph}}$Ind$^{\#}$)$_2$ZrCl$_2$. *: benzene, chloroform.

The ^{1}H NMR spectrum of a mixture of *rac*- and *meso*-($^{3\text{-Ph}}$Ind$^{\#}$)$_2$ZrCl$_2$ is shown in Figure 3.6. Since neither *rac* nor *meso* isomer was isolated, the two sets of resonances corresponding

to each isomer are indistinguishable. Resonances observed between 6.90 and 7.90 ppm are assigned to the phenyl protons of either isomers. Two singlet resonances at 5.86 and 6.52 ppm correspond to the Cp protons of each isomer. The methyl groups on the indenyl rings of both isomers are seen between 1.60 and 2.80 ppm as singlet resonances.

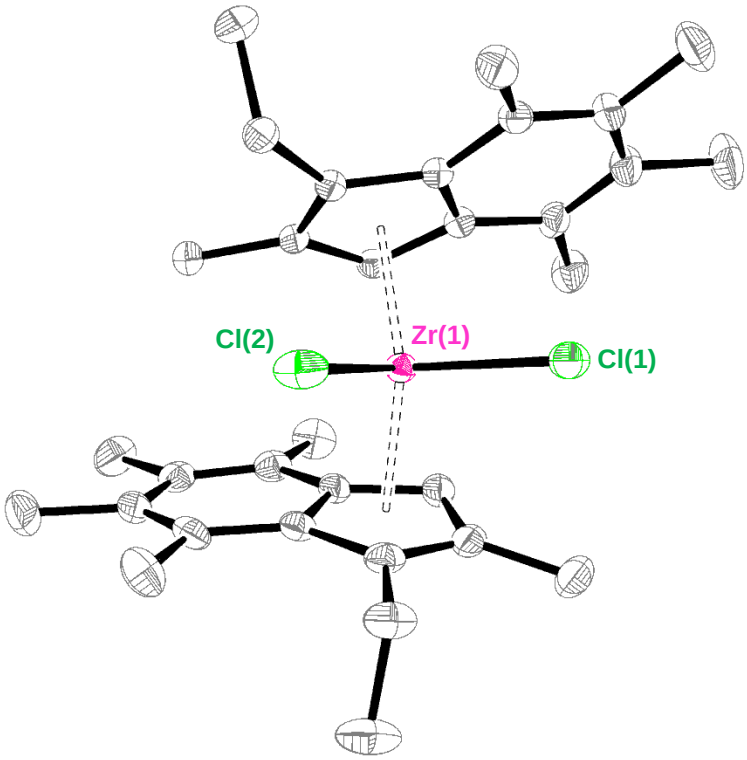


Figure 3.7. Molecular structure of *rac*-($^{3\text{-Et}}$Ind$^{\#}$)$_2$ZrCl$_2$. Hydrogen atoms omitted for clarity, ellipsoids drawn at 50% probability.

Table 3.1. Selected bond lengths and angles for *rac*-($^{3\text{-Et}}$Ind$^{\#}$)$_2$MCl$_2$ (M = Zr, Hf).

Parameter	**Bond lengths (Å) / Angles (°)**	
	M = Zr	M = Hf
M-Cl	2.4183(6), 2.4514(6)	2.3907(9), 2.4227(9)
M-Cp$_{cent}$	2.2453(8), 2.2374(8)	2.2273(15), 2.2236(14)
$\Delta_{M\text{-}C,\ max}$	0.071, 0.189	0.078, 0.198
$\Delta_{M\text{-}C,\ \eta^3}$	-0.018, 0.074	-0.012, 0.083
HA	8.06, 3.42	8.62, 3.24
α	51.72(10)	51.80(19)
δ	132.44(3)	132.56(5)
TA	173.14	173.01

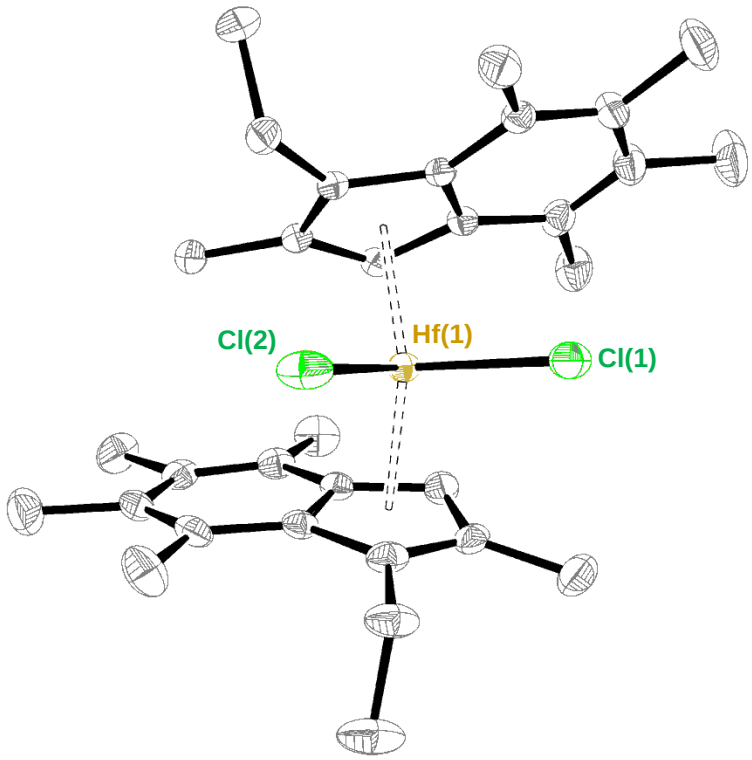


Figure 3.8. Molecular structure of *rac*-($^{3\text{-Et}}$Ind$^{\#}$)$_2$HfCl$_2$. Hydrogen atoms omitted for clarity, ellipsoids drawn at 50% probability.

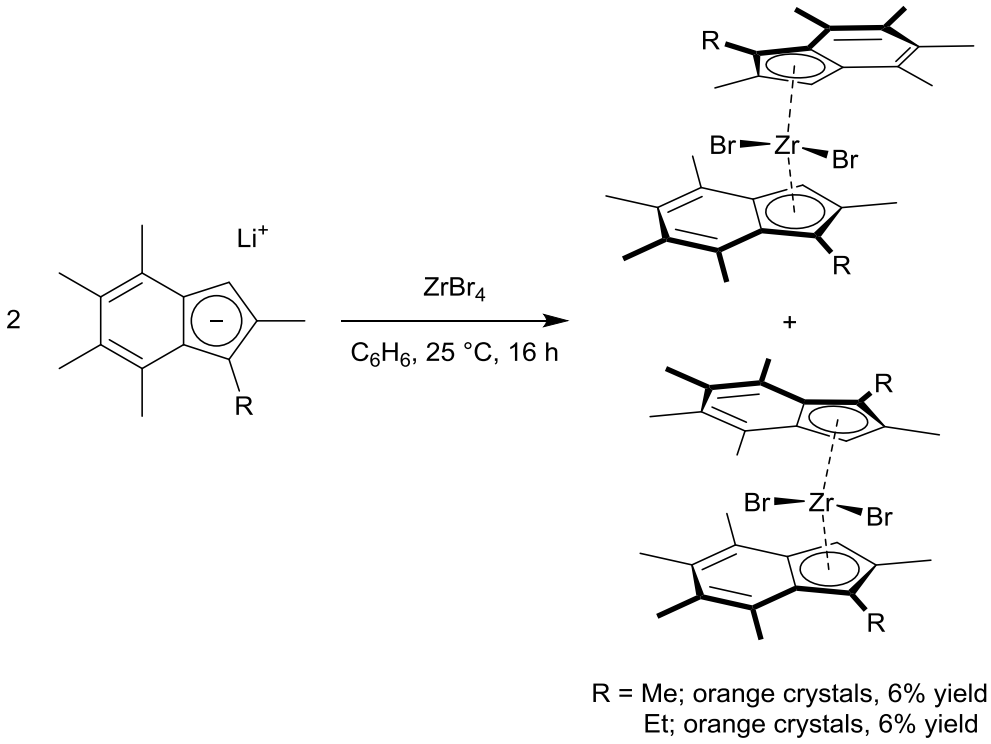
Yellow crystals of *rac*-($^{3\text{-Et}}$Ind$^{\#}$)$_2$ZrCl$_2$ suitable for single crystal X-ray diffraction were grown from a toluene solution of the isomeric mixture at -30 °C. Similarly, yellow crystals of *rac*-($^{3\text{-Et}}$Ind$^{\#}$)$_2$HfCl$_2$ were grown in Et$_2$O at -30 °C. The molecular structures are shown in Figure 3.7 and Figure 3.8, respectively. Both complexes crystallised in the monoclinic space group $P2_1/c$ as a racemic mixture. The selected bond lengths and angles for *rac*-($^{3\text{-Et}}$Ind$^{\#}$)$_2$ZrCl$_2$ and *rac*-($^{3\text{-Et}}$Ind$^{\#}$)$_2$HfCl$_2$ are listed in Table 3.1.

The average Zr-Cl and Hf-Cl bond lengths, 2.435 and 2.407 Å, respectively, are in close agreement with those for the 3-methyl analogues reported in the literature, *rac*-(Ind$^{\#}$)$_2$ZrCl$_2$ (2.421 Å) and *rac*-(Ind$^{\#}$)$_2$HfCl$_2$ (2.409 Å).[23] The same can be said of the average Zr-Cp$_{cent}$ and Hf-Cp$_{cent}$ distances, 2.241 Å compared to 2.228 Å and 2.225 Å compared to 2.217 Å, respectively, albeit very slightly larger due to the presence of the bulkier ethyl groups. The α value of 51.72° for *rac*-($^{3\text{-Et}}$Ind$^{\#}$)$_2$ZrCl$_2$ is comparable to those for *rac*-($^{3\text{-Et}}$Ind$^{\#}$)$_2$HfCl$_2$ (51.80°), *rac*-(Ind$^{\#}$)$_2$ZrCl$_2$ (51.6°) and *rac*-(Ind$^{\#}$)$_2$HfCl$_2$ (51.58°). The δ values for these complexes, 132.44, 132.56, 133.59 and 133.85°, respectively, are very similar. The TA values for these complexes are also relatively similar, 173.14, 173.01, 171.31 and 170.43°, respectively. These mentioned bond lengths and angles imply that the introduction of 3-ethyl

groups has little to no impact on the molecular frameworks of the unbridged substituted indenyl complexes.

Structure comparisons of *rac*-($^{3\text{-Et}}$Ind$^{\#}$)$_2$ZrCl$_2$ with its unmethylated analogue, *rac*-($^{1\text{-Et}}$Ind)$_2$ZrCl$_2$, show similar average Zr-Cl bond lengths (2.435 Å compared to 2.441 Å) and Zr-Cp$_{cent}$ distances (2.241 Å compared to 2.233 Å).[24] The α value for *rac*-($^{3\text{-Et}}$Ind$^{\#}$)$_2$ZrCl$_2$ (51.72°) is slightly larger than that for *rac*-($^{1\text{-Et}}$Ind)$_2$ZrCl$_2$ (50.0°). The δ values for these two zirconocenes are almost equal (132.44° compared to 132.34°). On the other hand, the TA value of 173.14° for *rac*-($^{3\text{-Et}}$Ind$^{\#}$)$_2$ZrCl$_2$ is significantly larger than that for *rac*-($^{1\text{-Et}}$Ind)$_2$ZrCl$_2$ (120.85°) as a result of the methylation of the indenyl ligands.

3.2.2 Synthesis of ($^{3\text{-R}}$Ind$^{\#}$)$_2$ZrBr$_2$ (R = Me, Et)



Scheme 3.2. Synthesis of ($^{3\text{-R}}$Ind$^{\#}$)$_2$ZrBr$_2$ (R = Me, Et).

Two equivalents of $^{3\text{-R}}$Ind$^{\#}$Li (R = Me, Et) and one equivalent of ZrBr$_4$ were mixed in benzene and left stirring for 16 hours at room temperature (Scheme 3.2). The reaction mixture was allowed to settle before being filtered. For R = Me, the red filtrate was dried *in vacuo* to afford an orange solid comprising of a 20:80 mixture of *rac*- and *meso*-(Ind$^{\#}$)$_2$ZrBr$_2$, and impurities. Recrystallisation of the isomeric mixture in toluene at -30 °C yielded *meso*-(Ind$^{\#}$)$_2$ZrBr$_2$ as orange crystals (6% yield). For R = Et, the orange filtrate was dried *in*

vacuo to afford an orange solid comprising of a 40:60 mixture of *rac*- and *meso*-($^{3\text{-Et}}$Ind$^{\#}$)$_2$ZrBr$_2$, and impurities. Recrystallisation of the isomeric mixture in DCM at -30 °C yielded *meso*-($^{3\text{-Et}}$Ind$^{\#}$)$_2$ZrBr$_2$ as orange crystals (6% yield).

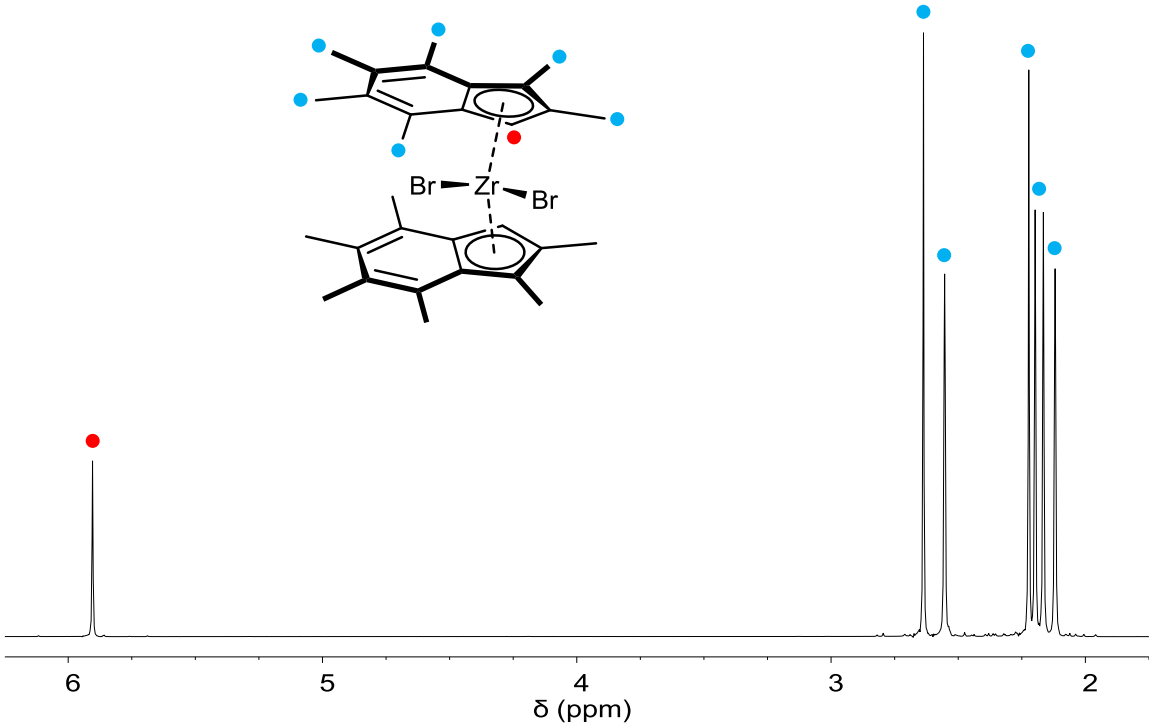


Figure 3.9. ^{1}H NMR spectrum (400 MHz, 298 K, chloroform-d_1) of *meso*-(Ind$^{\#}$)$_2$ZrBr$_2$.

The ^{1}H NMR spectrum of *meso*-(Ind$^{\#}$)$_2$ZrBr$_2$ is shown in Figure 3.9. The two indenyl rings are magnetically equivalent, hence, displaying as one set of resonances. The Cp protons are observed as a singlet resonance at 5.90 ppm. Six singlet resonances between 2.10 and 2.70 ppm are assigned to the methyl groups on the indenyl rings.

The ^{1}H NMR spectrum of *meso*-($^{3\text{-Et}}$Ind$^{\#}$)$_2$ZrBr$_2$ was recorded (Figure 3.10). A singlet resonance at 6.25 ppm corresponds to the Cp protons. Two doublet of quartets resonances at 2.69 and 3.22 ppm correspond to the diastereotopic methylene protons of the ethyl groups. The methyl groups on the indenyl rings are seen between 1.70 and 2.60 ppm as five singlet resonances, two of which are coincident at 2.54 ppm. A triplet resonance at 1.05 ppm is assigned to the methyl protons of the ethyl groups.

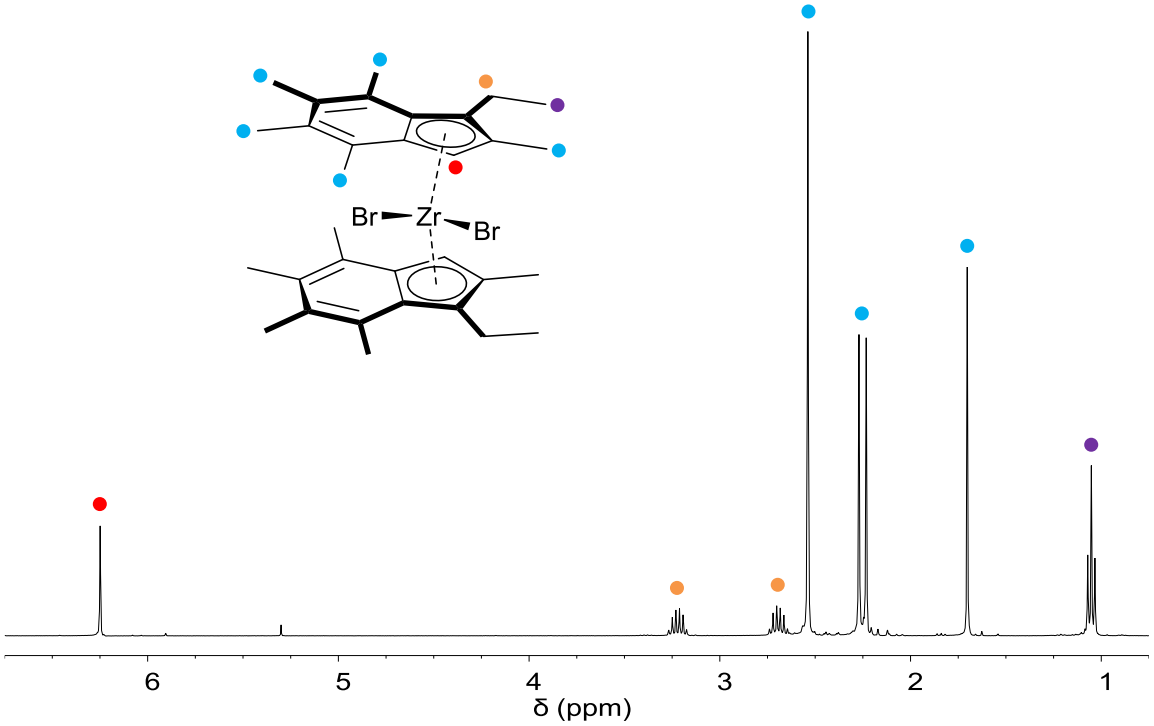


Figure 3.10. ^{1}H NMR spectrum (400 MHz, 298 K, chloroform-d_1) of *meso*-($^{3\text{-Et}}$Ind$^{\#}$)$_2$ZrBr$_2$.

Table 3.2. Selected bond lengths and angles for *meso*-($^{3\text{-R}}$Ind$^{\#}$)$_2$ZrBr$_2$ (R = Me, Et).

Parameter	**Bond lengths (Å) / Angles (°)**	
	R = Me	R = Et
Zr-Br	2.6133(4), 2.5745(4)	2.6041(5), 2.5927(5)
Zr-Cp$_{cent}$	2.2500(10), 2.2525(10)	2.2425(11), 2.2430(11)
$\Delta_{M\text{-}C,\ max}$	0.148, 0.197	0.039, 0.187
$\Delta_{M\text{-}C,\ \eta^3}$	0.039, 0.086	-0.042, 0.050
HA	3.65, 3.45	9.51, 4.57
α	54.35(13)	52.44(14)
δ	133.62(4)	131.93(4)
TA	35.46	81.49

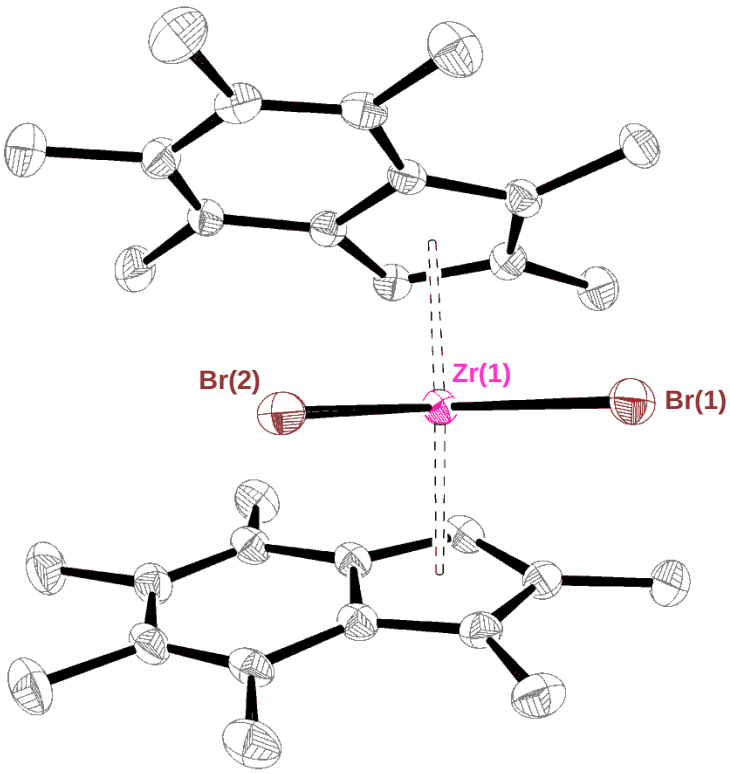


Figure 3.11. Molecular structure of *meso*-(Ind$^{\#}$)$_2$ZrBr$_2$. Hydrogen atoms omitted for clarity, ellipsoids drawn at 50% probability.

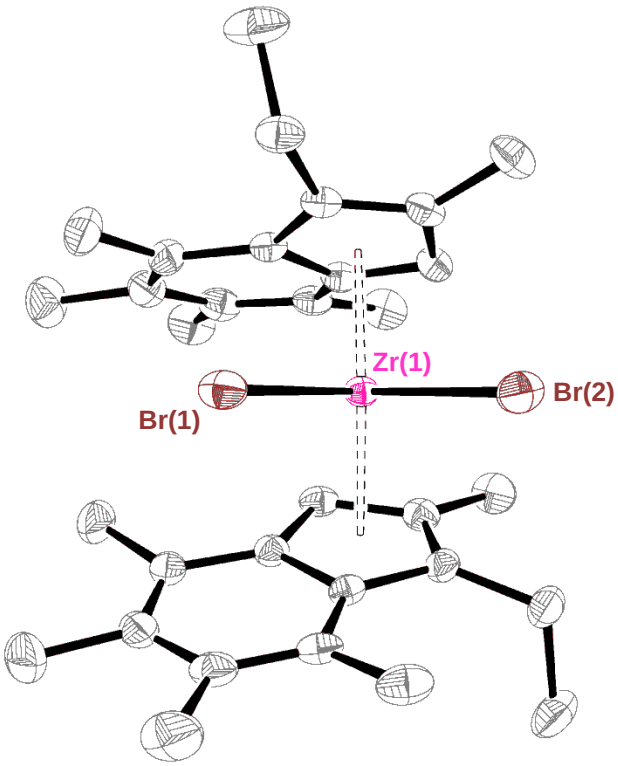
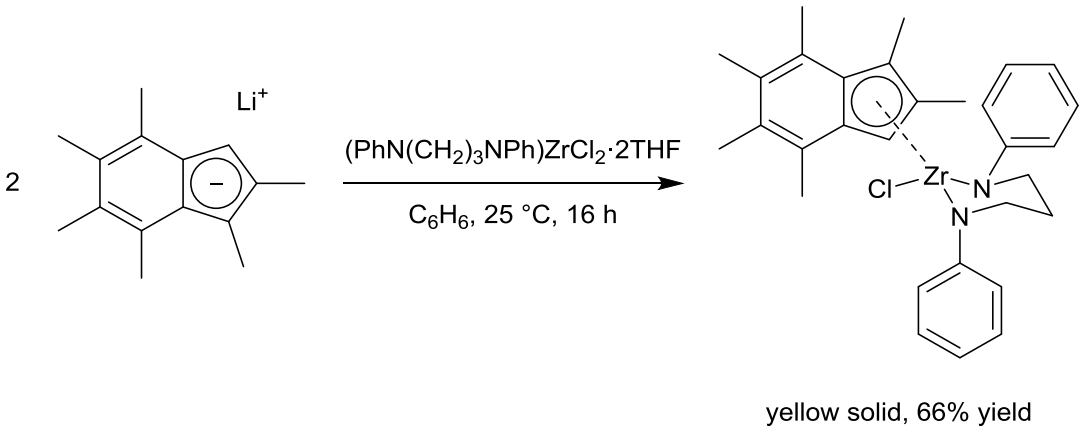


Figure 3.12. Molecular structure of *meso*-($^{3\text{-Et}}$Ind$^{\#}$)$_2$ZrBr$_2$. Hydrogen atoms omitted for clarity, ellipsoids drawn at 50% probability.

Orange crystals of *meso*-(Ind$^{\#}$)$_2$ZrBr$_2$ suitable for single crystal X-ray diffraction were grown from a toluene solution of the isomeric mixture at -30 °C. On the other hand, orange crystals of *meso*-($^{3\text{-Et}}$Ind$^{\#}$)$_2$ZrBr$_2$ were grown in pentane at room temperature. The molecular structures are shown in Figure 3.11 and Figure 3.12, respectively. *meso*-(Ind$^{\#}$)$_2$ZrBr$_2$ crystallised in the monoclinic space group $P2_1/c$ while *meso*-($^{3\text{-Et}}$Ind$^{\#}$)$_2$ZrBr$_2$ crystallised in the orthorhombic space group *Pbca*. The selected bond lengths and angles for *meso*-(Ind$^{\#}$)$_2$ZrBr$_2$ and *meso*-($^{3\text{-Et}}$Ind$^{\#}$)$_2$ZrBr$_2$ are listed in Table 3.2.

The average Zr-Br bond lengths of 2.594 and 2.598 Å, respectively, and Zr-Cp$_{cent}$ distances of 2.251 and 2.243 Å, respectively, are within the range of those for other unbridged dibromobisindenyl zirconocenes reported in the literature.[25–28] The α value of 54.35 and 52.44° for *meso*-(Ind$^{\#}$)$_2$ZrBr$_2$ and *meso*-($^{3\text{-Et}}$Ind$^{\#}$)$_2$ZrBr$_2$, respectively, are larger than those for *rac*-(Ind$^{\#}$)$_2$ZrCl$_2$ (51.6°) and *rac*-($^{3\text{-Et}}$Ind$^{\#}$)$_2$ZrCl$_2$ (51.72°) due to the larger Br ligands. To the contrary, the δ values for these complexes, 133.62, 131.93, 133.59 and 132.44°, respectively, are relatively similar. The TA value of 35.46° for *meso*-(Ind$^{\#}$)$_2$ZrBr$_2$ indicates the preference to orient the two unsubstituted Cp positions in the same direction to avoid steric clash with the methyl groups. The introduction of ethyl groups causes more steric strain with the large Br ligands resulting in *meso*-($^{3\text{-Et}}$Ind$^{\#}$)$_2$ZrBr$_2$ adopting 'gauche' conformation reflected in the TA value of 81.49°.

3.2.3 Synthesis of (Ind$^{\#}$)(PhN(CH$_2$)$_3$NPh)ZrCl



Scheme 3.3. Synthesis of (Ind$^{\#}$)(PhN(CH$_2$)$_3$NPh)ZrCl.

Two equivalents of Ind$^{\#}$Li and one equivalent of (PhN(CH$_2$)$_3$NPh)ZrCl$_2$·2THF were mixed in benzene and left stirring for 16 hours at room temperature (Scheme 3.3). The reaction mixture was dried *in vacuo* to yield a yellow solid which was then extracted with

benzene. The yellow filtrate was dried *in vacuo* to afford (Ind$^{\#}$)(PhN(CH$_2$)$_3$NPh)ZrCl as a yellow solid (66% yield).

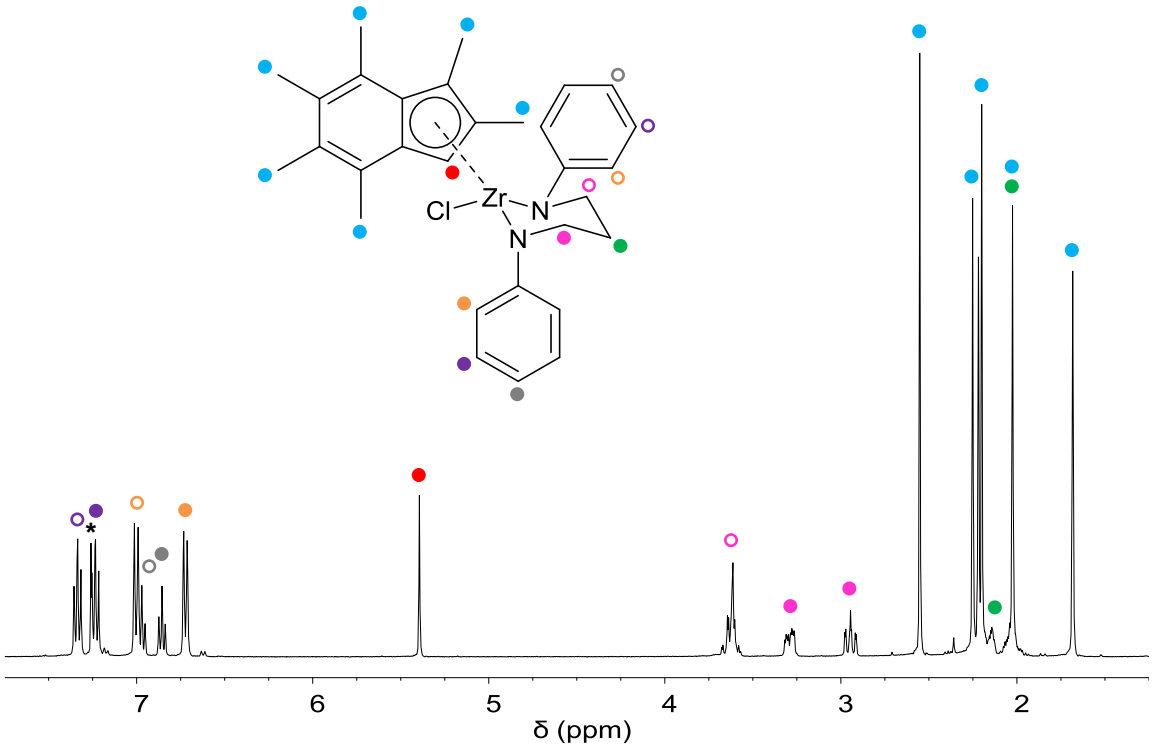


Figure 3.13. ^{1}H NMR spectrum (400 MHz, 298 K, chloroform-d_1) of (Ind$^{\#}$)(PhN(CH$_2$)$_3$NPh)ZrCl. *: chloroform.

The ^{1}H NMR spectrum of (Ind$^{\#}$)(PhN(CH$_2$)$_3$NPh)ZrCl is shown in Figure 3.13. Due to the lack of symmetry of the complex, both ends of the chelating diamine ligand are magnetically inequivalent. 2D NMR spectroscopic techniques, including COSY, HSQC and HMBC, are used to assist with resonance assignments. The *ortho*, *meta* and *para* protons of the first phenyl group are observed at 6.72 (doublet), 7.23 (doublet of doublets) and 6.86 ppm (triplet), respectively. Resonances at 7.00 (doublet), 7.33 (doublet of doublets) and 6.97 ppm (triplet) are assigned to the *ortho*, *meta* and *para* protons of the second phenyl group, respectively. All protons on the alkyl chain of the diamine ligand are diastereotopic. Two multiplet resonances at 2.95 and 3.29 ppm correspond to the -CH$_2$ group adjacent to the first phenyl group. The -CH$_2$ group adjacent to the second phenyl group is seen at 3.62 ppm as a multiplet resonance. Two multiplet resonances at 2.04 and 2.14 ppm are assigned to the -CH$_2$ group at the middle of the alkyl chain. The Cp proton is observed as a singlet resonance at 5.39 ppm. Six singlet resonances between 1.60 and 2.60 ppm correspond to the methyl groups on the indenyl ring.

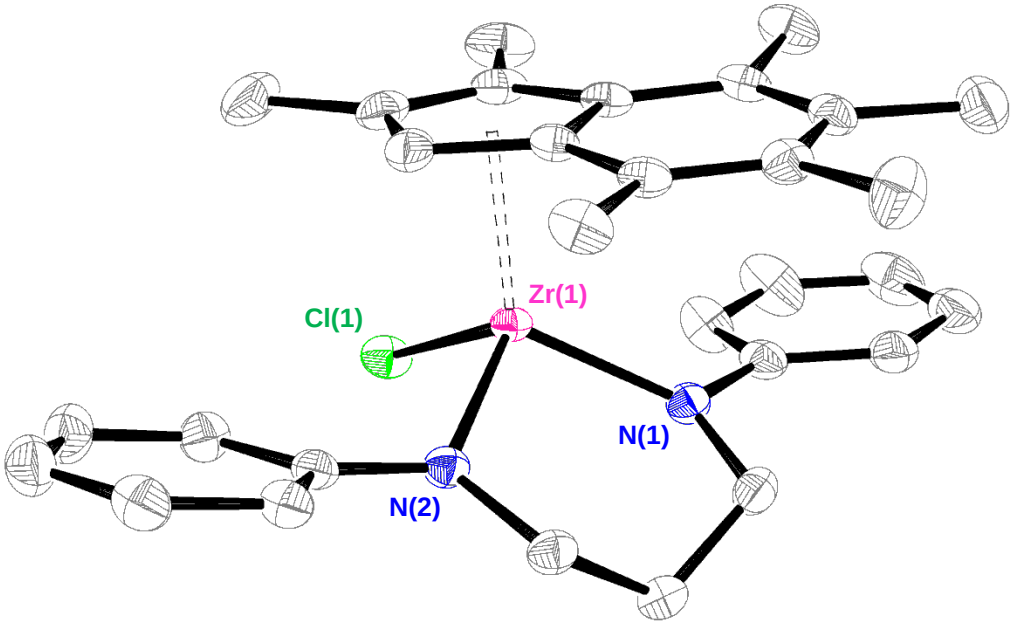


Figure 3.14. Molecular structure of (Ind$^{\#}$)(PhN(CH$_2$)$_3$NPh)ZrCl. Hydrogen atoms omitted for clarity, ellipsoids drawn at 50% probability.

Table 3.3. Selected bond lengths and angles for (Ind$^{\#}$)(PhN(CH$_2$)$_3$NPh)ZrCl.

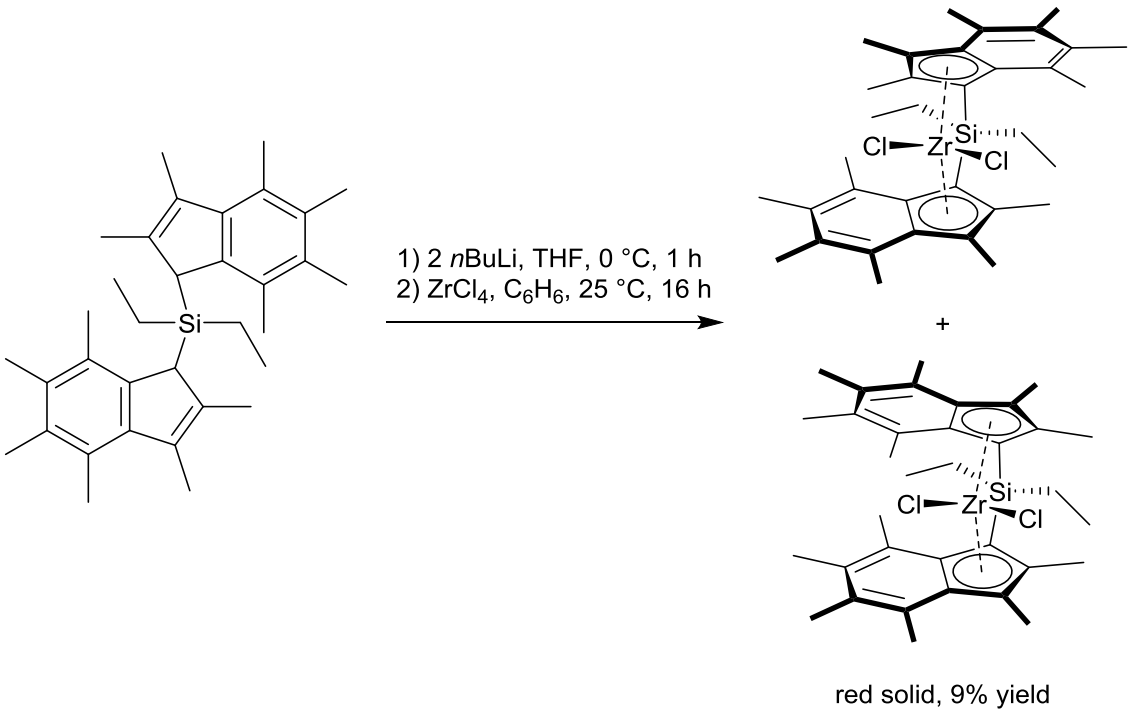
Parameter	Bond lengths (Å) / Angles (°)
Zr-N	2.0740(13), 2.0739(11)
Zr-Cl	2.4340(4)
Zr-Cp$_{cent}$	2.2141(8)
$\Delta_{M\text{-}C,\ max}$	0.099
$\Delta_{M\text{-}C,\ \eta^3}$	-0.117
HA	2.05
α	n/a
δ	n/a
TA	n/a

Yellow crystals of (Ind$^{\#}$)(PhN(CH$_2$)$_3$NPh)ZrCl suitable for single crystal X-ray diffraction were grown by slow evaporation of a benzene-d_6 solution of the complex. The molecular structure is shown in Figure 3.14. The complex crystallised in the monoclinic space group

*C*2/*c* as a racemic mixture. The selected bond lengths and angles for $(Ind^{\#})(PhN(CH_2)_3NPh)ZrCl$ are listed in Table 3.3.

3.3 Silyl bridged substituted indenyl complexes

3.3.1 Synthesis of ^{Et2}SBI*ZrCl$_2$



Scheme 3.4. Synthesis of ^{Et2}SBI*ZrCl$_2$.

One equivalent of *rac*-^{Et2}SBI*H$_2$ was reacted with two equivalents of *n*BuLi in THF at 0 °C (Scheme 3.4). The reaction was kept at 0 °C and stirred for 1 hour. The resulting dark brown solution was dried *in vacuo* at 0 °C to form a yellow solid, which was then washed with pentane. One equivalent of $ZrCl_4$ was mixed with *rac*-^{Et2}SBI*Li$_2$ (yellow solid) and benzene was then added to the mixture. The reaction slowly turned red and was left stirring for 16 hours at room temperature. The reaction mixture was allowed to settle before being filtered. The red filtrate was dried *in vacuo* to afford a red solid which was then washed with Et_2O to yield a 50:50 mixture of *rac*- and *meso*-^{Et2}SBI*ZrCl$_2$ as a red solid (9% yield). *rac*-^{Et2}SBI*ZrCl$_2$ was isolated as orange crystals from the Et_2O filtrate at -30 °C.

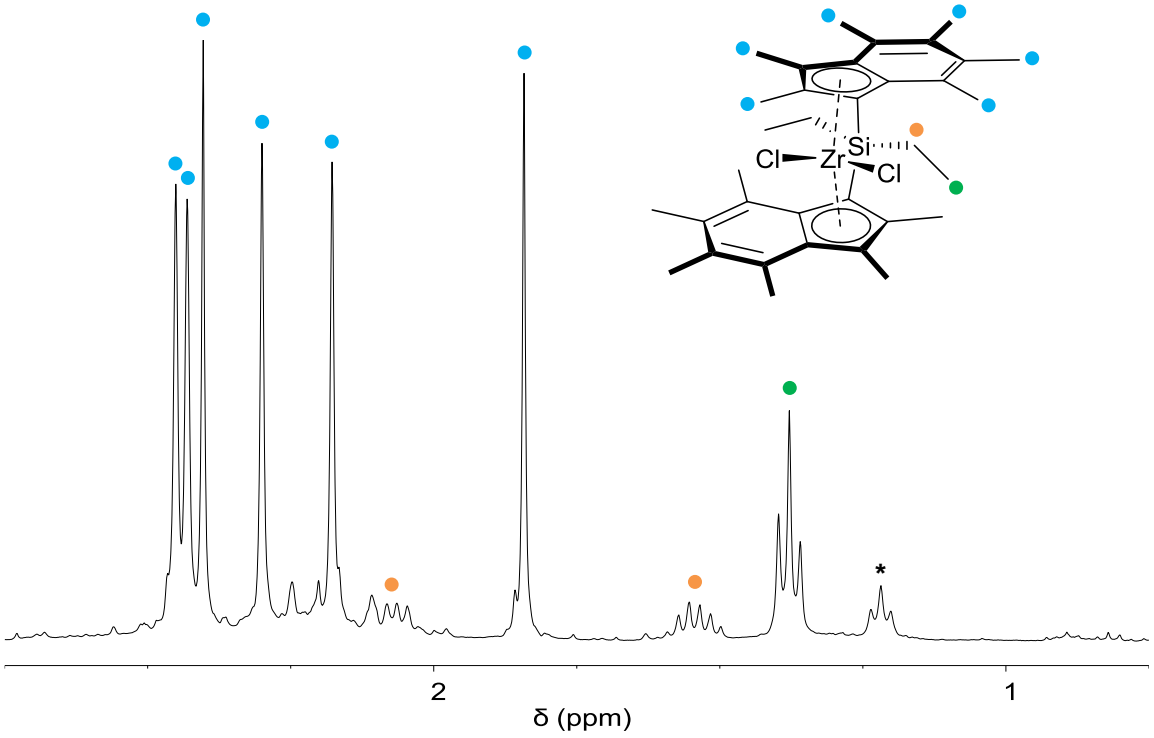


Figure 3.15. ^{1}H NMR spectrum (400 MHz, 298 K, chloroform-d_1) of *rac*-^{Et2}SBI*$ZrCl_2$. *: Et_2O.

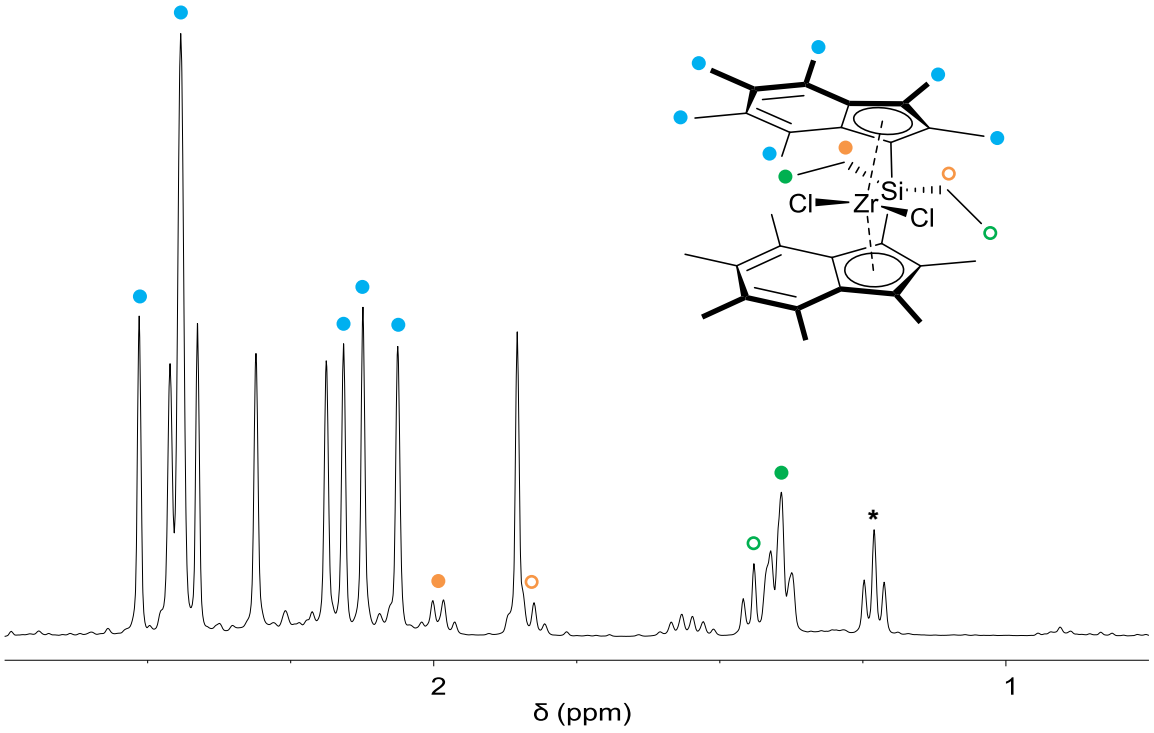


Figure 3.16. ^{1}H NMR spectrum (400 MHz, 298 K, chloroform-d_1) of a mixture of *rac*- and *meso*-^{Et2}SBI*$ZrCl_2$. *: Et_2O.

The ^{1}H NMR spectrum of *rac*-^{Et2}SBI*$ZrCl_2$ is shown in Figure 3.15. As the two indenyl rings are magnetically equivalent, the methyl groups on the indenyl rings are observed as six singlet resonances between 1.80 and 2.50 ppm. Due to the C_2 symmetry of the complex, the two ethyl groups are also magnetically equivalent. Two multiplet resonances at 1.54 and 2.07 ppm correspond to the diastereotopic methylene protons of the ethyl groups. The methyl signal of the ethyl groups is seen at 1.38 ppm as a triplet resonance.

The ^{1}H NMR spectrum of a mixture of *rac*- and *meso*-^{Et2}SBI*$ZrCl_2$ is shown in Figure 3.16. By accounting for the signals of the *rac* isomer from the spectrum, resonances corresponding to the *meso* isomer can be assigned. Six singlet resonances at 2.06, 2.12, 2.16, 2.44 (two coincident resonances) and 2.51 ppm are assigned to the methyl groups on the indenyl rings. Unlike the *rac* isomer, the two ethyl groups are diastereotopic, thus, displaying as two sets of resonances. A triplet resonance at 1.39 ppm and a quartet resonance at 1.99 ppm correspond respectively to the methyl and methylene protons of the first ethyl group. The methyl and methylene signals of the second ethyl group are seen at 1.44 (triplet) and 1.83 ppm (quartet), respectively. Interestingly, the methylene protons of the ethyl groups are no longer diastereotopic due to the C_s symmetry of the complex.

Table 3.4. Selected bond lengths and angles for *rac*-^{Et2}SBI*$ZrCl_2$.

Parameter	**Bond lengths (Å) / Angles (°)**
Zr-Cl	2.4267(5), 2.4261(5)
Zr-Cp_{cent}	2.2422(8), 2.2357(9)
$\Delta_{M\text{-}C,\ max}$	0.186, 0.211
$\Delta_{M\text{-}C,\ \eta^3}$	0.146, 0.141
HA	5.14, 3.24
α	58.36(10)
δ	129.79(3)
TA	144.08

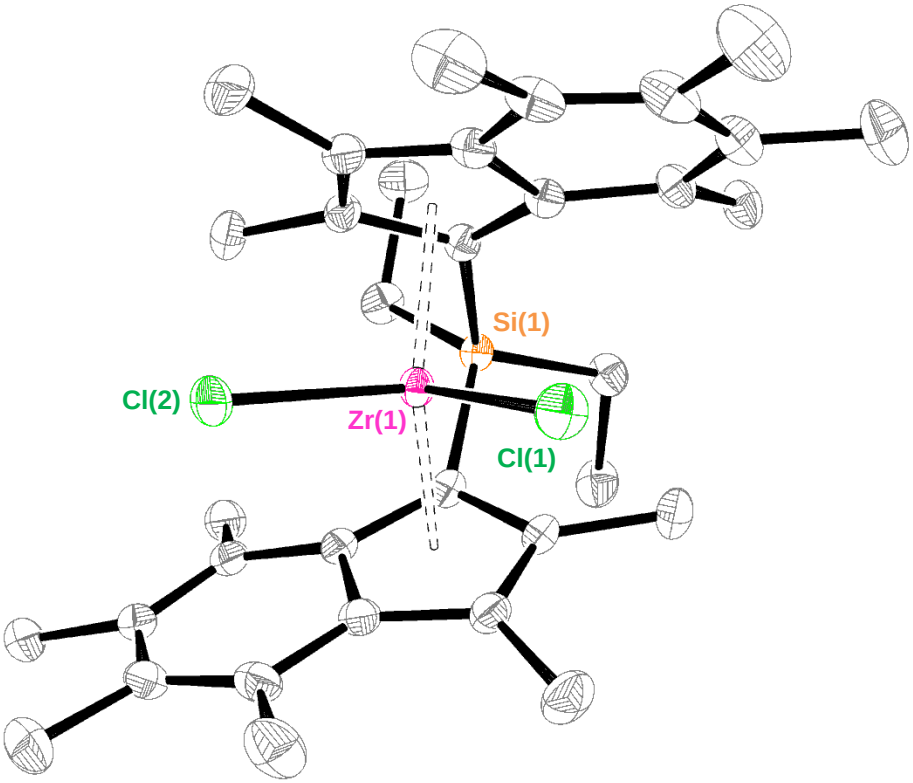
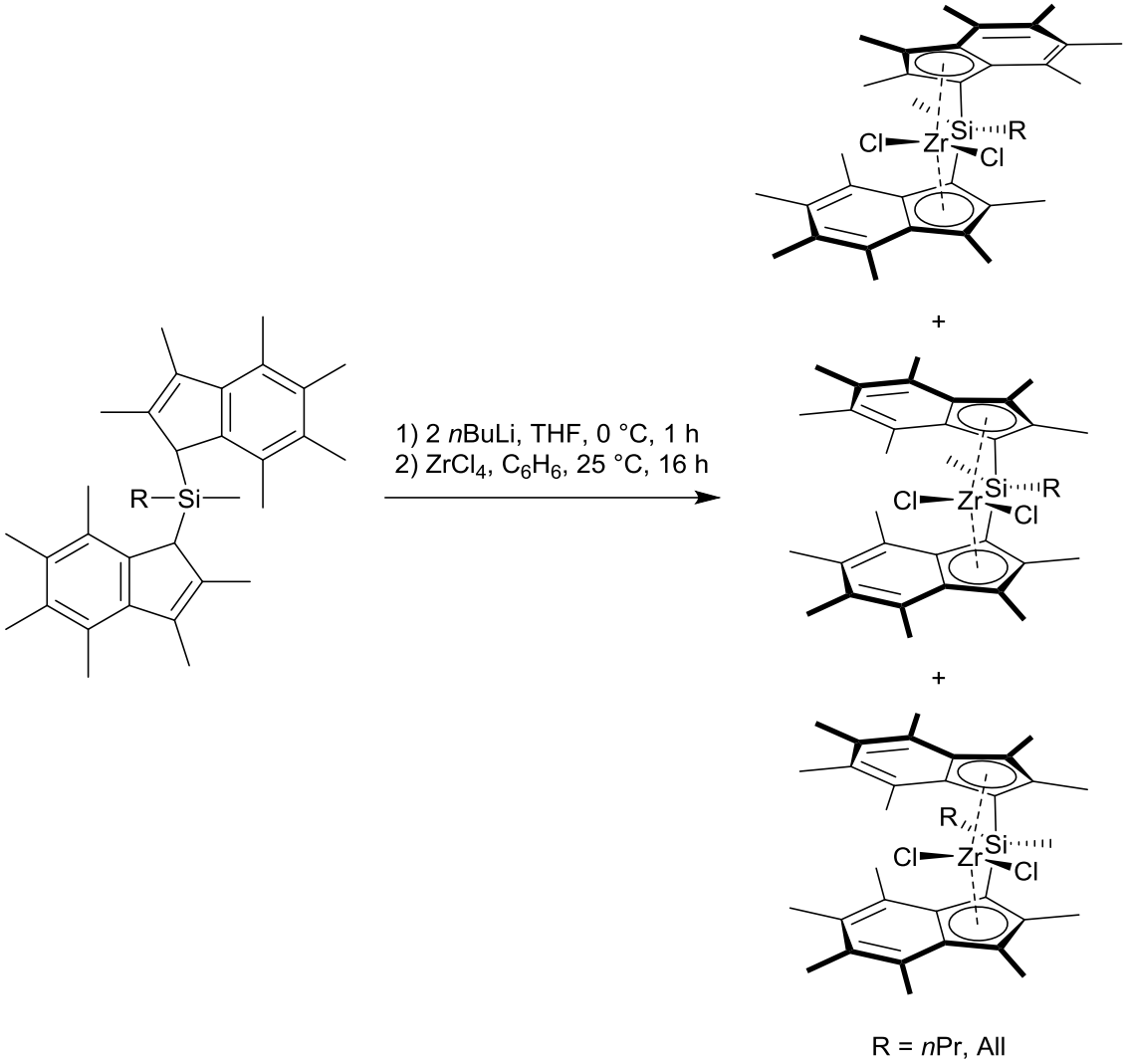


Figure 3.17. Molecular structure of *rac*-^{Et2}SBI*$ZrCl_2$. Hydrogen atoms omitted for clarity, ellipsoids drawn at 50% probability.

Orange crystals of *rac*-^{Et2}SBI*$ZrCl_2$ suitable for single crystal X-ray diffraction were grown by slow evaporation of a benzene-d_6 solution of the isomer. The molecular structure is shown in Figure 3.17. The complex crystallised in the triclinic space group $P\bar{1}$ as a racemic mixture. The selected bond lengths and angles for *rac*-^{Et2}SBI*$ZrCl_2$ are listed in Table 3.4.

Structure comparisons between *rac*-^{Et2}SBI*$ZrCl_2$ and, its permethylated analogue, *rac*-^{Me2}SBI*$ZrCl_2$, show that substituting methyl groups for ethyl groups on the silyl bridge has minimal impact on the molecular framework. The average Zr-Cl bond length and Zr-Cp_{cent} distance of 2.426 and 2.239 Å, respectively, for *rac*-^{Et2}SBI*$ZrCl_2$ are very comparable to those of *rac*-^{Me2}SBI*$ZrCl_2$ (2.423 and 2.251 Å, respectively).[29] Similarly, the α, δ and TA values of 58.36, 129.79 and 144.08°, respectively, are nearly identical compared to 58.49, 130.37 and 145.52°, respectively.

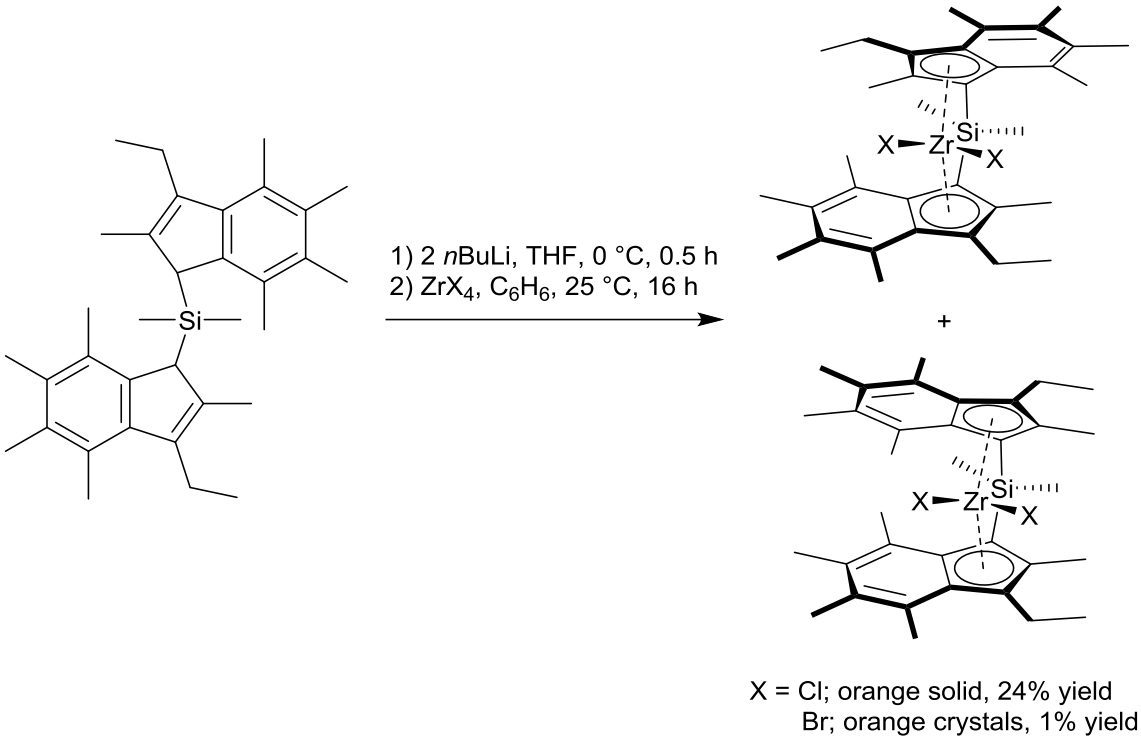
3.3.2 Attempted synthesis of ^{R,Me}SBI*ZrCl$_2$ (R = *n*Pr, All)



Scheme 3.5. Attempted synthesis of ^{R,Me}SBI*ZrCl$_2$ (R = *n*Pr, All).

The synthesis of ^{R,Me}SBI*ZrCl$_2$ (R = *n*Pr, All) has been attempted following the synthesis procedure for ^{Et2}SBI*ZrCl$_2$ (Scheme 3.5). One equivalent of *rac*-^{R,Me}SBI*H$_2$ was reacted with two equivalents of *n*BuLi in THF at 0 °C. The reaction was kept at 0 °C and stirred for 1 hour. The resulting dark brown solution was dried *in vacuo* at 0 °C to form a yellow solid, which was then washed with pentane. One equivalent of $ZrCl_4$ was mixed with *rac*-^{R,Me}SBI*Li$_2$ (yellow solid) and benzene was then added to the mixture. The reaction slowly turned red and was left stirring for 16 hours at room temperature. The reaction mixture was allowed to settle before being filtered. The red filtrate was dried *in vacuo* to afford a red solid which was analysed by ^{1}H NMR spectroscopy to contain multiple species. Attempts to isolate a product were unsuccessful.

3.3.3 Synthesis of ^{Me2}SB($^{3\text{-}Et}$I*)ZrX$_2$ (X = Cl, Br)



Scheme 3.6. Synthesis of ^{Me2}SB($^{3\text{-}Et}$I*)ZrX$_2$ (X = Cl, Br).

One equivalent of ^{Me2}SB($^{3\text{-}Et}$I*)H$_2$ was reacted with two equivalents of *n*BuLi in THF at 0 °C (Scheme 3.6). The reaction was kept at 0 °C and stirred for 30 minutes. The resulting dark brown solution was dried *in vacuo* at 0 °C to form a yellow solid, which was then washed with Et$_2$O and pentane. One equivalent of ZrX$_4$ (X = Cl, Br) was mixed with ^{Me2}SB($^{3\text{-}Et}$I*)Li$_2$ (yellow solid) and benzene was then added to the mixture. The reaction slowly turned red and was left stirring for 16 hours at room temperature. The reaction mixture was allowed to settle before being filtered. For X = Cl, the red filtrate was dried *in vacuo* to afford an orange solid which was then washed with Et$_2$O to yield a 50:50 mixture of *rac*- and *meso*-^{Me2}SB($^{3\text{-}Et}$I*)ZrCl$_2$ as an orange solid (24% yield). For X = Br, the red filtrate was dried *in vacuo* to afford a red solid comprising of a 50:50 mixture of *rac*- and *meso*-^{Me2}SB($^{3\text{-}Et}$I*)ZrBr$_2$, and impurities. Recrystallisation of the isomeric mixture in Et$_2$O at -30 °C yielded *rac*-^{Me2}SB($^{3\text{-}Et}$I*)ZrBr$_2$ as orange crystals (1% yield).

One-pot synthesis of ^{Me2}SB($^{3\text{-}Et}$I*)ZrCl$_2$ was carried out. Firstly, two equivalents of $^{3\text{-}Et}$Ind$^{\#}$H were reacted with two equivalents of *n*BuLi in pentane at 0 °C. The reaction was allowed to warm up to room temperature and stirred for 3 hours, during which time an off-white solid was formed. The resulting mixture was dried *in vacuo* and redissolved in THF

to form a dark brown solution of $^{3\text{-Et}}$Ind$^{\#}$Li. Secondly, one equivalent of Me_2SiCl_2 was dissolved in THF and then added dropwise to the $^{3\text{-Et}}$Ind$^{\#}$Li solution at 0 °C. The reaction was allowed to warm up to room temperature and left stirring for 16 hours after which an aliquot was taken showing that the reaction had gone to completion. Thirdly, two equivalents of *n*BuLi was added dropwise to the resulting pale yellow solution of ^{Me_2}SB($^{3\text{-Et}}$I*)H_2 at 0 °C. The reaction was kept at 0 °C and stirred for 30 minutes. The resulting dark brown solution was dried *in vacuo* at 0 °C to form a yellow solid, which was then washed with Et_2O and pentane. Lastly, one equivalent of $ZrCl_4$ was mixed with ^{Me_2}SB($^{3\text{-Et}}$I*)Li_2 (yellow solid) and benzene was then added to the mixture. The reaction slowly turned red and was left stirring for 16 hours at room temperature, after which the reaction mixture was dried *in vacuo* to yield a red solid. The red solid was then extracted with pentane and a 50:50 mixture of *rac*- and *meso*-^{Me_2}SB($^{3\text{-Et}}$I*)$ZrCl_2$ was precipitated from the pentane filtrate at -30 °C as an orange solid (7% yield). Recrystallisation of the isomeric mixture in Et_2O at -30 °C yielded *rac*-^{Me_2}SB($^{3\text{-Et}}$I*)$ZrCl_2$ as orange crystals.

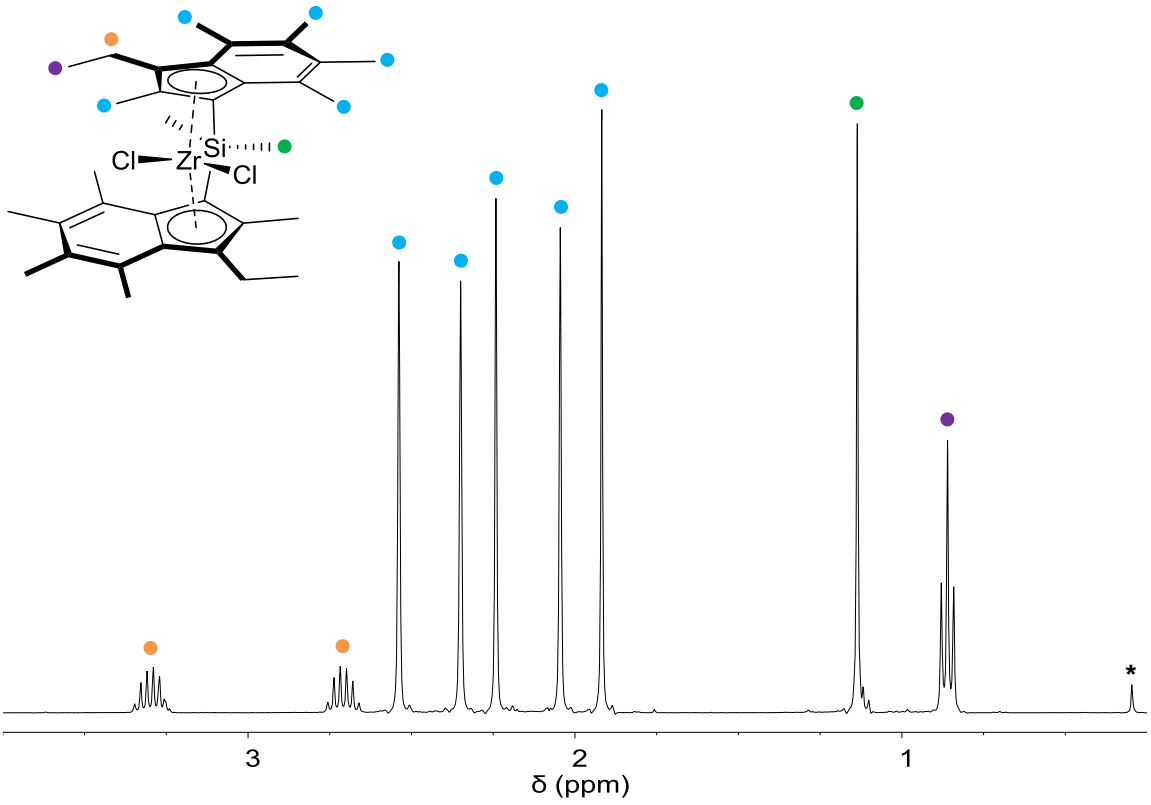


Figure 3.18. ^{1}H NMR spectrum (400 MHz, 298 K, benzene-d_6) of *rac*-^{Me_2}SB($^{3\text{-Et}}$I*)$ZrCl_2$. *: silicone grease.

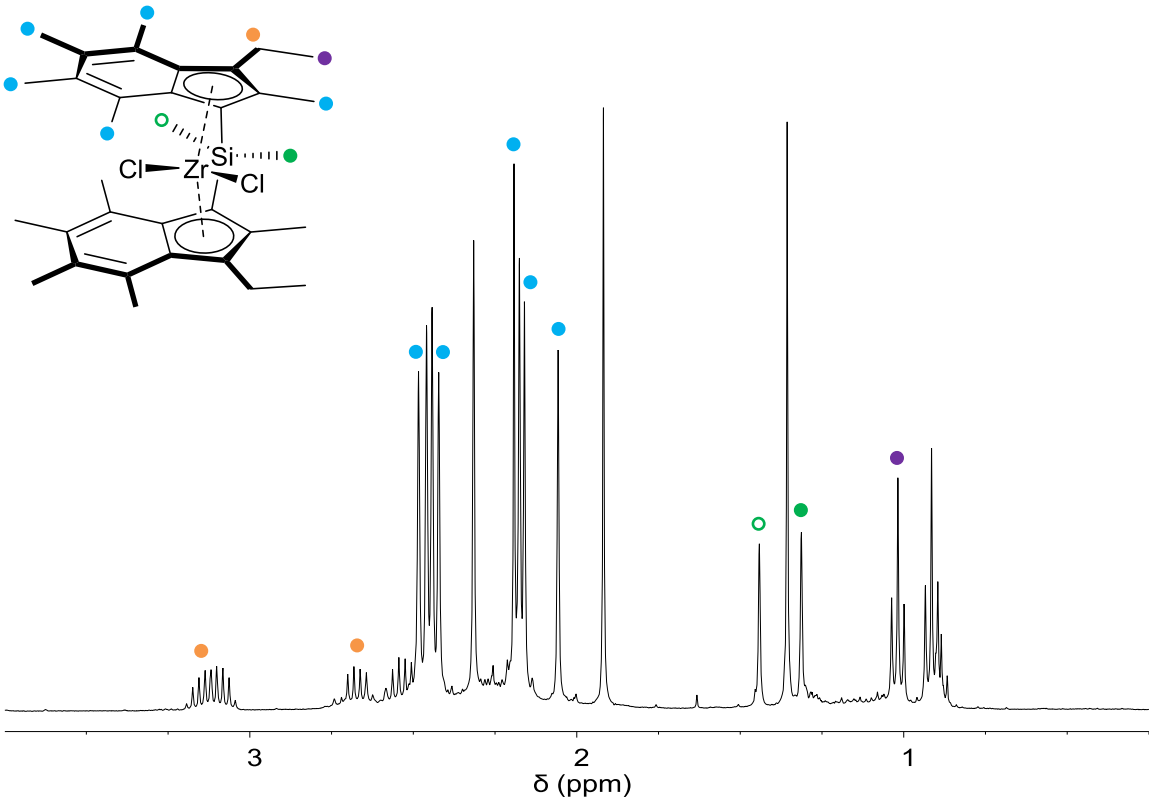


Figure 3.19. ^{1}H NMR spectrum (400 MHz, 298 K, chloroform-d_1) of *rac*- and *meso*-^{Me2}SB($^{3\text{-}Et}$I*)ZrCl$_2$.

The ^{1}H NMR spectrum of *rac*-^{Me2}SB($^{3\text{-}Et}$I*)ZrCl$_2$ is shown in Figure 3.18. Similar to *rac*-^{Et2}SBI*ZrCl$_2$, the indenyl rings and methyl groups on the silyl bridge are magnetically equivalent with respect to their counterpart. The diastereotopic methylene protons of the ethyl groups are observed as two doublet of quartets resonances at 2.71 and 3.30 ppm. Five singlet resonances between 1.90 and 2.60 ppm correspond to the methyl groups on the indenyl rings. A singlet resonance at 1.14 ppm is assigned to the methyl groups on the silyl bridge. The methyl signal of the ethyl groups is seen at 0.86 ppm as a triplet resonance.

The ^{1}H NMR spectrum of a mixture of *rac*- and *meso*-^{Me2}SB($^{3\text{-}Et}$I*)ZrCl$_2$ is shown in Figure 3.19. By subtracting the signals of the *rac* isomer from the spectrum, resonances corresponding to the *meso* isomer can be assigned. Two doublet of quartets resonances at 2.67 and 3.15 ppm correspond to the diastereotopic methylene protons of the ethyl groups. The methyl groups on the indenyl rings are observed as five singlet resonances at 2.06, 2.16, 2.19, 2.42 and 2.48 ppm. Similar to *meso*-^{Et2}SBI*ZrCl$_2$, the two methyl groups on the silyl bridge are diastereotopic and thus seen at 1.31 and 1.44 ppm as two singlet resonances. A triplet resonance at 1.02 ppm is assigned to the methyl protons of the ethyl groups.

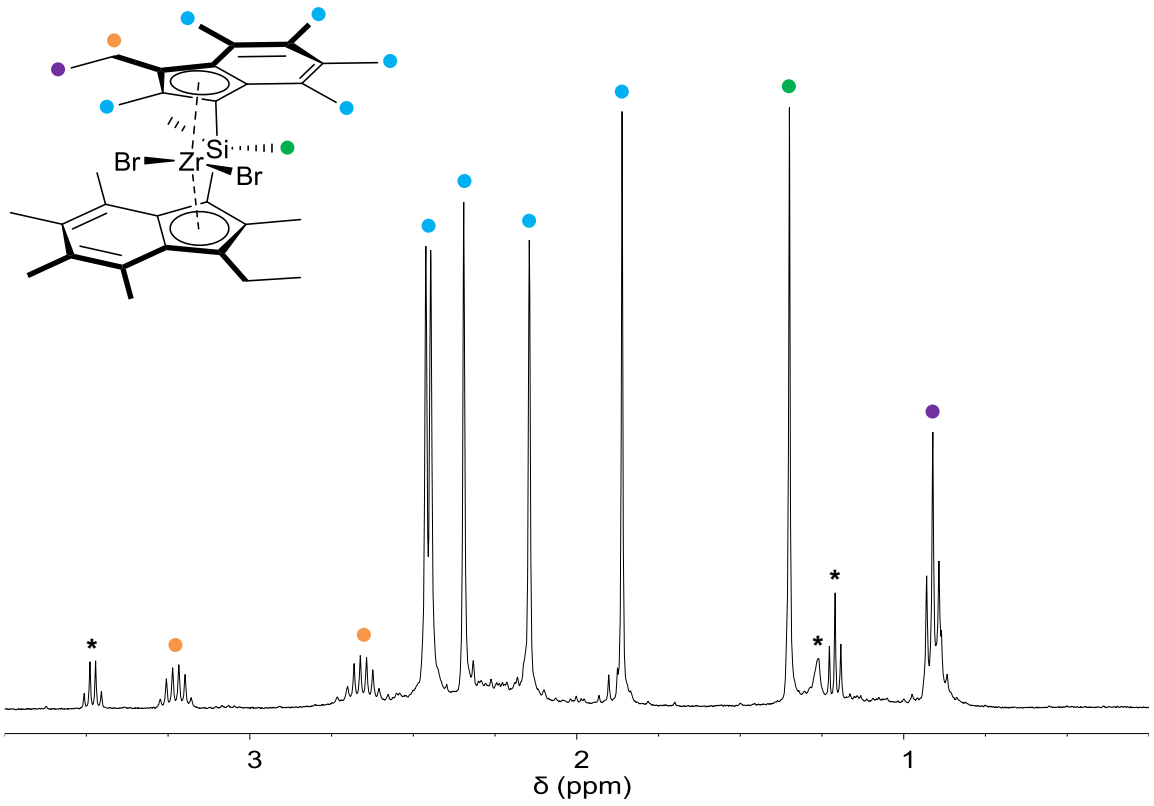


Figure 3.20. ^{1}H NMR spectrum (400 MHz, 298 K, chloroform-d_1) of *rac*-^{Me2}SB($^{3\text{-}Et}$I*)ZrBr$_2$. *: Et_2O, pentane.

The ^{1}H NMR spectrum of *rac*-^{Me2}SB($^{3\text{-}Et}$I*)ZrBr$_2$ (Figure 3.20) shows an identical pattern to that of the analogous dichloro zirconocene. The diastereotopic methylene protons of the ethyl groups are observed as two doublet of quartets resonances at 2.65 and 3.23 ppm. Five singlet resonances between 1.80 and 2.50 ppm correspond to the methyl groups on the indenyl rings. The methyl groups on the silyl bridge are observed as a singlet resonance at 1.35 ppm. A triplet resonance at 0.91 ppm is assigned to the methyl protons of the ethyl groups.

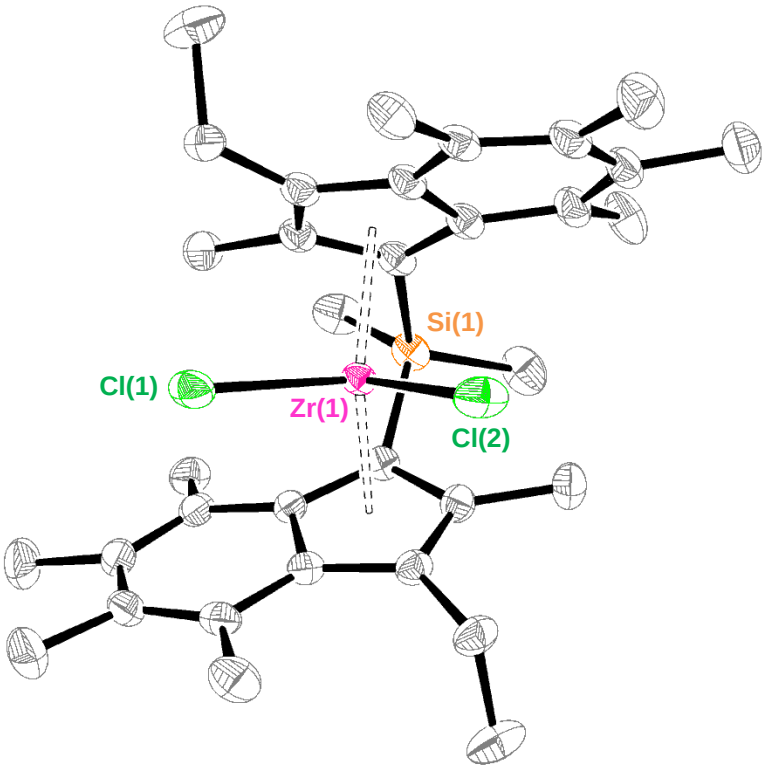


Figure 3.21. Molecular structure of *rac*-^{Me2}SB($^{3\text{-}Et}$I*)ZrCl$_2$. Hydrogen atoms omitted for clarity, ellipsoids drawn at 50% probability.

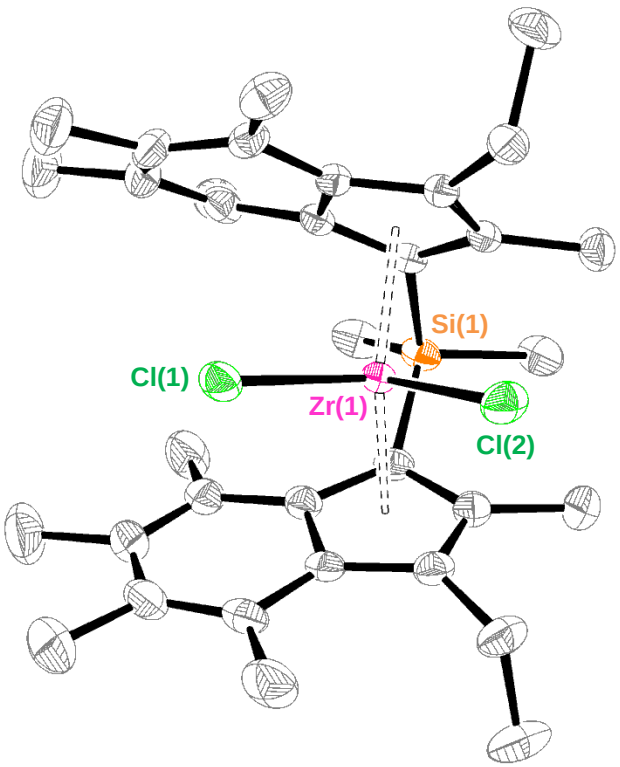


Figure 3.22. Molecular structure of *meso*-^{Me2}SB($^{3\text{-}Et}$I*)ZrCl$_2$. Hydrogen atoms omitted for clarity, ellipsoids drawn at 50% probability.

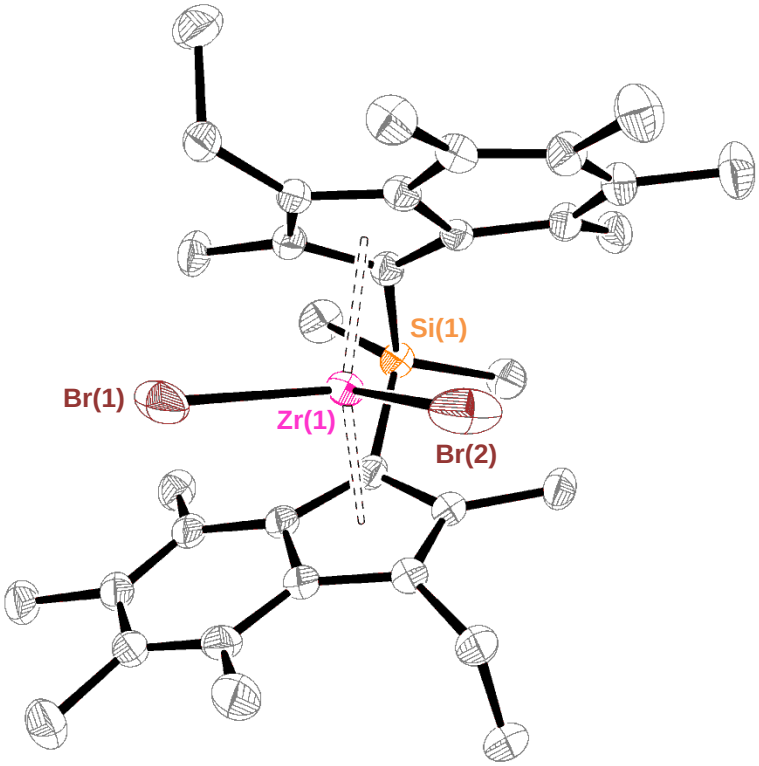


Figure 3.23. Molecular structure of *rac*-^{Me2}SB($^{3\text{-}Et}$I*)ZrBr$_2$. Hydrogen atoms omitted for clarity, ellipsoids drawn at 50% probability.

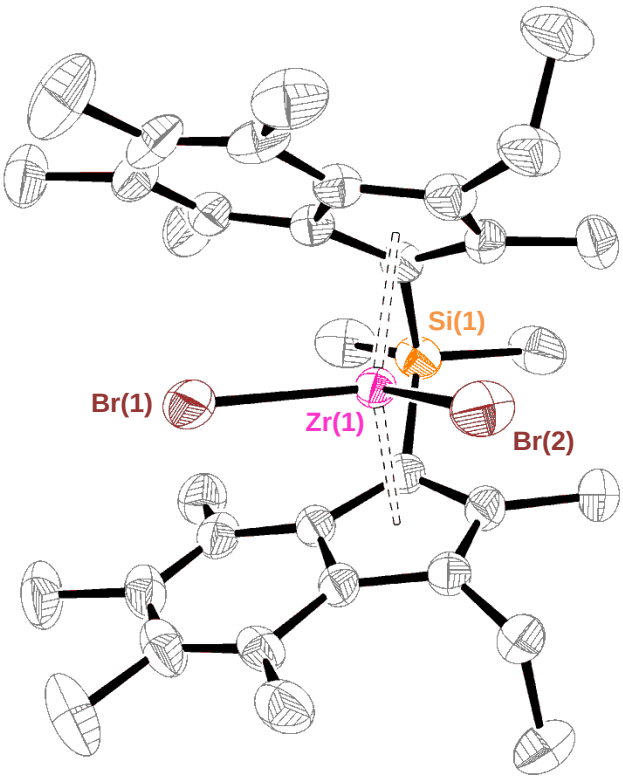


Figure 3.24. Molecular structure of *meso*-^{Me2}SB($^{3\text{-}Et}$I*)ZrBr$_2$. Hydrogen atoms omitted for clarity, ellipsoids drawn at 50% probability.

Table 3.5. Selected bond lengths and angles for *rac*- and *meso*-^{Me2}SB($^{3\text{-}Et}$I*)ZrCl$_2$.

Parameter	Bond lengths (Å) / Angles (°)	
	rac	*meso*
Zr-Cl	2.4186(7), 2.4295(7)	2.4136(6), 2.4357(7)
Zr-Cp$_{cent}$	2.2361(11), 2.2374(11)	2.2513(11), 2.2410(11)
$\Delta_{M\text{-}C,\ max}$	0.209, 0.197	0.179, 0.180
$\Delta_{M\text{-}C,\ \eta^3}$	0.165, 0.146	0.124, -0.026
HA	3.99, 3.61	3.57, 3.51
α	58.21(13)	57.13(14)
δ	129.54(4)	130.53(4)
TA	144.92	5.60

Table 3.6. Selected bond lengths and angles for *rac*- and *meso*-^{Me2}SB($^{3\text{-}Et}$I*)ZrBr$_2$.

Parameter	Bond lengths (Å) / Angles (°)	
	rac	*meso*
Zr-Br	2.5861(5), 2.5656(5)	2.5635(8), 2.5945(9)
Zr-Cp$_{cent}$	2.2511(14), 2.2435(14)	2.244(2), 2.2389(19)
$\Delta_{M\text{-}C,\ max}$	0.236, 0.217	0.145, 0.184
$\Delta_{M\text{-}C,\ \eta^3}$	0.179, 0.173	-0.004, 0.109
HA	4.42, 3.70	3.72, 4.34
α	59.65(18)	57.9(3)
δ	129.14(5)	130.09(8)
TA	144.99	2.89

Orange crystals of *rac*- and *meso*-^{Me2}SB($^{3\text{-}Et}$I*)ZrCl$_2$ suitable for single crystal X-ray diffraction were grown by slow cooling of a hot pentane extract of the isomeric mixture. The molecular structures are shown in Figure 3.21 and Figure 3.22. The *rac* and *meso* isomers co-crystallised in the triclinic space group $P\bar{1}$. The selected bond lengths and angles for *rac*- and *meso*-^{Me2}SB($^{3\text{-}Et}$I*)ZrCl$_2$ are listed in Table 3.5.

Orange crystals of *rac*- and *meso*-^{Me2}SB($^{3\text{-}Et}$I*)ZrBr$_2$ suitable for single crystal X-ray diffraction were grown by slow evaporation of a Et$_2$O solution of the *rac* isomer or a chloroform-d_1 solution of the isomeric mixture, respectively. The molecular structures are shown in Figure 3.23 and Figure 3.24, respectively. Both isomers crystallised in the

monoclinic space group $P2_1/c$ (as a racemic mixture for the *rac* isomer). The selected bond lengths and angles for *rac*- and *meso*-^{Me2}SB($^{3\text{-}Et}$I*)ZrBr$_2$ are listed in Table 3.6.

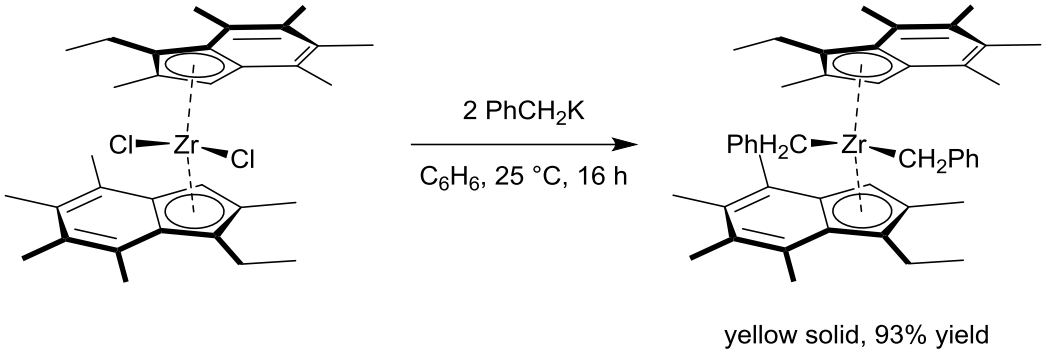
There is little deviation of the average Zr-Cl bond lengths of 2.424 and 2.245 Å for *rac*- and *meso*-^{Me2}SB($^{3\text{-}Et}$I*)ZrCl$_2$ compared to those of its unbridged and permethylated analogues (2.435 Å for *rac*-($^{3\text{-}Et}$Ind$^{\#}$)$_2$ZrCl$_2$ and 2.423 Å for *rac*-^{Me2}SBI*ZrCl$_2$, respectively). This is also the case for the average Zr-Br bond lengths of 2.576 and 2.579 Å for *rac*- and *meso*-^{Me2}SB($^{3\text{-}Et}$I*)ZrBr$_2$ compared to 2.598 Å for its unbridged analogue, *meso*-($^{3\text{-}Et}$Ind$^{\#}$)$_2$ZrBr$_2$. The Zr-Cp$_{cent}$ distances for the *rac* and *meso* isomers of ^{Me2}SB($^{3\text{-}Et}$I*)ZrCl$_2$ (2.237 and 2.246 Å, respectively) and ^{Me2}SB($^{3\text{-}Et}$I*)ZrBr$_2$ (2.247 and 2.241 Å, respectively) are also very similar.

The α value of 58.21° for *rac*-^{Me2}SB($^{3\text{-}Et}$I*)ZrCl$_2$ is in close agreement with 58.49° for *rac*-^{Me2}SBI*ZrCl$_2$ implying that introducing ethyl groups at the 3- position has no impact on the α value. On the other hand, by changing the Cl ligands to Br, the α value increases for *rac*-^{Me2}SB($^{3\text{-}Et}$I*)ZrBr$_2$ when comparing with its dichloro counterpart (59.65° compared to 58.21°). The same effect is not observed in the case of *meso*-^{Me2}SB($^{3\text{-}Et}$I*)ZrBr$_2$ (57.9° compared to 57.13°).

The TA values of 144.92 and 144.99° for *rac*-^{Me2}SB($^{3\text{-}Et}$I*)ZrCl$_2$ and *rac*-^{Me2}SB($^{3\text{-}Et}$I*)ZrBr$_2$, respectively, are nearly identical as well as with that of *rac*-^{Me2}SBI*ZrCl$_2$ (145.52°) due to the geometric restriction of the silyl bridge. In comparison, without the restriction, the unbridged analogue, *rac*-($^{3\text{-}Et}$Ind$^{\#}$)$_2$ZrCl$_2$, adopts near perfect 'anti' conformation, reflected in the TA value of 173.14°, to minimise steric interactions. The same structure restriction can also be observed in *meso*-^{Me2}SB($^{3\text{-}Et}$I*)ZrCl$_2$ and *meso*-^{Me2}SB($^{3\text{-}Et}$I*)ZrBr$_2$ with their TA values close to 0° (5.60 and 2.89°, respectively).

3.4 Dibenzyl substituted indenyl complexes

3.4.1 Synthesis of *rac*-($^{3\text{-Et}}$Ind$^{\#}$)$_2$Zr(CH$_2$Ph)$_2$



Scheme 3.7. Synthesis of *rac*-($^{3\text{-Et}}$Ind$^{\#}$)$_2$Zr(CH$_2$Ph)$_2$.

One equivalent of *rac*-($^{3\text{-Et}}$Ind$^{\#}$)$_2$ZrCl$_2$ was reacted with two equivalents of PhCH$_2$K in benzene for 16 hours at room temperature (Scheme 3.7). The reaction mixture was allowed to settle before being filtered. The yellow filtrate was dried *in vacuo* to afford *rac*-($^{3\text{-Et}}$Ind$^{\#}$)$_2$Zr(CH$_2$Ph)$_2$ as a yellow solid (93% yield).

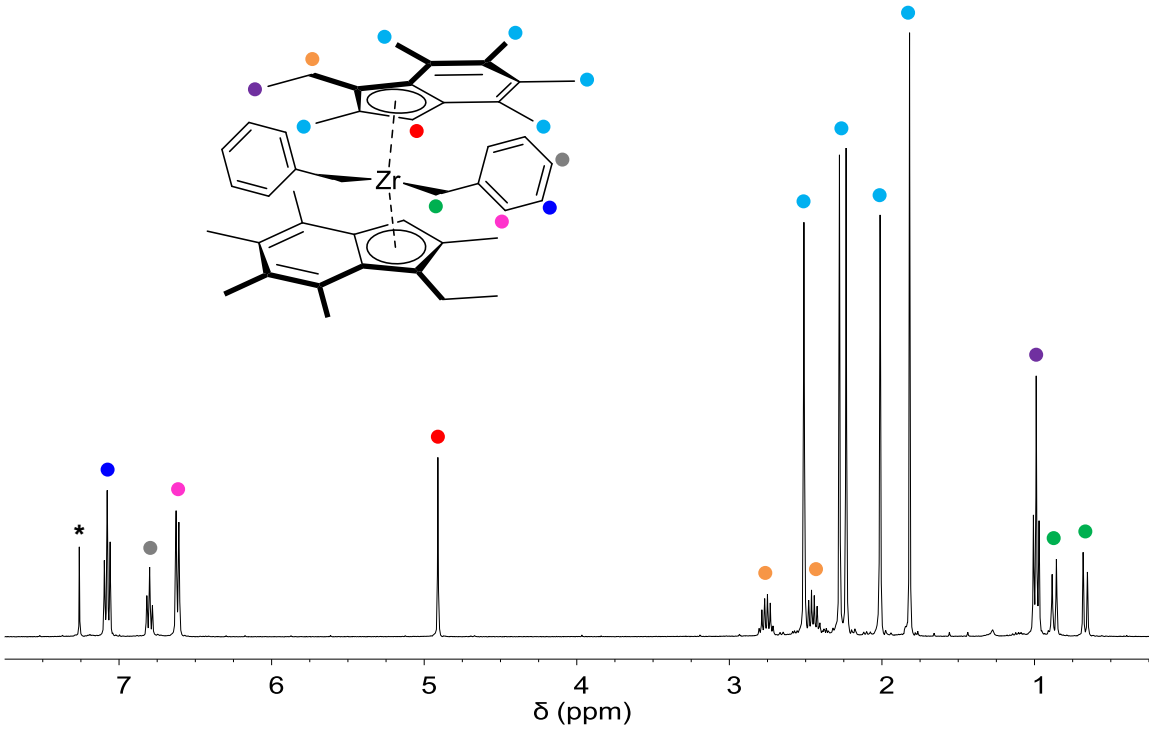


Figure 3.25. ^{1}H NMR spectrum (400 MHz, 298 K, chloroform-d_1) of *rac*-($^{3\text{-Et}}$Ind$^{\#}$)$_2$Zr(CH$_2$Ph)$_2$. *: chloroform.

The ^{1}H NMR spectrum of *rac*-($^{3\text{-Et}}$Ind$^{\#}$)$_2$Zr(CH$_2$Ph)$_2$ is shown in Figure 3.25. The complex has C_2 symmetry resulting in the indenyl rings and benzyl groups being magnetically equivalent with respect to their counterpart. 2D NMR spectroscopic techniques, including COSY, HSQC and HMBC, are used to assist with resonance assignments. The *ortho*, *meta* and *para* protons of the benzyl groups are seen at 6.62 (doublet), 7.08 (doublet of doublets) and 6.80 ppm (triplet), respectively. Two doublet resonances at 0.67 and 0.87 ppm are assigned to the diastereotopic benzylic protons of the benzyl groups. A singlet resonance at 4.91 ppm corresponds to the Cp protons. Two doublet of quartets resonances at 2.45 and 2.76 ppm are assigned to the diastereotopic methylene protons of the ethyl groups. The methyl groups on the indenyl rings are observed as five singlet resonances between 1.80 and 2.60 ppm. The methyl protons of the ethyl groups are observed as a triplet resonance at 0.99 ppm.

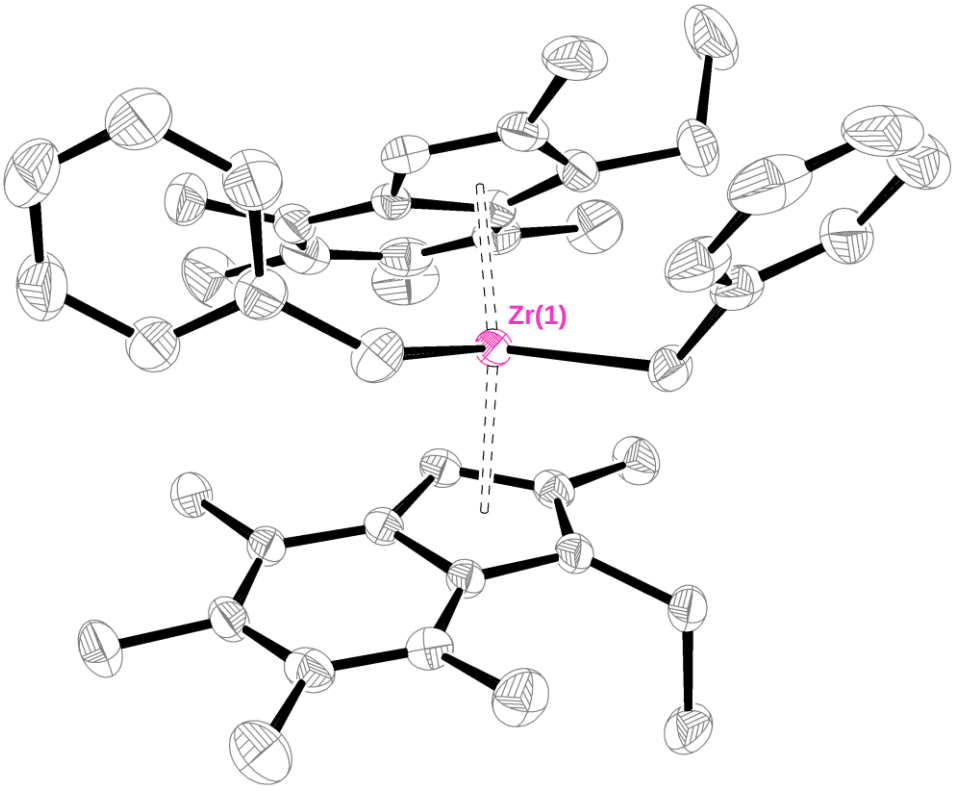


Figure 3.26. Molecular structure of *rac*-($^{3\text{-Et}}$Ind$^{\#}$)$_2$Zr(CH$_2$Ph)$_2$. Hydrogen atoms omitted for clarity, ellipsoids drawn at 50% probability.

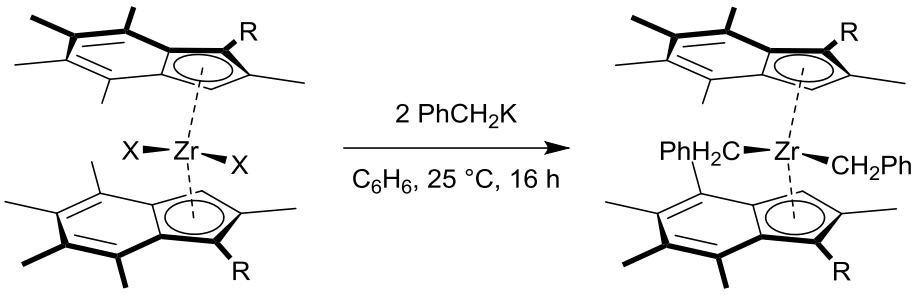
Table 3.7. Selected bond lengths and angles for *rac*-($^{3\text{-Et}}$Ind$^{\#}$)$_2$Zr(CH$_2$Ph)$_2$.

Parameter	Bond lengths (Å) / Angles (°)
Zr-CH$_2$Ph	2.307(2), 2.3284(19)
Zr-Cp$_{cent}$	2.3045(8), 2.2666(9)
$\Delta_{M\text{-}C,\ max}$	0.287, 0.137
$\Delta_{M\text{-}C,\ \eta^3}$	0.132, 0.017
HA	4.70, 2.29
α	51.80(11)
δ	132.99(3)
TA	102.95

Yellow crystals of *rac*-($^{3\text{-Et}}$Ind$^{\#}$)$_2$Zr(CH$_2$Ph)$_2$ suitable for single crystal X-ray diffraction were grown in pentane at -30 °C. The molecular structure is shown in Figure 3.26. The complex crystallised in the monoclinic space group $P2_1/c$ as a racemic mixture. The selected bond lengths and angles for *rac*-($^{3\text{-Et}}$Ind$^{\#}$)$_2$Zr(CH$_2$Ph)$_2$ are listed in Table 3.7.

The average Zr-CH$_2$Ph bond length of 2.318 Å for *rac*-($^{3\text{-Et}}$Ind$^{\#}$)$_2$Zr(CH$_2$Ph)$_2$ matches with that of its permethylated analogue, *rac*-(Ind$^{\#}$)$_2$Zr(CH$_2$Ph)$_2$ (2.320 Å)[23] and is slightly longer than that of another literature example, ($^{4,7\text{-F}_2}$Ind)$_2$Zr(CH$_2$Ph)$_2$ (2.294 Å).[30] Similar to *meso*-($^{3\text{-Et}}$Ind$^{\#}$)$_2$ZrBr$_2$, *rac*-($^{3\text{-Et}}$Ind$^{\#}$)$_2$Zr(CH$_2$Ph)$_2$ has the TA value of 102.95° adopting 'gauche' conformation to minimise the steric clash between the ethyl and benzyl groups.

3.4.2 Synthesis of *meso*-($^{3\text{-R}}$Ind$^{\#}$)$_2$Zr(CH$_2$Ph)$_2$ (R = Me, Et)



R = Me, X = Br; yellow solid, 88% yield
R = Et, X = Cl; yellow solid, 93% yield
R = Et, X = Br; yellow solid, 88% yield

Scheme 3.8. Synthesis of *meso*-($^{3\text{-R}}$Ind$^{\#}$)$_2$Zr(CH$_2$Ph)$_2$ (R = Me, Et).

For R = Me, one equivalent of *meso*-$(Ind^{\#})_2ZrBr_2$ was reacted with two equivalents of $PhCH_2K$ in benzene for 16 hours at room temperature (Scheme 3.8). The reaction mixture was allowed to settle before being filtered. The yellow filtrate was dried *in vacuo* to afford *meso*-$(Ind^{\#})_2Zr(CH_2Ph)_2$ as a yellow solid (88% yield).

For R = Et, one equivalent of *meso*-$(^{3\text{-Et}}Ind^{\#})_2ZrX_2$ (X = Cl, Br) was reacted with two equivalents of $PhCH_2K$ in benzene for 16 hours at room temperature (Scheme 3.8). The reaction mixture was allowed to settle before being filtered. The yellow filtrate was dried *in vacuo* to afford *meso*-$(^{3\text{-Et}}Ind^{\#})_2Zr(CH_2Ph)_2$ as a yellow solid (93% yield for X = Cl; 88% yield for X = Br).

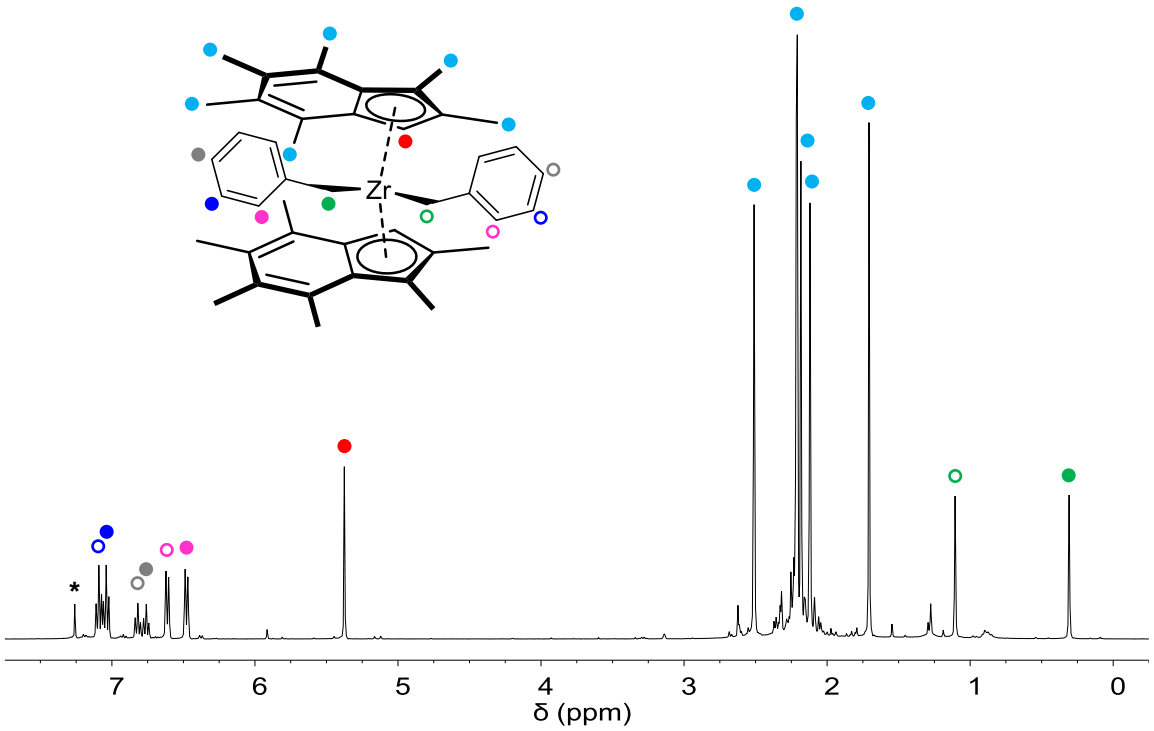


Figure 3.27. ^{1}H NMR spectrum (400 MHz, 298 K, chloroform-d_1) of *meso*-$(Ind^{\#})_2Zr(CH_2Ph)_2$. *: chloroform.

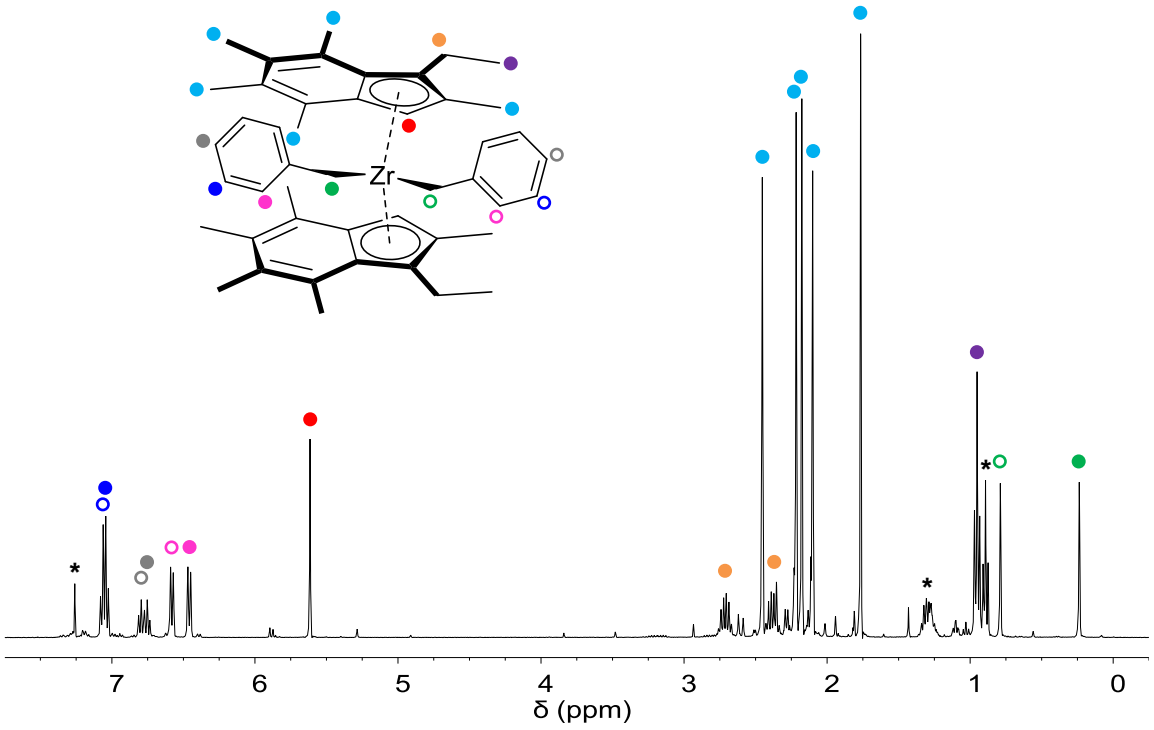


Figure 3.28. ^{1}H NMR spectrum (400 MHz, 298 K, chloroform-d_1) of *meso*-($^{3\text{-Et}}$Ind$^{\#}$)$_2$Zr(CH$_2$Ph)$_2$. *: chloroform, pentane.

The ^{1}H NMR spectrum of *meso*-(Ind$^{\#}$)$_2$Zr(CH$_2$Ph)$_2$ shows that the two benzyl groups are observed as two sets of resonances and hence are not magnetically equivalent (Figure 3.27). 2D NMR spectroscopic techniques, including COSY, HSQC and HMBC, are used to assist with resonance assignments. The *ortho*, *meta*, *para* and benzylic protons of the first benzyl group are seen at 6.48 (doublet), 7.04 (doublet of doublets), 6.76 (triplet) and 0.31 ppm (singlet), respectively. Resonances at 6.61 (doublet), 7.09 (doublet of doublets), 6.82 (triplet) and 1.11 ppm (singlet) correspond respectively to the *ortho*, *meta*, *para* and benzylic protons of the second benzyl group. The benzylic protons of the benzyl groups are not diastereotopic because the complex has C_s symmetry. The two indenyl rings are magnetically equivalent. A singlet resonance at 5.37 ppm is assigned to the Cp protons. The methyl groups on the indenyl rings are observed as six singlet resonances between 1.70 and 2.60 ppm.

The ^{1}H NMR spectrum of *meso*-($^{3\text{-Et}}$Ind$^{\#}$)$_2$Zr(CH$_2$Ph)$_2$ (Figure 3.28) shows a similar pattern to that of *meso*-(Ind$^{\#}$)$_2$Zr(CH$_2$Ph)$_2$. The *ortho*, *meta*, *para* and benzylic protons of the first benzyl group are seen at 6.46 (doublet), 7.04 (doublet of doublets), 6.75 (triplet) and 0.24 ppm (singlet), respectively. Resonances at 6.58 (doublet), 7.06 (doublet of doublets), 6.79 (triplet) and 0.79 ppm (singlet) correspond respectively to the *ortho*, *meta*, *para* and

benzylic protons of the second benzyl group. A singlet resonance at 5.61 ppm is assigned to the Cp protons. Two doublet of quartets resonances at 2.38 and 2.71 ppm correspond to the diastereotopic methylene protons of the ethyl groups. The methyl groups on the indenyl rings are observed as five singlet resonances between 1.70 and 2.50 ppm. Lastly, the methyl signal of the ethyl groups is seen at 0.95 ppm as a triplet resonance.

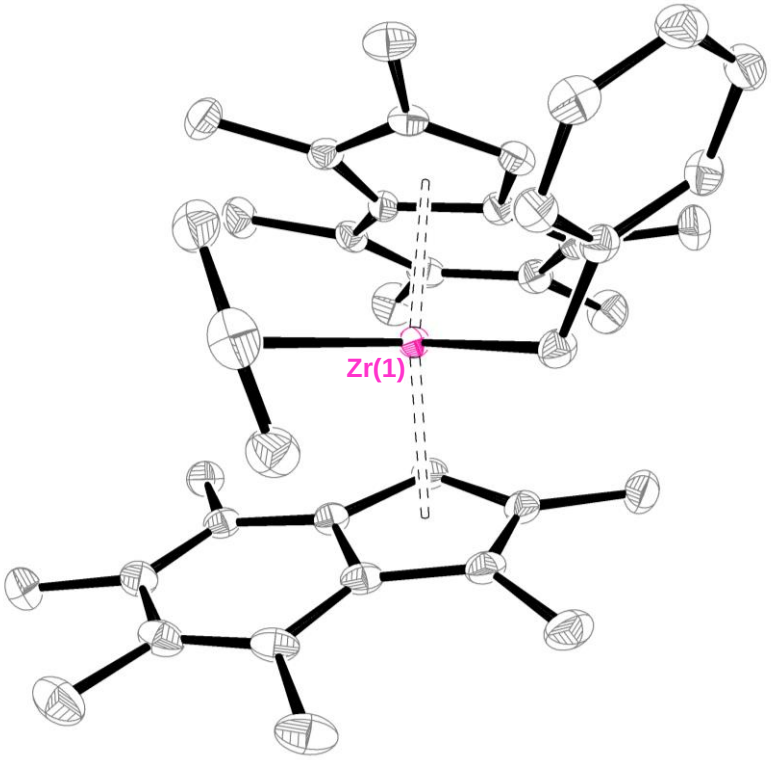


Figure 3.29. Molecular structure of *meso*-(Ind$^{\#}$)$_2$Zr(CH$_2$Ph)$_2$. Hydrogen atoms omitted for clarity, ellipsoids drawn at 50% probability.

Table 3.8. Selected bond lengths and angles for *meso*-($^{3\text{-R}}$Ind$^{\#}$)$_2$Zr(CH$_2$Ph)$_2$ (R = Me, Et).

Parameter	**Bond lengths (Å) / Angles (°)**	
	R = Me	R = Et
Zr-CH$_2$Ph	2.3302(18), 2.3132(18)	2.307(7), 2.299(7)
Zr-Cp$_{cent}$	2.2763(9), 2.3419(10)	2.322(3), 2.281(3)
$\Delta_{M\text{-}C,\ max}$	0.146, 0.366	0.218, 0.126
$\Delta_{M\text{-}C,\ \eta^3}$	0.022, 0.141	0.081, 0.098
HA	2.54, 3.86	1.72, 3.99
α	53.66(10)	51.9(4)
Δ	133.92(3)	133.63(11)
TA	112.56	157.30

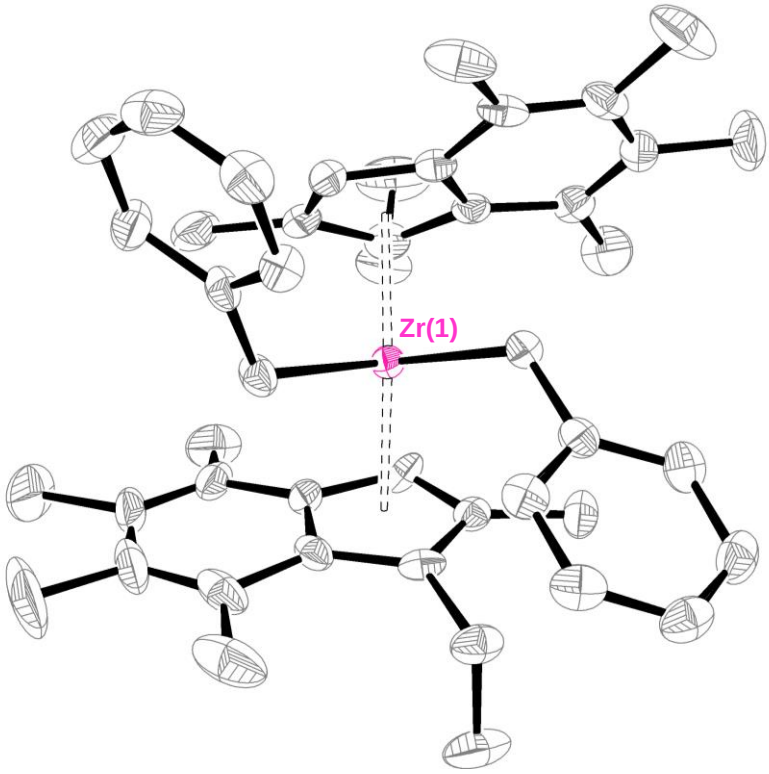
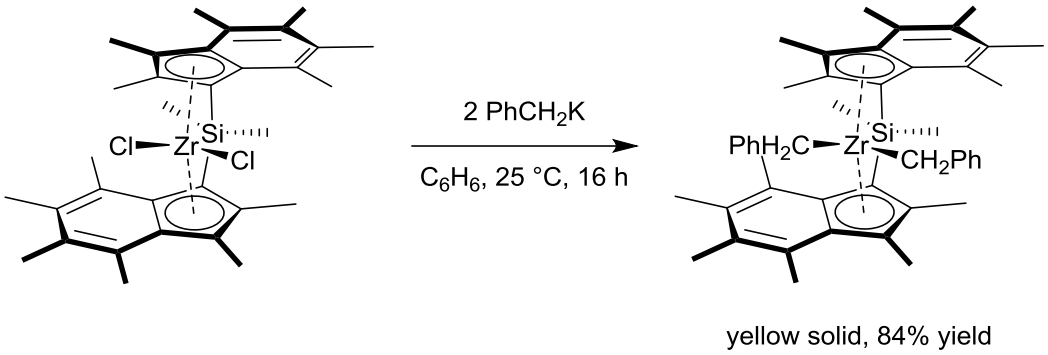


Figure 3.30. Molecular structure of *meso*-($^{3\text{-Et}}$Ind$^{\#}$)$_2$Zr(CH$_2$Ph)$_2$. Hydrogen atoms omitted for clarity, ellipsoids drawn at 50% probability.

Yellow crystals of *meso*-(Ind$^{\#}$)$_2$Zr(CH$_2$Ph)$_2$ and orange crystals of *meso*-($^{3\text{-Et}}$Ind$^{\#}$)$_2$Zr(CH$_2$Ph)$_2$ suitable for single crystal X-ray diffraction were grown in toluene at room temperature or in pentane at -30 °C, respectively. The molecular structures are shown in Figure 3.29 and Figure 3.30, respectively. *meso*-(Ind$^{\#}$)$_2$Zr(CH$_2$Ph)$_2$ co-crystallised with toluene in the monoclinic space group *C*2/*c* while *meso*-($^{3\text{-Et}}$Ind$^{\#}$)$_2$Zr(CH$_2$Ph)$_2$ crystallised in the monoclinic space group *P*2/*c*. The selected bond lengths and angles for *meso*-(Ind$^{\#}$)$_2$Zr(CH$_2$Ph)$_2$ and *meso*-($^{3\text{-Et}}$Ind$^{\#}$)$_2$Zr(CH$_2$Ph)$_2$ are listed in Table 3.8.

The average Zr-CH$_2$Ph bond lengths of 2.322 and 2.303 Å for *meso*-(Ind$^{\#}$)$_2$Zr(CH$_2$Ph)$_2$ and *meso*-($^{3\text{-Et}}$Ind$^{\#}$)$_2$Zr(CH$_2$Ph)$_2$ are similar to those of *rac*-(Ind$^{\#}$)$_2$Zr(CH$_2$Ph)$_2$ and *rac*-($^{3\text{-Et}}$Ind$^{\#}$)$_2$Zr(CH$_2$Ph)$_2$ (2.320 and 2.318 Å, respectively). Comparisons between the α values of the unbridged dibenzyl complexes are difficult because the complexes adopt different conformations, reflected in the difference in the TA values, in order to minimise the steric interactions between the indenyl and benzyl ligands.

3.4.3 Synthesis of *rac*-^{Me2}SBI*Zr(CH$_2$Ph)$_2$



Scheme 3.9. Synthesis of *rac*-^{Me2}SBI*Zr(CH$_2$Ph)$_2$.

One equivalent of *rac*-^{Me2}SBI*ZrCl$_2$ was reacted with two equivalents of PhCH$_2$K in benzene for 16 hours at room temperature (Scheme 3.9). The reaction mixture was allowed to settle before being filtered. The yellow filtrate was dried *in vacuo* to afford *rac*-^{Me2}SBI*Zr(CH$_2$Ph)$_2$ as a yellow solid (84% yield).

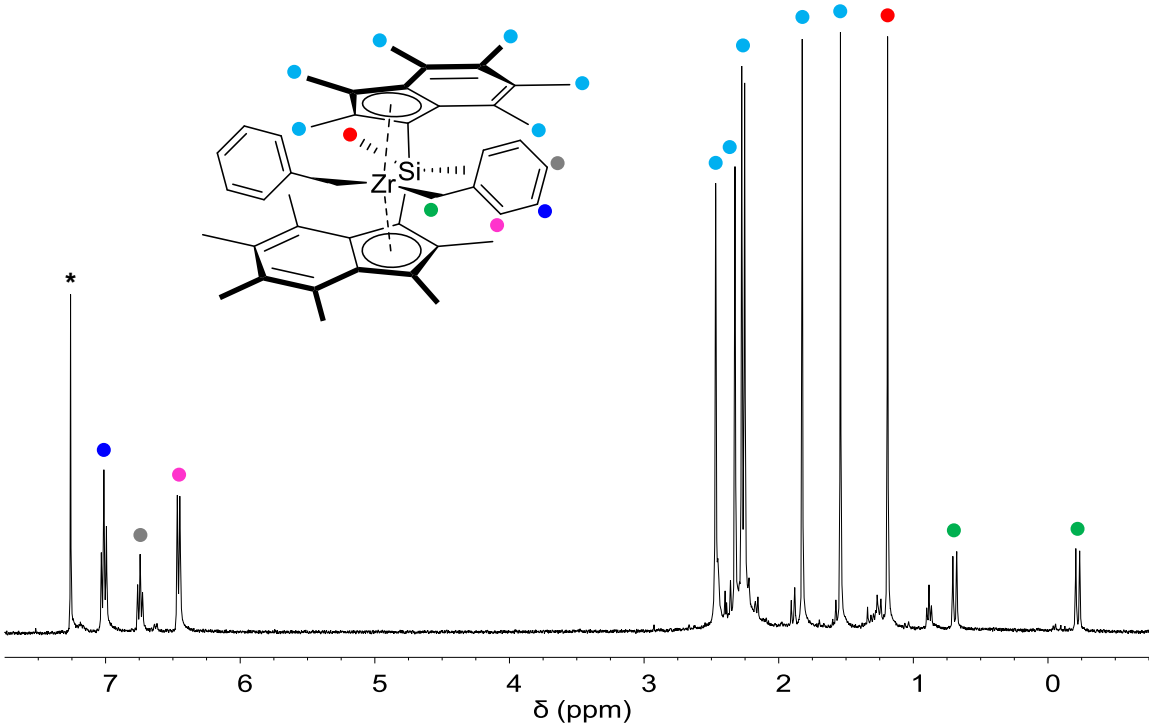
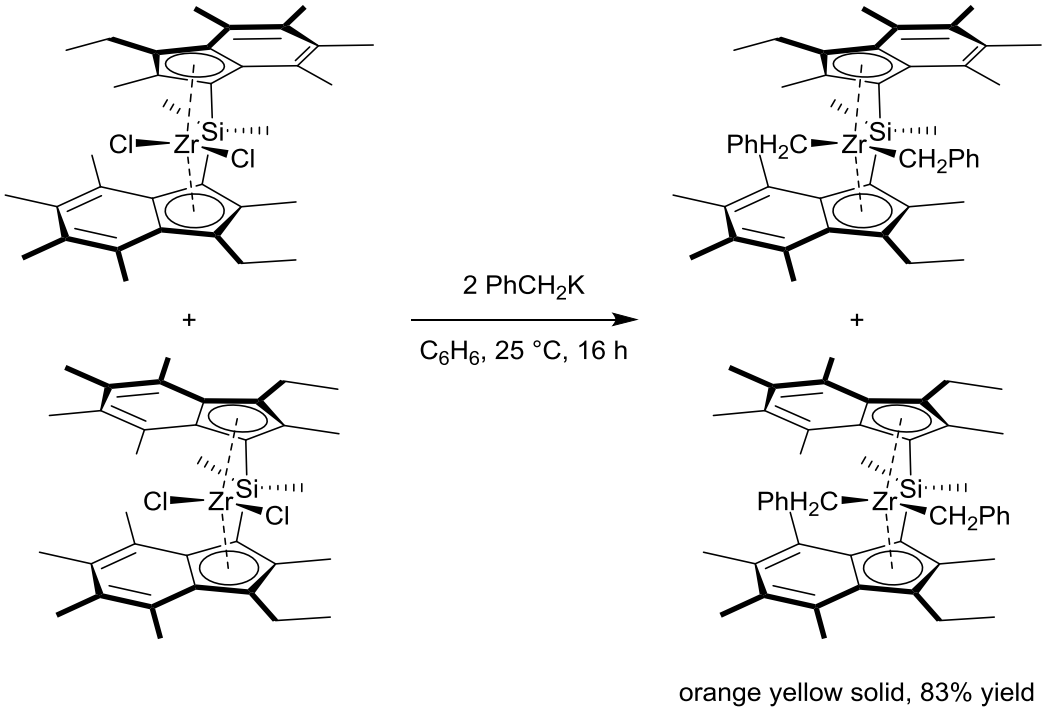


Figure 3.31. ^{1}H NMR spectrum (400 MHz, 298 K, chloroform-d_1) of *rac*-^{Me2}SBI*Zr(CH$_2$Ph)$_2$. *: chloroform.

The ^{1}H NMR spectrum of *rac*-^{Me2}SBI*Zr(CH$_2$Ph)$_2$ is shown in Figure 3.31. Due to the C_2 symmetry of the complex, the indenyl rings, benzyl groups and methyl groups on the silyl bridge are magnetically equivalent with respect to their counterpart. 2D NMR spectroscopic techniques, including COSY, HSQC and HMBC, are used to assist with resonance assignments. Resonances at 6.46 (doublet), 7.01 (doublet of doublets) and 6.74 ppm (triplet) correspond respectively to the *ortho*, *meta* and *para* protons of the benzyl groups. Two doublet resonances at -0.22 and 0.69 ppm are assigned to the diastereotopic benzylic protons of the benzyl groups. Six singlet resonances between 1.50 and 2.50 ppm correspond to the methyl groups on the indenyl rings. The methyl groups on the silyl bridge are observed as a singlet resonance at 1.19 ppm.

3.4.4 Synthesis of ^{Me2}SB($^{3\text{-}Et}$I*)Zr(CH$_2$Ph)$_2$



Scheme 3.10. Synthesis of ^{Me2}SB($^{3\text{-}Et}$I*)Zr(CH$_2$Ph)$_2$.

One equivalent of a 50:50 mixture of *rac*- and *meso*-^{Me2}SB($^{3\text{-}Et}$I*)ZrCl$_2$ was reacted with two equivalents of PhCH$_2$K in benzene for 16 hours at room temperature (Scheme 3.10). The reaction mixture was allowed to settle before being filtered. The orange filtrate was dried *in vacuo* to afford a 75:25 mixture of *rac*- and *meso*-^{Me2}SB($^{3\text{-}Et}$I*)Zr(CH$_2$Ph)$_2$ as an orange yellow solid (83% yield). The change in the isomeric ratio suggests the possibility of isomerisation between the *rac* and *meso* isomers although this has not been observed in other

benzylation reactions. A more likely explanation is due to the difference in solubility of the two isomers impacting the ratio during the filtration.

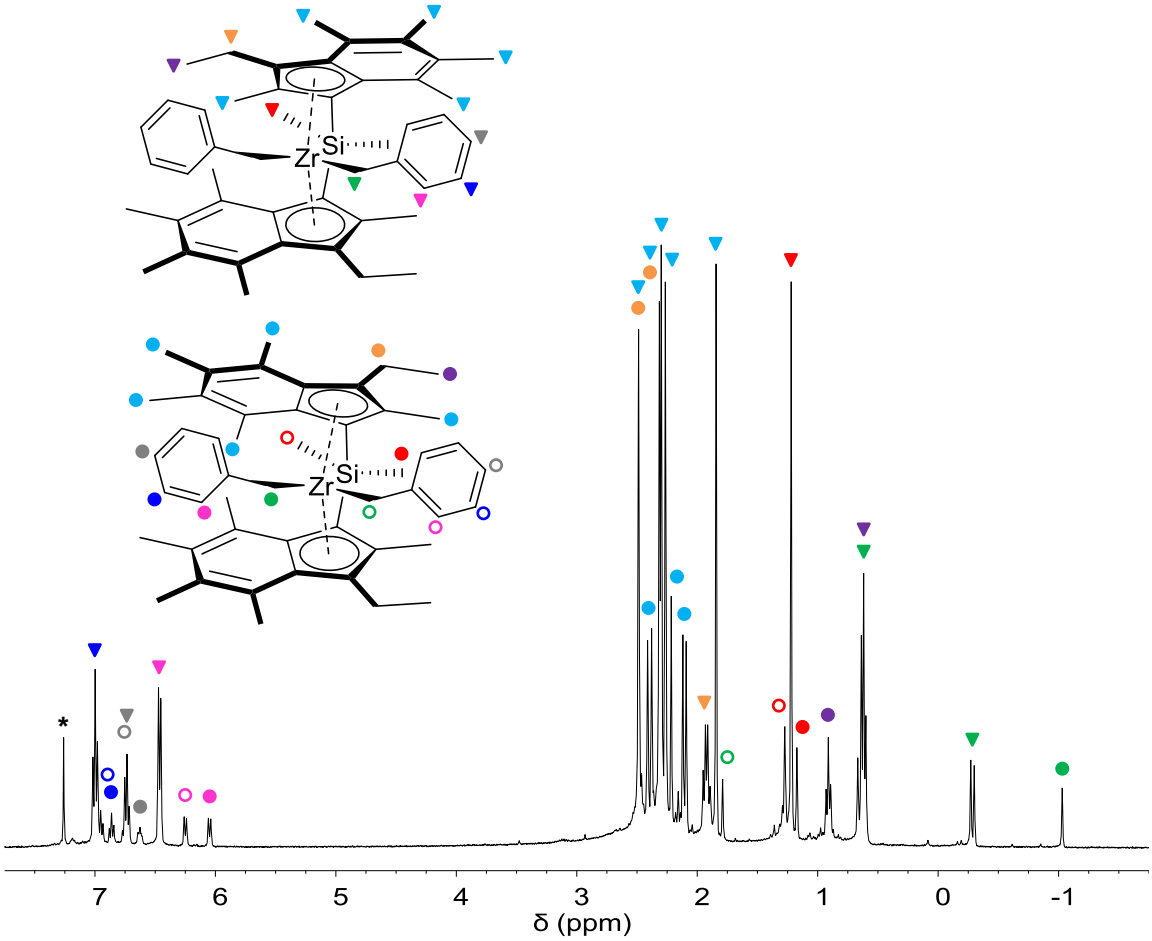


Figure 3.32. ^{1}H NMR spectrum (400 MHz, 298 K, chloroform-d_1) of a mixture of *rac*- and *meso*-^{Me2}SB($^{3\text{-}Et}$I*)Zr(CH_2Ph)$_2$. *: chloroform.

The ^{1}H NMR spectrum of a mixture of *rac*- and *meso*-^{Me2}SB($^{3\text{-}Et}$I*)Zr(CH_2Ph)$_2$ is shown in Figure 3.32. 2D NMR spectroscopic techniques, including COSY, HSQC and HMBC, are used to assist with resonance assignments. Two sets of resonances can be distinguished from each other by the difference in integration and 2D NMR spectroscopy correlations. For both isomers, the two indenyl rings are magnetically equivalent.

The *rac* isomer has C_2 symmetry resulting in the benzyl groups and the methyl groups on the silyl bridge being magnetically equivalent. The *ortho*, *meta* and *para* protons of the benzyl groups are seen at 6.46 (doublet), 7.00 (doublet of doublets) and 6.73 ppm (triplet), respectively. The diastereotopic benzylic protons of the benzyl groups are observed as two doublet resonances at -0.29 and 0.65 ppm. Five singlet resonances at 1.84, 2.26, 2.30, 2.31 and 2.49 ppm correspond to the methyl groups on the indenyl rings. Interestingly, the

methylene protons of the ethyl groups are not diastereotopic and thus observed as a quartet resonance at 1.92 ppm. A singlet resonance at 1.22 ppm is assigned to the methyl groups on the silyl bridge. Lastly, a triplet resonance at 0.62 ppm corresponds to the methyl protons of the ethyl groups.

On the other hand, *meso*-^{Me2}SB($^{3\text{-}Et}$I*)Zr($CH_2Ph)_2$ generated two sets of resonances in the spectrum corresponding to the two magnetically inequivalent benzyl groups. The *ortho*, *meta*, *para* and benzylic protons of the first benzyl group are seen at 6.05 (doublet), 6.86 (doublet of doublets), 6.63 (triplet) and -1.03 ppm (singlet), respectively. Resonances at 6.25 (doublet), 6.95 (doublet of doublets), 6.75 (triplet) and 1.79 ppm (singlet) correspond respectively to the *ortho*, *meta*, *para* and benzylic protons of the second benzyl group. The *meso* isomer shares its C_s symmetry with *meso*-(Ind$^{\#}$)$_2$Zr($CH_2Ph)_2$ and *meso*-($^{3\text{-}Et}$Ind$^{\#}$)$_2$Zr($CH_2Ph)_2$ and, as a consequence, the benzylic protons of the benzyl groups are not diastereotopic. Two multiplet resonances at 2.32 and 2.49 ppm are assigned to the diastereotopic methylene protons of the ethyl groups. The methyl groups on the indenyl rings are observed as five singlet resonances at 2.09, 2.12, 2.22, 2.38 and 2.41 ppm. Two singlet resonances at 1.17 and 1.27 ppm correspond to the diastereotopic methyl groups on the silyl bridge. Lastly, a triplet resonance at 0.91 ppm is assigned to the methyl protons of the ethyl groups.

Notably, the separation between the singlet resonances at -1.03 and 1.79 ppm of the *meso* isomer, corresponding respectively to the benzylic protons of each benzyl group, is significantly large in comparison to those of *meso*-(Ind$^{\#}$)$_2$Zr($CH_2Ph)_2$ (0.31 and 1.11 ppm) and *meso*-($^{3\text{-}Et}$Ind$^{\#}$)$_2$Zr($CH_2Ph)_2$ (0.24 and 0.79 ppm). A similar large separation has been observed for *meso*-EBI*Zr($CH_2Ph)_2$ (-0.70 and 1.83 ppm) by O'Hare and co-workers.[31] After a comprehensive analysis, it is concluded that ring current effects play a major role influencing the chemical shifts of the benzylic protons. Using rotating frame nuclear Overhauser effect spectroscopy (ROESY) in combination with the molecular structure determined by single crystal X-ray diffraction, the benzylic protons of one of the benzyl groups are found to position directly in between the two benzene rings of the indenyl groups, hence, experienced shielding effect of the ring currents.

Ring current effects, first conceptualised by Pople in 1956,[32] can positively (deshielding) or negatively (shielding) affect the chemical shift of a proton depending on its position relative to the conjugated system.[33] One of the classic examples of shielding ring current effect was reported by Waugh and Fessenden on l,4-polymethylenebenzenes whose methylene protons are forced to lie directly above the benzene ring, thus, experienced a strong upfield shift.[34] A more recent example in metallocene chemistry was reported concerning the

chemical shift of the β-agostic proton of an alkyltitanocene complex negatively affected by the Cp ring currents.[35]

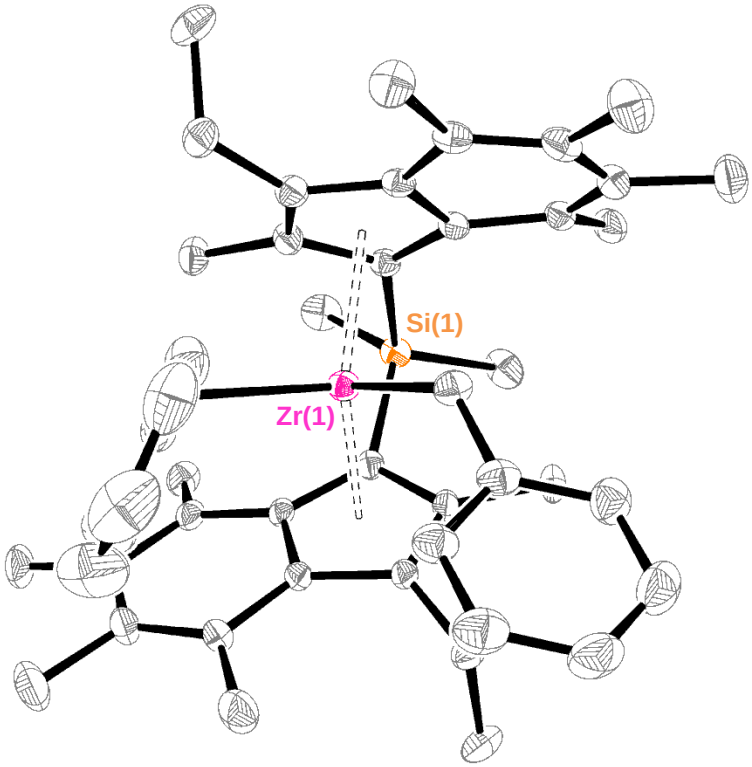


Figure 3.33. Molecular structure of *rac*-^{Me2}SB($^{3\text{-}Et}$I*)Zr(CH_2Ph)$_2$. Hydrogen atoms omitted for clarity, ellipsoids drawn at 50% probability.

Table 3.9. Selected bond lengths and angles for *rac*-^{Me2}SB($^{3\text{-}Et}$I*)Zr(CH_2Ph)$_2$.

Parameter	Bond lengths (Å) / Angles (°)
Zr-CH_2Ph	2.273(4), 2.334(4)
Zr-Cp_{cent}	2.2923(18), 2.3146(18)
$\Delta_{M\text{-}C,\ max}$	0.246, 0.358
$\Delta_{M\text{-}C,\ \eta^3}$	0.164, 0.301
HA	3.50, 2.70
α	63.2(2)
δ	128.84(7)
TA	146.78

Orange crystals of *rac*-^{Me2}SB($^{3\text{-}Et}$I*)Zr(CH_2Ph)$_2$ suitable for single crystal X-ray diffraction were grown from a pentane solution of the isomeric mixture at room temperature. The molecular structure is shown in Figure 3.33. The isomer crystallised in the triclinic space

group $P\bar{1}$ as a racemic mixture. The selected bond lengths and angles for *rac*-^{Me_2}SB($^{3\text{-}Et}$I*)Zr(CH_2Ph)$_2$ are listed in Table 3.9.

Structure comparisons between *rac*-^{Me_2}SB($^{3\text{-}Et}$I*)Zr(CH_2Ph)$_2$ and its dichoro counterpart, *rac*-^{Me_2}SB($^{3\text{-}Et}$I*)$ZrCl_2$, highlight structure distortions caused the steric effects of the bulky benzyl ligands. There is a larger disparity between the Zr-CH_2Ph bond lengths for *rac*-^{Me_2}SB($^{3\text{-}Et}$I*)Zr(CH_2Ph)$_2$ compared to the Zr-Cl bonds of *rac*-^{Me_2}SB($^{3\text{-}Et}$I*)$ZrCl_2$. Both α and TA values of 63.2 and 146.78°, respectively, for *rac*-^{Me_2}SB($^{3\text{-}Et}$I*)Zr(CH_2Ph)$_2$ are significantly larger than those of *rac*-^{Me_2}SB($^{3\text{-}Et}$I*)$ZrCl_2$ (58.21 and 144.92°, respectively) due to the large steric effects of the benzyl ligands.

3.5 Conclusions

Chapter Three describes the syntheses of novel substituted indenyl group 4 complexes using the pro-ligands synthesised in Chapter Two. All complexes were fully characterised by NMR spectroscopy, mass spectrometry, elemental analysis and, when possible, single crystal X-ray diffraction. Unbridged ($^{3\text{-}R}$Ind$^{\#}$)$_2$$MCl_2$ (R = Et, Ph; M = Zr, Hf) were successfully synthesised as 50:50 mixtures of the corresponding *rac* and *meso* isomers. The synthesis of ($^{3\text{-}R}$Ind$^{\#}$)$_2$$ZrBr_2$ (R = Me, Et) was accomplished but undesirably favoured the formation of the *meso* isomers. Jordan's reagent was also used but only formed the monosubstituted product. Silyl bridged substituted indenyl zirconocenes, including ^{Et_2}SBI*$ZrCl_2$ and ^{Me_2}SB($^{3\text{-}Et}$I*)ZrX_2 (X = Cl, Br), were synthesised and no selectivity towards the formation of the *rac* isomers was observed. Dibenzylation of the synthesised dichloro and dibromo zirconocenes were successfully carried out.

3.6 References

1 G. G. Hlatky, *Coord. Chem. Rev.*, 1999, **181**, 243–296.
2 G. G. Hlatky, *Coord. Chem. Rev.*, 2000, **199**, 235–329.
3 W. Kaminsky, *Macromol. Chem. Phys.*, 1996, **197**, 3907–3945.
4 G. M. Diamond, S. Rodewald and R. F. Jordan, *Organometallics*, 1995, **14**, 5–7.
5 G. M. Diamond, R. F. Jordan and J. L. Petersen, *J. Am. Chem. Soc.*, 1996, **118**, 8024–8033.
6 G. M. Diamond, R. F. Jordan and J. L. Petersen, *Organometallics*, 1996, **15**, 4030–4037.
7 J. N. Christopher, G. M. Diamond, R. F. Jordan and J. L. Petersen, *Organometallics*, 1996, **15**, 4038–4044.
8 X. Zhang, Q. Zhu, I. A. Guzei and R. F. Jordan, *J. Am. Chem. Soc.*, 2000, **122**, 8093–8094.
9 M. D. LoCoco and R. F. Jordan, *Organometallics*, 2003, **22**, 5498–5503.
10 A. R. Dunn, L. E. Sweet, D. C. Wiser, M. D. LoCoco and R. F. Jordan, *Organometallics*, 2004, **23**, 5671–5680.
11 M. D. LoCoco, X. Zhang and R. F. Jordan, *J. Am. Chem. Soc.*, 2004, **126**, 15231–15244.

12 M. D. LoCoco and R. F. Jordan, *J. Am. Chem. Soc.*, 2004, **126**, 13918–13919.
13 R. M. Buck, N. Vinayavekhin and R. F. Jordan, *J. Am. Chem. Soc.*, 2007, **129**, 3468–3469.
14 H.-R. H. Damrau, E. Royo, S. Obert, F. Schaper, A. Weeber and H.-H. Brintzinger, *Organometallics*, 2001, **20**, 5258–5265.
15 L. Resconi, F. Piemontesi, I. Camurati, D. Balboni, A. Sironi, M. Moret, H. Rychlicki and R. Zeigler, *Organometallics*, 1996, **15**, 5046–5059.
16 I. E. Nifant'ev and P. V. Ivchenko, *Organometallics*, 1997, **16**, 713–715.
17 I. E. Nifant'ev, P. V. Ivchenko, V. V. Bagrov, A. V. Churakov and P. Mercandelli, *Organometallics*, 2012, **31**, 4962–4970.
18 I. E. Nifant'ev, P. V. Ivchenko, V. V. Bagrov, A. V. Churakov and R. Chevalier, *Organometallics*, 2012, **31**, 4340–4348.
19 S. A. Westcott, A. K. Kakkar, G. Stringer, N. J. Taylor and T. B. Marder, *J. Organomet. Chem.*, 1990, **394**, 777–794.
20 P. J. Shapiro, *Coord. Chem. Rev.*, 2002, **231**, 67–81.
21 D. E. Herbert, U. F. J. Mayer and I. Manners, *Angew. Chemie, Int. Ed.*, 2007, **46**, 5060–5081.
22 M. J. Calhorda, V. Félix and L. F. Veiros, *Coord. Chem. Rev.*, 2002, **230**, 49–64.
23 T. A. Q. Arnold, J.-C. Buffet, Z. R. Turner and D. O'Hare, *J. Organomet. Chem.*, 2015, **792**, 55–65.
24 N. E. Grimmer, N. J. Coville, C. B. de Koning, J. M. Smith and L. M. Cook, *J. Organomet. Chem.*, 2000, **616**, 112–127.
25 J. L. M. Petoff, M. D. Bruce, R. M. Waymouth, A. Masood, T. K. Lal, R. W. Quan and S. J. Behrend, *Organometallics*, 1997, **16**, 5909–5916.
26 C. D. Tagge, R. L. Kravchenko, T. K. Lal and R. M. Waymouth, *Organometallics*, 1999, **18**, 380–388.
27 A. Y. Lebedev, V. V. Izmer, A. F. Asachenko, A. A. Tzarev, D. V. Uborsky, Y. A. Homutova, E. R. Shperber, J. A. M. Canich and A. Z. Voskoboynikov, *Organometallics*, 2009, **28**, 1800–1816.
28 M. G. Medvedev, I. S. Borisov, P. S. Kulyabin, V. V. Izmer, D. S. Kononovich, D. V. Uborsky and A. Z. Voskoboynikov, *Acta Crystallogr. Sect. E Crystallogr. Commun.*, 2016, **72**, 1599–1602.
29 J.-C. Buffet, T. A. Q. Arnold, Z. R. Turner, P. Angpanitcharoen and D. O'Hare, *RSC Adv.*, 2015, **5**, 87456–87464.
30 N. Piccolrovazzi, P. Pino, G. Consiglio, A. Sironi and M. Moret, *Organometallics*, 1990, **9**, 3098–3105.
31 T. A. Q. Arnold, Z. R. Turner, J.-C. Buffet and D. O'Hare, *J. Organomet. Chem.*, 2016, **822**, 85–90.
32 J. A. Pople, *J. Chem. Phys.*, 1956, **24**, 1111.
33 C. W. Haigh and R. B. Mallion, *Prog. Nucl. Magn. Reson. Spectrosc.*, 1979, **13**, 303–344.
34 J. S. Waugh and R. W. Fessenden, *J. Am. Chem. Soc.*, 1957, **79**, 846–849.
35 F. Sauriol, J. F. Sonnenberg, S. J. Chadder, A. F. Dunlop-Brière, M. C. Baird and P. H. M. Budzelaar, *J. Am. Chem. Soc.*, 2010, **132**, 13357–13370.

Chapter Four – Ethylene polymerisation studies

4.1 Introduction

Group 4 metallocene complexes have been shown to be highly active for ethylene polymerisation.[1,2] Studies have demonstrated that minor alterations to the complex framework can have a strong influence on the catalyst activity.[3–8] Therefore, small optimisations to the metallocene structure can significantly improve productivity.[9–11]

The ethylene polymerisation activity of metallocene complexes depends on a multitude of factors including polymerisation temperature, complex concentration, co-catalyst concentration, chain transfer agent and ethylene partial pressure.[12] As a result, comparisons of activities with the literature must be done with caution.

In this Chapter, homogeneous and heterogeneous ethylene polymerisation using the substituted indenyl group 4 complexes described in Chapter 3 are studied. The resulting polyethylenes are characterised.

4.2 Homogeneous ethylene polymerisation

The discovery of methylaluminoxane (MAO) and its stupendous capability as a co-catalyst ignited the interest in homogeneous ethylene polymerisation using group 4 metallocene complexes.[13,14] Despite mostly dominated by slurry- and gas-phase processes, a number of industrial, homogeneous polymerisation processes exist for the production of polyethylene including Compact Process by DEX Plastomers, Dowlex by Dow and Sclairtech by Nova Chemicals.[15] Furthermore, homogeneous ethylene polymerisation is very useful for academic purposes given the ability to more easily control and probe the catalyst active site.

For a homogeneous ethylene polymerisation test, a metallocene complex (0.5 mg, 1.0 eq), MAO (500 eq) and hexane (50 mL) were added to a 150 mL Rotaflo ampoule containing a stirrer bar. The ampoule was sealed and degassed before being heated to the desired temperature at the stirring speed of 1000 rpm. The ampoule was then opened to ethylene (2 bar). On completion of the test, the ampoule was closed to ethylene and degassed. The resulting polyethylene was filtered on a glass sintered frit, washed with pentane (2 x 25 mL) and dried. All polymerisation tests were carried out for 30 minutes or until the stirring ceased entirely. The molecular weights of the resulting polyethylenes were determined by gel

permeation chromatography (GPC) and reported with their corresponding polydispersity index (PDI) values, which indicate the broadness of the molecular weight distributions.

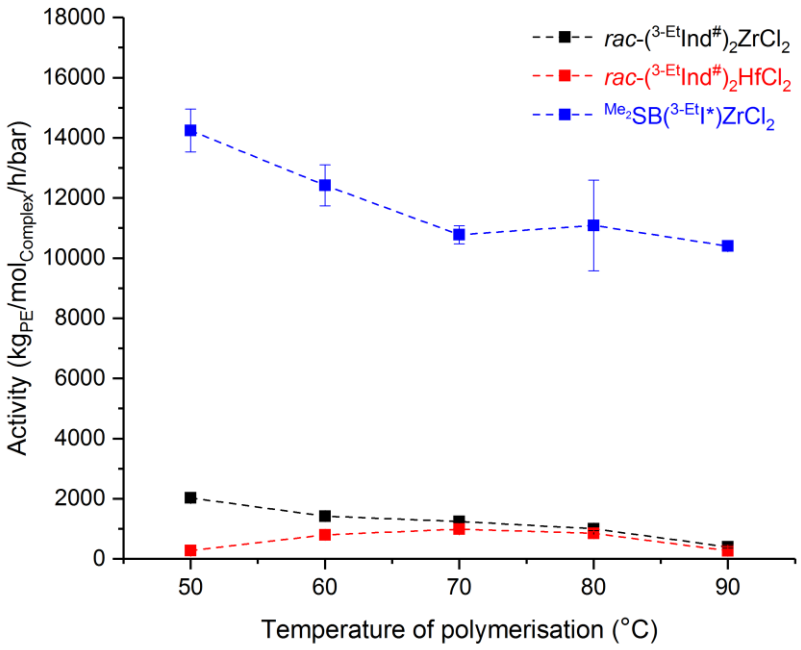


Figure 4.1. Homogeneous ethylene polymerisation activity of *rac*-($^{3\text{-Et}}$Ind$^{\#}$)$_2$ZrCl$_2$, *rac*-($^{3\text{-Et}}$Ind$^{\#}$)$_2$HfCl$_2$ and $^{\text{Me}_2}$SB($^{3\text{-Et}}$I*)ZrCl$_2$ as a function of temperature of polymerisation.

Homogeneous ethylene polymerisation using *rac*-($^{3\text{-Et}}$Ind$^{\#}$)$_2$ZrCl$_2$, *rac*-($^{3\text{-Et}}$Ind$^{\#}$)$_2$HfCl$_2$ and $^{\text{Me}_2}$SB($^{3\text{-Et}}$I*)ZrCl$_2$ (50:50 mixture of *rac* and *meso* isomers) complexes were carried out. The activities were recorded over a temperature range of 50 to 90 °C (Figure 4.1). The activities of *rac*-($^{3\text{-Et}}$Ind$^{\#}$)$_2$ZrCl$_2$ and $^{\text{Me}_2}$SB($^{3\text{-Et}}$I*)ZrCl$_2$ show declining trends with respect to increasing temperature while those of *rac*-($^{3\text{-Et}}$Ind$^{\#}$)$_2$HfCl$_2$ display a maximum of 988 kg$_{\text{PE}}$/mol$_{\text{Complex}}$/h/bar at 70 °C. The decreased activities at higher temperatures are believed to be, at least in part, a result of the lack of thermal stability of metallocene complexes.[16]

$^{\text{Me}_2}$SB($^{3\text{-Et}}$I*)ZrCl$_2$ is shown to be significantly more active than its unbridged analogue, *rac*-($^{3\text{-Et}}$Ind$^{\#}$)$_2$ZrCl$_2$ (14242 kg$_{\text{PE}}$/mol$_{\text{Complex}}$/h/bar compared to 2029 kg$_{\text{PE}}$/mol$_{\text{Complex}}$/h/bar at 50 °C). Comparisons of both silyl bridged and unbridged zirconocenes with their permethylated counterparts show contradicting results. The maximum activity of $^{\text{Me}_2}$SB($^{3\text{-Et}}$I*)ZrCl$_2$ is lower than that of *rac*-$^{\text{Me}_2}$SBI*ZrCl$_2$ (22622 kg$_{\text{PE}}$/mol$_{\text{Complex}}$/h/bar at 60 °C)[17] while the maximum activity of *rac*-($^{3\text{-Et}}$Ind$^{\#}$)$_2$ZrCl$_2$ compares favourably with that of

rac-(Ind$^{\#}$)$_2$ZrCl$_2$ (433 kg$_{PE}$/mol$_{Complex}$/h/bar at 50 °C).[18] *rac*-($^{3\text{-Et}}$Ind$^{\#}$)$_2$HfCl$_2$ is less active than its zirconocene counterpart which is consistent with the literature on their permethylated analogues.[18] Comparison of the activity of *rac*-($^{3\text{-Et}}$Ind$^{\#}$)$_2$ZrCl$_2$ with that of its unmethylated analogue, *rac*-($^{1\text{-Et}}$Ind)$_2$ZrCl$_2$, (10650 kg$_{PE}$/mol$_{Complex}$/h/bar at 50 °C) is difficult due to the significant difference in polymerisation conditions used.[19] The same can be said for ^{Me2}SB($^{3\text{-Et}}$I*)ZrCl$_2$ when compared with its unmethylated counterpart, ^{Me2}SB($^{3\text{-Et}}$I)ZrCl$_2$ (9150 and 7600 kg$_{PE}$/mol$_{Complex}$/h/bar for the *rac* and *meso* isomers, respectively).[20]

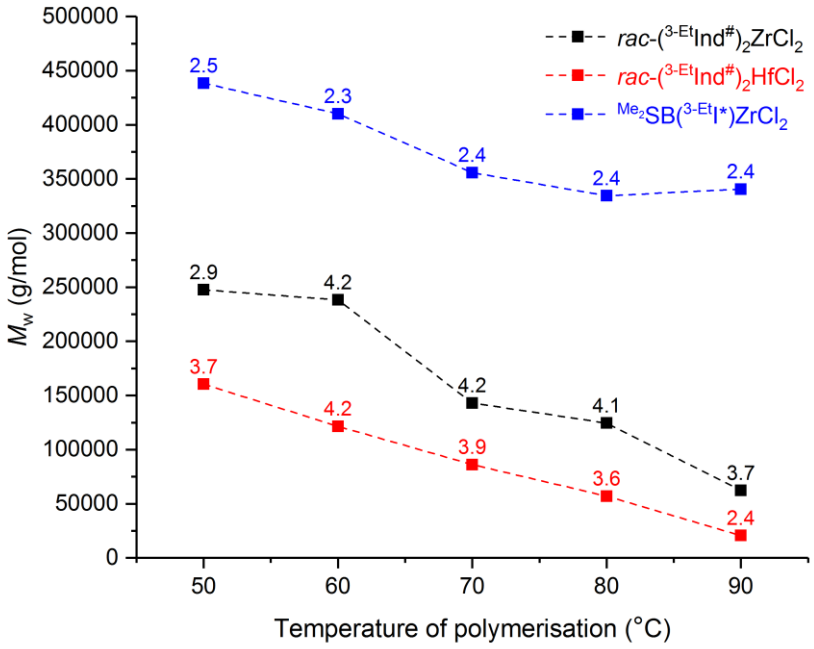


Figure 4.2. Molecular weight of the resulting polyethylenes of homogeneous ethylene polymerisation using *rac*-($^{3\text{-Et}}$Ind$^{\#}$)$_2$ZrCl$_2$, *rac*-($^{3\text{-Et}}$Ind$^{\#}$)$_2$HfCl$_2$ and ^{Me2}SB($^{3\text{-Et}}$I*)ZrCl$_2$ as a function of temperature of polymerisation.

The molecular weights of the resulting polyethylenes of homogeneous ethylene polymerisation using *rac*-($^{3\text{-Et}}$Ind$^{\#}$)$_2$ZrCl$_2$, *rac*-($^{3\text{-Et}}$Ind$^{\#}$)$_2$HfCl$_2$ and ^{Me2}SB($^{3\text{-Et}}$I*)ZrCl$_2$ complexes are shown in Figure 4.2 with their corresponding PDI values. All three complexes show general decreases in molecular weight with respect to temperature. This is due to the increase in the termination rate of ethylene polymerisation relative to the propagation rate at higher temperatures.[12] In general, the molecular weight and activity values are directly proportional which are the case for ^{Me2}SB($^{3\text{-Et}}$I*)ZrCl$_2$, *rac*-($^{3\text{-Et}}$Ind$^{\#}$)$_2$ZrCl$_2$ and *rac*-($^{3\text{-Et}}$Ind$^{\#}$)$_2$HfCl$_2$ (438500, 247600 and 160400 g/mol at 50 °C, respectively).

4.3 Complex immobilisation

4.3.1 Synthesis of sMAO supported metallocene catalysts

Since the discovery of MAO, metallocene catalysts have increasingly taken the main stage in the field of ethylene polymerisation. In order to avoid reactor fouling caused by hot spots in homogeneous processes, while maintaining the single-site nature of metallocenes, it is beneficial to immobilise the active catalytic components onto a heterogeneous support.[15]

Solid polymethylaluminoxane (sMAO) is a type of MAO which is insoluble in hydrocarbon solvents. As a result, sMAO can simultaneously act as both co-catalyst and heterogeneous support in ethylene polymerisation. Metallocene complexes immobilised on sMAO have been shown to display excellent ethylene polymerisation activities.[21]

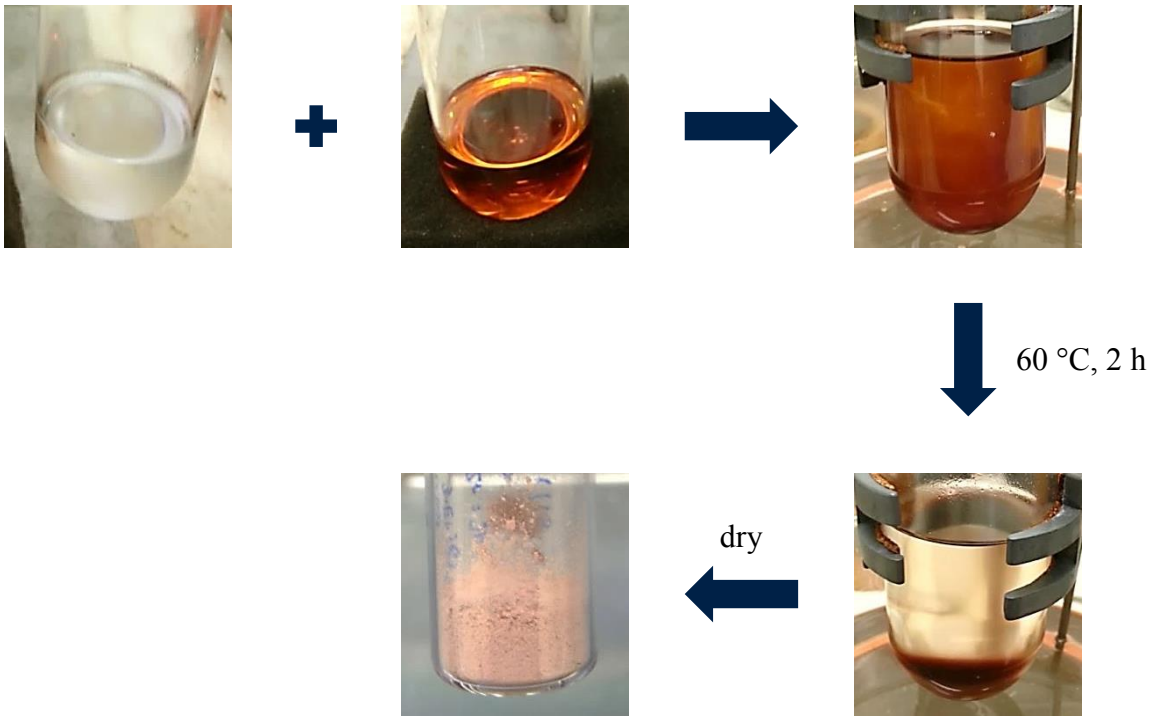


Figure 4.3. Synthesis of sMAO-[^{Me2}SB($^{3\text{-}Et}$I*)ZrCl$_2$].

An example of the immobilisation process is shown in Figure 4.3. An orange toluene solution of a 50:50 mixture of *rac*- and *meso*-^{Me2}SB($^{3\text{-}Et}$I*)ZrCl$_2$ was added to a colourless toluene slurry of sMAO. The mixture was then heated at 60 °C for 2 hours with occasional swirling. Since polymer morphology replicates that of the catalyst support, swirling instead of using a magnetic stirrer prevents aggregation of the support during the immobilisation process and hence preserves the catalyst morphology. After 2 hours, the mixture was left to cool to

room temperature resulting in a dark red suspension and a clear, colourless solution. Since the zirconocene solution is very intensely coloured, by observing the colour intensity of the solution phase during the immobilisation process, the colourless solution ensured that all zirconocene complex was adsorbed onto the sMAO. The solution was then decanted and the solid was dried *in vacuo* to afford sMAO-[^{Me2}SB($^{3\text{-}Et}$I*)ZrCl$_2$] catalyst as a pale pink, free-flowing powder.

4.3.2 Characterisation of sMAO-[^{Me2}SB($^{3\text{-}Et}$I*)ZrCl$_2$] catalyst

sMAO-[^{Me2}SB($^{3\text{-}Et}$I*)ZrCl$_2$] catalyst was characterised by ^{13}C CPMAS, ^{27}Al Hahn-echo MAS and ^{29}Si CPMAS solid state NMR spectroscopy as well as scanning electron microscopy.

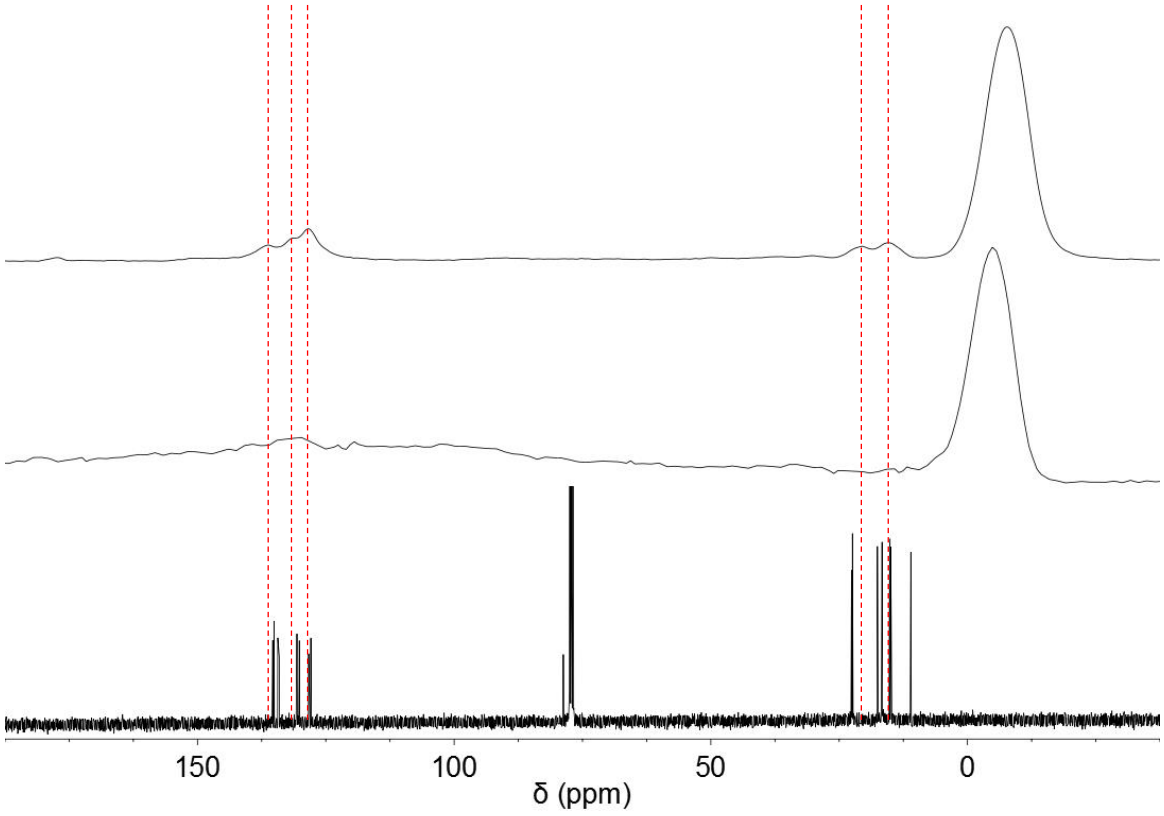


Figure 4.4. Stack plot of (top) ^{13}C CPMAS SSNMR spectrum (400 MHz, 298 K, 10 kHz) of sMAO-[^{Me2}SB($^{3\text{-}Et}$I*)ZrCl$_2$], (middle) ^{13}C CPMAS SSNMR spectrum (400 MHz, 298 K, 10 kHz) of sMAO and (bottom) ^{13}C{^{1}H} NMR spectrum (400 MHz, 298 K, chloroform-d_1) of *rac*-^{Me2}SB($^{3\text{-}Et}$I*)ZrCl$_2$.

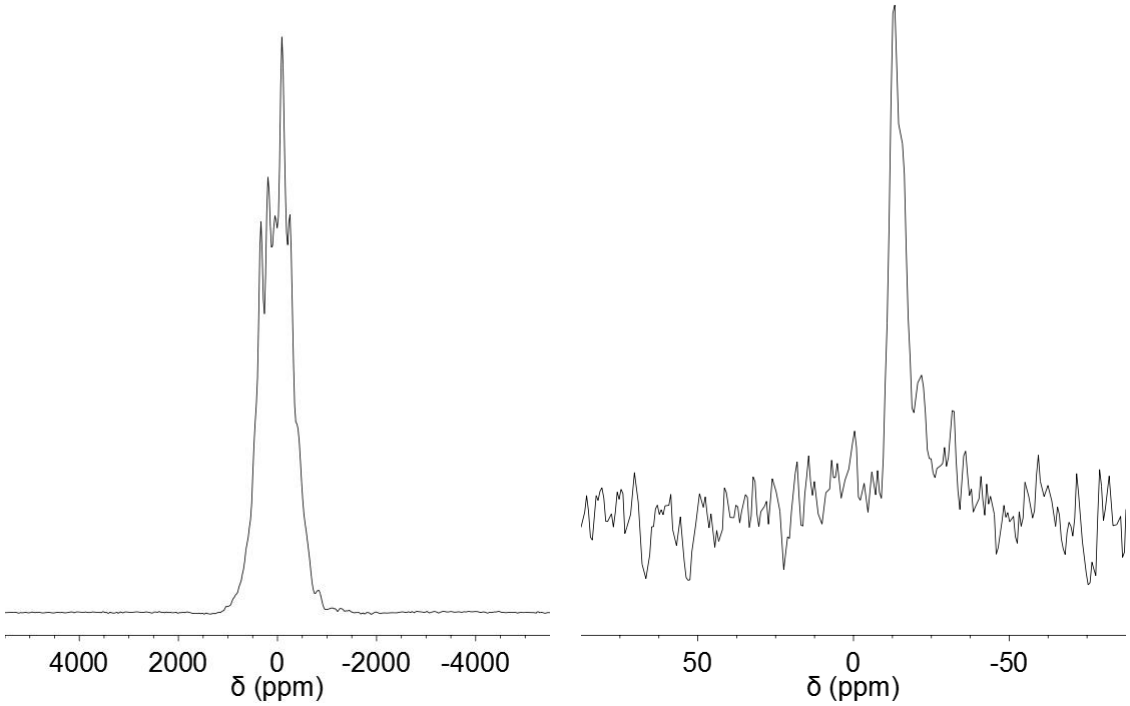


Figure 4.5. ^{27}Al Hahn-echo MAS SSNMR spectrum (400 MHz, 298 K, 15 kHz, left) and ^{29}Si CPMAS SSNMR spectrum (400 MHz, 298 K, 10 kHz, right) of sMAO-[^{Me2}SB($^{3\text{-}Et}$I*)ZrCl$_2$].

The ^{13}C CPMAS SSNMR spectrum of sMAO-[^{Me2}SB($^{3\text{-}Et}$I*)ZrCl$_2$] catalyst is shown in Figure 4.4 (top). A broad resonance at -8 ppm corresponds to the methyl groups of the sMAO support. The resonance slightly shifts in comparison with the corresponding signal of the unsupported sMAO (-5 ppm) shown in Figure 4.4 (middle). Due to the amorphous nature of sMAO, both resonances are very broad. Three broad resonances at 128, 131 and 136 ppm in the aromatic region are assigned to the indenyl signals of the immobilised ^{Me2}SB($^{3\text{-}Et}$I*)ZrCl$_2$ complex. Similarly, two broad resonances at 15 and 21 ppm are assigned to the alkyl signals of the complex. Both sets of resonances show slight shifts when compared to the ^{13}C{^{1}H} NMR spectrum of unsupported *rac*-^{Me2}SB($^{3\text{-}Et}$I*)ZrCl$_2$ in chloroform-d_1 (Figure 4.4, bottom). The ^{27}Al Hahn-echo MAS SSNMR spectrum of the catalyst shows a multiplet resonance at -92 ppm corresponding to the Al signals of the sMAO (Figure 4.5, left). The ^{29}Si CPMAS SSNMR spectrum of the catalyst shows a singlet resonance at -13 ppm corresponding to the silyl bridge of the ^{Me2}SB($^{3\text{-}Et}$I*)ZrCl$_2$. A shoulder observed on the right side of the peak infers a presence of, at least, two Si species which is consistent with the fact that a 50:50 mixture of the *rac* and *meso* isomers was used in the immobilision process. These NMR findings confirm that ^{Me2}SB($^{3\text{-}Et}$I*)ZrCl$_2$ was successfully immobilised onto sMAO and the ligand framework remained intact during the process.

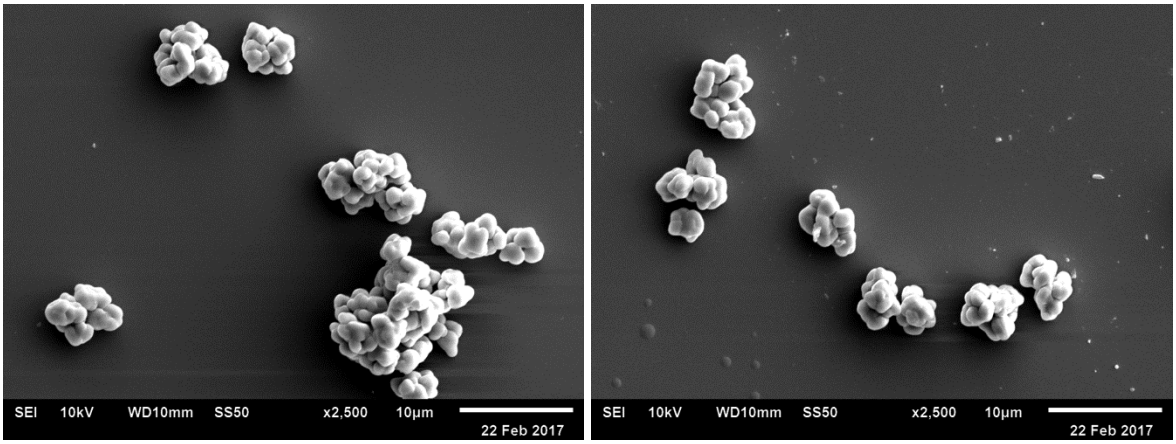


Figure 4.6. SEM images of sMAO before (left) and after (right) complex immobilisation.

The morphology of sMAO support shown in Figure 4.6 (left) resembles aggregated popcorn shaped particles. After the immobilisation process, the sMAO-[^{Me_2}SB($^{3\text{-}Et}$I*)ZrCl$_2$] catalyst retained the support morphology albeit less aggregated (Figure 4.6, right).

4.4 Heterogeneous ethylene polymerisation

Heterogeneous ethylene polymerisation using the synthesised substituted indenyl group 4 complexes immobilised onto sMAO were carried out. For a heterogeneous ethylene polymerisation test, a supported metallocene catalyst (10.0 mg, 1.0 eq$_{Complex}$), TIBA (1000 eq) and hexane (50 mL) were added to a 150 mL Rotaflo ampoule containing a stirrer bar. The ampoule was sealed and degassed before being heated to the desired temperature at the stirring speed of 1000 rpm. The ampoule was then opened to ethylene (2 bar). On completion of the test, the ampoule was closed to ethylene and degassed. The resulting polyethylene was filtered on a glass sintered frit, washed with pentane (2 x 25 mL) and dried. All polymerisation tests were run for 30 minutes.

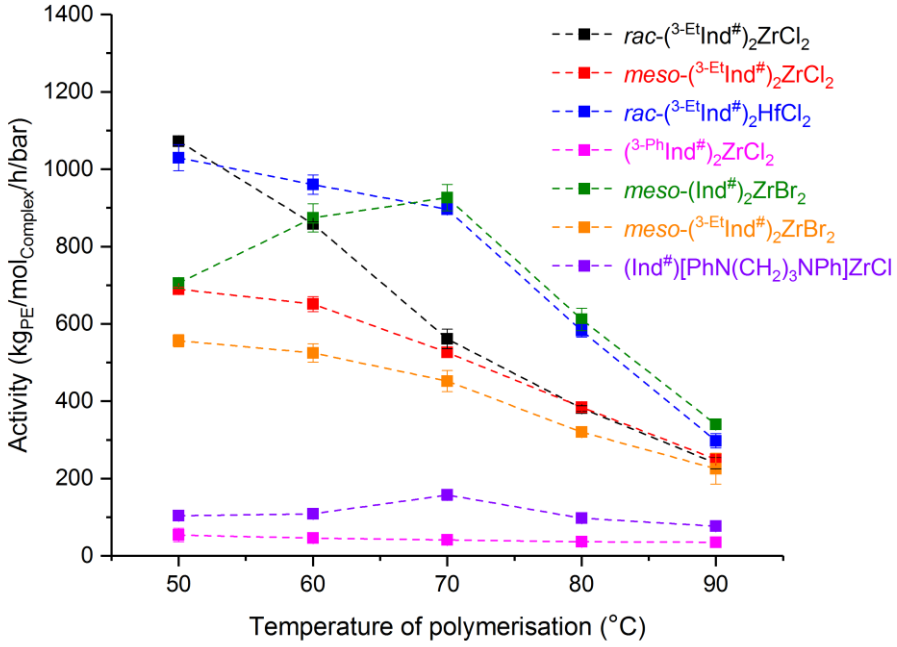


Figure 4.7. Heterogeneous ethylene polymerisation activity of sMAO supported unbridged substituted indenyl complexes as a function of temperature of polymerisation.

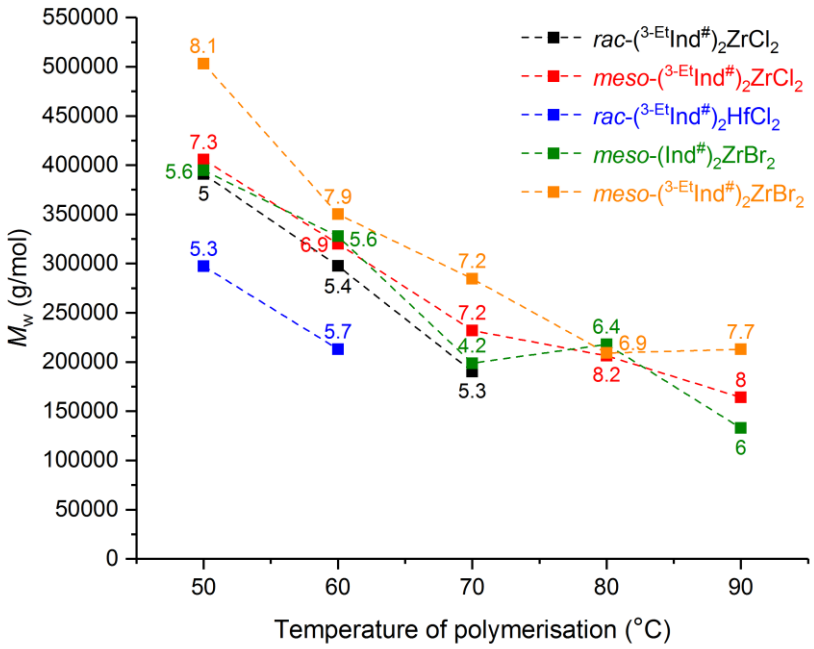


Figure 4.8. Molecular weight of the resulting polyethylenes of heterogeneous ethylene polymerisation using sMAO supported unbridged substituted indenyl complexes as a function of temperature of polymerisation.

The heterogeneous ethylene polymerisation activities of *rac*-($^{3\text{-Et}}$Ind$^{\#}$)$_2$ZrCl$_2$, *meso*-($^{3\text{-Et}}$Ind$^{\#}$)$_2$ZrCl$_2$, *rac*-($^{3\text{-Et}}$Ind$^{\#}$)$_2$HfCl$_2$, ($^{3\text{-Ph}}$Ind$^{\#}$)$_2$ZrCl$_2$, *meso*-(Ind$^{\#}$)$_2$ZrBr$_2$, *meso*-($^{3\text{-Et}}$Ind$^{\#}$)$_2$ZrBr$_2$ and (Ind$^{\#}$)(PhN(CH$_2$)$_3$NPh)ZrCl immobilised onto sMAO were recorded over a temperature range of 50 to 90 °C (Figure 4.7). ($^{3\text{-Ph}}$Ind$^{\#}$)$_2$ZrCl$_2$ and (Ind$^{\#}$)(PhN(CH$_2$)$_3$NPh)ZrCl display abysmal activities with the maximum values of 54 (50 °C) and 158 kg$_{PE}$/mol$_{Complex}$/h/bar (70 °C), respectively, possibly due to the steric hindrance of the phenyl groups. The remaining complexes exhibit similar activities with decreasing trends with respect to increasing temperature, with the exception of *meso*-(Ind$^{\#}$)$_2$ZrBr$_2$ which has a maximum activity of 927 kg$_{PE}$/mol$_{Complex}$/h/bar at 70 °C. *rac*-($^{3\text{-Et}}$Ind$^{\#}$)$_2$ZrCl$_2$, *meso*-($^{3\text{-Et}}$Ind$^{\#}$)$_2$ZrCl$_2$, *rac*-($^{3\text{-Et}}$Ind$^{\#}$)$_2$HfCl$_2$ and *meso*-($^{3\text{-Et}}$Ind$^{\#}$)$_2$ZrBr$_2$ display their maximum activities at 50 °C (1072, 690, 1030 and 557 kg$_{PE}$/mol$_{Complex}$/h/bar, respectively). From these comparisons, it can be concluded that, with the exception of 3-Ph modification, the complex alterations only have small impacts on the ethylene polymerisation activity.

The molecular weights of the resulting polyethylenes of heterogeneous ethylene polymerisation using the sMAO supported unbridged substituted indenyl complexes are shown in Figure 4.8 with their corresponding PDI values. One of the prominent features of the trends are the very high molecular weight of 503100 g/mol for *meso*-($^{3\text{-Et}}$Ind$^{\#}$)$_2$ZrCl$_2$ at 50 °C despite having comparatively low activity. The other interesting feature is that *rac*-($^{3\text{-Et}}$Ind$^{\#}$)$_2$HfCl$_2$ produced relatively low molecular weight polyethylenes (297300 g/mol at 50 °C).

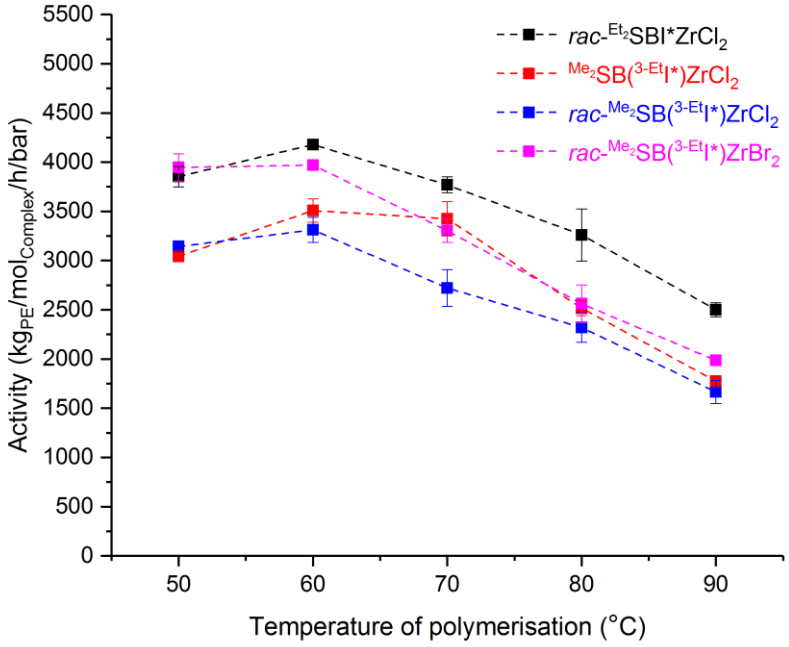


Figure 4.9. Heterogeneous ethylene polymerisation activity of sMAO supported silyl bridged substituted indenyl complexes as a function of temperature of polymerisation.

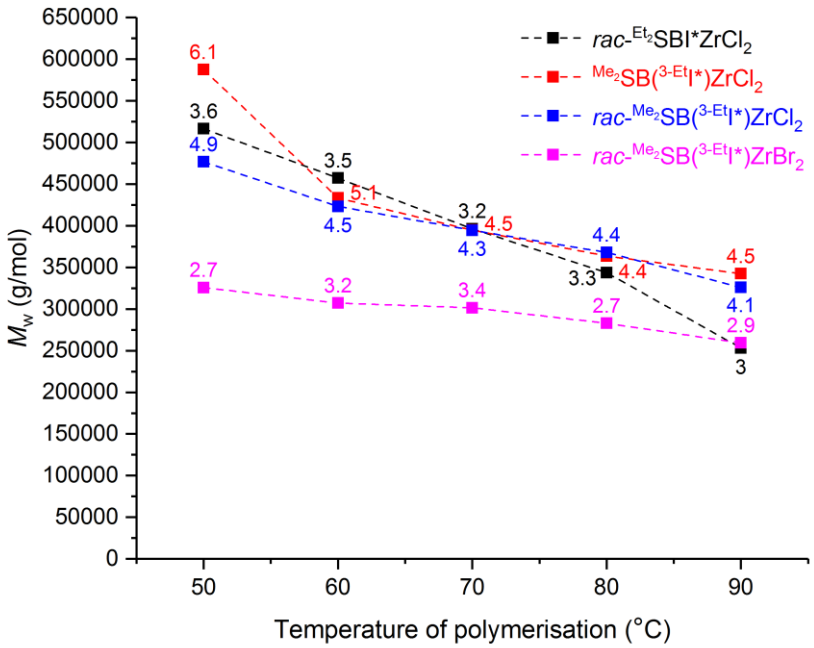


Figure 4.10. Molecular weight of the resulting polyethylenes of heterogeneous ethylene polymerisation using sMAO supported silyl bridged substituted indenyl complexes as a function of temperature of polymerisation.

The heterogeneous ethylene polymerisation activities of *rac*-^{Et_2}SBI*ZrCl$_2$, ^{Me_2}SB($^{3\text{-}Et}$I*)ZrCl$_2$, *rac*-^{Me_2}SB($^{3\text{-}Et}$I*)ZrCl$_2$, and *rac*-^{Me_2}SB($^{3\text{-}Et}$I*)ZrBr$_2$ immobilised onto sMAO were recorded over a temperature range of 50 to 90 °C (Figure 4.9). All silyl bridged complexes display similar trends with their maximum activities at 60 °C and are shown to be substantially more active than their unbridged counterparts. *rac*-^{Et_2}SBI*ZrCl$_2$ is shown to be the most active followed closely by *rac*-^{Me_2}SB($^{3\text{-}Et}$I*)ZrBr$_2$ and *rac*-^{Me_2}SB($^{3\text{-}Et}$I*)ZrCl$_2$ (4179, 3971 and 3312 kg$_{PE}$/mol$_{Complex}$/h/bar, respectively). Unusually, a 50:50 mixture of *rac*- and *meso*-^{Me_2}SB($^{3\text{-}Et}$I*)ZrCl$_2$ is shown to be slightly more active than the pure *rac* isomer (3507 kg$_{PE}$/mol$_{Complex}$/h/bar compared to 3312 kg$_{PE}$/mol$_{Complex}$/h/bar at 60 °C) implying that both isomers have similar activities.

The molecular weights of the resulting polyethylenes of heterogeneous ethylene polymerisation using the sMAO supported silyl bridged substituted indenyl complexes are shown in Figure 4.10 with their corresponding PDI values. Interestingly, *rac*-^{Me_2}SB($^{3\text{-}Et}$I*)ZrBr$_2$ produced polyethylene with significantly lower molecular weight compared to its dichloro analogue while maintaining similar polymerisation activity (325700 g/mol compared to 476700 g/mol at 50 °C).

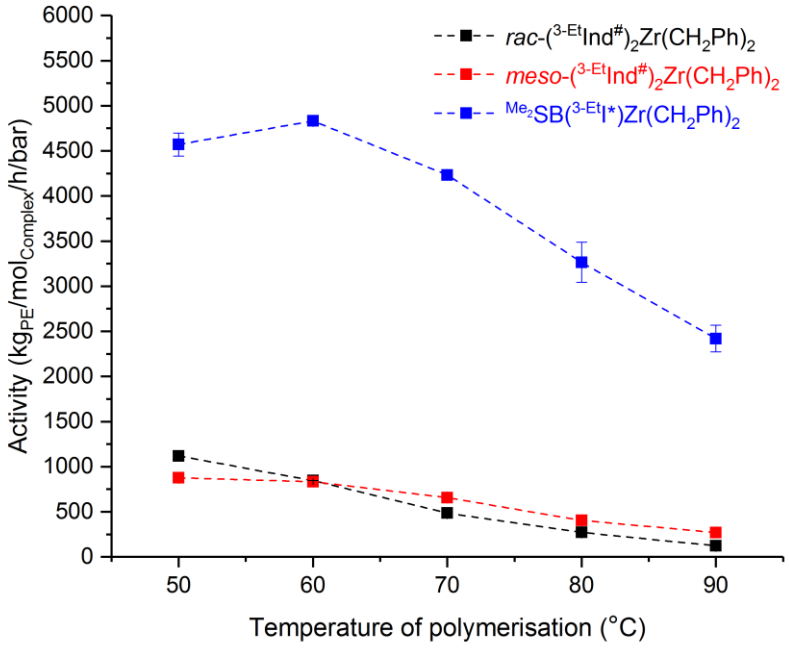


Figure 4.11. Heterogeneous ethylene polymerisation activity of sMAO supported dibenzyl substituted indenyl complexes as a function of temperature of polymerisation.

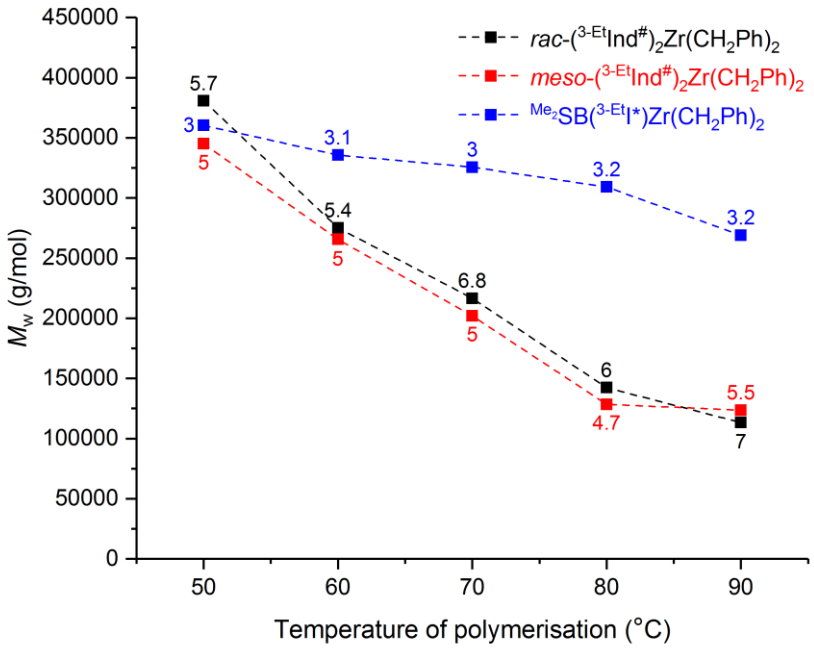


Figure 4.12. Molecular weight of the resulting polyethylenes of heterogeneous ethylene polymerisation using sMAO supported dibenzyl substituted indenyl complexes as a function of temperature of polymerisation.

The heterogeneous ethylene polymerisation activities of *rac*-($^{3\text{-Et}}$Ind$^{\#}$)$_2$Zr(CH$_2$Ph)$_2$, *meso*-($^{3\text{-Et}}$Ind$^{\#}$)$_2$Zr(CH$_2$Ph)$_2$ and ^{Me2}SB($^{3\text{-Et}}$I*)Zr(CH$_2$Ph)$_2$ immobilised onto sMAO were recorded over a temperature range of 50 to 90 °C (Figure 4.11). ^{Me2}SB($^{3\text{-Et}}$I*)Zr(CH$_2$Ph)$_2$ exhibits a maximum activity of 4832 kg$_{PE}$/mol$_{Complex}$/h/bar at 60 °C which is considerably higher than that of its dichloro analogue, ^{Me2}SB($^{3\text{-Et}}$I*)ZrCl$_2$ (3507 kg$_{PE}$/mol$_{Complex}$/h/bar). Likewise, *rac*- and *meso*-($^{3\text{-Et}}$Ind$^{\#}$)$_2$Zr(CH$_2$Ph)$_2$ show slight increases in their maximum activities at 50 °C (1119 and 877 kg$_{PE}$/mol$_{Complex}$/h/bar, respectively) in comparison to their dichloro counterparts (1072 and 690 kg$_{PE}$/mol$_{Complex}$/h/bar, respectively). The maximum activity of ^{Me2}SB($^{3\text{-Et}}$I*)Zr(CH$_2$Ph)$_2$ is similar to that of *meso*-EBI*Zr(CH$_2$Ph)$_2$ (5179 kg$_{PE}$/mol$_{Complex}$/h/bar at 60 °C).[21]

The molecular weights of the resulting polyethylenes of heterogeneous ethylene polymerisation using the sMAO supported dibenzyl substituted indenyl complexes are shown in Figure 4.12 with their corresponding PDI values. The molecular weight trends for *rac*- and *meso*-($^{3\text{-Et}}$Ind$^{\#}$)$_2$Zr(CH$_2$Ph)$_2$ show similar sharp decline with respect to increasing temperature. In contrast, the molecular weight trend for ^{Me2}SB($^{3\text{-Et}}$I*)Zr(CH$_2$Ph)$_2$ displays more tolerant response towards temperature increase. Coincidentally, all three complexes produced

polyethylenes with similar molecular weights at 50 °C (380700 g/mol for *rac*-($^{3\text{-Et}}$Ind$^{\#}$)$_2$Zr(CH$_2$Ph)$_2$, 345100 g/mol for *meso*-($^{3\text{-Et}}$Ind$^{\#}$)$_2$Zr(CH$_2$Ph)$_2$ and 360400 g/mol for ^{Me2}SB($^{3\text{-Et}}$I*)Zr(CH$_2$Ph)$_2$).

4.5 Polymer characterisation

The resulting polyethylene of heterogeneous ethylene polymerisation using sMAO-[^{Me2}SB($^{3\text{-Et}}$I*)ZrCl$_2$] catalyst was characterised by powder X-ray diffraction (XRD) and SEM.

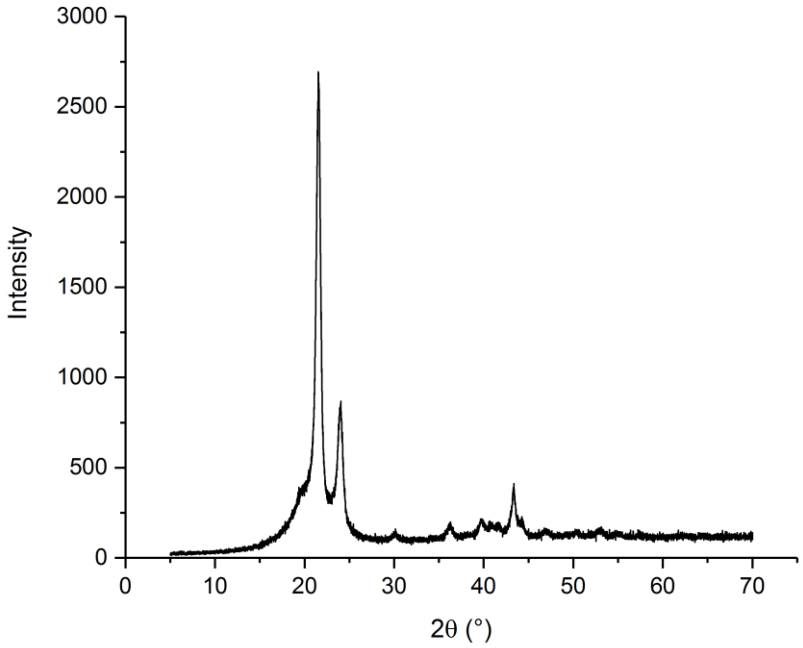


Figure 4.13. XRD spectrum of the resulting polyethylene of heterogeneous ethylene polymerisation using sMAO-[^{Me2}SB($^{3\text{-Et}}$I*)ZrCl$_2$].

Figure 4.13 shows peaks at 21.5° and 24° corresponding to (110) and (200) planes of high-density polyethylene (HDPE), respectively.[22] The sharp nature of the XRD spectrum confirms the high crystallinity of the HDPE polymer.[23]

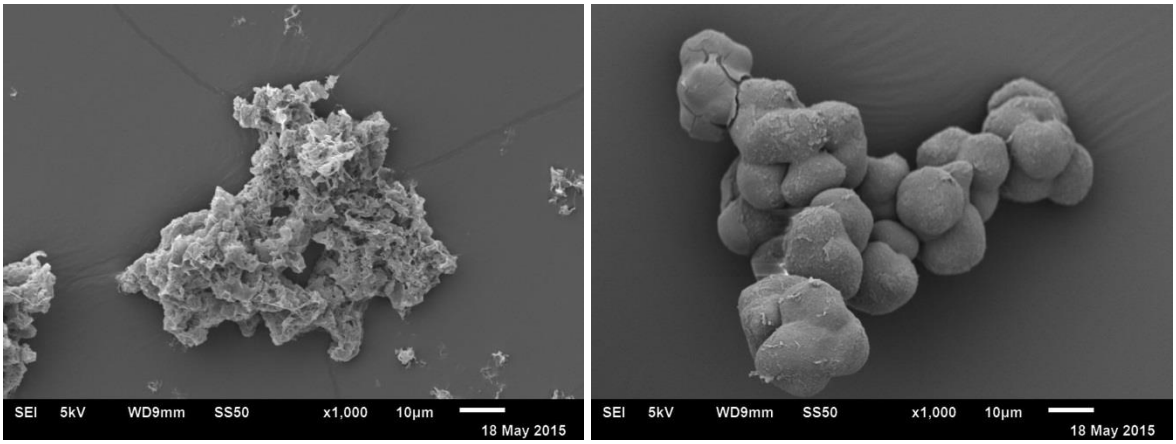


Figure 4.14. SEM images of the resulting polyethylenes of homogeneous ethylene polymerisation using $^{Me2}SB(^{3\text{-}Et}I^*)ZrCl_2$ (left) and heterogeneous ethylene polymerisation using sMAO-[$^{Me2}SB(^{3\text{-}Et}I^*)ZrCl_2$] (right).

The resulting polyethylene of homogeneous ethylene polymerisation using $^{Me2}SB(^{3\text{-}Et}I^*)ZrCl_2$ complex shows very poorly undefined morphology (Figure 4.14, left). On the other hand, the morphology of the resulting polyethylene of heterogeneous ethylene polymerisation using sMAO-[$^{Me2}SB(^{3\text{-}Et}I^*)ZrCl_2$] catalyst closely resembles that of the corresponding sMAO support albeit more aggregated (Figure 4.14, right).

4.6 Conclusions

Chapter Four describes homogeneous and heterogeneous ethylene polymerisation using the synthesised substituted indenyl group 4 complexes. The complexes were immobilised onto a highly unique sMAO support. The sMAO-[$^{Me2}SB(^{3\text{-}Et}I^*)ZrCl_2$] catalyst was characterised by solid state NMR spectroscopy and SEM showing that the complex ligand framework and support morphology are retained after the immobilisation. The ethylene polymerisation results show that the silyl bridged complexes are substantially more active compared to their unbridged relatives with *rac*-$^{Et2}SBI^*ZrCl_2$ being the most active. Interestingly, *rac*- and *meso*-$^{Me2}SB(^{3\text{-}Et}I^*)ZrCl_2$ display similar activities. Dibenzylation of the dichloro complexes increases the ethylene polymerisation activity. The resulting polyethylenes were characterised by GPC, XRD and SEM.

4.7 References

1 G. G. Hlatky, *Coord. Chem. Rev.*, 1999, **181**, 243–296.
2 G. G. Hlatky, *Coord. Chem. Rev.*, 2000, **199**, 235–329.

3 P. C. Möhring and N. J. Coville, *J. Mol. Catal.*, 1992, **77**, 41–50.
4 P. C. Möhring and N. J. Coville, *J. Organomet. Chem.*, 1994, **479**, 1–29.
5 P. C. Möhring, N. Vlachakis, N. E. Grimmer and N. J. Coville, *J. Organomet. Chem.*, 1994, **483**, 159–166.
6 P. C. Möhring and N. J. Coville, *J. Mol. Catal. A Chem.*, 1995, **96**, 181–195.
7 P. C. Möhring and N. J. Coville, *Coord. Chem. Rev.*, 2006, **250**, 18–35.
8 B. Wang, *Coord. Chem. Rev.*, 2006, **250**, 242–258.
9 W. Kaminsky, *Macromol. Chem. Phys.*, 1996, **197**, 3907–3945.
10 W. Kaminsky, *J. Chem. Soc. Dalt. Trans.*, 1998, 1413–1418.
11 W. Kaminsky and A. Laban, *Appl. Catal. A Gen.*, 2001, **222**, 47–61.
12 L. D'Agnillo, J. B. P. Soares and A. Penlidis, *Macromol. Chem. Phys.*, 1998, **199**, 955–962.
13 H. Sinn, W. Kaminsky, H.-J. Vollmer and R. Woldt, *Angew. Chemie*, 1980, **92**, 396–402.
14 W. Kaminsky, M. Miri, H. Sinn and R. Woldt, *Die Makromol. Chemie, Rapid Commun.*, 1983, **4**, 417–421.
15 J. R. Severn, J. C. Chadwick, R. Duchateau and N. Friederichs, *Chem. Rev.*, 2005, **105**, 4073–4147.
16 F. Azimfar, I. Kohsari and S. M. Pourmortazavi, *J. Inorg. Organomet. Polym. Mater.*, 2009, **19**, 181–186.
17 J.-C. Buffet, T. A. Q. Arnold, Z. R. Turner, P. Angpanitcharoen and D. O'Hare, *RSC Adv.*, 2015, **5**, 87456–87464.
18 T. A. Q. Arnold, J.-C. Buffet, Z. R. Turner and D. O'Hare, *J. Organomet. Chem.*, 2015, **792**, 55–65.
19 N. E. Grimmer, N. J. Coville and C. B. de Koning, *J. Organomet. Chem.*, 2002, **642**, 195–202.
20 I. Bravo, C. Alonso-Moreno, F. Carrillo-Hermosilla, I. López-Solera, A. Antiñolo and J. Albaladejo, *Chempluschem*, 2015, **80**, 963–972.
21 T. A. Q. Arnold, Z. R. Turner, J.-C. Buffet and D. O'Hare, *J. Organomet. Chem.*, 2016, **822**, 85–90.
22 K.-T. Li, C.-L. Dai and C.-W. Kuo, *Catal. Commun.*, 2007, **8**, 1209–1213.
23 F. M. Mirabella Jr. and E. A. Ford, *J. Polym. Sci. Part B Polym. Phys.*, 1987, **25**, 777–790.

Chapter Five – ^{Me2}SB($^{3\text{-}Et}$I*)ZrCl$_2$ polymerisation studies

5.1 Introduction

There are three critical components to heterogeneous ethylene polymerisation; a metallocene complex, a co-catalyst (MAO is the most commonly used) and a solid support.[1] Extensive research has shown that the best immobilisation method for hydroxyl based supports is to precontact a solution of MAO with a calcined support prior to complex immobilisation.[2] This helps reduce the concentration of hydroxyl groups on the support surface and, hence, minimise the deactivation of metallocene complex. Additionally, the trace amount of TMA left in MAO from its synthesis reacts with the surface hydroxyl groups. This can lead to increased activity in metallocene-catalysed polymerisation as the presence of TMA can depress activity via the formation of dormant alkyl-bridged species, $[Cp_2Zr(\mu\text{-}R)(\mu\text{-}Me)AlMe_2]^+$, blocking monomer coordination to the metal centre. TMA has a particularly large depressing rate effect with hafnocenes due to their high stability.[3,4]

Ethylene polymerisation using metallocene catalysts has a wide range of industrial applications depending on the chosen polymerisation conditions. With the addition of hydrogen as a chain transfer agent, metallocene catalysts can produce very low molecular weight polyethylene waxes.[5] Linear low-density polyethylene (LLDPE) can be produced by the copolymerisation of ethylene and 1-hexene co-monomer using metallocene catalysts.[6–9]

5.2 Heterogeneous supports

5.2.1 Synthesis of SSMAO- and LDHMAO-[^{Me2}SB($^{3\text{-}Et}$I*)ZrCl$_2$] catalysts

Silica or AMO-LDH ($Mg_{0.75}Al_{0.25}(OH)_2(CO_3)_{0.125}$) was dispersed in toluene to form a colourless slurry and MAO was dissolved in toluene to form a colourless solution which was then quickly added to the previous slurry at room temperature. The reaction mixture was heated to 80 °C for 2 hours with occasional swirling. The resulting colourless slurry was then left to cool down to room temperature and dried *in vacuo* to afford silica supported methylaluminoxane (SSMAO) or layered double hydroxide supported methylaluminoxane (LDHMAO) as a white solid.



Figure 5.1. Synthesis of LDHMAO-[$^{Me2}SB(^{3\text{-}Et}I^{*})ZrCl_2$].

The pictural respresentation of the synthesis of LDHMAO-[$^{Me2}SB(^{3\text{-}Et}I^{*})ZrCl_2$] solid catalyst is shown in Figure 5.1. LDHMAO was dispersed in toluene to form a colourless slurry. A 50:50 mixture of *rac*- and *meso*-$^{Me2}SB(^{3\text{-}Et}I^{*})ZrCl_2$ was dissolved in toluene to form an orange solution which was then quickly added to the LDHMAO at room temperature. The reaction mixture was heated to 60 °C for 2 hours with occasional swirling. The yellow solid was allowed to settle from the clear, colourless solution which was decanted, and the solid was dried *in vacuo* to afford the product as an off-white solid in 94% yield. SSMAO-[$^{Me2}SB(^{3\text{-}Et}I^{*})ZrCl_2$] synthesis also followed the synthetic procedure described above in 90% yield.

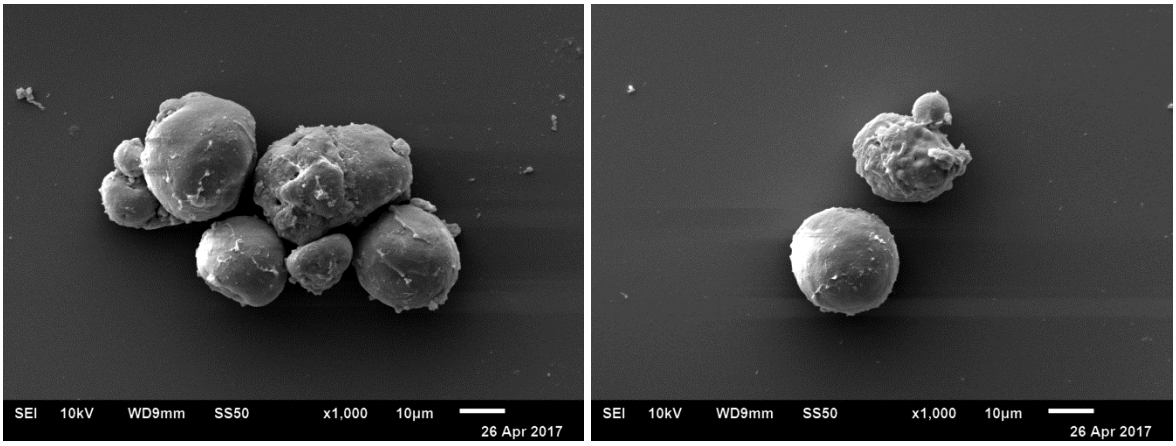


Figure 5.2. SEM images of SSMAO before (left) and after (right) complex immobilisation.

Figure 5.2 shows the spherical morphology of SSMAO support (left) which became less aggregated after the immobilisation process (right) while maintained the spherical shape. The morphology of LDHMAO is shown in Figure 5.3 (left). The unique morphology of AMO-LDH has small platelets forming loose flower-shape agglomerates, which have a more exposed surface compared to the densely stacked morphology of conventional LDHs.[10] Similar to other supports, LDHMAO became less aggregated after complex immobilisation as a result of being dispersed in a hydrocarbon solvent (Figure 5.3, right).

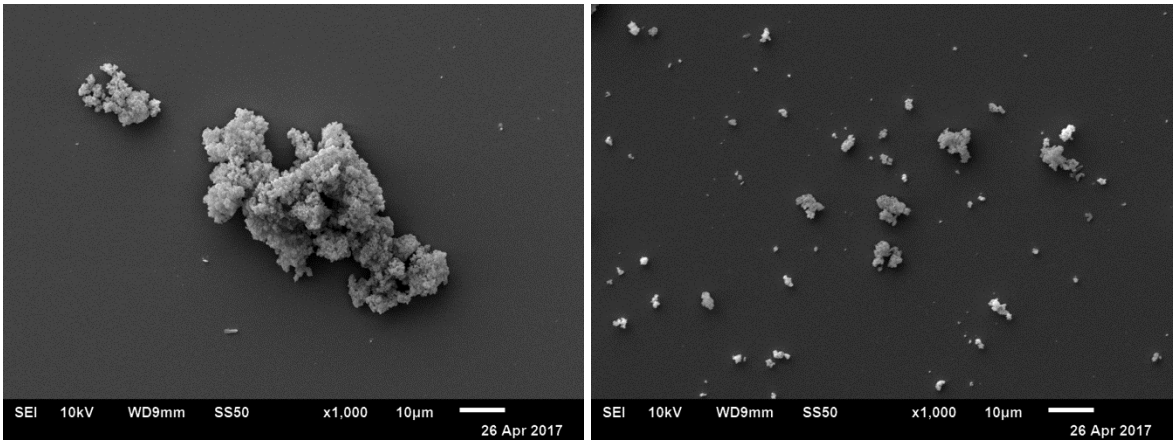


Figure 5.3. SEM images of LDHMAO before (left) and after (right) complex immobilisation.

5.2.2 Support comparisons

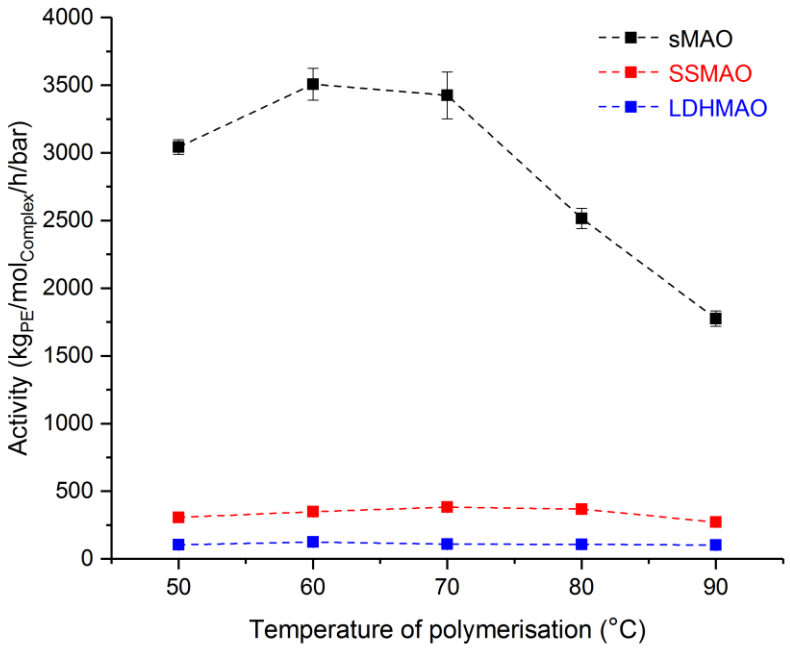


Figure 5.4. Heterogeneous ethylene polymerisation activity of ^{Me2}SB($^{3\text{-}Et}$I*)ZrCl$_2$ immobilised onto sMAO, SSMAO and LDHMAO as a function of temperature of polymerisation.

The heterogeneous ethylene polymerisation activities of ^{Me2}SB($^{3\text{-}Et}$I*)ZrCl$_2$ immobilised onto sMAO, SSMAO and LDHMAO were recorded over a temperature range of 50 to 90 °C (Figure 5.4). All three catalysts exhibit curve trends with a maximum activity at 60 °C for sMAO- and LDHMAO-[^{Me2}SB($^{3\text{-}Et}$I*)ZrCl$_2$], and 70 °C for SSMAO-[^{Me2}SB($^{3\text{-}Et}$I*)ZrCl$_2$]. ^{Me2}SB($^{3\text{-}Et}$I*)ZrCl$_2$ immobilised onto sMAO is significantly more active when compared to

SSMAO and LDHMAO (3507, 383 and 125 $kg_{PE}/mol_{Complex}/h/bar$, respectively). Similar to the homogeneous polymerisation comparison, the maximum activity of ^{Me2}SB($^{3\text{-}Et}$I*)ZrCl$_2$ immobilised onto SSMAO compares unfavourably with that of its permethylated analogue, SSMAO-[*rac*-^{Me2}SBI*ZrCl$_2$] (725 $kg_{PE}/mol_{Complex}/h/bar$ at 80 °C).[11]

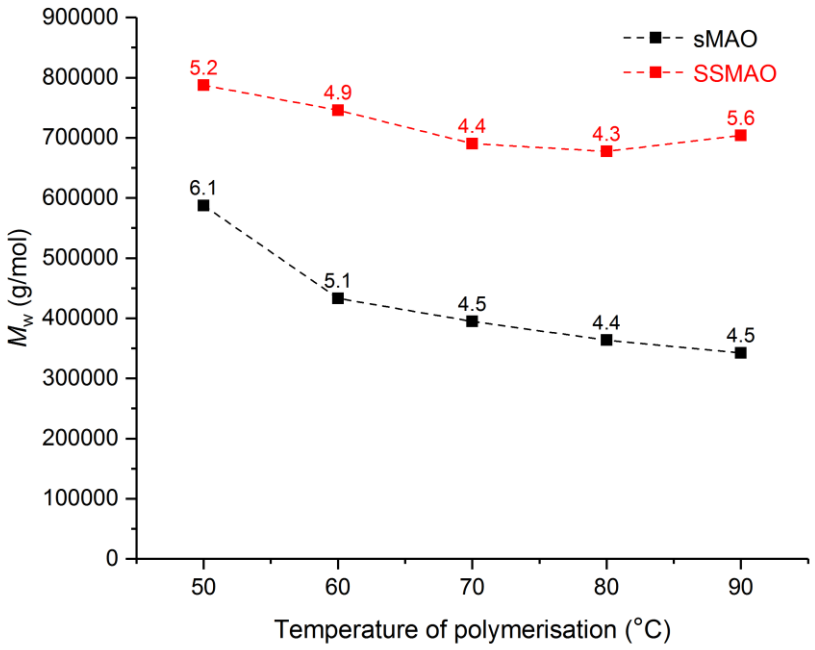


Figure 5.5. Molecular weight of the resulting polyethylenes of heterogeneous ethylene polymerisation using ^{Me2}SB($^{3\text{-}Et}$I*)ZrCl$_2$ immobilised onto sMAO and SSMAO as a function of temperature of polymerisation.

The molecular weights of the resulting polyethylenes of heterogeneous ethylene polymerisation using sMAO- and SSMAO-^{Me2}SB($^{3\text{-}Et}$I*)ZrCl$_2$ are shown in Figure 5.5 with their corresponding PDI values. SSMAO-^{Me2}SB($^{3\text{-}Et}$I*)ZrCl$_2$ produced polyethylenes with significantly higher molecular weights in comparisons with the sMAO catalyst (787400 g/mol compared to 587400 g/mol at 50 °C). Therefore, despite compromising on the activity, silica can potentially be the support of choice for high molecular weight polyethylene production.

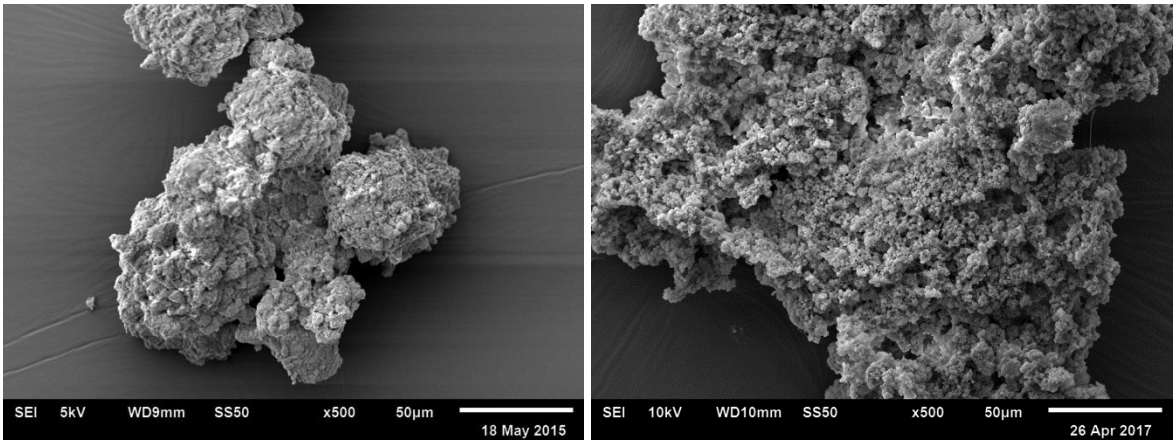


Figure 5.6. SEM images of the resulting polyethylenes of heterogeneous ethylene polymerisation using $^{Me2}SB(^{3\text{-}Et}I^*)ZrCl_2$ immobilised onto SSMAO (left) and LDHMAO (right).

SEM images of the resulting polyethylenes of heterogeneous ethylene polymerisation using SSMAO- and LDHMAO-$^{Me2}SB(^{3\text{-}Et}I^*)ZrCl_2$ catalysts are shown in Figure 5.6. Both display very poor undefined morphologies which are potentially troublesome for post-synthesis process in industrial settings.

5.3 Polymerisation condition optimisation

5.3.1 Impurity scavenger

Trialkylaluminiums play an important role in ethylene polymerisation as impurity scavenger. They react with any traces of moisture or reactive functional groups present in the polymerisation setup and, hence, prevent the decomposition of the critical metallocene complex.[12] However, they can also depress activity via the formation of dormant alkyl-bridged species, $[Cp_2Zr(\mu\text{-}R)(\mu\text{-}Me)AlMe_2]^+$, blocking monomer coordination to the transition metal.[3,4]

Figure 5.7 shows the heterogeneous ethylene polymerisation activities of sMAO-$[^{Me2}SB(^{3\text{-}Et}I^*)ZrCl_2]$ with MAO, TMA, TEA and TIBA as impurity scavenger. Comparison between the trialkylaluminiums shows TIBA to be the most effective scavenger followed in order by TEA and TMA (4533, 4390 and 3562 $kg_{PE}/mol_{Complex}/h/bar$, respectively). This order is consistent with the tendency of the trialkylaluminiums to form the dormant alkyl-bridged species (TMA > TEA > TIBA). Using MAO as the impurity scavenger caused leaching of the metallocene complex into the solution initiating homogeneous polymerisation instead. This disrupted the stirring of the reactor and reduced the activity.

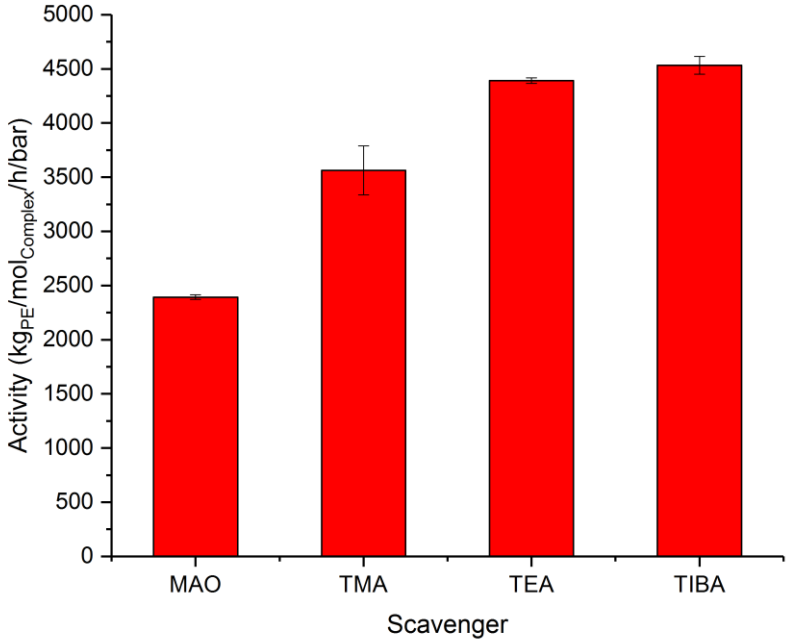


Figure 5.7. Heterogeneous ethylene polymerisation activity of sMAO-[$^{Me2}SB(^{3\text{-}Et}I^{*})ZrCl_2$] with MAO, TMA, TEA and TIBA as impurity scavenger.

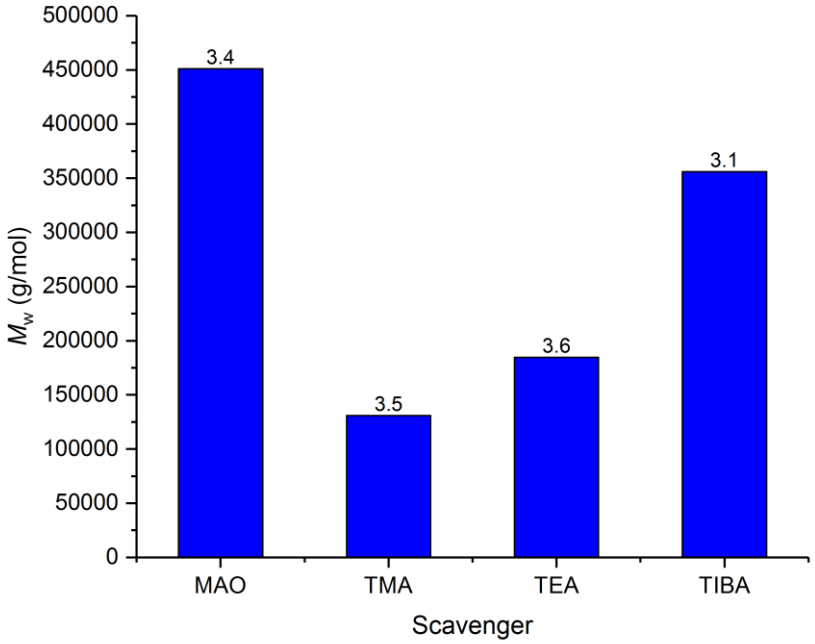


Figure 5.8. Molecular weight of the resulting polyethylenes of heterogeneous ethylene polymerisation using sMAO-[$^{Me2}SB(^{3\text{-}Et}I^{*})ZrCl_2$] with MAO, TMA, TEA and TIBA as impurity scavenger.

The molecular weights of the resulting polyethylenes of heterogeneous ethylene polymerisation using sMAO-[^{Me2}SB($^{3\text{-}Et}$I*)ZrCl$_2$] with the aforementioned impurity scavengers are consistent with the activity trend and the fact that, in the case of MAO, the reaction was essentially transformed into an homogeneous polymerisation (Figure 5.8). In summary, TIBA was found to be the best performing impurity scavenger for this system.

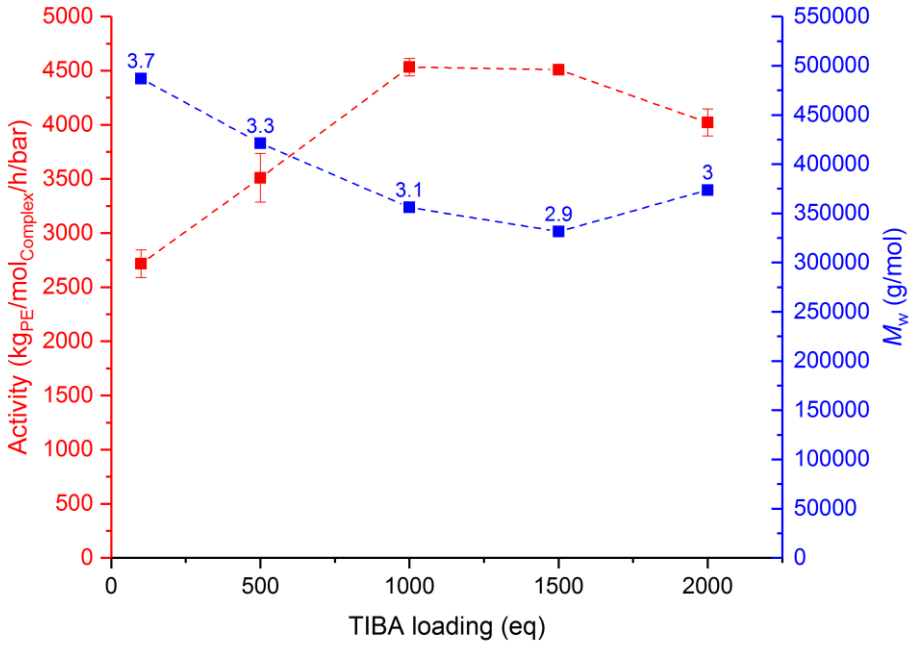


Figure 5.9. Activity (red) and molecular weight (blue) of the resulting polyethylenes of heterogeneous ethylene polymerisation using sMAO-[^{Me2}SB($^{3\text{-}Et}$I*)ZrCl$_2$] as a function of TIBA loading.

To balance between the opposing effects of TIBA, the optimisation of the catalyst activity with respect to TIBA loading was carried out (Figure 5.9, red). 1000 equivalents of TIBA are shown to be the optimal concentration to remove impurities from the system but not high enough to retard the polymerisation (4533 kg$_{PE}$/mol$_{Complex}$/h/bar).

The molecular weight trend of the resulting polyethylenes as a function of TIBA loading, shown in Figure 5.9 (blue), nearly mirrors the activity trend. A decrease in the molecular weight from 487000 to 331500 g/mol (from 100 to 1500 eq) was observed. This is because, at high concentrations, TIBA can act as a chain transfer agent increasing the termination rate of ethylene polymerisation.[13] Interestingly, the PDI also decreases with respect to increased TIBA loading.

5.3.2 Complex loading

The complex loading, inferring to the surface concentration of immobilised metallocene complex, was also optimised (Figure 5.10). As the loading decreases (increase in Al/Zr ratio), the ethylene polymerisation activity (red) increases due to the easier access to the monomer by each metallocene complex. However, when the productivity (blue) is considered, there is an optimal Al/Zr ratio of 200 which maximises the polymerisation capability per gram of the catalyst (0.329 $kg_{PE}/g_{Catalyst}/h/bar$).

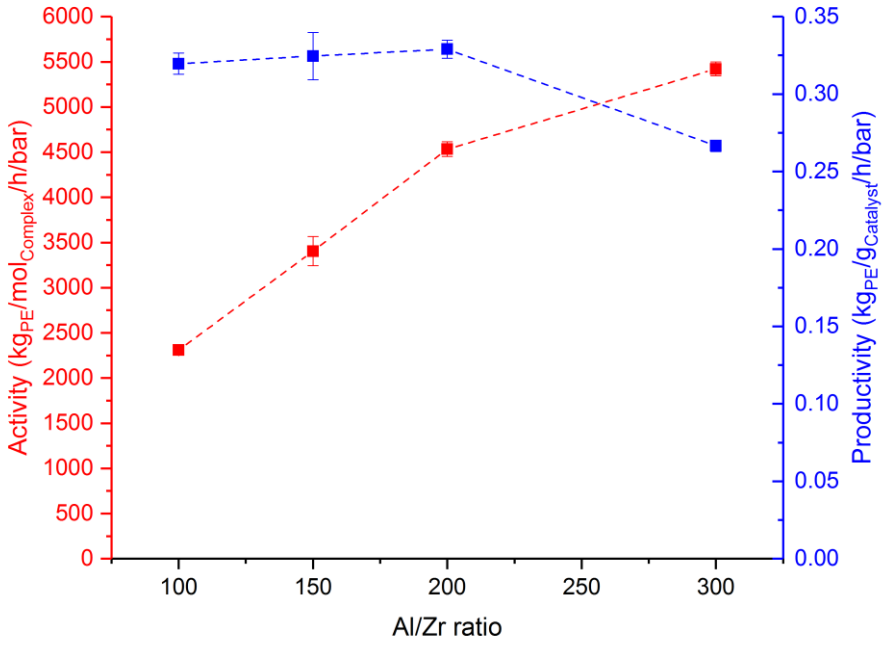


Figure 5.10. Heterogeneous ethylene polymerisation activity (red) and productivity (blue) of sMAO-[$^{Me2}SB(^{3\text{-}Et}I^{*})ZrCl_2$] as a function of Al/Zr ratio.

5.3.3 Catalyst loading and reaction volume

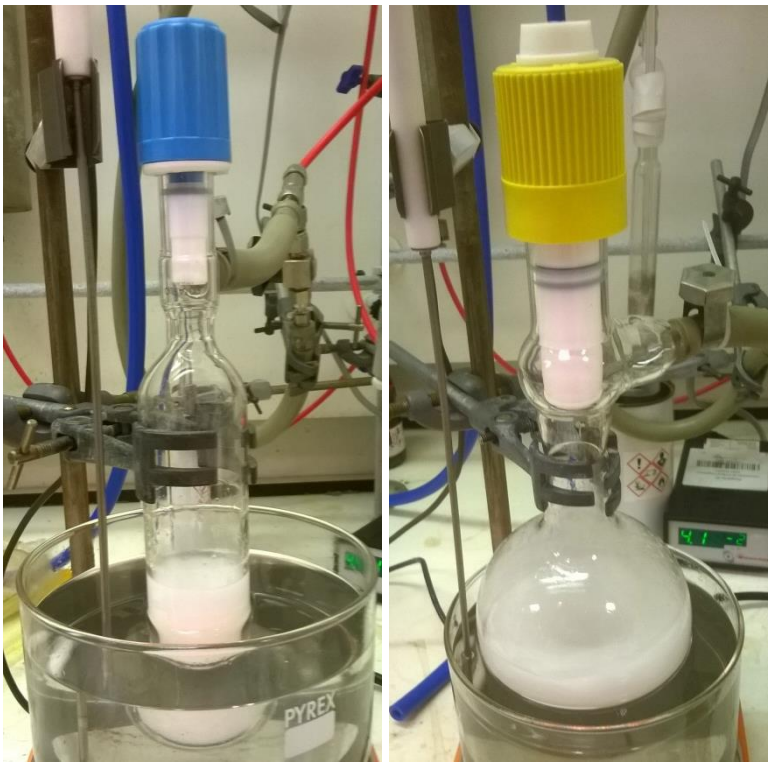


Figure 5.11. 50 mL (left) and 250 mL (right) ethylene polymerisation.

A 50 mL ethylene polymerisation setup, consisting of a 150 mL Rotaflo ampoule in a temperature controlled oil bath, connected to an ethylene gas line (2 bar), is shown in Figure 5.11 (left). Heterogeneous ethylene polymerisation using varied loadings of sMAO-[$^{Me2}SB(^{3\text{-}Et}I^{*})ZrCl_2$] catalyst were carried out. As expected, the catalyst loading of 20 mg resulted in a lower activity than the typical catalyst loading of 10 mg (2809 and 4533 $kg_{PE}/mol_{Complex}/h/bar$, respectively) due to the physical limitations of the reactor. However, the same logic does not apply to the catalyst loading of 5 mg which surprisingly also yielded a slightly lower activity (3747 $kg_{PE}/mol_{Complex}/h/bar$).

To study the effect of increased reaction volume, heterogeneous ethylene polymerisation using the catalyst loading of 10 mg was performed in a 250 mL ethylene polymerisation setup (Figure 5.11, right). A lower activity of 3812 $kg_{PE}/mol_{Complex}/h/bar$ was again observed. It can be concluded that, although the physical saturation of the reactor can lower the activity, there is a minimum concentration of the catalyst loading per reaction volume needed in order for the ethylene polymerisation to function optimally.

The sMAO-[$^{Me2}SB(^{3\text{-}Et}I^{*})ZrCl_2$] catalyst was subjected to large-scale 1 L ethylene polymerisation test under 8 bar of ethylene, an activity of 3261 $kg_{PE}/mol_{Complex}/h/bar$ was

recorded. This is surprising, as in general, polymerisation activity increases under higher pressure of ethylene.

5.4 Hydrogen as chain transfer agent

sMAO-[*rac*-^{Me2}SB($^{3\text{-}Et}$I*)ZrCl$_2$] catalyst was chosen for further testing under a variety of polymerisation conditions using a high throughput screening process. 120 psi of ethylene was used. Prior to polymerisation tests, the Zr content of the catalyst was measured by inductively coupled plasma (ICP) analysis. The measured value of 0.61 wt% is in good agreement with the expected value of 0.64 wt%.

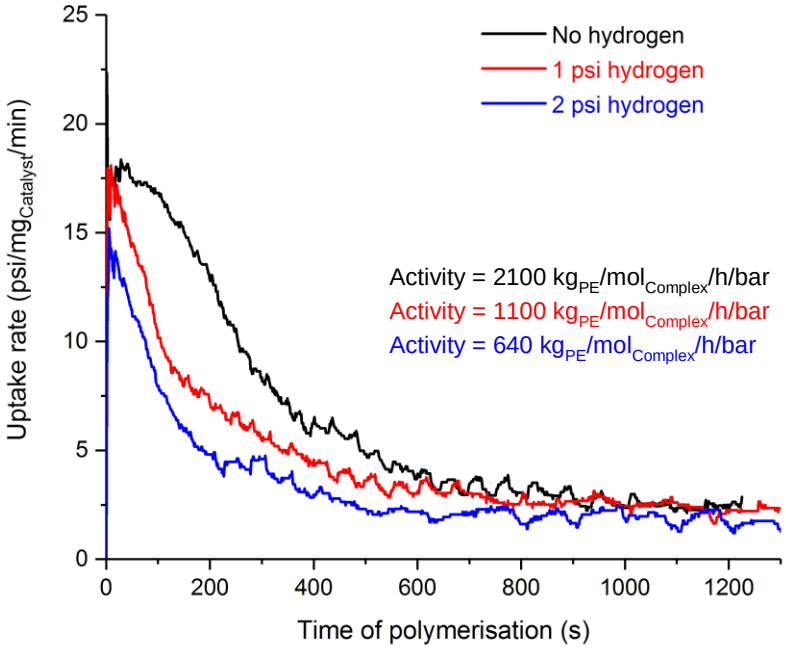


Figure 5.12. Ethylene uptake rate during heterogeneous ethylene polymerisation using sMAO-[*rac*-^{Me2}SB($^{3\text{-}Et}$I*)ZrCl$_2$] under different hydrogen partial pressure (0, 1 and 2 psi) as a function of time of polymerisation.

Heterogeneous ethylene polymerisation using sMAO-[*rac*-^{Me2}SB($^{3\text{-}Et}$I*)ZrCl$_2$] under different hydrogen partial pressure (0, 1 and 2 psi) was performed. The ethylene uptake rates during the polymerisation, which reflect the rate of polymerisation, are shown in Figure 5.12. All three tests show very high initial polymerisation rates after which sharply decline to low but stable rates. The activity of the catalyst decreases from 2100 to 640 kg$_{PE}$/mol$_{Complex}$/h/bar with respect to increased hydrogen partial pressure (from 0 to 2 psi). The molecular weight

distributions of the resulting polyethylenes are shown in Figure 5.13. Acting as a chain transfer agent, increase in hydrogen partial pressure significantly lowers the molecular weight of the resulting polyethylenes (from 1009 kg/mol at 0 psi to 20 kg/mol at 2 psi).[14]

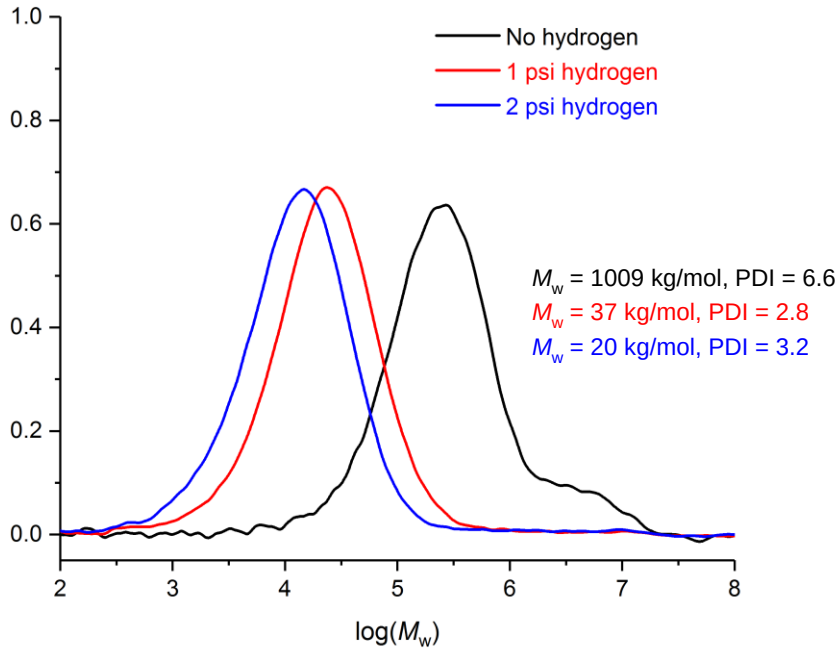


Figure 5.13. Molecular weight distribution of the resulting polyethylenes of heterogeneous ethylene polymerisation using sMAO-[*rac*-^{Me2}SB($^{3\text{-}Et}$I*)ZrCl$_2$] under different hydrogen partial pressure (0, 1 and 2 psi).

5.5 1-Hexene copolymerisation

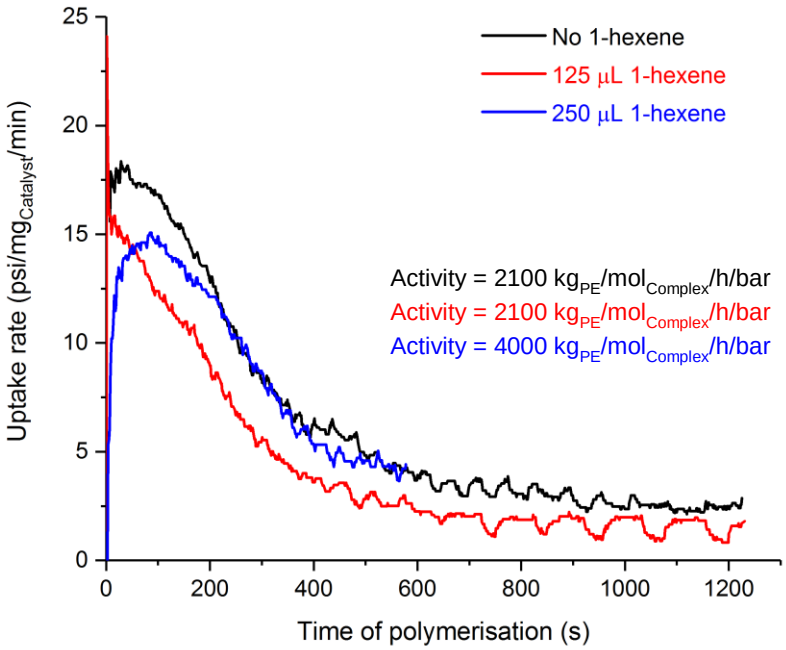


Figure 5.14. Ethylene uptake rate during heterogeneous ethylene copolymerisation with 1-hexene (0, 125 and 250 µL) using sMAO-[*rac*-^{Me2}SB($^{3\text{-}Et}$I*)ZrCl$_2$] as a function of time of polymerisation.

Using high throughput screening process, heterogeneous ethylene copolymerisation with 1-hexene (0, 125 and 250 µL) using sMAO-[*rac*-^{Me2}SB($^{3\text{-}Et}$I*)ZrCl$_2$] was performed. The ethylene uptake rates during the polymerisation show similar profiles to those in the hydrogen tests (Figure 5.14). However, here, the catalyst becomes more active (from 2100 to 4000 kg$_{PE}$/mol$_{Complex}$/h/bar) as the amount of the co-monomer increases (from 0 to 250 µL) due to the co-monomer effect.

The molecular weight of the resulting polyethylenes, shown in Figure 5.15, is slightly lowered upon the increase in 1-hexene concentration (1009 to 383 kg/mol). The resulting polyethylenes have very low 1-hexene incorporation of 0.3 and 0.7 mol% for 125 and 250 µL, respectively. These findings verify that the sMAO-[*rac*-^{Me2}SB($^{3\text{-}Et}$I*)ZrCl$_2$] catalyst is not suitable for copolymerisation of ethylene and 1-hexene.

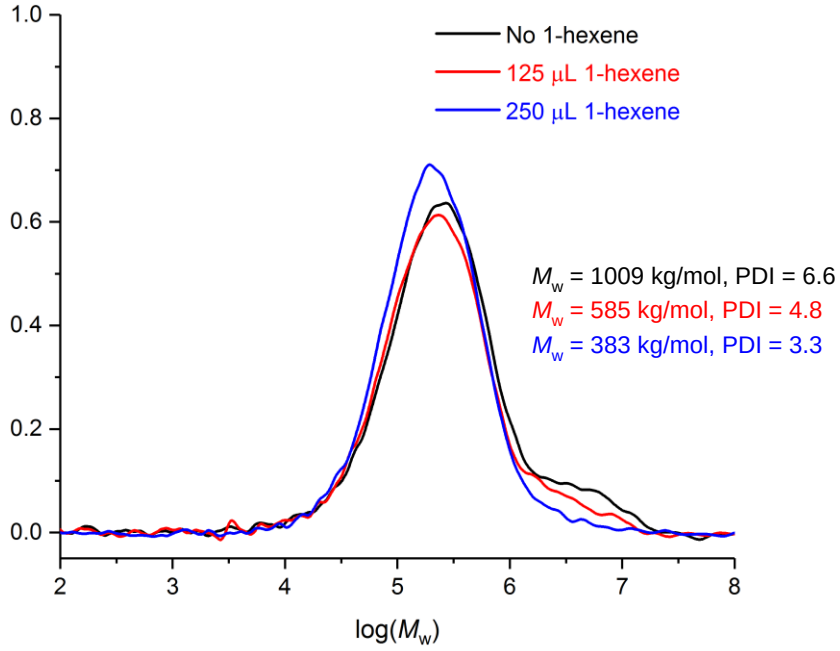


Figure 5.15. Molecular weight distribution of the resulting polyethylenes of heterogeneous ethylene copolymerisation with 1-hexene (0, 125 and 250 μL) using sMAO-[*rac*-^{Me2}SB($^{3\text{-}Et}$I*)ZrCl$_2$].

5.6 Conclusions

Chapter Five describes ethylene polymerisation studies of supported ^{Me2}SB($^{3\text{-}Et}$I*)ZrCl$_2$ catalysts. The complex was immobilised onto SSMAO, LDHMAO and sMAO supports and the resulting catalysts were tested for ethylene polymerisation activity. Polymerisation conditions, including scavenger type and loading, complex loading, catalyst loading and reaction volume, were optimised for sMAO-[^{Me2}SB($^{3\text{-}Et}$I*)ZrCl$_2$] catalyst. sMAO-[*rac*-^{Me2}SB($^{3\text{-}Et}$I*)ZrCl$_2$] catalyst was subjected to high throughput screening process and found to be responsive to hydrogen but not suitable for copolymerisation of ethylene and 1-hexene. The resulting polyethylenes were characterised by GPC and SEM.

5.7 References

1 J. R. Severn, J. C. Chadwick, R. Duchateau and N. Friederichs, *Chem. Rev.*, 2005, **105**, 4073–4147.
2 J. R. Severn and J. C. Chadwick, *Dalt. Trans.*, 2013, **42**, 8979–87.
3 K. P. Bryliakov, E. P. Talsi, A. Z. Voskoboynikov, S. J. Lancaster and M. Bochmann, *Organometallics*, 2008, **27**, 6333–6342.
4 V. Busico, R. Cipullo, R. Pellecchia, G. Talarico and A. Razavi, *Macromolecules*, 2009, **42**,

1789–1791.
5 M. Napoli, R. De Vita, I. Immediata, P. Longo and G. Guerra, *Polym. Adv. Technol.*, 2011, **22**, 458–462.
6 M. L. Britto, G. B. Galland, J. H. Z. dos Santos and M. C. Forte, *Polymer (Guildf).*, 2001, **42**, 6355–6361.
7 P. Mi, S. Xu, L. Qu, Z. Deshun, C. Qian and W. Sihan, *J. Appl. Polym. Sci.*, 2011, **121**, 21–26.
8 B. Paredes, R. van Grieken, A. Carrero, I. Suarez and J. B. P. Soares, *Macromol. Chem. Phys.*, 2011, **212**, 1590–1599.
9 T. M. Ushakova, E. E. Starchak, V. G. Krasheninnikov, A. A. Samoilenko, P. V. Ivchenko, I. E. Nifant'ev and L. A. Novokshonova, *Kinet. Catal.*, 2012, **53**, 75–83.
10 C. Chen, M. Yang, Q. Wang, J.-C. Buffet and D. O'Hare, *J. Mater. Chem. A*, 2014, **2**, 15102–15110.
11 J.-C. Buffet, T. A. Q. Arnold, Z. R. Turner, P. Angpanitcharoen and D. O'Hare, *RSC Adv.*, 2015, **5**, 87456–87464.
12 A. Maneshi, J. B. P. Soares and L. C. Simon, *Macromol. Chem. Phys.*, 2011, **212**, 2017–2028.
13 J. Zhang, X. Wang and G.-X. Jin, *Coord. Chem. Rev.*, 2006, **250**, 95–109.
14 L. D'Agnillo, J. B. P. Soares and A. Penlidis, *Macromol. Chem. Phys.*, 1998, **199**, 955–962.

Chapter Six – Experimental details

6.1 Characterisation techniques

6.1.1 Solution phase NMR spectroscopy

Air and moisture sensitive samples were prepared using dry deuterated solvents in a glove box under a N_2 atmosphere and sealed in Young's tap NMR tubes. NMR spectra were recorded on a Bruker Avance III HD Nanobay 400 MHz NMR spectrometer equipped with a 9.4 T magnet or a Bruker Avance III 500 MHz NMR spectrometer equipped with a 11.75 T magnet. ^{1}H and $^{13}C\{^{1}H\}$ NMR spectra were referenced internally to the residual *protio*-solvent resonance. ^{7}Li NMR spectra were referenced externally to LiCl. NMR spectra were recorded at 25 °C unless stated otherwise.

6.1.2 Solid state NMR spectroscopy

Samples were prepared in a glove box under a N_2 atmosphere and sealed in 4 mm ZrO_2 rotors. Solid state NMR spectra were recorded by Dr. Nicholas Rees, University of Oxford, on a Bruker Avance III HD Solid state 400 MHz NMR spectrometer equipped with a 9.4 T magnet. Samples were spun at the magic angle (54.71°) at spin rates of 10 kHz for ^{13}C CPMAS and ^{29}Si CPMAS, and 15 kHz for ^{27}Al Hahn-echo MAS SSNMR experiments. ^{13}C, ^{27}Al and ^{29}Si SSNMR spectra were referenced externally to adamantane, $Al(NO_3)_3$ and kaolinite, respectively. Solid state NMR spectra were recorded at 25 °C unless stated otherwise.

6.1.3 Infrared spectroscopy

Air and moisture sensitive samples were prepared in a glove box under a N_2 atmosphere, ground with anhydrous KBr, then formed into discs using a specially designed press and sealed in airtight holders. IR spectra were recorded on a Thermo Scientific Nicolet iS5 FT-IR spectrometer (range = 4000-400 cm^{-1}, resolution = 1 cm^{-1}) in transmission mode. Air stable samples were recorded on the same instrument using an iS3 diamond surface. A background spectrum was recorded prior to each sample and subtracted from the IR spectrum.

6.1.4 Mass spectrometry

Samples were tested using either electron ionisation (EI) or electrospray ionisation (ESI). Mass spectra were recorded by Dr. James Wickens and Mr. Colin Sparrow, University of Oxford.

6.1.5 Elemental analysis

Air and moisture sensitive samples were prepared in a glove box under a N_2 atmosphere and sealed in glass vials. CHN analyses were carried out in duplicate by Dr. Stephen Boyer, London Metropolitan University.

6.1.6 Single crystal X-ray diffraction

Data collection and structure determination were performed by Dr. Zoë Turner and Dr. Thomas Arnold, University of Oxford. Crystals were mounted on MiTeGen MicroMounts using a perfluoropolyether oil (Fomblin YR-1800, Alfa Aesar) and cooled rapidly to 150 K using an Oxford Cryosystems Cryostream unit.[1] Two different diffractometer setups were used as follows:

1) An Enraf-Nonius Kappa CCD diffractometer using graphite monochromated Mo K_α radiation (λ = 0.71073 Å). Raw frame data were reduced using DENZO-SMN package,[2] and corrected for absorption using SORTAV.[3] Intensity data were collected using a multi-scan method with SCALEPACK (within DENZO-SMN).

2) An Oxford Diffraction Supernova diffractometer using multilayer, orthogonal, micro-focus Cu K_α radiation (λ = 1.5405 Å). Raw frame data were collected, reduced and processed using CrysAlisPRO.[4]

The structures were solved using either direct methods with SHELXS[5] or using charge flipping with SuperFlip,[6] and refined using a full-matrix least squares refinement on all F^2 data using CRYSTALS[7,8] or WinGX[9] program suite. In general, distances were calculated using the full variance/co-variance matrix. Dihedral angles were calculated using CCDC's Mercury[10] or PLATON.[11] Illustrations of the solid state molecular structures were created using ORTEP.[9] Thermal ellipsoids were shown at 50% probability.

6.1.7 Powder X-ray diffraction

Powder X-ray diffraction data were collected by Dr. Kanittika Ruengkajorn, University of Oxford, on a PANAnalytical X'Pert Pro diffractometer in reflection mode at 45 kV and 40 mA using Cu K_α radiation (α_1 = 1.54057 Å, α_2 = 1.54433 Å). Scans were recorded in the range of $5° \leq 2\theta \leq 70°$ over 30 minutes. Samples were mounted onto aluminium sample holders, accounting for the reflections in the region of 44°.

6.1.8 Gel permeation chromatography

Gel permeation chromatography (GPC) of polyethylene samples was carried out at Norner AS, Norway.

6.1.9 Scanning electron microscopy

Air and moisture sensitive samples were prepared in a glove box under a N_2 atmosphere and dispersed onto silicon wafers. Air stable samples were dispersed onto carbon tapes. Samples were then coated with platinum (20 nm thickness) using a Quorum Q150T ES sputter coater. Scanning electron microscopy (SEM) images were recorded on a JEOL JSM-6610LV scanning electron microscope. Energy dispersive X-ray spectroscopy (EDS) was also performed on this instrument. For EDS, samples were coated with palladium (20 nm thickness) instead of platinum.

6.2 General procedures

Air and moisture sensitive compounds were manipulated under a N_2 atmosphere using standard Schlenk techniques on a dual vacuum/N_2 gas manifold or a MBraun UNIlab glove box. All glassware was dried in an oven at 160 °C for a minimum of two hours prior to use. Molecular sieves (3 Å, 8-12 mesh) were supplied by ACROS Organics and dried at 140 °C *in vacuo* for 16 hours prior to use.

For dry solvents, pentane, hexane, benzene, toluene and dichloromethane (DCM) were dried on a MBraun SPS-800 solvent purification system and degassed prior to use. The non-chlorinated solvents were stored in ampoules over a potassium mirror while DCM was stored over molecular sieves. Tetrahydrofuran (THF) was distilled from sodium benzophenone ketyl and stored in ampoules over molecular sieves. Diethyl ether (Et_2O) was distilled from Na/K and stored in ampoules over a potassium mirror.

Benzene-d_6 (99.6%, Sigma Aldrich) and toluene-d_8 (99.5%, Goss Scientific) were dried over Na/K. Chloroform-d_1 (99.8%, Sigma Aldrich), pyridine-d_5 (99.5%, Goss Scientific) and tetrahydrofuran-d_8 (99.6%, Goss Scientific) were dried over CaH_2. All deuterated solvents were vacuum transferred and freeze-pump-thaw degassed three times prior to use.

Large-scale ligand preparation procedures were carried out in a Chemglass ChemRxnHub 2 L reactor.

6.3 Starting materials

6.3.1 Commercially supplied reagents

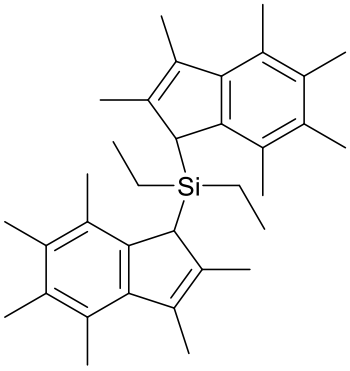
All reagents were used as received unless stated otherwise. Benzophenone and oxalyl chloride were supplied by Alfa Aesar. Sodium, potassium, CaH_2, (E)-2-methylpent-2-enoic acid, (E)-α-methylcinnamic acid, N,N-dimethylformamide (DMF), $AlCl_3$ (anhydrous), $LiAlH_4$ (2.0 M in THF), *n*BuLi (2.5 M in hexanes), trimethylaluminium (TMA), triethylaluminium (TEA) and triisobutylaluminium (TIBA) were supplied by Sigma Aldrich. 1,2,3,4-tetramethylbenzene was supplied by SCG Chemicals Co., Ltd.. HCl (concentrated), $MgSO_4$ (anhydrous) and H_2SO_4 (concentrated) were supplied by Fisher Scientific. $NaHCO_3$ was supplied by ACROS Organics. Dichlorodiethylsilane (Et_2SiCl_2), dichloro(methyl)propylsilane (*n*PrMeSiCl_2), allyl(dichloro)methylsilane (AllMeSiCl_2) and dichlorodimethylsilane (Me_2SiCl_2) were supplied by Sigma Aldrich, dried over molecular sieves and freeze-pump-thaw degassed three times prior to use. $ZrBr_4$, $ZrCl_4$ and $HfCl_4$ were supplied by Sigma Aldrich and dried at 140 °C for 16 hours prior to use. Methylaluminoxane (MAO; 10% wt in toluene) was supplied by Sigma Aldrich and dried *in vacuo* prior to use. Solid polymethylaluminoxane (sMAO; 12.40% wt in toluene) was supplied by SCG Chemicals Co., Ltd. and dried *in vacuo* prior to use. Ethylene gas (99.9%, BOC Industrial Gases) was passed through a drying column containing molecular sieves prior to use. Silica was supplied by SCG Chemicals Co., Ltd. and calcined at 600 °C for 6 hours.

6.3.2 Literature preparations

The following compounds were prepared according to literature procedures: Ind$^{\#}$Li,[12] (PhN(CH_2)$_3$NPh)ZrCl_2·2THF,[13–15] PhCH_2K,[16] *rac*-^{Me2}SBI*ZrCl_2,[17] AMO-LDH ($Mg_{0.75}Al_{0.25}(OH)_2(CO_3)_{0.125}$; calcined at 150 °C for 6 hours *in vacuo*).[18,19]

6.4 Experimental details for Chapter Two

6.4.1 Synthesis of ^{Et2}SBI*H$_2$



$C_{34}H_{48}Si$, M_r = 484.84

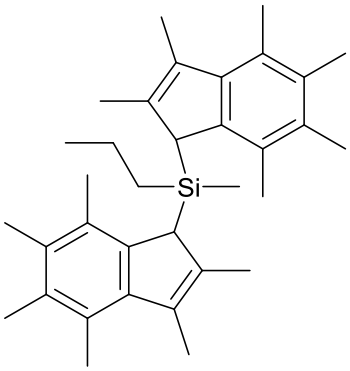
Ind$^{\#}$Li (4.00 g, 19.4 mmol, 2.2 eq) was dissolved in THF (200 mL) to form a dark brown solution. Et_2SiCl_2 (1.38 g, 8.81 mmol, 1.0 eq) was diluted in THF (50 mL) to form a colourless solution which was then added dropwise to the Ind$^{\#}$Li solution at 0 °C. The reaction was allowed to warm up to room temperature and left stirring for 16 hours. The resulting brown solution was dried *in vacuo* to remove all volatiles. Extraction using DCM (200 mL) was carried out and the resulting yellow filtrate was dried *in vacuo* to yield a yellow viscous oil containing *rac*-^{Et2}SBI*H$_2$, *meso*-^{Et2}SBI*H$_2$ and Ind$^{\#}$H. The oil was washed with pentane (50 mL) to yield the product, *rac*-^{Et2}SBI*H$_2$, as a white solid (0.500 g, 1.03 mmol, 12% yield). Colourless crystals of *rac*-^{Et2}SBI*H$_2$ suitable for single crystal X-ray diffraction were grown in pentane at 0 °C.

***rac*-^{Et2}SBI*H$_2$:**

^{1}H NMR (400.2 MHz, 298 K, chloroform-d$_1$): δ (ppm) 0.40 (m, 2H, Si-C**H$_a$**H$_b$-CH$_3$), 0.41 (bt, 6H, Si-CH$_2$-C**H$_3$**), 0.51 (m, 2H, Si-CH$_a$**H$_b$**-CH$_3$), 1.86 (s, 6H, Ind-C**H$_3$**), 2.11 (s, 6H, Ind-C**H$_3$**), 2.17 (s, 6H, Ind-C**H$_3$**), 2.20 (s, 6H, Ind-C**H$_3$**), 2.25 (s, 6H, Ind-C**H$_3$**), 2.47 (s, 6H, Ind-C**H$_3$**), 3.18 (s, 2H, Ind-**H**).

^{13}C{^{1}H} NMR (100.6 MHz, 298 K, chloroform-d$_1$): δ (ppm) 5.03 (Si-**C**H$_2$-CH$_3$), 7.19 (Si-CH$_2$-**C**H$_3$), 15.31 (Ind-**C**H$_3$), 15.61 (Ind-**C**H$_3$), 16.24 (Ind-**C**H$_3$), 16.24 (Ind-**C**H$_3$), 16.32 (Ind-**C**H$_3$), 18.10 (Ind-**C**H$_3$), 45.37 (**Ind**-H), 126.13 (**Ind**), 127.16 (**Ind**), 129.69 (**Ind**), 132.18 (**Ind**), 132.67 (**Ind**), 140.64 (**Ind**), 141.57 (**Ind**), 143.10 (**Ind**).

6.4.2 Synthesis of $^{n\text{Pr,Me}}$SBI*H$_2$



$C_{34}H_{48}Si$, M_r = 484.84

Ind$^{\#}$Li (5.00 g, 24.2 mmol, 2.5 eq) was dissolved in THF (200 mL) to form a dark brown solution. *n*PrMeSiCl$_2$ (1.52 g, 9.70 mmol, 1.0 eq) was diluted in THF (50 mL) to form a colourless solution which was then added dropwise to the Ind$^{\#}$Li solution at 0 °C. The reaction was allowed to warm up to room temperature and left stirring for 16 hours. The resulting brown solution was dried *in vacuo* to remove all volatiles. Extraction using DCM (200 mL) was carried out and the resulting yellow filtrate was dried *in vacuo* to yield a yellow viscous oil containing *rac*-$^{n\text{Pr,Me}}$SBI*H$_2$, *meso*-$^{n\text{Pr,Me}}$SBI*H$_2$ and Ind$^{\#}$H. The oil was washed with pentane (50 mL) to yield the product, *rac*-$^{n\text{Pr,Me}}$SBI*H$_2$, as a white solid (0.672 g, 1.39 mmol, 14% yield).

***rac*-$^{n\text{Pr,Me}}$SBI*H$_2$:**

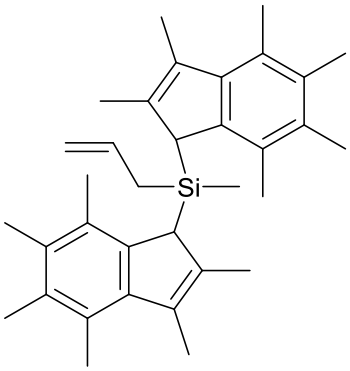
^{1}H NMR (400.1 MHz, 298 K, chloroform-d$_1$): δ (ppm) -0.39 (s, 3H, Si-C**H$_3$**), 0.27 (m, 2H, Si-C**H$_2$**-CH$_2$-CH$_3$), 0.54 (m, 2H, $^3J_{HH}$ = 7.0 Hz, Si-CH$_2$-C**H$_2$**-CH$_3$), 0.69 (t, 3H, $^3J_{HH}$ = 7.0 Hz, Si-CH$_2$-CH$_2$-C**H$_3$**), 2.01 (s, 3H, Ind-C**H$_3$**), 2.17 (s, 3H, Ind-C**H$_3$**), 2.21 (s, 6H, Ind-C**H$_3$**), 2.24 (s, 6H, Ind-C**H$_3$**), 2.25 (s, 3H, Ind-C**H$_3$**), 2.27 (s, 3H, Ind-C**H$_3$**), 2.32 (s, 6H, Ind-C**H$_3$**), 2.54 (s, 3H, Ind-C**H$_3$**), 2.55 (s, 3H, Ind-C**H$_3$**), 3.45 (s, 1H, Ind$_a$-**H**), 3.58 (s, 1H, Ind$_b$-**H**).

^{13}C{^{1}H} NMR (100.6 MHz, 298 K, chloroform-d$_1$): δ (ppm) -4.48 (Si-**C**H$_3$), 15.16 (Ind-**C**H$_3$), 15.24 (Ind-**C**H$_3$), 15.75 (Ind-**C**H$_3$), 15.87 (Ind-**C**H$_3$), 16.21 (Ind-**C**H$_3$), 16.27 (Ind-**C**H$_3$), 16.27 (Ind-**C**H$_3$), 16.27 (Ind-**C**H$_3$), 16.33 (Ind-**C**H$_3$), 16.36 (Ind-**C**H$_3$), 16.78 (Si-**C**H$_2$-CH$_2$-CH$_3$), 17.59 (Si-CH$_2$-**C**H$_2$-CH$_3$), 18.47 (Ind-**C**H$_3$), 18.62 (Si-CH$_2$-CH$_2$-**C**H$_3$), 18.86 (Ind-**C**H$_3$), 46.32 (**Ind$_a$**-H), 47.12 (**Ind$_b$**-H), 126.14 (**Ind**), 126.19 (**Ind**), 127.13 (**Ind**), 127.18 (**Ind**), 129.67 (**Ind**), 129.76 (**Ind**), 132.16 (**Ind**), 132.24 (**Ind**), 132.70 (**Ind**), 132.79 (**Ind**), 140.08 (**Ind**), 140.26 (**Ind**), 141.52 (**Ind**), 141.56 (**Ind**), 142.50 (**Ind**), 142.95 (**Ind**).

HRMS (EI): *m*/*z* = found 484.3515; calculated 484.3520, $[M]^+$.

CHN analysis (%): found: C 84.00, H 10.04; calculated: C 84.23, H 9.98.

6.4.3 Synthesis of ^{All,Me}SBI*H$_2$



$C_{34}H_{46}Si$, M_r = 482.83

Ind$^{\#}$Li (5.00 g, 24.2 mmol, 2.5 eq) was dissolved in THF (200 mL) to form a dark brown solution. AllMeSiCl$_2$ (1.50 g, 9.70 mmol, 1.0 eq) was diluted in THF (50 mL) to form a colourless solution which was then added dropwise to the Ind$^{\#}$Li solution at 0 °C. The reaction was allowed to warm up to room temperature and left stirring for 16 hours. The resulting brown solution was dried *in vacuo* to remove all volatiles. Extraction using DCM (200 mL) was carried out and the resulting yellow filtrate was dried *in vacuo* to yield a yellow viscous oil containing *rac*-^{All,Me}SBI*H$_2$, *meso*-^{All,Me}SBI*H$_2$ and Ind$^{\#}$H. The oil was washed with pentane (50 mL) to yield the product, *rac*-^{All,Me}SBI*H$_2$, as a white solid (0.600 g, 1.24 mmol, 13% yield).

***rac*-^{All,Me}SBI*H$_2$:**

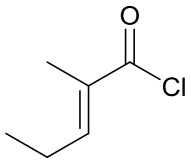
^{1}H NMR (400.1 MHz, 298 K, chloroform-d$_1$): δ (ppm) -0.39 (s, 3H, Si-C**H$_3$**), 1.30 (d, 2H, $^3J_{HH}$ = 7.9 Hz, Si-C**H$_2$**-CH=CH$_2$), 1.94 (s, 3H, Ind-C**H$_3$**), 2.09 (s, 3H, Ind-C**H$_3$**), 2.12 (s, 3H, Ind-C**H$_3$**), 2.13 (s, 3H, Ind-C**H$_3$**), 2.17 (s, 3H, Ind-C**H$_3$**), 2.20 (s, 3H, Ind-C**H$_3$**), 2.21 (s, 3H, Ind-C**H$_3$**), 2.23 (s, 3H, Ind-C**H$_3$**), 2.26 (s, 6H, Ind-C**H$_3$**), 2.49 (s, 3H, Ind-C**H$_3$**), 2.50 (s, 3H, Ind-C**H$_3$**), 3.34 (s, 1H, Ind$_a$-**H**), 3.49 (s, 1H, Ind$_b$-**H**), 4.52 (d, 1H, $^3J_{HH}$ = 5.8 Hz, Si-CH$_2$-CH=C**H$_a$**H$_b$), 4.55 (s, 1H, Si-CH$_2$-CH=CH$_a$**H$_b$**), 5.04 (m, 1H, $^3J_{HH}$ = 5.8, 7.9 Hz, Si-CH$_2$-C**H**=CH$_2$).

^{13}C{^{1}H} NMR (100.6 MHz, 298 K, chloroform-d$_1$): δ (ppm) -3.69 (Si-**C**H$_3$), 15.18 (Ind-**C**H$_3$), 15.30 (Ind-**C**H$_3$), 15.56 (Ind-**C**H$_3$), 15.75 (Ind-**C**H$_3$), 16.22 (Ind-**C**H$_3$), 16.27 (Ind-**C**H$_3$), 16.27 (Ind-**C**H$_3$), 16.27 (Ind-**C**H$_3$), 16.36 (Ind-**C**H$_3$), 16.36 (Ind-**C**H$_3$), 18.39 (Ind-**C**H$_3$), 18.81 (Ind-**C**H$_3$), 22.31 (Si-**C**H$_2$-CH=CH$_2$), 45.66 (**Ind$_a$**-H), 46.55 (**Ind$_b$**-H), 113.69 (Si-CH$_2$-CH=**C**H$_2$), 126.24 (**Ind**), 126.35 (**Ind**), 127.08 (**Ind**), 127.13 (**Ind**), 129.82 (**Ind**), 129.98 (**Ind**), 132.35 (**Ind**), 132.50 (**Ind**), 133.01 (**Ind**), 133.20 (**Ind**), 135.15

(Si-CH_2-**C**H=CH_2), 139.80 (**Ind**), 140.00 (**Ind**), 141.52 (**Ind**), 141.61 (**Ind**), 142.14 (**Ind**), 142.73 (**Ind**).

HRMS (EI): *m*/*z* = found 482.3362; calculated 482.3363, $[M]^+$.

6.4.4 Synthesis of EtCH=CMeCOCl



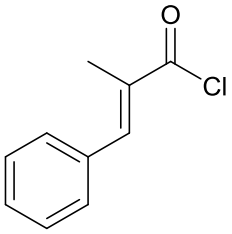
C_6H_9OCl, M_r = 132.59

(E)-2-methylpent-2-enoic acid (23.6 g, 207 mmol, 1.0 eq) was dissolved in DCM (500 mL) to form a colourless solution. Under a flow of N_2, oxalyl chloride (28.9 g, 228 mmol, 1.1 eq) was quickly added to the solution and dry DMF (5 drops) was then introduced to the mixture creating effervescence. The reaction was stirred for 2 hours after which an aliquot was taken showing that the reaction had gone to completion. Due to the high moisture sensitivity of the product, the resulting pale yellow solution was immediately used in the next step of the synthesis (100% yield assumed).

^{1}H NMR (499.9 MHz, 298 K, chloroform-d$_1$): δ (ppm) 1.11 (t, 3H, $^3J_{HH}$ = 7.6 Hz, C=CH-CH_2-C**H$_3$**), 1.89 (s, 3H, C=C-C**H$_3$**), 2.29 (dq, 2H, $^3J_{HH}$ = 7.4, 7.6 Hz, C=CH-C**H$_2$**-CH_3), 7.17 (t, 1H, $^3J_{HH}$ = 7.4 Hz, C=C**H**-CH_2-CH_3).

^{13}C{^{1}H} NMR (125.7 MHz, 298 K, chloroform-d$_1$): δ (ppm) 12.72 (C=CH-CH_2-**C**H_3), 13.37 (C=C-**C**H_3), 23.05 (C=CH-**C**H_2-CH_3), 132.26 (C=**C**-CH_3), 154.34 (C=**C**H-CH_2-CH_3), 169.42 (C=C-**C**OCl).

6.4.5 Synthesis of PhCH=CMeCOCl



$C_{10}H_9OCl$, M_r = 180.63

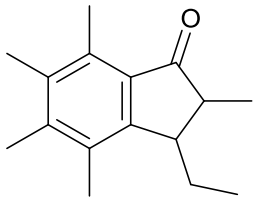
(E)-α-methylcinnamic acid (33.6 g, 207 mmol, 1.0 eq) was dissolved in DCM (500 mL) to form a colourless solution. Under a flow of N_2, oxalyl chloride (28.9 g, 228 mmol, 1.1 eq)

was quickly added to the solution and dry DMF (5 drops) was then introduced to the mixture creating effervescence. The reaction was stirred for 2 hours after which an aliquot was taken showing that the reaction had gone to completion. Due to the high moisture sensitivity of the product, the resulting pale yellow solution was immediately used in the next step of the synthesis (100% yield assumed).

^{1}H NMR (400.2 MHz, 298 K, chloroform-d$_1$): δ (ppm) 2.20 (s, 3H, C=C-C**H$_3$**), 7.43 (m, 1H, *p*-Ph-**H**), 7.46 (bd, 4H, *o*,*m*-Ph-**H**), 8.05 (s, 1H, C=C**H**-Ph).

^{13}C{^{1}H} NMR (100.6 MHz, 298 K, chloroform-d$_1$): δ (ppm) 15.30 (C=C-**C**H$_3$), 128.79 (*o*,*m*-**Ph**), 129.89 (*p*-**Ph**), 130.20 (*o*,*m*-**Ph**), 132.52 (C=**C**-CH$_3$), 134.64 (C=CH-**Ph**), 147.61 (C=**C**H-Ph), 170.28 (C=C-**C**OCl).

6.4.6 Synthesis of $^{3\text{-Et}}$Ind$^{\#}$=O



$C_{16}H_{22}O$, M_r = 230.35

Under a flow of N_2, $AlCl_3$ (41.4 g, 310 mmol, 1.5 eq) was slowly added to the EtCH=CMeCOCl solution (27.4 g, 207 mmol, 1.0 eq) to yield an orange solution. 1,2,3,4-tetramethylbenzene (25.0 g, 186 mmol, 0.9 eq) was diluted in DCM (100 mL) and then added dropwise to the reaction mixture over 30 minutes with colour change from orange to blood red. The reaction was then stirred for 4 hours after which a 1:1 mixture of concentrated HCl and ice (200 mL) was added slowly to quench the reaction. The reaction mixture changed colour from blood red to light orange during the work-up. The product was extracted with DCM (3 x 100 mL) and the combined organic layers were washed with saturated $NaHCO_3$ solution (100 mL) and deionised water (2 x 100 mL) before being dried using anhydrous $MgSO_4$. The mixture was filtered and the resulting filtrate was dried *in vacuo* to afford the product as a light brown solid (42.9 g, 186 mmol, 100% yield). The crude product contained several diastereomers most of which can be extracted by pentane leaving only the *cis* isomer as a white solid. Colourless crystals of $^{3\text{-Et}}$Ind$^{\#}$=O suitable for single crystal X-ray diffraction were grown in hexane at 0 °C.

***cis*-$^{3\text{-Et}}$Ind$^{\#}$=O:**

^{1}H NMR (400.2 MHz, 298 K, chloroform-d$_1$): δ (ppm) 0.56 (t, 3H, $^{3}J_{HH}$ = 7.5 Hz, CH-CH$_2$-C**H$_3$**), 1.27 (d, 3H, $^{3}J_{HH}$ = 7.2 Hz, CH-C**H$_3$**), 1.63 (m, 2H, $^{3}J_{HH}$ = 7.5 Hz, CH-C**H$_2$**-CH$_3$), 2.23 (s, 3H, Ph-C**H$_3$**), 2.28 (s, 6H, Ph-C**H$_3$**), 2.62 (s, 3H, Ph-C**H$_3$**), 2.74 (dq, 1H, $^{3}J_{HH}$ = 7.2, 7.2 Hz, C**H**-CH$_3$), 3.45 (m, 1H, $^{3}J_{HH}$ = 7.2 Hz, C**H**-CH$_2$-CH$_3$).

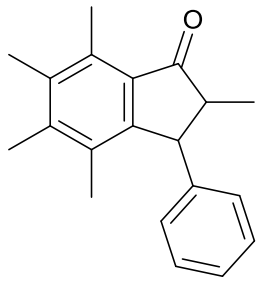
^{13}C{^{1}H} NMR (100.6 MHz, 298 K, chloroform-d$_1$): δ (ppm) 10.20 (CH-**C**H$_3$), 11.28 (CH-CH$_2$-**C**H$_3$), 14.08 (Ph-**C**H$_3$), 15.53 (Ph-**C**H$_3$), 15.71 (Ph-**C**H$_3$), 17.15 (Ph-**C**H$_3$), 24.17 (CH-**C**H$_2$-CH$_3$), 41.69 (**C**H-CH$_2$-CH$_3$), 48.38 (**C**H-CH$_3$), 130.38 (**Ph**), 131.43 (**Ph**), 133.69 (**Ph**), 135.20 (**Ph**), 141.76 (**Ph**), 153.07 (**Ph**), 209.99 (**C**=O).

IR: $\bar{\upsilon}$ (cm^{-1}) 1691.52 (C=O).

HRMS (ESI): *m*/*z* = found 231.17446; calculated 231.17434, [M + H]$^{+}$.

CHN analysis (%): found: C 83.53, H 9.75; calculated: C 83.43, H 9.63.

6.4.7 Synthesis of $^{3\text{-Ph}}$Ind$^{\#}$=O



$C_{20}H_{22}O$, M_r = 278.40

Under a flow of N_2, $AlCl_3$ (41.4 g, 310 mmol, 1.5 eq) was slowly added to the PhCH=CMeCOCl solution (37.4 g, 207 mmol, 1.0 eq) to yield an orange solution. 1,2,3,4-tetramethylbenzene (25.0 g, 186 mmol, 0.9 eq) was diluted in DCM (100 mL) and then added dropwise to the reaction mixture over 30 minutes with colour change from orange to blood red. The reaction was then stirred for 4 hours after which a 1:1 mixture of concentrated HCl and ice (200 mL) was added slowly to quench the reaction. The reaction mixture changed colour from blood red to light orange during the work-up. The product was extracted with DCM (3 x 100 mL) and the combined organic layers were washed with saturated $NaHCO_3$ solution (100 mL) and deionised water (2 x 100 mL) before being dried using anhydrous $MgSO_4$. The mixture was filtered and the resulting filtrate was dried *in vacuo* to afford the product as a light brown oil (51.9 g, 186 mmol, 100% yield). The crude product contained several diastereomers most of which can be extracted by pentane leaving

only the *cis* isomer as a white solid. Colourless crystals of $^{3\text{-Ph}}$Ind$^{\#}$=O suitable for single crystal X-ray diffraction were grown in hexane at 0 °C.

***cis*-$^{3\text{-Ph}}$Ind$^{\#}$=O:**

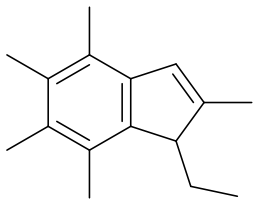
^{1}H NMR (400.2 MHz, 298 K, chloroform-d$_1$): δ (ppm) 0.81 (d, 3H, $^{3}J_{HH}$ = 7.3 Hz, CH-C**H$_3$**), 2.00 (s, 3H, Ph-C**H$_3$**), 2.24 (s, 3H, Ph-C**H$_3$**), 2.27 (s, 3H, Ph-C**H$_3$**), 2.71 (s, 3H, Ph-C**H$_3$**), 3.00 (dq, 1H, $^{3}J_{HH}$ = 7.3, 8.2 Hz, C**H**-CH$_3$), 4.61 (d, 1H, $^{3}J_{HH}$ = 8.2 Hz, C**H**-Ph), 6.82 (bs, 2H, *o*-Ph-**H**), 7.18 (m, 3H, *m*,*p*-Ph-**H**).

^{13}C{^{1}H} NMR (100.6 MHz, 298 K, chloroform-d$_1$): δ (ppm) 12.07 (CH-**C**H$_3$), 14.13 (Ph-**C**H$_3$), 15.62 (Ph-**C**H$_3$), 15.66 (Ph-**C**H$_3$), 17.14 (Ph-**C**H$_3$), 48.52 (**C**H-Ph), 48.78 (**C**H-CH$_3$), 126.53 (*p*-**Ph**), 128.37 (*m*-**Ph**), 128.90 (*o*-**Ph**), 131.31 (**Ph**), 131.76 (**Ph**), 133.71 (**Ph**), 136.06 (**Ph**), 141.33 (CH-**Ph**), 142.79 (**Ph**), 152.31 (**Ph**), 210.04 (**C**=O).

HRMS (ESI): *m*/*z* = found 301.15625; calculated 301.15629, $[M + Na]^+$.

CHN analysis (%): found: C 84.86, H 7.57; calculated: C 86.29, H 7.97.

6.4.8 Synthesis of $^{3\text{-Et}}$Ind$^{\#}$H



$C_{16}H_{22}$, M_r = 214.35

$^{3\text{-Et}}$Ind$^{\#}$=O (43.6 g, 189 mmol, 1.0 eq) was dissolved in THF (200 mL) to form an orange solution. Under a flow of N_2, $LiAlH_4$ (2.0 M in THF, 47.3 mL, 94.6 mmol, 0.5 eq) was added dropwise to the solution over 30 minutes and the resulting yellow solution was stirred for 2 hours. The reaction was cooled to 0 °C and then slowly quenched by addition of deionised water (3.42 mL, 189 mmol, 1.0 eq). Concentrated H_2SO_4 (50.4 mL, 946 mmol, 5.0 eq) was added dropwise to the reaction mixture over 30 minutes after which the reaction mixture turned dark brown. The reaction was then quenched with deionised water (200 mL) and extracted with DCM (3 x 100 mL). The combined organic layers were washed with saturated $NaHCO_3$ solution (100 mL) and deionised water (2 x 100 mL), dried over anhydrous $MgSO_4$ and filtered. The resulting yellow solution was dried *in vacuo* to afford the product as a light brown solid (37.6 g, 175 mmol, 93% yield). Colourless crystals of $^{3\text{-Et}}$Ind$^{\#}$H suitable for single crystal X-ray diffraction were grown in toluene at 0 °C.

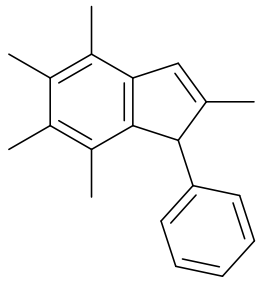
^{1}H NMR (400.2 MHz, 298 K, chloroform-d$_1$): δ (ppm) 0.44 (t, 3H, $^{3}J_{HH}$ = 7.4 Hz, CH-CH$_2$-C**H$_3$**), 1.94 (m, 1H, $^{3}J_{HH}$ = 4.0, 7.4 Hz, CH-C**H$_a$**H$_b$-CH$_3$), 2.07 (s, 3H, C=C-C**H$_3$**), 2.18 (m, 1H, $^{3}J_{HH}$ = 4.0, 7.4 Hz, CH-CH$_a$**H$_b$**-CH$_3$), 2.26 (s, 6H, Ph-C**H$_3$**), 2.34 (s, 3H, Ph-C**H$_3$**), 2.34 (s, 3H, Ph-C**H$_3$**), 3.43 (t, 1H, $^{3}J_{HH}$ = 4.0 Hz, C**H**-CH$_2$-CH$_3$), 6.59 (s, 1H, C=C-**H**).

^{13}C{^{1}H} NMR (100.6 MHz, 298 K, chloroform-d$_1$): δ (ppm) 7.56 (CH-CH$_2$-**C**H$_3$), 15.42 (C=C-**C**H$_3$), 16.04 (Ph-**C**H$_3$), 16.22 (Ph-**C**H$_3$), 16.23 (Ph-**C**H$_3$), 16.54 (Ph-**C**H$_3$), 21.09 (CH-**C**H$_2$-CH$_3$), 52.93 (**C**H-CH$_2$-CH$_3$), 124.83 (**Ph**), 126.10 (C=**C**-H), 128.88 (**Ph**), 130.66 (**Ph**), 133.00 (**Ph**), 141.92 (C=**C**-CH$_3$), 142.07 (**Ph**), 146.67 (**Ph**).

HRMS (ESI): *m*/*z* = found 215.17966; calculated 215.17943, $[M + H]^+$.

CHN analysis (%): found: C 89.62, H 10.47; calculated: C 89.65, H 10.35.

6.4.9 Synthesis of $^{3\text{-Ph}}$Ind$^{\#}$H



$C_{20}H_{22}$, M_r = 262.40

$^{3\text{-Ph}}$Ind$^{\#}$=O (54.8 g, 197 mmol, 1.0 eq) was dissolved in THF (200 mL) to form an orange solution. Under a flow of N_2, $LiAlH_4$ (2.0 M in THF, 49.2 mL, 98.4 mmol, 0.5 eq) was added dropwise to the solution over 30 minutes and the resulting yellow solution was stirred for 2 hours. The reaction was cooled to 0 °C and then slowly quenched by the addition of deionised water (3.55 mL, 197 mmol, 1.0 eq). Concentrated H_2SO_4 (52.4 mL, 984 mmol, 5.0 eq) was added dropwise to the reaction mixture over 30 minutes after which the reaction mixture turned dark brown. The reaction was then quenched with deionised water (200 mL) and extracted with DCM (3 x 100 mL). The combined organic layers were washed with saturated $NaHCO_3$ solution (100 mL) and deionised water (2 x 100 mL), dried over anhydrous $MgSO_4$ and filtered. The resulting yellow solution was dried *in vacuo* to afford the product as a light brown solid (48.8 g, 186 mmol, 94% yield). Colourless crystals of $^{3\text{-Ph}}$Ind$^{\#}$H suitable for single crystal X-ray diffraction were grown in hexane at 0 °C.

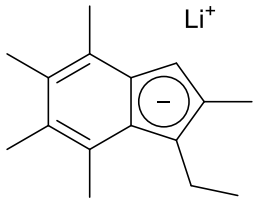
^{1}H NMR (400.2 MHz, 298 K, chloroform-d$_1$): δ (ppm) 1.84 (s, 3H, C=C-C**H$_3$**), 1.93 (s, 3H, Ph-C**H$_3$**), 2.17 (s, 3H, Ph-C**H$_3$**), 2.25 (s, 3H, Ph-C**H$_3$**), 2.37 (s, 3H, Ph-C**H$_3$**), 4.29 (s, 1H, C**H**-Ph), 6.56 (s, 1H, C=C-**H**), 6.99 (d, 2H, $^{3}J_{HH}$ = 6.9 Hz, *o*-Ph-**H**), 7.20 (m, 3H, $^{3}J_{HH}$ = 6.9 Hz, *m*,*p*-Ph-**H**).

^{13}C{^{1}H} NMR (100.6 MHz, 298 K, chloroform-d$_1$): δ (ppm) 15.38 (C=C-**C**H$_3$), 16.03 (Ph-**C**H$_3$), 16.34 (Ph-**C**H$_3$), 16.38 (Ph-**C**H$_3$), 16.47 (Ph-**C**H$_3$), 59.96 (**C**H-Ph), 125.17 (**Ph**), 125.30 (C=**C**-H), 126.37 (*p*-**Ph**), 128.28 (*o*-**Ph**), 128.64 (*m*-**Ph**), 129.59 (**Ph**), 131.25 (**Ph**), 133.83 (**Ph**), 140.54 (CH-**Ph**), 141.84 (**Ph**), 144.01 (**Ph**), 148.88 (C=**C**-CH$_3$).

HRMS (EI): *m*/*z* = found 262.1721; calculated 262.1716, $[M]^{+}$.

CHN analysis (%): found: C 91.36, H 8.57; calculated: C 91.55, H 8.45.

6.4.10 Synthesis of $^{3\text{-Et}}$Ind$^{\#}$Li



$C_{16}H_{21}Li$, M_r = 220.28

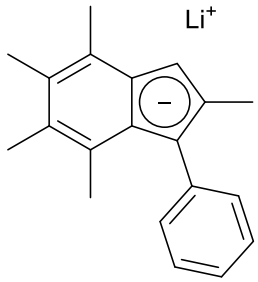
$^{3\text{-Et}}$Ind$^{\#}$H (10.0 g, 46.7 mmol, 1.0 eq) was dissolved in pentane (200 mL) to form a yellow solution. *n*BuLi (2.5 M in hexanes, 20.5 mL, 51.3 mmol, 1.1 eq) was added dropwise to the solution at 0 °C. The reaction was allowed to warm up to room temperature and left stirring for 16 hours. The resulting yellow suspension was filtered to yield a solid, which was washed with pentane (50 mL) and then dried *in vacuo* to afford the product as an off-white solid (8.66 g, 39.3 mmol, 84% yield).

^{1}H NMR (400.2 MHz, 298 K, pyridine-d$_5$): δ (ppm) 1.45 (t, 3H, $^{3}J_{HH}$ = 7.3 Hz, Cp-CH$_2$-C**H$_3$**), 2.43 (s, 3H, Ph-C**H$_3$**), 2.45 (s, 3H, Ph-C**H$_3$**), 2.60 (s, 3H, Ph-C**H$_3$**), 2.63 (s, 3H, Ph-C**H$_3$**), 2.85 (s, 3H, Cp-C**H$_3$**), 3.27 (q, 2H, $^{3}J_{HH}$ = 7.3 Hz, Cp-C**H$_2$**-CH$_3$), 6.32 (s, 1H, Cp-**H**).

^{13}C{^{1}H} NMR (100.6 MHz, 298 K, pyridine-d$_5$): δ (ppm) 15.69 (Ph-**C**H$_3$), 17.11 (Ph-**C**H$_3$), 17.24 (Ph-**C**H$_3$), 17.37 (Ph-**C**H$_3$), 17.69 (Cp-**C**H$_3$), 20.63 (Cp-CH$_2$-**C**H$_3$), 22.66 (Cp-**C**H$_2$-CH$_3$), 91.24 (**Cp**-H), 108.67 (**Cp**-CH$_2$-CH$_3$), 118.30 (**Ph**), 119.21 (**Ph**), 121.74 (**Ph**), 122.93 (**Ph**), 124.52 (**Cp**-CH$_3$), 125.26 (**Ph**), 128.39 (**Ph**).

^{7}Li NMR (155.5 MHz, 298 K, pyridine-d$_5$): δ (ppm) -1.81 (s).

6.4.11 Synthesis of $^{3\text{-Ph}}$Ind$^{\#}$Li



$C_{20}H_{21}Li$, M_r = 268.33

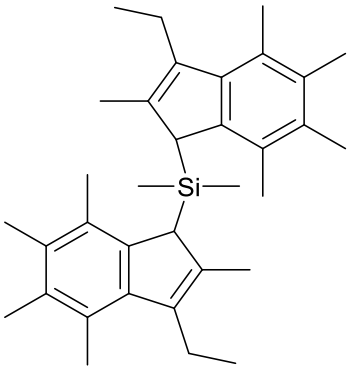
$^{3\text{-Ph}}$Ind$^{\#}$H (6.21 g, 23.7 mmol, 1.0 eq) was dissolved in Et_2O (200 mL) to form a yellow solution. *n*BuLi (2.5 M in hexanes, 14.2 mL, 35.5 mmol, 1.5 eq) was added dropwise to the solution at 0 °C. The reaction was allowed to warm up to room temperature and left stirring for 16 hours. The resulting yellow suspension was filtered to yield a solid, which was washed with pentane (50 mL) and then dried *in vacuo* to afford the product as an off-white solid (5.62 g, 20.9 mmol, 88% yield).

^{1}H NMR (400.2 MHz, 298 K, pyridine-d$_5$): δ (ppm) 2.55 (s, 3H, Ph-C**H$_3$**), 2.56 (s, 3H, Ph-C**H$_3$**), 2.75 (s, 3H, Ph-C**H$_3$**), 2.86 (s, 3H, Ph-C**H$_3$**), 2.92 (s, 3H, Cp-C**H$_3$**), 6.67 (s, 1H, Cp-**H**), 7.06 (t, 1H, $^3J_{HH}$ = 7.2 Hz, *p*-Ph-**H**), 7.42 (dd, 2H, $^3J_{HH}$ = 7.2, 7.9 Hz, *m*-Ph-**H**), 7.78 (d, 2H, $^3J_{HH}$ = 7.9 Hz, *o*-Ph-**H**).

^{13}C{^{1}H} NMR (100.6 MHz, 298 K, pyridine-d$_5$): δ (ppm) 17.37 (Ph-**C**H$_3$), 17.54 (Ph-**C**H$_3$), 17.69 (Ph-**C**H$_3$), 17.96 (Cp-**C**H$_3$), 20.90 (Ph-**C**H$_3$), 96.93 (**Cp**-H), 110.49 (**Cp**-Ph), 117.96 (**Ph**), 119.38 (**Ph**), 120.49 (*p*-**Ph**), 120.89 (**Ph**), 122.24 (**Ph**), 127.11 (*m*-**Ph**), 127.33 (**Cp**-CH$_3$), 128.50 (**Ph**), 131.92 (**Ph**), 132.39 (*o*-**Ph**), 147.18 (Cp-**Ph**).

^{7}Li NMR (155.5 MHz, 298 K, pyridine-d$_5$): δ (ppm) 2.58 (s).

6.4.12 Synthesis of ^{Me2}SB($^{3\text{-}Et}$I*)H$_2$



$C_{34}H_{48}Si$, M_r = 484.84

$^{3\text{-}Et}$Ind$^{\#}$Li (2.00 g, 9.08 mmol, 2.0 eq) was dissolved in THF (100 mL) to form a dark brown solution. Me_2SiCl_2 (0.586 g, 4.54 mmol, 1.0 eq) was diluted in THF (50 mL) to form a colourless solution which was then added dropwise to the $^{3\text{-}Et}$Ind$^{\#}$Li solution at 0 °C. The reaction was allowed to warm up to room temperature and left stirring for 16 hours. The resulting pale yellow solution was dried *in vacuo* to remove all volatiles. Extraction using DCM (200 mL) was carried out and the resulting pale yellow filtrate was dried *in vacuo* to yield the product, a 1:1 mixture of *rac*-^{Me2}SB($^{3\text{-}Et}$I*)H$_2$ and *meso*-^{Me2}SB($^{3\text{-}Et}$I*)H$_2$, as an off-white solid (1.16 g, 2.39 mmol, 53% yield). Colourless crystals of *rac*-^{Me2}SB($^{3\text{-}Et}$I*)H$_2$ suitable for single crystal X-ray diffraction were grown in Et_2O at -30 °C.

HRMS (EI): *m*/*z* = found 484.3523; calculated 484.3520, $[M]^+$.

CHN analysis (%): found: C 84.10, H 10.15; calculated: C 84.23, H 9.98.

***rac*-^{Me2}SB($^{3\text{-}Et}$I*)H$_2$:**

^{1}H NMR (400.2 MHz, 298 K, chloroform-d$_1$): δ (ppm) -0.63 (s, 6H, Si-C**H$_3$**), 1.17 (t, 6H, $^3J_{HH}$ = 7.5 Hz, Ind-CH$_2$-C**H$_3$**), 2.16 (s, 12H, Ind-C**H$_3$**), 2.20 (s, 6H, Ind-C**H$_3$**), 2.27 (s, 6H, Ind-C**H$_3$**), 2.46 (s, 6H, Ind-C**H$_3$**), 2.74 (q, 4H, $^3J_{HH}$ = 7.5 Hz, Ind-C**H$_2$**-CH$_3$), 3.74 (s, 2H, Ind-**H**).

^{13}C{^{1}H} NMR (100.6 MHz, 298 K, chloroform-d$_1$): δ (ppm) -3.96 (Si-**C**H$_3$), 14.78 (Ind-CH$_2$-**C**H$_3$), 15.69 (Ind-**C**H$_3$), 15.95 (Ind-**C**H$_3$), 16.37 (Ind-**C**H$_3$), 16.37 (Ind-**C**H$_3$), 19.17 (Ind-**C**H$_3$), 20.98 (Ind-**C**H$_2$-CH$_3$), 47.20 (**Ind**-H), 125.77 (**Ind**), 127.15 (**Ind**), 129.75 (**Ind**), 132.35 (**Ind**), 139.38 (**Ind**), 139.56 (**Ind**), 140.63 (**Ind**), 142.59 (**Ind**).

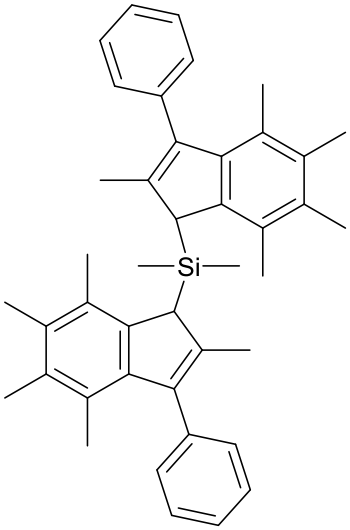
***meso*-^{Me2}SB($^{3\text{-}Et}$I*)H$_2$:**

^{1}H NMR (400.2 MHz, 298 K, chloroform-d$_1$): δ (ppm) -0.61 (s, 3H, Si-C$_a$**H$_3$**), -0.43 (s, 3H, Si-C$_b$**H$_3$**), 1.12 (t, 6H, $^3J_{HH}$ = 7.5 Hz, Ind-CH$_2$-C**H$_3$**), 1.98 (s, 6H, Ind-C**H$_3$**), 2.17 (s, 12H,

Ind-C**H₃**), 2.21 (s, 6H, Ind-C**H₃**), 2.46 (s, 6H, Ind-C**H₃**), 2.67 (q, 4H, $^{3}J_{HH}$ = 7.5 Hz, Ind-C**H₂**-CH_3), 3.60 (s, 2H, Ind-**H**).

$^{13}C\{^{1}H\}$ NMR (100.6 MHz, 298 K, chloroform-d₁): δ (ppm) -2.55 (Si-**C$_b$**H_3), -2.07 (Si-**C$_a$**H_3), 14.78 (Ind-CH_2-**C**H_3), 15.02 (Ind-**C**H_3), 15.91 (Ind-**C**H_3), 16.37 (Ind-**C**H_3), 16.37 (Ind-**C**H_3), 19.10 (Ind-**C**H_3), 20.92 (Ind-**C**H_2-CH_3), 47.13 (**Ind**-H), 125.77 (**Ind**), 126.99 (**Ind**), 129.78 (**Ind**), 132.28 (**Ind**), 139.04 (**Ind**), 140.10 (**Ind**), 140.50 (**Ind**), 143.00 (**Ind**).

6.4.13 Synthesis of $^{Me2}SB(^{3\text{-}Ph}I^*)H_2$



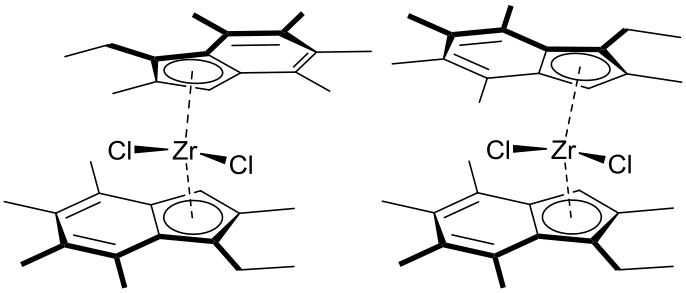
$C_{42}H_{48}Si$, M_r = 580.93

$^{3\text{-}Ph}Ind^{\#}Li$ (3.00 g, 11.2 mmol, 2.0 eq) was dissolved in THF (100 mL) to form a dark brown solution. Me_2SiCl_2 (0.721 g, 5.59 mmol, 1.0 eq) was diluted in THF (50 mL) to form a colourless solution which was then added dropwise to the $^{3\text{-}Ph}Ind^{\#}Li$ solution at 0 °C. The reaction was allowed to warm up to room temperature and left stirring for 16 hours. The resulting brown solution was dried *in vacuo* to remove all volatiles. Extraction using DCM (200 mL) was carried out and the resulting yellow filtrate was dried *in vacuo* to yield a yellow viscous oil containing *rac*-$^{Me2}SB(^{3\text{-}Ph}I^*)H_2$, *meso*-$^{Me2}SB(^{3\text{-}Ph}I^*)H_2$ and $^{3\text{-}Ph}Ind^{\#}H$. The product was not separable.

^{1}H NMR (400.2 MHz, 298 K, chloroform-d₁): δ (ppm) -0.33 (s, 6H, *rac*-Si-C**H₃**), -0.31 (s, 3H, *meso*-Si-C_a**H₃**), -0.12 (s, 3H, *meso*-Si-C_b**H₃**), 1.81 (s, 6H, Ind-C**H₃**), 1.82 (s, 6H, Ind-C**H₃**), 1.87 (s, 6H, Ind-C**H₃**), 2.16 (s, 6H, Ind-C**H₃**), 2.17 (s, 12H, Ind-C**H₃**), 2.23 (s, 6H, Ind-C**H₃**), 2.23 (s, 6H, Ind-C**H₃**), 2.27 (s, 6H, Ind-C**H₃**), 2.31 (s, 6H, Ind-C**H₃**), 3.89 (s, 2H, *meso*-Ind-**H**), 4.02 (s, 2H, *rac*-Ind-**H**), 7.32 (m, 20H, Ph-**H**).

6.5 Experimental details for Chapter Three

6.5.1 Synthesis of ($^{3\text{-Et}}$Ind$^{\#}$)$_2$ZrCl$_2$



$C_{32}H_{42}Cl_2Zr$, M_r = 588.81

$^{3\text{-Et}}$Ind$^{\#}$Li (3.00 g, 13.6 mmol, 2.0 eq) and $ZrCl_4$ (1.59 g, 6.81 mmol, 1.0 eq) were mixed in benzene (100 mL) and left stirring for 16 hours at room temperature. The reaction mixture was allowed to settle before being filtered. The orange filtrate was dried *in vacuo* to afford the product, a 50:50 mixture of *rac*-($^{3\text{-Et}}$Ind$^{\#}$)$_2$ZrCl$_2$ and *meso*-($^{3\text{-Et}}$Ind$^{\#}$)$_2$ZrCl$_2$, as an orange yellow solid (1.23 g, 2.09 mmol, 31% yield). Recrystallisation of the isomeric mixture in toluene at -30 °C yielded *rac*-($^{3\text{-Et}}$Ind$^{\#}$)$_2$ZrCl$_2$ as yellow crystals suitable for single crystal X-ray diffraction. Fractional crystallisation from the toluene filtrate at -30 °C yielded *meso*-($^{3\text{-Et}}$Ind$^{\#}$)$_2$ZrCl$_2$ as orange yellow crystals.

***rac*-($^{3\text{-Et}}$Ind$^{\#}$)$_2$ZrCl$_2$:**

^{1}H NMR (400.2 MHz, 298 K, chloroform-d$_1$): δ (ppm) 1.05 (t, 6H, $^3J_{HH}$ = 7.5 Hz, Ind-CH$_2$-C**H$_3$**), 1.64 (s, 6H, Ind-C**H$_3$**), 2.27 (s, 6H, Ind-C**H$_3$**), 2.28 (s, 6H, Ind-C**H$_3$**), 2.52 (s, 6H, Ind-C**H$_3$**), 2.59 (s, 6H, Ind-C**H$_3$**), 2.60 (dq, 2H, $^2J_{HH}$ = 15.0 Hz, $^3J_{HH}$ = 7.5 Hz, Ind-C**H$_a$**H$_b$-CH$_3$), 3.10 (dq, 2H, $^2J_{HH}$ = 15.0 Hz, $^3J_{HH}$ = 7.5 Hz, Ind-CH$_a$**H$_b$**-CH$_3$), 6.23 (s, 2H, Ind-**H**).

^{13}C{^{1}H} NMR (100.6 MHz, 298 K, chloroform-d$_1$): δ (ppm) 13.64 (Ind-**C**H$_3$), 15.57 (Ind-CH$_2$-**C**H$_3$), 16.57 (Ind-**C**H$_3$), 16.70 (Ind-**C**H$_3$), 16.81 (Ind-**C**H$_3$), 17.63 (Ind-**C**H$_3$), 21.71 (Ind-**C**H$_2$-CH$_3$), 94.19 (**Ind**-H), 124.61 (**Ind**), 124.90 (**Ind**), 125.31 (**Ind**), 127.86 (**Ind**), 130.32 (**Ind**), 131.05 (**Ind**), 133.08 (**Ind**), 133.66 (**Ind**).

HRMS (EI): *m*/*z* = found 586.1703; calculated 586.1705, $[M]^+$.

CHN analysis (%): found: 65.90, H 7.96; calculated: C 65.28, H 7.19.

***meso*-($^{3\text{-Et}}$Ind$^{\#}$)$_2$ZrCl$_2$:**

^{1}H NMR (400.2 MHz, 298 K, chloroform-d$_1$): δ (ppm) 1.09 (t, 6H, $^3J_{HH}$ = 7.5 Hz, Ind-CH$_2$-C**H$_3$**), 2.14 (s, 6H, Ind-C**H$_3$**), 2.20 (s, 6H, Ind-C**H$_3$**), 2.21 (s, 6H, Ind-C**H$_3$**), 2.27 (s,

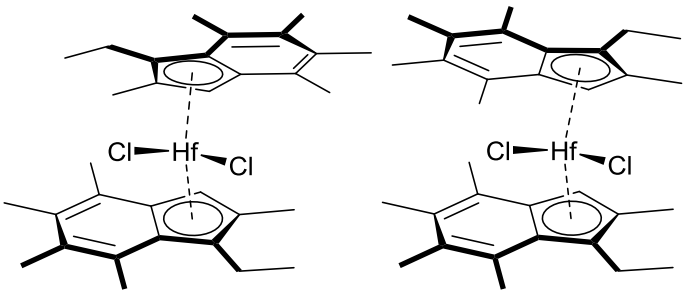
6H, Ind-C**H₃**), 2.50 (s, 6H, Ind-C**H₃**), 2.64 (dq, 2H, $^{2}J_{HH}$ = 15.0 Hz, $^{3}J_{HH}$ = 7.5 Hz, Ind-C**H$_a$**H$_b$-CH$_3$), 3.26 (dq, 2H, $^{2}J_{HH}$ = 15.0 Hz, $^{3}J_{HH}$ = 7.5 Hz, Ind-CH$_a$**H$_b$**-CH$_3$), 5.86 (s, 2H, Ind-**H**).

^{13}C{^{1}H} NMR (100.6 MHz, 298 K, chloroform-d$_1$): δ (ppm) 15.33 (Ind-CH$_2$-**C**H$_3$), 15.46 (Ind-**C**H$_3$), 16.33 (Ind-**C**H$_3$), 16.59 (Ind-**C**H$_3$), 16.59 (Ind-**C**H$_3$), 16.74 (Ind-**C**H$_3$), 22.00 (Ind-**C**H$_2$-CH$_3$), 97.14 (**Ind**-H), 125.44 (**Ind**), 126.28 (**Ind**), 126.87 (**Ind**), 126.90 (**Ind**), 129.11 (**Ind**), 130.14 (**Ind**), 133.14 (**Ind**), 133.66 (**Ind**).

HRMS (EI): *m*/*z* = found 586.1695; calculated 586.1705, [M]$^{+}$.

CHN analysis (%): found: C 65.35, H 7.27; calculated: C 65.28, H 7.19.

6.5.2 Synthesis of ($^{3\text{-Et}}$Ind$^{\#}$)$_2$HfCl$_2$



$C_{32}H_{42}Cl_2Hf$, M_r = 676.08

$^{3\text{-Et}}$Ind$^{\#}$Li (2.00 g, 9.08 mmol, 2.0 eq) and $HfCl_4$ (1.45 g, 4.54 mmol, 1.0 eq) were mixed in benzene (100 mL) and left stirring for 16 hours at room temperature. The reaction mixture was allowed to settle before being filtered. The yellow filtrate was dried *in vacuo* to afford the product, a 50:50 mixture of *rac*-($^{3\text{-Et}}$Ind$^{\#}$)$_2$HfCl$_2$ and *meso*-($^{3\text{-Et}}$Ind$^{\#}$)$_2$HfCl$_2$, as a yellow solid (1.44 g, 2.13 mmol, 47% yield). Recrystallisation of the isomeric mixture in toluene at -30 °C yielded *rac*-($^{3\text{-Et}}$Ind$^{\#}$)$_2$HfCl$_2$ as yellow crystals. Yellow crystals of *rac*-($^{3\text{-Et}}$Ind$^{\#}$)$_2$HfCl$_2$ suitable for single crystal X-ray diffraction were grown in Et_2O at -30 °C.

***rac*-($^{3\text{-Et}}$Ind$^{\#}$)$_2$HfCl$_2$:**

^{1}H NMR (400.2 MHz, 298 K, chloroform-d$_1$): δ (ppm) 1.05 (t, 6H, $^{3}J_{HH}$ = 7.5 Hz, Ind-CH$_2$-C**H₃**), 1.76 (s, 6H, Ind-C**H₃**), 2.28 (s, 12H, Ind-C**H₃**), 2.50 (s, 6H, Ind-C**H₃**), 2.56 (s, 6H, Ind-C**H₃**), 2.56 (dq, 2H, $^{2}J_{HH}$ = 15.0 Hz, $^{3}J_{HH}$ = 7.5 Hz, Ind-C**H$_a$**H$_b$-CH$_3$), 3.11 (dq, 2H, $^{2}J_{HH}$ = 15.0 Hz, $^{3}J_{HH}$ = 7.5 Hz, Ind-CH$_a$**H$_b$**-CH$_3$), 6.06 (s, 2H, Ind-**H**).

^{13}C{^{1}H} NMR (100.6 MHz, 298 K, chloroform-d$_1$): δ (ppm) 13.75 (Ind-**C**H$_3$), 15.73 (Ind-CH$_2$-**C**H$_3$), 16.49 (Ind-**C**H$_3$), 16.68 (Ind-**C**H$_3$), 16.74 (Ind-**C**H$_3$), 17.62 (Ind-**C**H$_3$), 21.58

(Ind-**C**H_2-CH_3), 92.68 (**Ind**-H), 122.24 (**Ind**), 124.15 (**Ind**), 125.42 (**Ind**), 126.66 (**Ind**), 129.61 (**Ind**), 130.09 (**Ind**), 132.91 (**Ind**), 133.42 (**Ind**).

HRMS (EI): *m*/*z* = found 676.2133; calculated 676.2124, $[M]^+$.

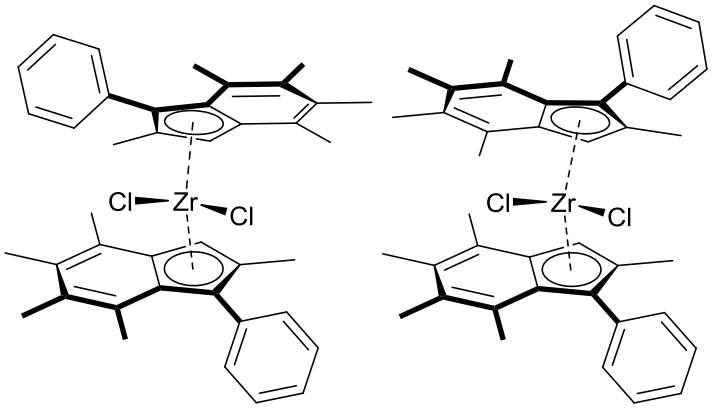
CHN analysis (%): found: C 57.77, H 6.94; calculated: C 56.85, H 6.26.

***meso*-($^{3\text{-Et}}$Ind$^{\#}$)$_2$HfCl$_2$:**

^{1}H NMR (400.2 MHz, 298 K, chloroform-d$_1$): δ (ppm) 1.08 (t, 6H, $^3J_{HH}$ = 7.5 Hz, Ind-CH_2-C**H$_3$**), 2.12 (s, 6H, Ind-C**H$_3$**), 2.21 (s, 12H, Ind-C**H$_3$**), 2.34 (s, 6H, Ind-C**H$_3$**), 2.48 (s, 6H, Ind-C**H$_3$**), 2.63 (dq, 2H, $^2J_{HH}$ = 15.0 Hz, $^3J_{HH}$ = 7.5 Hz, Ind-C**H$_a$**H$_b$-CH_3), 3.26 (dq, 2H, $^2J_{HH}$ = 15.0 Hz, $^3J_{HH}$ = 7.5 Hz, Ind-CH_a**H$_b$**-CH_3), 5.70 (s, 2H, Ind-**H**).

^{13}C{^{1}H} NMR (100.6 MHz, 298 K, chloroform-d$_1$): δ (ppm) 15.43 (Ind-**C**H_3), 15.57 (Ind-CH_2-**C**H_3), 16.34 (Ind-**C**H_3), 16.51 (Ind-**C**H_3), 16.64 (Ind-**C**H_3), 16.64 (Ind-**C**H_3), 21.78 (Ind-**C**H_2-CH_3), 94.79 (**Ind**-H), 123.63 (**Ind**), 124.26 (**Ind**), 126.16 (**Ind**), 126.72 (**Ind**), 128.20 (**Ind**), 129.96 (**Ind**), 132.93 (**Ind**), 133.31 (**Ind**).

6.5.3 Synthesis of ($^{3\text{-Ph}}$Ind$^{\#}$)$_2$ZrCl$_2$



$C_{40}H_{42}Cl_2Zr$, M_r = 684.90

$^{3\text{-Ph}}$Ind$^{\#}$Li (2.00 g, 7.45 mmol, 2.0 eq) and $ZrCl_4$ (0.868 g, 3.73 mmol, 1.0 eq) were mixed in benzene (100 mL) and left stirring for 16 hours at room temperature. The reaction mixture was allowed to settle before being filtered. The orange filtrate was dried *in vacuo* to afford the product, a 50:50 mixture of *rac*-($^{3\text{-Ph}}$Ind$^{\#}$)$_2$ZrCl$_2$ and *meso*-($^{3\text{-Ph}}$Ind$^{\#}$)$_2$ZrCl$_2$, as an orange yellow solid (1.15 g, 1.68 mmol, 45% yield).

^{1}H NMR (499.9 MHz, 298 K, chloroform-d$_1$): δ (ppm) 1.64 (s, 6H, Ind-C**H$_3$**), 1.98 (s, 6H, Ind-C**H$_3$**), 2.02 (s, 6H, Ind-C**H$_3$**), 2.18 (s, 6H, Ind-C**H$_3$**), 2.21 (s, 12H, Ind-C**H$_3$**), 2.27 (s, 12H, Ind-C**H$_3$**), 2.29 (s, 6H, Ind-C**H$_3$**), 2.73 (s, 6H, Ind-C**H$_3$**), 5.86 (s, 2H, Ind-**H**), 6.52 (s, 2H,

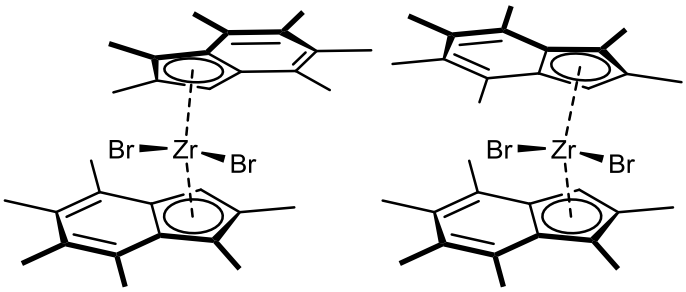
Ind-**H**), 6.98 (bd, 2H, Ph-**H**), 7.01 (m, 2H, Ph-**H**), 7.24 (bt, 2H, Ph-**H**), 7.28 (m, 6H, Ph-**H**), 7.38 (m, 4H, Ph-**H**), 7.66 (bd, 2H, Ph-**H**), 7.85 (bd, 2H, Ph-**H**).

^{13}C{^{1}H} NMR (125.7 MHz, 298 K, chloroform-d$_1$): δ (ppm) 15.06 (Ind-**C**H$_3$), 16.58 (Ind-**C**H$_3$), 16.69 (Ind-**C**H$_3$), 16.69 (Ind-**C**H$_3$), 16.78 (Ind-**C**H$_3$), 16.86 (Ind-**C**H$_3$), 17.10 (Ind-**C**H$_3$), 18.26 (Ind-**C**H$_3$), 18.49 (Ind-**C**H$_3$), 18.75 (Ind-**C**H$_3$), 94.42 (**Ind**-H), 98.62 (**Ind**-H), 124.40 (**Ind**), 125.06 (**Ind**), 125.38 (**Ind**), 125.81 (**Ind**), 126.98 (**Ph**-H), 127.00 (**Ph**-H), 127.05 (**Ph**-H), 127.26 (**Ph**-H), 127.30 (**Ph**-H), 127.57 (**Ind**), 127.61 (**Ind**), 127.66 (**Ph**-H), 127.90 (**Ind**), 130.50 (**Ind**), 130.50 (**Ind**), 130.72 (**Ind**), 131.76 (**Ind**), 132.09 (**Ph**-H), 132.21 (**Ph**-H), 132.44 (**Ph**-H), 132.54 (**Ind**), 133.58 (**Ind**), 133.69 (**Ind**), 134.04 (**Ph**-H), 134.78 (**Ind**), 134.86 (**Ind**), 135.95 (Ind-**Ph**), 136.06 (Ind-**Ph**).

HRMS (EI): *m*/*z* = found 682.1736; calculated 682.1705, $[M]^+$.

CHN analysis (%): found: C 70.26, H 6.38; calculated: C 70.15, H 6.18.

6.5.4 Synthesis of (Ind$^{\#}$)$_2$ZrBr$_2$



$C_{30}H_{38}Br_2Zr$, M_r = 649.67

Ind$^{\#}$Li (2.00 g, 9.70 mmol, 2.0 eq) and $ZrBr_4$ (1.99 g, 4.85 mmol, 1.0 eq) were mixed in benzene (100 mL) and left stirring for 16 hours at room temperature. The reaction mixture was allowed to settle before being filtered. The red filtrate was dried *in vacuo* to afford an orange solid comprising of a 20:80 mixture of *rac*-(Ind$^{\#}$)$_2$ZrBr$_2$ and *meso*-(Ind$^{\#}$)$_2$ZrBr$_2$, and impurities. Recrystallisation of the isomeric mixture in toluene at -30 °C yielded the product, *meso*-(Ind$^{\#}$)$_2$ZrBr$_2$, as orange crystals suitable for single crystal X-ray diffraction (0.180 g, 0.277 mmol, 6% yield).

***meso*-(Ind$^{\#}$)$_2$ZrBr$_2$:**

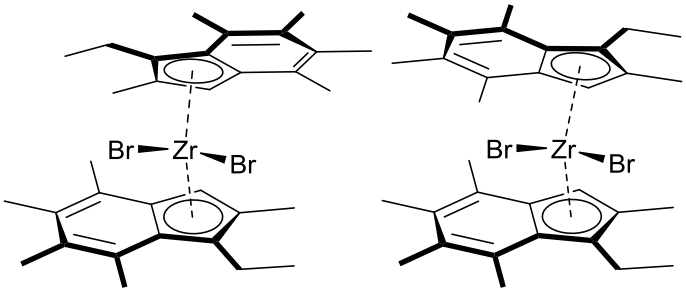
^{1}H NMR (400.2 MHz, 298 K, chloroform-d$_1$): δ (ppm) 2.12 (s, 6H, Ind-C**H$_3$**), 2.17 (s, 6H, Ind-C**H$_3$**), 2.20 (s, 6H, Ind-C**H$_3$**), 2.22 (s, 6H, Ind-C**H$_3$**), 2.55 (s, 6H, Ind-C**H$_3$**), 2.64 (s, 6H, Ind-C**H$_3$**), 5.90 (s, 2H, Ind-**H**).

^{13}C{^{1}H} NMR (100.6 MHz, 298 K, chloroform-d$_1$): δ (ppm) 16.23 (Ind-**C**H$_3$), 16.57 (Ind-**C**H$_3$), 16.59 (Ind-**C**H$_3$), 16.64 (Ind-**C**H$_3$), 16.72 (Ind-**C**H$_3$), 17.46 (Ind-**C**H$_3$), 96.73 (**Ind**-H), 121.24 (**Ind**), 126.82 (**Ind**), 127.35 (**Ind**), 127.36 (**Ind**), 129.59 (**Ind**), 130.98 (**Ind**), 133.40 (**Ind**), 133.95 (**Ind**).

HRMS (EI): *m*/*z* = found 646.0366; calculated 646.0382, $[M]^+$.

CHN analysis (%): found: C 55.50, H 6.02; calculated: C 55.46, H 5.90.

6.5.5 Synthesis of ($^{3\text{-Et}}$Ind$^{\#}$)$_2$ZrBr$_2$



$C_{32}H_{42}Br_2Zr$, M_r = 677.72

$^{3\text{-Et}}$Ind$^{\#}$Li (2.00 g, 9.08 mmol, 2.0 eq) and $ZrBr_4$ (1.87 g, 4.54 mmol, 1.0 eq) were mixed in benzene (100 mL) and left stirring for 16 hours at room temperature. The reaction mixture was allowed to settle before being filtered. The orange filtrate was dried *in vacuo* to afford an orange solid comprising of a 40:60 mixture of *rac*-($^{3\text{-Et}}$Ind$^{\#}$)$_2$ZrBr$_2$ and *meso*-($^{3\text{-Et}}$Ind$^{\#}$)$_2$ZrBr$_2$, and impurities. Recrystallisation of the isomeric mixture in DCM at -30 °C yielded the product, *meso*-($^{3\text{-Et}}$Ind$^{\#}$)$_2$ZrBr$_2$, as orange crystals (0.178 g, 0.263 mmol, 6% yield). Orange crystals of *meso*-($^{3\text{-Et}}$Ind$^{\#}$)$_2$ZrBr$_2$ suitable for single crystal X-ray diffraction were grown in pentane at room temperature.

***meso*-($^{3\text{-Et}}$Ind$^{\#}$)$_2$ZrBr$_2$:**

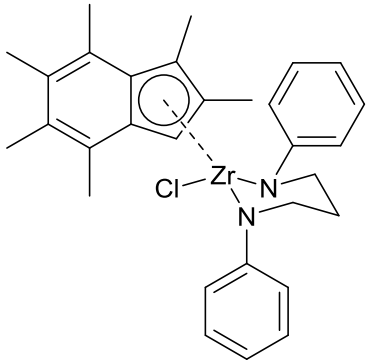
^{1}H NMR (400.2 MHz, 298 K, chloroform-d$_1$): δ (ppm) 1.05 (t, 6H, $^3J_{HH}$ = 7.5 Hz, Ind-CH$_2$-C**H$_3$**), 1.70 (s, 6H, Ind-C**H$_3$**), 2.23 (s, 6H, Ind-C**H$_3$**), 2.27 (s, 6H, Ind-C**H$_3$**), 2.54 (s, 12H, Ind-C**H$_3$**), 2.69 (dq, 2H, $^2J_{HH}$ = 15.0 Hz, $^3J_{HH}$ = 7.5 Hz, Ind-C**H$_a$**H$_b$-CH$_3$), 3.22 (dq, 2H, $^2J_{HH}$ = 15.0 Hz, $^3J_{HH}$ = 7.5 Hz, Ind-CH$_a$**H$_b$**-CH$_3$), 6.25 (s, 2H, Ind-**H**).

^{13}C{^{1}H} NMR (100.6 MHz, 298 K, chloroform-d$_1$): δ (ppm) 14.60 (Ind-**C**H$_3$), 15.64 (Ind-CH$_2$-**C**H$_3$), 16.62 (Ind-**C**H$_3$), 16.84 (Ind-**C**H$_3$), 17.05 (Ind-**C**H$_3$), 17.62 (Ind-**C**H$_3$), 22.99 (Ind-**C**H$_2$-CH$_3$), 94.57 (**Ind**-H), 125.19 (**Ind**), 125.59 (**Ind**), 126.00 (**Ind**), 127.82 (**Ind**), 130.83 (**Ind**), 130.94 (**Ind**), 133.42 (**Ind**), 134.18 (**Ind**).

HRMS (EI): *m*/*z* = found 674.0724; calculated 674.0695, $[M]^+$.

CHN analysis (%): found: C 56.61, H 6.33; calculated: C 56.71, H 6.25.

6.5.6 Synthesis of (Ind$^{\#}$)(PhN(CH$_2$)$_3$NPh)ZrCl



$C_{30}H_{35}N_2ClZr$, M_r = 550.30

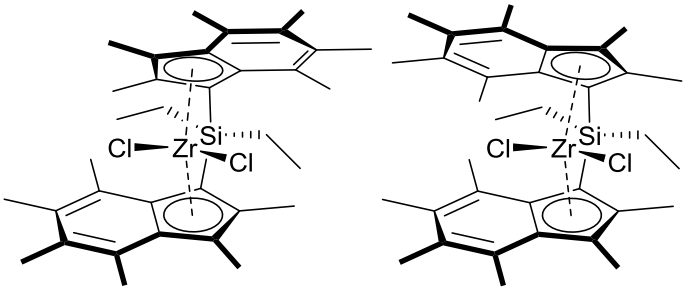
Ind$^{\#}$Li (1.00 g, 4.85 mmol, 2.0 eq) and (PhN(CH$_2$)$_3$NPh)ZrCl$_2$·2THF (1.29 g, 2.42 mmol, 1.0 eq) were mixed in benzene (50 mL) and left stirring for 16 hours at room temperature. The reaction mixture was dried *in vacuo* to yield a yellow solid which was then extracted with benzene (50 mL). The yellow filtrate was dried *in vacuo* to afford the product as a yellow solid (0.880 g, 1.60 mmol, 66% yield). Yellow crystals of (Ind$^{\#}$)(PhN(CH$_2$)$_3$NPh)ZrCl suitable for single crystal X-ray diffraction were grown by slow evaporation of a benzene-d$_6$ solution of the product.

^{1}H NMR (400.2 MHz, 298 K, chloroform-d$_1$): δ (ppm) 1.68 (s, 3H, Ind-C**H$_3$**), 2.02 (s, 3H, Ind-C**H$_3$**), 2.04 (m, 1H, Ph$_a$N-CH$_2$-C**H$_a$**H$_b$-CH$_2$-NPh$_b$), 2.14 (m, 1H, Ph$_a$N-CH$_2$-CH$_a$**H$_b$**-CH$_2$-NPh$_b$), 2.20 (s, 3H, Ind-C**H$_3$**), 2.22 (s, 3H, Ind-C**H$_3$**), 2.25 (s, 3H, Ind-C**H$_3$**), 2.55 (s, 3H, Ind-C**H$_3$**), 2.95 (m, 1H, Ph$_a$N-C**H$_a$**H$_b$-CH$_2$-CH$_2$-NPh$_b$), 3.29 (m, 1H, Ph$_a$N-CH$_a$**H$_b$**-CH$_2$-CH$_2$-NPh$_b$), 3.62 (m, 2H, Ph$_a$N-CH$_2$-CH$_2$-C**H$_2$**-NPh$_b$), 5.39 (s, 1H, Ind-**H**), 6.72 (d, 2H, $^3J_{HH}$ = 8.4 Hz, *o*-Ph$_a$-**H**), 6.86 (t, 1H, $^3J_{HH}$ = 7.3 Hz, *p*-Ph$_a$-**H**), 6.97 (t, 1H, $^3J_{HH}$ = 7.3 Hz, *p*-Ph$_b$-**H**), 7.00 (d, 2H, $^3J_{HH}$ = 8.4 Hz, *o*-Ph$_b$-**H**), 7.23 (dd, 2H, $^3J_{HH}$ = 7.3, 8.4 Hz, *m*-Ph$_a$-**H**), 7.33 (dd, 2H, $^3J_{HH}$ = 7.3, 8.4 Hz, *m*-Ph$_b$-**H**).

^{13}C{^{1}H} NMR (100.6 MHz, 298 K, chloroform-d$_1$): δ (ppm) 14.21 (Ind-**C**H$_3$), 14.56 (Ind-**C**H$_3$), 15.92 (Ind-**C**H$_3$), 16.50 (Ind-**C**H$_3$), 16.50 (Ind-**C**H$_3$), 16.77 (Ind-**C**H$_3$), 33.21 (Ph$_a$N-CH$_2$-**C**H$_2$-CH$_2$-NPh$_b$), 54.75 (Ph$_a$N-CH$_2$-CH$_2$-**C**H$_2$-NPh$_b$), 55.18 (Ph$_a$N-**C**H$_2$-CH$_2$-CH$_2$-NPh$_b$), 100.34 (**Ind**-H), 114.03 (**Ind**), 118.40 (*o*-**Ph$_a$**), 118.95 (*o*-**Ph$_b$**), 120.83 (*p*-**Ph$_a$**), 121.60 (*p*-**Ph$_b$**), 124.31 (**Ind**), 125.25 (**Ind**), 126.61 (**Ind**), 129.11 (*m*-**Ph$_a$**), 129.16 (*m*-**Ph$_b$**), 131.46 (**Ind**), 131.56 (**Ind**), 132.52 (**Ind**), 133.02 (**Ind**) 152.60 (N-**Ph$_a$**), 154.71 (N-**Ph$_b$**).

CHN analysis (%): found: C 65.36, H 6.52, N 5.14; calculated: C 65.48, H 6.41, N 5.09.

6.5.7 Synthesis of ^{Et2}SBI*ZrCl$_2$



$C_{34}H_{46}SiCl_2Zr$, M_r = 644.95

rac-^{Et2}SBI*H$_2$ (0.640 g, 1.32 mmol, 1.0 eq) was dissolved in THF (50 mL) to form a colourless solution. *n*BuLi (2.5 M in hexanes, 1.16 mL, 2.90 mmol, 2.2 eq) was added dropwise to the solution at 0 °C. The reaction was kept at 0 °C and stirred for 1 hour. The resulting dark brown solution was dried *in vacuo* at 0 °C to form a yellow solid, which was then washed with pentane (2 x 25 mL). $ZrCl_4$ (0.308 g, 1.32 mmol, 1.0 eq) was mixed with *rac*-^{Et2}SBI*Li$_2$ (yellow solid), and benzene (50 mL) was then added to the mixture. The reaction slowly turned red and was left stirring for 16 hours at room temperature. The reaction mixture was allowed to settle before being filtered. The red filtrate was dried *in vacuo* to afford a red solid which was then washed with Et_2O (25 mL) to yield the product, a 50:50 mixture of *rac*-^{Et2}SBI*ZrCl$_2$ and *meso*-^{Et2}SBI*ZrCl$_2$, as a red solid (77.1 mg, 0.120 mmol, 9% yield). *rac*-^{Et2}SBI*ZrCl$_2$ was isolated as orange crystals from the Et_2O filtrate at -30 °C. Orange crystals of *rac*-^{Et2}SBI*ZrCl$_2$ suitable for single crystal X-ray diffraction were grown by slow evaporation of a benzene-d_6 solution of the isomer.

***rac*-^{Et2}SBI*ZrCl$_2$:**

^{1}H NMR (400.2 MHz, 298 K, chloroform-d$_1$): δ (ppm) 1.38 (t, 6H, $^3J_{HH}$ = 7.6 Hz, Si-CH$_2$-C**H$_3$**), 1.54 (m, 2H, $^3J_{HH}$ = 7.6 Hz, Si-C**H$_a$**H$_b$-CH$_3$), 1.84 (s, 6H, Ind-C**H$_3$**), 2.07 (m, 2H, $^3J_{HH}$ = 7.6 Hz, Si-CH$_a$**H$_b$**-CH$_3$), 2.18 (s, 6H, Ind-C**H$_3$**), 2.30 (s, 6H, Ind-C**H$_3$**), 2.40 (s, 6H, Ind-C**H$_3$**), 2.43 (s, 6H, Ind-C**H$_3$**), 2.45 (s, 6H, Ind-C**H$_3$**).

^{13}C{^{1}H} NMR (100.6 MHz, 298 K, chloroform-d$_1$): δ (ppm) 8.26 (Si-CH$_2$-**C**H$_3$), 11.75 (Si-**C**H$_2$-CH$_3$), 14.94 (Ind-**C**H$_3$), 16.13 (Ind-**C**H$_3$), 16.45 (Ind-**C**H$_3$), 17.50 (Ind-**C**H$_3$), 17.72 (Ind-**C**H$_3$), 21.93 (Ind-**C**H$_3$), 78.46 (**Ind**-Si), 127.46 (**Ind**), 129.85 (**Ind**), 129.88 (**Ind**), 130.08 (**Ind**), 130.98 (**Ind**), 134.23 (**Ind**), 134.73 (**Ind**), 135.28 (**Ind**).

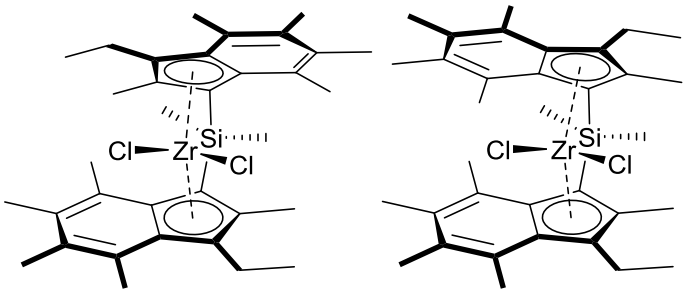
CHN analysis (%): found: C 63.40, H 7.24; calculated: C 63.32, H 7.19.

***meso*-^{Et2}SBI*ZrCl$_2$:**

^{1}H NMR (400.2 MHz, 298 K, chloroform-d$_1$): δ (ppm) 1.39 (t, 3H, $^3J_{HH}$ = 7.5 Hz, Si-CH$_2$-C$_a$**H$_3$**), 1.44 (t, 3H, $^3J_{HH}$ = 7.5 Hz, Si-CH$_2$-C$_b$**H$_3$**), 1.83 (q, 2H, $^3J_{HH}$ = 7.5 Hz, Si-C**H$_2$**-C$_b$H$_3$), 1.99 (q, 2H, $^3J_{HH}$ = 7.5 Hz, Si-C**H$_2$**-C$_a$H$_3$), 2.06 (s, 6H, Ind-C**H$_3$**), 2.12 (s, 6H, Ind-C**H$_3$**), 2.16 (s, 6H, Ind-C**H$_3$**), 2.44 (s, 12H, Ind-C**H$_3$**), 2.51 (s, 6H, Ind-C**H$_3$**).

^{13}C{^{1}H} NMR (100.6 MHz, 298 K, chloroform-d$_1$): δ (ppm) 7.95 (Si-CH$_2$-**C$_a$**H$_3$), 8.15 (Si-CH$_2$-**C$_b$**H$_3$), 10.02 (Si-**C**H$_2$-C$_b$H$_3$), 12.78 (Si-**C**H$_2$-C$_a$H$_3$), 16.14 (Ind-**C**H$_3$), 16.29 (Ind-**C**H$_3$), 16.43 (Ind-**C**H$_3$), 17.25 (Ind-**C**H$_3$), 17.81 (Ind-**C**H$_3$), 22.20 (Ind-**C**H$_3$), 77.48 (**Ind**-Si), 128.47 (**Ind**), 129.88 (**Ind**), 130.82 (**Ind**), 131.30 (**Ind**), 133.93 (**Ind**), 134.04 (**Ind**), 134.06 (**Ind**), 134.12 (**Ind**).

6.5.8 Synthesis of ^{Me2}SB($^{3\text{-}Et}$I*)ZrCl$_2$



C$_{34}$H$_{46}$SiCl$_2$Zr, M_r = 644.95

Method A:

^{Me2}SB($^{3\text{-}Et}$I*)H$_2$ (2.64 g, 5.45 mmol, 1.0 eq) was dissolved in THF (100 mL) to form a pale yellow solution. *n*BuLi (2.5 M in hexanes, 4.79 mL, 12.0 mmol, 2.2 eq) was added dropwise to the solution at 0 °C. The reaction was kept at 0 °C and stirred for 30 minutes. The resulting dark brown solution was dried *in vacuo* at 0 °C to form a yellow solid, which was then washed with Et$_2$O (50 mL) and pentane (2 x 50 mL). ZrCl$_4$ (1.27 g, 5.45 mmol, 1.0 eq) was mixed with ^{Me2}SB($^{3\text{-}Et}$I*)Li$_2$ (yellow solid), and benzene (100 mL) was then added to the mixture. The reaction slowly turned red and was left stirring for 16 hours at room temperature. The reaction mixture was allowed to settle before being filtered. The red filtrate was dried *in vacuo* to afford an orange solid which was then washed with Et$_2$O (50 mL) to yield the product, a 50:50 mixture of *rac*-^{Me2}SB($^{3\text{-}Et}$I*)ZrCl$_2$ and *meso*-^{Me2}SB($^{3\text{-}Et}$I*)ZrCl$_2$, as an orange solid (0.850 g, 1.32 mmol, 24% yield).

Method B:

$^{3\text{-Et}}$Ind$^{\#}$H (3.40 g, 15.9 mmol, 2.0 eq) was dissolved in pentane (100 mL) to form a pale yellow solution. *n*BuLi (2.5 M in hexanes, 6.98 mL, 17.4 mmol, 2.2 eq) was added dropwise to the solution at 0 °C. The reaction was allowed to warm up to room temperature and stirred for 3 hours, during which time an off-white solid was formed. The resulting mixture was dried *in vacuo* and redissolved in THF (100 mL) to form a dark brown solution of $^{3\text{-Et}}$Ind$^{\#}$Li. Me_2SiCl_2 (1.02 g, 7.93 mmol, 1.0 eq) was dissolved in THF (50 mL) to form a colourless solution and then added dropwise to the $^{3\text{-Et}}$Ind$^{\#}$Li solution at 0 °C. The reaction was allowed to warm up to room temperature and left stirring for 16 hours after which an aliquot was taken showing that the reaction had gone to completion. *n*BuLi (2.5 M in hexanes, 6.98 mL, 17.4 mmol, 2.2 eq) was added dropwise to the resulting pale yellow solution of ^{Me2}SB($^{3\text{-Et}}$I*)H_2 at 0 °C. The reaction was kept at 0 °C and stirred for 30 minutes. The resulting dark brown solution was dried *in vacuo* at 0 °C to form a yellow solid, which was then washed with Et_2O (50 mL) and pentane (2 x 50 mL). $ZrCl_4$ (1.85 g, 7.93 mmol, 1.0 eq) was mixed with ^{Me2}SB($^{3\text{-Et}}$I*)Li_2 (yellow solid), and benzene (100 mL) was then added to the mixture. The reaction slowly turned red and was left stirring for 16 hours at room temperature, after which the reaction mixture was dried *in vacuo* to yield a red solid. The red solid was then extracted with pentane (100 mL) and the product, a 50:50 mixture of *rac*-^{Me2}SB($^{3\text{-Et}}$I*)$ZrCl_2$ and *meso*-^{Me2}SB($^{3\text{-Et}}$I*)$ZrCl_2$, was precipitated from the pentane filtrate at -30 °C as an orange solid (0.353 g, 0.547 mmol, 7% yield). Recrystallisation of the isomeric mixture in Et_2O at -30 °C yielded *rac*-^{Me2}SB($^{3\text{-Et}}$I*)$ZrCl_2$ as orange crystals. Orange crystals of *rac*-^{Me2}SB($^{3\text{-Et}}$I*)$ZrCl_2$ and *meso*-^{Me2}SB($^{3\text{-Et}}$I*)$ZrCl_2$ suitable for single crystal X-ray diffraction were grown by slow cooling of hot pentane extract of the isomeric mixture.

HRMS (EI): *m*/*z* = found 642.1750; calculated 642.1787, $[M]^+$.

CHN analysis (%): found: C 63.16, H 7.29; calculated: C 63.32, H 7.19.

***rac*-^{Me2}SB($^{3\text{-Et}}$I*)$ZrCl_2$:**

^{1}H NMR (400.2 MHz, 298 K, benzene-d_6): δ (ppm) 0.86 (t, 6H, $^3J_{HH}$ = 7.6 Hz, Ind-CH_2-C**H**$_3$), 1.14 (s, 6H, Si-C**H**$_3$), 1.92 (s, 6H, Ind-C**H**$_3$), 2.04 (s, 6H, Ind-C**H**$_3$), 2.24 (s, 6H, Ind-C**H**$_3$), 2.35 (s, 6H, Ind-C**H**$_3$), 2.54 (s, 6H, Ind-C**H**$_3$), 2.71 (dq, 2H, $^2J_{HH}$ = 15.2 Hz, $^3J_{HH}$ = 7.6 Hz, Ind-C**H**$_a$H$_b$-CH_3), 3.30 (dq, 2H, $^2J_{HH}$ = 15.2 Hz, $^3J_{HH}$ = 7.6 Hz, Ind-CH_a**H**$_b$-CH_3).

^{13}C{^{1}H} NMR (100.6 MHz, 298 K, benzene-d_6): δ (ppm) 10.84 (Si-**C**H_3), 15.00 (Ind-CH_2-**C**H_3), 15.26 (Ind-**C**H_3), 16.70 (Ind-**C**H_3), 16.97 (Ind-**C**H_3), 17.48 (Ind-**C**H_3), 22.37 (Ind-**C**H_3), 23.03 (Ind-**C**H_2-CH_3), 79.17 (**Ind**-Si), 127.94 (**Ind**), 128.71 (**Ind**), 129.88 (**Ind**), 131.04 (**Ind**), 134.34 (**Ind**), 134.57 (**Ind**), 135.25 (**Ind**), 135.26 (**Ind**).

^{1}H NMR (400.2 MHz, 298 K, chloroform-d$_1$): δ (ppm) 0.91 (t, 6H, $^{3}J_{HH}$ = 7.6 Hz, Ind-CH$_2$-C**H$_3$**), 1.36 (s, 6H, Si-C**H$_3$**), 1.92 (s, 6H, Ind-C**H$_3$**), 2.18 (s, 6H, Ind-C**H$_3$**), 2.32 (s, 6H, Ind-C**H$_3$**), 2.44 (s, 6H, Ind-C**H$_3$**), 2.46 (s, 6H, Ind-C**H$_3$**), 2.54 (dq, 2H, $^{2}J_{HH}$ = 15.2 Hz, $^{3}J_{HH}$ = 7.6 Hz, Ind-C**H$_a$**H$_b$-CH$_3$), 3.09 (dq, 2H, $^{2}J_{HH}$ = 15.2 Hz, $^{3}J_{HH}$ = 7.6 Hz, Ind-CH$_a$**H$_b$**-CH$_3$).

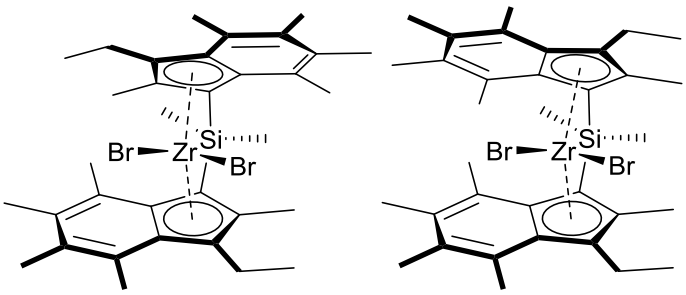
^{13}C{^{1}H} NMR (100.6 MHz, 298 K, chloroform-d$_1$): δ (ppm) 11.02 (Si-**C**H$_3$), 14.95 (Ind-CH$_2$-**C**H$_3$), 15.14 (Ind-**C**H$_3$), 16.64 (Ind-**C**H$_3$), 16.70 (Ind-**C**H$_3$), 17.55 (Ind-**C**H$_3$), 22.41 (Ind-**C**H$_3$), 22.59 (Ind-**C**H$_2$-CH$_3$), 78.73 (**Ind**-Si), 127.92 (**Ind**), 128.35 (**Ind**), 130.16 (**Ind**), 130.63 (**Ind**), 134.07 (**Ind**), 134.36 (**Ind**), 135.07 (**Ind**), 135.34 (**Ind**).

***meso*-^{Me2}SB($^{3\text{-}Et}$I*)ZrCl$_2$:**

^{1}H NMR (400.2 MHz, 298 K, chloroform-d$_1$): δ (ppm) 1.02 (t, 6H, $^{3}J_{HH}$ = 7.6 Hz, Ind-CH$_2$-C**H$_3$**), 1.31 (s, 3H, Si-C$_a$**H$_3$**), 1.44 (s, 3H, Si-C$_b$**H$_3$**), 2.06 (s, 6H, Ind-C**H$_3$**), 2.16 (s, 6H, Ind-C**H$_3$**), 2.19 (s, 6H, Ind-C**H$_3$**), 2.42 (s, 6H, Ind-C**H$_3$**), 2.48 (s, 6H, Ind-C**H$_3$**), 2.67 (dq, 2H, $^{2}J_{HH}$ = 15.2 Hz, $^{3}J_{HH}$ = 7.6 Hz, Ind-C**H$_a$**H$_b$-CH$_3$), 3.15 (dq, 2H, $^{2}J_{HH}$ = 15.2 Hz, $^{3}J_{HH}$ = 7.6 Hz, Ind-CH$_a$**H$_b$**-CH$_3$).

^{13}C{^{1}H} NMR (100.6 MHz, 298 K, chloroform-d$_1$): δ (ppm) 9.62 (Si-**C$_a$**H$_3$), 14.00 (Si-**C$_b$**H$_3$), 14.22 (Ind-CH$_2$-**C**H$_3$), 15.55 (Ind-**C**H$_3$), 16.57 (Ind-**C**H$_3$), 16.60 (Ind-**C**H$_3$), 17.30 (Ind-**C**H$_3$), 22.65 (Ind-**C**H$_2$-CH$_3$), 22.76 (Ind-**C**H$_3$), 78.16 (**Ind**-Si), 128.77 (**Ind**), 129.41 (**Ind**), 130.56 (**Ind**), 133.45 (**Ind**), 134.12 (**Ind**), 134.15 (**Ind**), 134.49 (**Ind**), 134.91 (**Ind**).

6.5.9 Synthesis of ^{Me2}SB($^{3\text{-}Et}$I*)ZrBr$_2$



C$_{34}$H$_{46}$SiBr$_2$Zr, M_r = 733.86

^{Me2}SB($^{3\text{-}Et}$I*)H$_2$ (3.30 g, 6.81 mmol, 1.0 eq) was dissolved in THF (100 mL) to form a pale yellow solution. *n*BuLi (2.5 M in hexanes, 5.99 mL, 15.0 mmol, 2.2 eq) was added dropwise to the solution at 0 °C. The reaction was kept at 0 °C and stirred for 30 minutes. The resulting dark brown solution was dried *in vacuo* at 0 °C to form a yellow solid, which was then washed with Et$_2$O (50 mL) and pentane (2 x 50 mL). ZrBr$_4$ (2.80 g, 6.81 mmol, 1.0 eq) was

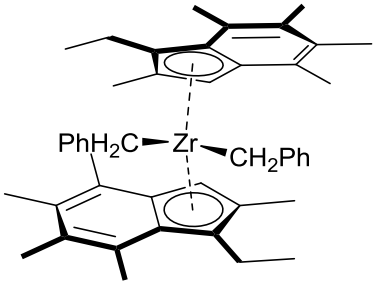
mixed with ^{Me2}SB($^{3\text{-}Et}$I*)Li$_2$ (yellow solid), and benzene (100 mL) was then added to the mixture. The reaction slowly turned red and was left stirring for 16 hours at room temperature. The reaction mixture was allowed to settle before being filtered. The red filtrate was dried *in vacuo* to afford a red solid comprising of a 50:50 mixture of *rac*-^{Me2}SB($^{3\text{-}Et}$I*)ZrBr$_2$ and *meso*-^{Me2}SB($^{3\text{-}Et}$I*)ZrBr$_2$, and impurities. Recrystallisation of the isomeric mixture in Et$_2$O at -30 °C yielded the product, *rac*-^{Me2}SB($^{3\text{-}Et}$I*)ZrBr$_2$, as orange crystals (68.6 mg, 0.0935 mmol, 1% yield). Orange crystals of *rac*-^{Me2}SB($^{3\text{-}Et}$I*)ZrBr$_2$ suitable for single crystal X-ray diffraction were grown by slow evaporation of a Et$_2$O solution of the isomer. Orange crystals of *meso*-^{Me2}SB($^{3\text{-}Et}$I*)ZrBr$_2$ suitable for single crystal X-ray diffraction were grown by slow evaporation of a chloroform-d$_1$ solution of the isomeric mixture.

***rac*-^{Me2}SB($^{3\text{-}Et}$I*)ZrBr$_2$:**

^{1}H NMR (400.2 MHz, 298 K, chloroform-d$_1$): δ (ppm) 0.91 (t, 6H, $^3J_{HH}$ = 7.6 Hz, Ind-CH$_2$-C**H$_3$**), 1.35 (s, 6H, Si-C**H$_3$**), 1.86 (s, 6H, Ind-C**H$_3$**), 2.15 (s, 6H, Ind-C**H$_3$**), 2.35 (s, 6H, Ind-C**H$_3$**), 2.45 (s, 6H, Ind-C**H$_3$**), 2.46 (s, 6H, Ind-C**H$_3$**), 2.65 (dq, 2H, $^2J_{HH}$ = 15.2 Hz, $^3J_{HH}$ = 7.6 Hz, Ind-C**H$_a$**H$_b$-CH$_3$), 3.23 (dq, 2H, $^2J_{HH}$ = 15.2 Hz, $^3J_{HH}$ = 7.6 Hz, Ind-CH$_a$**H$_b$**-CH$_3$).

^{13}C{^{1}H} NMR (100.6 MHz, 298 K, chloroform-d$_1$): δ (ppm) 11.15 (Si-**C**H$_3$), 15.30 (Ind-CH$_2$-**C**H$_3$), 15.70 (Ind-**C**H$_3$), 16.71 (Ind-**C**H$_3$), 17.01 (Ind-**C**H$_3$), 17.62 (Ind-**C**H$_3$), 22.26 (Ind-**C**H$_3$), 24.04 (Ind-**C**H$_2$-CH$_3$), 77.59 (**Ind**-Si), 128.43 (**Ind**), 128.58 (**Ind**), 130.19 (**Ind**), 131.28 (**Ind**), 134.24 (**Ind**), 134.81 (**Ind**), 135.58 (**Ind**), 135.71 (**Ind**).

6.5.10 Synthesis of *rac*-($^{3\text{-}Et}$Ind$^{\#}$)$_2$Zr(CH$_2$Ph)$_2$



C$_{46}$H$_{56}$Zr, M_r = 700.18

rac-($^{3\text{-}Et}$Ind$^{\#}$)$_2$ZrCl$_2$ (45.2 mg, 0.0768 mmol, 1.0 eq) and PhCH$_2$K (20.0 mg, 0.154 mmol, 2.0 eq) were mixed in benzene (1 mL) and left stirring for 16 hours at room temperature. The reaction mixture was allowed to settle before being filtered. The yellow filtrate was dried *in*

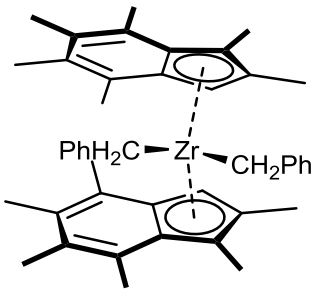
vacuo to afford the product as a yellow solid (50.2 mg, 0.0717 mmol, 93% yield). Yellow crystals of *rac*-($^{3\text{-Et}}$Ind$^{\#}$)$_2$Zr(CH$_2$Ph)$_2$ suitable for single crystal X-ray diffraction were grown in pentane at -30 °C.

^{1}H NMR (400.2 MHz, 298 K, chloroform-d$_1$): δ (ppm) 0.67 (d, 2H, $^2J_{HH}$ = 11.2 Hz, Zr-C**H$_a$**H$_b$-Ph), 0.87 (d, 2H, $^2J_{HH}$ = 11.2 Hz, Zr-CH$_a$**H$_b$**-Ph), 0.99 (t, 6H, $^3J_{HH}$ = 7.4 Hz, Ind-CH$_2$-C**H$_3$**), 1.82 (s, 6H, Ind-C**H$_3$**), 2.01 (s, 6H, Ind-C**H$_3$**), 2.23 (s, 6H, Ind-C**H$_3$**), 2.28 (s, 6H, Ind-C**H$_3$**), 2.45 (dq, 2H, $^2J_{HH}$ = 14.8 Hz, $^3J_{HH}$ = 7.4 Hz, Ind-C**H$_a$**H$_b$-CH$_3$), 2.51 (s, 6H, Ind-C**H$_3$**), 2.76 (dq, 2H, $^2J_{HH}$ = 14.8 Hz, $^3J_{HH}$ = 7.4 Hz, Ind-CH$_a$**H$_b$**-CH$_3$), 4.91 (s, 2H, Ind-**H**), 6.62 (d, 4H, $^3J_{HH}$ = 7.4 Hz, *o*-Ph-**H**), 6.80 (t, 2H, $^3J_{HH}$ = 7.3 Hz, *p*-Ph-**H**), 7.08 (dd, 4H, $^3J_{HH}$ = 7.3, 7.4 Hz, *m*-Ph-**H**).

^{13}C{^{1}H} NMR (100.6 MHz, 298 K, chloroform-d$_1$): δ (ppm) 13.13 (Ind-**C**H$_3$), 16.00 (Ind-CH$_2$-**C**H$_3$), 16.56 (Ind-**C**H$_3$), 16.65 (Ind-**C**H$_3$), 16.76 (Ind-**C**H$_3$), 17.08 (Ind-**C**H$_3$), 21.55 (Ind-**C**H$_2$-CH$_3$), 66.01 (Zr-**C**H$_2$-Ph), 100.76 (**Ind**-H), 119.81 (**Ind**), 121.00 (*p*-**Ph**), 123.22 (**Ind**), 126.39 (**Ind**), 127.14 (*o*-**Ph**), 127.59 (*m*-**Ph**), 127.80 (**Ind**), 127.86 (**Ind**), 128.27 (**Ind**), 130.95 (**Ind**), 133.28 (**Ind**), 152.80 (Zr-CH$_2$-**Ph**).

CHN analysis (%): found: C 78.91, H 8.15; calculated: C 78.91, H 8.06.

6.5.11 Synthesis of *meso*-(Ind$^{\#}$)$_2$Zr(CH$_2$Ph)$_2$



C$_{44}$H$_{52}$Zr, M_r = 672.12

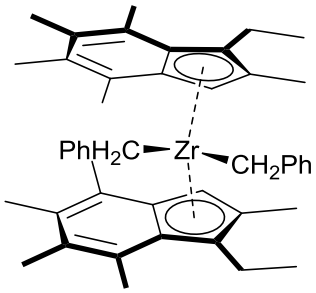
meso-(Ind$^{\#}$)$_2$ZrBr$_2$ (49.9 mg, 0.0768 mmol, 1.0 eq) and PhCH$_2$K (20.0 mg, 0.154 mmol, 2.0 eq) were mixed in benzene (1 mL) and left stirring for 16 hours at room temperature. The reaction mixture was allowed to settle before being filtered. The yellow filtrate was dried *in vacuo* to afford the product as a yellow solid (45.6 mg, 0.0678 mmol, 88% yield). Yellow crystals of *meso*-(Ind$^{\#}$)$_2$Zr(CH$_2$Ph)$_2$ suitable for single crystal X-ray diffraction were grown in toluene at room temperature.

^{1}H NMR (400.2 MHz, 298 K, chloroform-d$_1$): δ (ppm) 0.31 (s, 2H, Zr-C**H$_2$**-Ph$_a$), 1.11 (s, 2H, Zr-C**H$_2$**-Ph$_b$), 1.71 (s, 6H, Ind-C**H$_3$**), 2.12 (s, 6H, Ind-C**H$_3$**), 2.18 (s, 6H, Ind-C**H$_3$**), 2.21

(s, 6H, Ind-C**H**$_3$), 2.22 (s, 6H, Ind-C**H**$_3$), 2.51 (s, 6H, Ind-C**H**$_3$), 5.37 (s, 2H, Ind-**H**), 6.48 (d, 2H, $^3J_{HH}$ = 7.6 Hz, *o*-Ph$_a$-**H**), 6.61 (d, 2H, $^3J_{HH}$ = 7.6 Hz, *o*-Ph$_b$-**H**), 6.76 (t, 1H, $^3J_{HH}$ = 7.3 Hz, *p*-Ph$_a$-**H**), 6.82 (t, 1H, $^3J_{HH}$ = 7.3 Hz, *p*-Ph$_b$-**H**), 7.04 (dd, 2H, $^3J_{HH}$ = 7.3, 7.6 Hz, *m*-Ph$_a$-**H**), 7.09 (dd, 2H, $^3J_{HH}$ = 7.3, 7.6 Hz, *m*-Ph$_b$-**H**).

^{13}C{^{1}H} NMR (125.7 MHz, 298 K, chloroform-d$_1$): δ (ppm) 13.46 (Ind-**C**H$_3$), 14.92 (Ind-**C**H$_3$), 16.53 (Ind-**C**H$_3$), 16.64 (Ind-**C**H$_3$), 16.94 (Ind-**C**H$_3$), 17.56 (Ind-**C**H$_3$), 66.77 (Zr-**C**H$_2$-Ph$_a$), 67.64 (Zr-**C**H$_2$-Ph$_b$), 100.06 (**Ind**-H), 113.63 (**Ind**), 120.73 (*p*-**Ph$_a$**), 121.09 (*p*-**Ph$_b$**), 125.09 (**Ind**), 126.26 (**Ind**), 126.81 (*o*-**Ph$_a$**), 127.08 (*o*-**Ph$_b$**), 127.37 (**Ind**), 127.49 (*m*-**Ph$_a$**), 127.69 (*m*-**Ph$_b$**), 127.91 (**Ind**), 127.97 (**Ind**), 131.53 (**Ind**), 132.92 (**Ind**), 152.75 (Zr-CH$_2$-**Ph$_b$**), 152.87 (Zr-CH$_2$-**Ph$_a$**).

6.5.12 Synthesis of *meso*-(3-EtInd#)$_2$Zr(CH$_2$Ph)$_2$



$C_{46}H_{56}Zr$, M_r = 700.18

Method A:

meso-(3-EtInd#)$_2$ZrCl$_2$ (45.2 mg, 0.0768 mmol, 1.0 eq) and PhCH$_2$K (20.0 mg, 0.154 mmol, 2.0 eq) were mixed in benzene (1 mL) and left stirring for 16 hours at room temperature. The reaction mixture was allowed to settle before being filtered. The yellow filtrate was dried *in vacuo* to afford the product as a yellow solid (49.9 mg, 0.0713 mmol, 93% yield). Orange crystals of *meso*-(3-EtInd#)$_2$Zr(CH$_2$Ph)$_2$ suitable for single crystal X-ray diffraction were grown in pentane at -30 °C.

Method B:

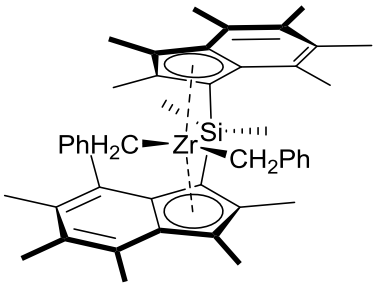
meso-(3-EtInd#)$_2$ZrBr$_2$ (52.0 mg, 0.0768 mmol, 1.0 eq) and PhCH$_2$K (20.0 mg, 0.154 mmol, 2.0 eq) were mixed in benzene (1 mL) and left stirring for 16 hours at room temperature. The reaction mixture was allowed to settle before being filtered. The yellow filtrate was dried *in vacuo* to afford the product as a yellow solid (47.3 mg, 0.0676 mmol, 88% yield).

^{1}H NMR (400.2 MHz, 298 K, chloroform-d$_1$): δ (ppm) 0.24 (s, 2H, Zr-C**H$_2$**-Ph$_a$), 0.79 (s, 2H, Zr-C**H$_2$**-Ph$_b$), 0.95 (t, 6H, $^{3}J_{HH}$ = 7.4 Hz, Ind-CH$_2$-C**H$_3$**), 1.77 (s, 6H, Ind-C**H$_3$**), 2.10 (s, 6H, Ind-C**H$_3$**), 2.18 (s, 6H, Ind-C**H$_3$**), 2.22 (s, 6H, Ind-C**H$_3$**), 2.38 (dq, 2H, $^{2}J_{HH}$ = 14.8 Hz, $^{3}J_{HH}$ = 7.4 Hz, Ind-C**H$_a$**H$_b$-CH$_3$), 2.45 (s, 6H, Ind-C**H$_3$**), 2.71 (dq, 2H, $^{2}J_{HH}$ = 14.8 Hz, $^{3}J_{HH}$ = 7.4 Hz, Ind-CH$_a$**H$_b$**-CH$_3$), 5.61 (s, 2H, Ind-**H**), 6.46 (d, 2H, $^{3}J_{HH}$ = 7.6 Hz, *o*-Ph$_a$-**H**), 6.58 (d, 2H, $^{3}J_{HH}$ = 7.6 Hz, *o*-Ph$_b$-**H**), 6.75 (t, 1H, $^{3}J_{HH}$ = 7.3 Hz, *p*-Ph$_a$-**H**), 6.79 (t, 1H, $^{3}J_{HH}$ = 7.3 Hz, *p*-Ph$_b$-**H**), 7.04 (dd, 2H, $^{3}J_{HH}$ = 7.3, 7.6 Hz, *m*-Ph$_a$-**H**), 7.06 (dd, 2H, $^{3}J_{HH}$ = 7.3, 7.6 Hz, *m*-Ph$_b$-**H**).

^{13}C{^{1}H} NMR (100.6 MHz, 298 K, chloroform-d$_1$): δ (ppm) 13.11 (Ind-**C**H$_3$), 16.18 (Ind-CH$_2$-**C**H$_3$), 16.57 (Ind-**C**H$_3$), 16.68 (Ind-**C**H$_3$), 16.75 (Ind-**C**H$_3$), 17.06 (Ind-**C**H$_3$), 21.98 (Ind-**C**H$_2$-CH$_3$), 66.30 (Zr-**C**H$_2$-Ph$_b$), 67.51 (Zr-**C**H$_2$-Ph$_a$), 100.69 (**Ind**-H), 118.88 (**Ind**), 120.67 (*p*-**Ph$_a$**), 121.07 (*p*-**Ph$_b$**), 123.33 (**Ind**), 126.45 (**Ind**), 126.58 (*o*-**Ph$_a$**), 126.92 (**Ind**), 127.24 (*o*-**Ph$_b$**), 127.33 (**Ind**), 127.51 (*m*-**Ph$_b$**), 127.53 (**Ind**), 127.57 (*m*-**Ph$_a$**), 131.78 (**Ind**), 133.13 (**Ind**), 152.67 (Zr-CH$_2$-**Ph$_b$**), 153.76 (Zr-CH$_2$-**Ph$_a$**).

CHN analysis (%): found: C 78.79, H 8.16; calculated: C 78.91, H 8.06.

6.5.13 Synthesis of *rac*-^{Me2}SBI*Zr(CH$_2$Ph)$_2$



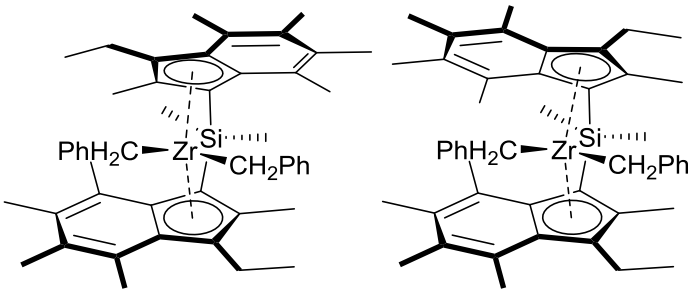
C$_{46}$H$_{56}$SiZr, M_r = 728.26

rac-^{Me2}SBI*ZrCl$_2$ (47.4 mg, 0.0768 mmol, 1.0 eq) and PhCH$_2$K (20.0 mg, 0.154 mmol, 2.0 eq) were mixed in benzene (1 mL) and left stirring for 16 hours at room temperature. The reaction mixture was allowed to settle before being filtered. The yellow filtrate was dried *in vacuo* to afford the product as a yellow solid (46.9 mg, 0.0644 mmol, 84% yield).

^{1}H NMR (400.2 MHz, 298 K, chloroform-d$_1$): δ (ppm) -0.22 (d, 2H, $^{2}J_{HH}$ = 11.5 Hz, Zr-C**H$_a$**H$_b$-Ph), 0.69 (d, 2H, $^{2}J_{HH}$ = 11.5 Hz, Zr-CH$_a$**H$_b$**-Ph), 1.19 (s, 6H, Si-C**H$_3$**), 1.54 (s, 6H, Ind-C**H$_3$**), 1.83 (s, 6H, Ind-C**H$_3$**), 2.25 (s, 6H, Ind-C**H$_3$**), 2.27 (s, 6H, Ind-C**H$_3$**), 2.32 (s, 6H, Ind-C**H$_3$**), 2.47 (s, 6H, Ind-C**H$_3$**), 6.46 (d, 4H, $^{3}J_{HH}$ = 7.4 Hz, *o*-Ph-**H**), 6.74 (t, 2H, $^{3}J_{HH}$ = 7.3 Hz, *p*-Ph-**H**), 7.01 (dd, 4H, $^{3}J_{HH}$ = 7.3, 7.4 Hz, *m*-Ph-**H**).

^{13}C{^{1}H} NMR (100.6 MHz, 298 K, chloroform-d$_1$): δ (ppm) 11.35 (Si-**C**H$_3$), 13.88 (Ind-**C**H$_3$), 15.15 (Ind-**C**H$_3$), 16.60 (Ind-**C**H$_3$), 17.59 (Ind-**C**H$_3$), 17.78 (Ind-**C**H$_3$), 21.96 (Ind-**C**H$_3$), 69.92 (Zr-**C**H$_2$-Ph), 75.80 (**Ind**-Si), 120.97 (*p*-**Ph**), 124.19 (**Ind**), 126.36 (*o*-**Ph**), 127.73 (*m*-**Ph**), 128.48 (**Ind**), 129.22 (**Ind**), 129.26 (**Ind**), 130.72 (**Ind**), 133.12 (**Ind**), 133.94 (**Ind**), 134.12 (**Ind**), 152.10 (Zr-CH$_2$-**Ph**).

6.5.14 Synthesis of ^{Me2}SB($^{3\text{-}Et}$I*)Zr(CH$_2$Ph)$_2$



$C_{48}H_{60}SiZr$, M_r = 756.32

^{Me2}SB($^{3\text{-}Et}$I*)ZrCl$_2$ (49.5 mg, 0.0768 mmol, 1.0 eq) and PhCH$_2$K (20.0 mg, 0.154 mmol, 2.0 eq) were mixed in benzene (1 mL) and left stirring for 16 hours at room temperature. The reaction mixture was allowed to settle before being filtered. The orange filtrate was dried *in vacuo* to afford the product, a 75:25 mixture of *rac*-^{Me2}SB($^{3\text{-}Et}$I*)Zr(CH$_2$Ph)$_2$ and *meso*-^{Me2}SB($^{3\text{-}Et}$I*)Zr(CH$_2$Ph)$_2$, as an orange yellow solid (48.4 mg, 0.0640 mmol, 83% yield). Orange crystals of *rac*-^{Me2}SB($^{3\text{-}Et}$I*)Zr(CH$_2$Ph)$_2$ suitable for single crystal X-ray diffraction were grown from a pentane solution of the isomeric mixture at room temperature.

***rac*-^{Me2}SB($^{3\text{-}Et}$I*)Zr(CH$_2$Ph)$_2$:**

^{1}H NMR (400.2 MHz, 298 K, chloroform-d$_1$): δ (ppm) -0.29 (d, 2H, $^{2}J_{HH}$ = 11.5 Hz, Zr-C**H$_a$**H$_b$-Ph), 0.62 (t, 6H, $^{3}J_{HH}$ = 7.4 Hz, Ind-CH$_2$-C**H$_3$**), 0.65 (d, 2H, $^{2}J_{HH}$ = 11.5 Hz, Zr-CH$_a$**H$_b$**-Ph), 1.22 (s, 6H, Si-C**H$_3$**), 1.84 (s, 6H, Ind-C**H$_3$**), 1.92 (q, 4H, $^{3}J_{HH}$ = 7.4 Hz, Ind-C**H$_2$**-CH$_3$), 2.26 (s, 6H, Ind-C**H$_3$**), 2.30 (s, 6H, Ind-C**H$_3$**), 2.31 (s, 6H, Ind-C**H$_3$**), 2.49 (s, 6H, Ind-C**H$_3$**), 6.46 (d, 4H, $^{3}J_{HH}$ = 7.4 Hz, *o*-Ph-**H**), 6.73 (t, 2H, $^{3}J_{HH}$ = 7.3 Hz, *p*-Ph-**H**), 7.00 (dd, 4H, $^{3}J_{HH}$ = 7.3, 7.4 Hz, *m*-Ph-**H**).

^{13}C{^{1}H} NMR (100.6 MHz, 298 K, chloroform-d$_1$): δ (ppm) 11.44 (Si-**C**H$_3$), 14.53 (Ind-**C**H$_3$), 15.87 (Ind-CH$_2$-**C**H$_3$), 16.69 (Ind-**C**H$_3$), 16.84 (Ind-**C**H$_3$), 17.61 (Ind-**C**H$_3$), 19.93 (Ind-**C**H$_2$-CH$_3$), 22.21 (Ind-**C**H$_3$), 69.86 (Zr-**C**H$_2$-Ph), 76.41 (**Ind**-Si), 121.00 (*p*-**Ph**), 126.48 (*o*-**Ph**), 127.48 (*m*-**Ph**), 128.53 (**Ind**), 128.69 (**Ind**), 128.81 (**Ind**), 128.89 (**Ind**), 129.64 (**Ind**), 133.17 (**Ind**), 133.71 (**Ind**), 134.01 (**Ind**), 152.38 (Zr-CH$_2$-**Ph**).

***meso*-^{Me2}SB($^{3\text{-}Et}$I*)Zr($CH_2Ph)_2$:**

^{1}H NMR (400.2 MHz, 298 K, chloroform-d_1): δ (ppm) -1.03 (s, 2H, Zr-C**H$_2$**-Ph$_a$), 0.91 (t, 6H, $^3J_{HH}$ = 7.4 Hz, Ind-CH$_2$-C**H$_3$**), 1.17 (s, 3H, Si-C$_a$**H$_3$**), 1.27 (s, 3H, Si-C$_b$**H$_3$**), 1.79 (s, 2H, Zr-C**H$_2$**-Ph$_b$), 2.09 (s, 6H, Ind-C**H$_3$**), 2.12 (s, 6H, Ind-C**H$_3$**), 2.22 (s, 6H, Ind-C**H$_3$**), 2.32 (m, 2H, $^3J_{HH}$ = 7.4 Hz, Ind-C**H$_a$**H$_b$-CH$_3$), 2.38 (s, 6H, Ind-C**H$_3$**), 2.41 (s, 6H, Ind-C**H$_3$**), 2.49 (m, 2H, $^3J_{HH}$ = 7.4 Hz, Ind-CH$_a$**H$_b$**-CH$_3$), 6.05 (d, 2H, $^3J_{HH}$ = 7.6 Hz, *o*-Ph$_a$-**H**), 6.25 (d, 2H, $^3J_{HH}$ = 7.6 Hz, *o*-Ph$_b$-**H**), 6.63 (t, 1H, $^3J_{HH}$ = 7.3 Hz, *p*-Ph$_a$-**H**), 6.75 (t, 1H, $^3J_{HH}$ = 7.3 Hz, *p*-Ph$_b$-**H**), 6.86 (dd, 2H, $^3J_{HH}$ = 7.3, 7.6 Hz, *m*-Ph$_a$-**H**), 6.95 (dd, 2H, $^3J_{HH}$ = 7.3, 7.6 Hz, *m*-Ph$_b$-**H**).

^{13}C{^{1}H} NMR (100.6 MHz, 298 K, chloroform-d_1): δ (ppm) 10.38 (Si-**C$_a$**H$_3$), 14.63 (Ind-CH$_2$-**C**H$_3$), 14.79 (Si-**C$_b$**H$_3$), 15.20 (Ind-**C**H$_3$), 16.80 (Ind-**C**H$_3$), 17.26 (Ind-**C**H$_3$), 17.40 (Ind-**C**H$_3$), 21.64 (Ind-**C**H$_2$-CH$_3$), 23.07 (Ind-**C**H$_3$), 65.52 (Zr-**C**H$_2$-Ph$_a$), 67.39 (Zr-**C**H$_2$-Ph$_b$), 76.63 (**Ind**-Si), 120.73 (*p*-**Ph$_a$**), 121.23 (*p*-**Ph$_b$**), 126.66 (*o*-**Ph$_a$**), 126.89 (*m*-**Ph$_a$**), 127.24 (*m*-**Ph$_b$**), 127.38 (*o*-**Ph$_b$**), 128.76 (**Ind**), 129.18 (**Ind**), 129.91 (**Ind**), 130.73 (**Ind**), 131.23 (**Ind**), 132.74 (**Ind**), 133.39 (**Ind**), 133.65 (**Ind**), 150.00 (Zr-CH$_2$-**Ph$_a$**), 151.97 (Zr-CH$_2$-**Ph$_b$**).

6.6 Experimental details for Chapter Four

6.6.1 Synthesis of sMAO supported metallocene catalysts

sMAO (39.7 or 41.1% wt$_{Al}$; 0.300 g, 4.41 or 4.57 mmol$_{Al}$, 200 eq) was dispersed in toluene (25 mL) to form a colourless slurry. A metallocene complex (0.0221 or 0.0229 mmol, 1.0 eq) was dissolved in toluene (25 mL) to form a coloured solution which was then quickly added to the sMAO at room temperature. A mixture of *rac*- and *meso*-isomer of the complex, and the Al:complex molar ratio of 200:1 were used unless stated otherwise. The reaction mixture was heated to 60 °C for 2 hours with occasional swirling. The coloured solid was allowed to settle from the clear, colourless solution which was decanted, and the solid was dried *in vacuo* to afford the product as follows:

sMAO-[*rac*-($^{3\text{-}Et}$Ind$^{\#}$)$_2$ZrCl$_2$]: a pale orange solid (0.251 g, 80% yield).

sMAO-[*meso*-($^{3\text{-}Et}$Ind$^{\#}$)$_2$ZrCl$_2$]: a pale orange solid (0.276 g, 88% yield).

sMAO-[*rac*-($^{3\text{-}Et}$Ind$^{\#}$)$_2$HfCl$_2$]: a gold solid (0.259 g, 82% yield).

sMAO-[($^{3\text{-}Ph}$Ind$^{\#}$)$_2$ZrCl$_2$]: a pink solid (0.276 g, 88% yield).

sMAO-[*meso*-(Ind$^{\#}$)$_2$ZrBr$_2$]: a pink solid (0.293 g, 93% yield).

sMAO-[*meso*-($^{3\text{-}Et}$Ind$^{\#}$)$_2$ZrBr$_2$]: a pale orange solid (0.290 g, 92% yield).

sMAO-[(Ind$^{\#}$)(PhN(CH$_2$)$_3$NPh)ZrCl]: a pale orange solid (0.260 g, 83% yield).

sMAO-[*rac*-^{Et_2}SBI*ZrCl$_2$]: a pink solid (0.280 g, 89% yield).

sMAO-[^{Me_2}SB($^{3\text{-}Et}$I*)ZrCl$_2$]: a pale pink solid (0.254 g, 81% yield).

^{13}C CPMAS SSNMR: δ (ppm) -8 (**C**H$_3$ in sMAO), 15 (Ind-**R**), 21 (Ind-**R**), 128 (**Ind**), 131 (**Ind**), 136 (**Ind**).

^{27}Al Hahn-echo MAS SSNMR: δ (ppm) -92 (**Al** in sMAO).

^{29}Si CPMAS SSNMR: δ (ppm) -13 (**Si**-CH$_3$).

sMAO-[^{Me_2}SB($^{3\text{-}Et}$I*)ZrCl$_2$] (300:1): a pale pink solid (0.240 g, 78% yield).

sMAO-[^{Me_2}SB($^{3\text{-}Et}$I*)ZrCl$_2$] (150:1): a pale pink solid (0.236 g, 74% yield).

sMAO-[^{Me_2}SB($^{3\text{-}Et}$I*)ZrCl$_2$] (100:1): a pale pink solid (0.242 g, 73% yield).

sMAO-[*rac*-^{Me_2}SB($^{3\text{-}Et}$I*)ZrCl$_2$]: a pale pink solid (0.290 g, 92% yield).

ICP analysis (%): found: Al 33.4, Zr 0.61; calculated: Al 37.9, Zr 0.64.

sMAO-[*rac*-^{Me_2}SB($^{3\text{-}Et}$I*)ZrBr$_2$]: a purple solid (0.292 g, 92% yield).

sMAO-[*rac*-($^{3\text{-}Et}$Ind$^{\#}$)$_2$Zr(CH$_2$Ph)$_2$]: a pale pink solid (0.274 g, 87% yield).

sMAO-[*meso*-($^{3\text{-}Et}$Ind$^{\#}$)$_2$Zr(CH$_2$Ph)$_2$]: a pale pink solid (0.285 g, 90% yield).

sMAO-[^{Me_2}SB($^{3\text{-}Et}$I*)Zr(CH$_2$Ph)$_2$]: a pale pink solid (0.276 g, 87% yield).

^{13}C CPMAS SSNMR: δ (ppm) -8 (**C**H$_3$ in sMAO), 16 (Ind-**R**), 21 (Ind-**R**), 128 (**Ind**), 131 (**Ind**), 136 (**Ind**).

^{27}Al Hahn-echo MAS SSNMR: δ (ppm) -91 (**Al** in sMAO).

^{29}Si CPMAS SSNMR: δ (ppm) -15 (**Si**-CH$_3$), -13 (**Si**-CH$_3$).

6.6.2 50 mL ethylene polymerisation

For a heterogeneous ethylene polymerisation test, a supported metallocene catalyst (10.0 mg, 1.0 eq$_{Complex}$), TIBA (1000 eq) and hexane (50 mL) were added to a 150 mL Rotaflo ampoule containing a stirrer bar. For a homogeneous ethylene polymerisation test, a metallocene complex (0.5 mg, 1.0 eq), MAO (500 eq) and hexane (50 mL) were added instead. The ampoule was sealed and degassed before being heated to the desired temperature at the stirring speed of 1000 rpm. The ampoule was then opened to ethylene (2 bar). On completion of the test, the ampoule was closed to ethylene and degassed. The resulting polyethylene was filtered on a glass sintered frit, washed with pentane (2 x 25 mL) and dried. All polymerisation tests were carried out, at least, in duplicate and run for 30 minutes, unless stated otherwise, or until the stirring ceased entirely. The activities were reported as an average with ±1 ESD error. The molecular weights of the resulting polyethylenes were determined by GPC and reported with their corresponding polydispersity index (PDI) values.

6.6.3 Polymerisation data

Table 6.1. Homogeneous ethylene polymerisation.

Complex	Temperature (°C)	Activity ($kg_{PE}/mol_{Complex}/h/bar$)	M_w (g/mol)	M_w/M_n
rac-($^{3\text{-Et}}Ind^{\#}$)$_2ZrCl_2$	50	2029 ± 142	247600	2.9
	60	1422 ± 17	238200	4.2
	70	1243 ± 37	143100	4.2
	80	1006 ± 71	124500	4.1
	90	398 ± 43	62200	3.7
rac-($^{3\text{-Et}}Ind^{\#}$)$_2HfCl_2$	50	274 ± 86	160400	3.7
	60	799 ± 52	121600	4.2
	70	988 ± 35	86200	3.9
	80	851 ± 52	57000	3.6
	90	270 ± 11	20600	2.4
$^{Me2}SB(^{3\text{-Et}}I^{*})ZrCl_2$	50	14242 ± 712	438500	2.5
	60	12423 ± 684	410200	2.3
	70	10778 ± 301	355800	2.4
	80	11088 ± 1505	334500	2.4
	90	10401 ± 151	340600	2.4

Polymerisation conditions: 50 mL_{Hexane}, 2 $bar_{Ethylene}$, 0.5 $mg_{Complex}$, 500 eq_{MAO}, 15 minutes (2 minutes for $^{Me2}SB(^{3\text{-Et}}I^{*})ZrCl_2$).

Table 6.2. Heterogeneous ethylene polymerisation using sMAO support.

Complex	Temperature (°C)	Activity ($kg_{PE}/mol_{Complex}/h/bar$)	M_w (g/mol)	M_w/M_n
rac-($^{3\text{-Et}}Ind^{\#}$)$_2ZrCl_2$	50	1072 ± 10	391000	5.0
	60	858 ± 5	297500	5.4

	70	561 ± 25	190400	5.3
	80	382 ± 7	-	-
	90	239 ± 14	-	-
meso-($^{3\text{-Et}}$Ind$^{\#}$)$_2$ZrCl$_2$	50	690 ± 5	405600	7.3
	60	651 ± 20	320100	6.9
	70	526 ± 0	232100	7.2
	80	385 ± 9	206400	8.2
	90	249 ± 3	164000	8.0
rac-($^{3\text{-Et}}$Ind$^{\#}$)$_2$HfCl$_2$	50	1030 ± 33	297300	5.3
	60	960 ± 25	213100	5.7
	70	896 ± 10	-	-
	80	582 ± 16	-	-
	90	297 ± 18	-	-
($^{3\text{-Ph}}$Ind$^{\#}$)$_2$ZrCl$_2$	50	54 ± 18	-	-
	60	46 ± 1	-	-
	70	41 ± 2	-	-
	80	36 ± 1	-	-
	90	35 ± 0	-	-
meso-(Ind$^{\#}$)$_2$ZrBr$_2$	50	705 ± 8	394700	5.6
	60	874 ± 36	327700	5.6
	70	927 ± 34	198700	4.2
	80	612 ± 29	218000	6.4
	90	340 ± 4	132900	6.0
meso-($^{3\text{-Et}}$Ind$^{\#}$)$_2$ZrBr$_2$	50	557 ± 16	503100	8.1
	60	525 ± 24	350200	7.9

	70	452 ± 28	284600	7.2
	80	320 ± 9	209100	6.9
	90	225 ± 40	212900	7.7
(Ind$^{\#}$)(PhN(CH$_2$)$_3$NPh)ZrCl	50	104 ± 2	-	-
	60	108 ± 8	-	-
	70	158 ± 14	-	-
	80	97 ± 4	-	-
	90	77 ± 3	-	-
rac-^{Et_2}SBI*ZrCl$_2$	50	3854 ± 105	516400	3.6
	60	4179 ± 47	457200	3.5
	70	3770 ± 81	396300	3.2
	80	3260 ± 265	343500	3.3
	90	2501 ± 72	253200	3.0
^{Me_2}SB($^{3\text{-}Et}$I*)ZrCl$_2$	50	3044 ± 54	587400	6.1
	60	3507 ± 118	433300	5.1
	70	3425 ± 174	394800	4.5
	80	2516 ± 75	363700	4.4
	90	1775 ± 57	342500	4.5
rac-^{Me_2}SB($^{3\text{-}Et}$I*)ZrCl$_2$	50	3144 ± 20	476700	4.9
	60	3312 ± 127	423300	4.5
	70	2721 ± 188	394500	4.3
	80	2321 ± 149	368100	4.4
	90	1665 ± 117	326000	4.1
rac-^{Me_2}SB($^{3\text{-}Et}$I*)ZrBr$_2$	50	3946 ± 138	325700	2.7
	60	3971 ± 43	307200	3.2

	70	3304 ± 118	301500	3.4
	80	2561 ± 191	282900	2.7
	90	1986 ± 30	259400	2.9
rac-($^{3\text{-Et}}$Ind$^{\#}$)$_2$Zr(CH$_2$Ph)$_2$	50	1119 ± 0	380700	5.7
	60	846 ± 0	275200	5.4
	70	486 ± 24	216600	6.8
	80	272 ± 23	142400	6.0
	90	123 ± 10	113300	7.0
meso-($^{3\text{-Et}}$Ind$^{\#}$)$_2$Zr(CH$_2$Ph)$_2$	50	877 ± 34	345100	5.0
	60	834 ± 44	265600	5.0
	70	657 ± 24	201900	5.0
	80	404 ± 39	128500	4.7
	90	270 ± 17	123700	5.5
^{Me2}SB($^{3\text{-Et}}$I*)Zr(CH$_2$Ph)$_2$	50	4570 ± 127	360400	3.0
	60	4832 ± 7	335700	3.1
	70	4233 ± 60	325600	3.0
	80	3265 ± 223	309200	3.2
	90	2419 ± 148	269000	3.2

Polymerisation conditions: 50 mL$_{Hexane}$, 2 bar$_{Ethylene}$, 10.0 mg$_{Catalyst}$, 200 Al/Zr, 1000 eq$_{TIBA}$, 30 minutes.

6.7 Experimental details for Chapter Five

6.7.1 Synthesis of silica supported methylaluminoxane (SSMAO)

Silica (SiO_2, M_r = 60.08; 2.00 g, 33.3 mmol, 2.0 eq) was dispersed in toluene (25 mL) to form a colourless slurry. MAO ($Al(CH_3)O$, M_r = 58.02; 0.966 g, 16.6 mmol, 1.0 eq) was dissolved in toluene (25 mL) to form a colourless solution which was then quickly added to the silica slurry at room temperature. The reaction mixture was heated to 80 °C for 2 hours with occasional swirling. The resulting colourless slurry was then left to cool down to room

temperature and dried *in vacuo* to afford the product as a white solid (2.62 g, 14.7 mmol, 88% yield).

6.7.2 Synthesis of layered double hydroxide supported methylaluminoxane (LDHMAO)

AMO-LDH ($Mg_{0.75}Al_{0.25}(OH)_2(CO_3)_{0.125}$, M_r = 66.49; 2.00 g, 30.1 mmol, 2.0 eq) was dispersed in toluene (25 mL) to form a colourless slurry. MAO ($Al(CH_3)O$, M_r = 58.02; 0.873 g, 15.0 mmol, 1.0 eq) was dissolved in toluene (25 mL) to form a colourless solution which was then quickly added to the AMO-LDH slurry at room temperature. The reaction mixture was heated to 80 °C for 2 hours with occasional swirling. The resulting colourless slurry was then left to cool down to room temperature and dried *in vacuo* to afford the product as a white solid (2.64 g, 13.8 mmol, 92% yield).

6.7.3 Synthesis of SSMAO-[^{Me2}SB($^{3\text{-}Et}$I*)$ZrCl_2$] catalyst

SSMAO (0.300 g, 1.68 mmol, 200 eq) was dispersed in toluene (25 mL) to form a colourless slurry. A 50:50 mixture of *rac*-^{Me2}SB($^{3\text{-}Et}$I*)$ZrCl_2$ and *meso*-^{Me2}SB($^{3\text{-}Et}$I*)$ZrCl_2$ (5.4 mg, 0.00842 mmol, 1.0 eq) was dissolved in toluene (25 mL) to form an orange solution which was then quickly added to the SSMAO slurry at room temperature. The reaction mixture was heated to 60 °C for 2 hours with occasional swirling. The orange solid was allowed to settle from the clear, colourless solution which was decanted, and the solid was dried *in vacuo* to afford the product as a pale orange solid (0.276 g, 90% yield).

6.7.4 Synthesis of LDHMAO-[^{Me2}SB($^{3\text{-}Et}$I*)$ZrCl_2$] catalyst

LDHMAO (0.300 g, 1.57 mmol, 200 eq) was dispersed in toluene (25 mL) to form a colourless slurry. A 50:50 mixture of *rac*-^{Me2}SB($^{3\text{-}Et}$I*)$ZrCl_2$ and *meso*-^{Me2}SB($^{3\text{-}Et}$I*)$ZrCl_2$ (5.1 mg, 0.00785 mmol, 1.0 eq) was dissolved in toluene (25 mL) to form an orange solution which was then quickly added to the LDHMAO at room temperature. The reaction mixture was heated to 60 °C for 2 hours with occasional swirling. The yellow solid was allowed to settle from the clear, colourless solution which was decanted, and the solid was dried *in vacuo* to afford the product as an off-white solid (0.288 g, 94% yield).

6.7.5 250 mL ethylene polymerisation

For a heterogeneous ethylene polymerisation test, a supported metallocene catalyst (10.0 mg, 1.0 $eq_{Complex}$), TIBA (1000 or 5000 eq) and hexane (250 mL) were added to a 500 mL Rotaflo ampoule containing a stirrer bar. The ampoule was sealed and degassed before being heated to the desired temperature at the stirring speed of 1000 rpm. The ampoule was then opened to ethylene (2 bar). On completion of the test, the ampoule was closed to ethylene and degassed. The resulting polyethylene was filtered on a glass sintered frit, washed with pentane (2 x 25 mL) and dried. All polymerisation tests were carried out, at least, in duplicate and run for 30 minutes, unless stated otherwise, or until the stirring ceased entirely. The activities were reported as an average with ±1 ESD error. The molecular weights of the resulting polyethylenes were determined by GPC and reported with their corresponding PDI values.

6.7.6 1 L ethylene polymerisation

Large-scale 1 L ethylene polymerisation tests and characterisations of the resulting polyethylene, including $^{13}C\{^{1}H\}$ NMR spectroscopy and GPC, were carried out at SCG Chemicals Co., Ltd., Thailand.

6.7.7 High throughput ethylene polymerisation

High throughput ethylene polymerisation tests, inductively coupled plasma (ICP) analysis of the sMAO-[*rac*-^{Me2}SB($^{3\text{-}Et}$I*)$ZrCl_2$] catalyst, and characterisations of the resulting polyethylene, including $^{13}C\{^{1}H\}$ NMR spectroscopy, crystallisation elution fractionation (CEF) and GPC, were carried out at HTExplore, Italy.

6.7.8 Polymerisation data

Table 6.3. Heterogeneous ethylene polymerisation using ^{Me2}SB($^{3\text{-}Et}$I*)$ZrCl_2$ complex.

Support	Temperature (°C)	Activity ($kg_{PE}/mol_{Complex}/h/bar$)	M_w (g/mol)	M_w/M_n
sMAO	50	3044 ± 54	587400	6.1
	60	3507 ± 118	433300	5.1

	70	3425 ± 174	394800	4.5
	80	2516 ± 75	363700	4.4
	90	1775 ± 57	342500	4.5
SSMAO	50	307 ± 27	787400	5.2
	60	348 ± 16	745900	4.9
	70	383 ± 13	690500	4.4
	80	368 ± 18	677300	4.3
	90	272 ± 18	703900	5.6
LDHMAO	50	104 ± 23	-	-
	60	125 ± 6	-	-
	70	108 ± 2	-	-
	80	108 ± 2	-	-
	90	102 ± 10	-	-

Polymerisation conditions: 50 mL_{Hexane}, 2 $bar_{Ethylene}$, 10.0 $mg_{Catalyst}$, 200 Al/Zr, 1000 eq_{TIBA}, 30 minutes.

Table 6.4. Heterogeneous ethylene polymerisation using sMAO-[^{Me2}SB($^{3\text{-}Et}$I*)$ZrCl_2$] catalyst.

Scavenger	**Loading (eq)**	**Activity ($kg_{PE}/mol_{Complex}/h/bar$)**	M_w **(g/mol)**	M_w/M_n
MAO	1000	2393 ± 22	450900	3.4
TMA	1000	3562 ± 226	130800	3.5
TEA	1000	4390 ± 25	184600	3.6
TIBA	100	2717 ± 127	487000	3.7
	500	3511 ± 224	421100	3.3
	1000	4533 ± 81	356100	3.1
	1500	4509 ± 11	331500	2.9
	2000	4022 ± 125	373600	3.0

Polymerisation conditions: 50 mL_{Hexane}, 2 $bar_{Ethylene}$, 10.0 $mg_{Catalyst}$, 200 Al/Zr, 60 °C, 30 minutes.

Table 6.5. Heterogeneous ethylene polymerisation using sMAO-[^{Me2}SB($^{3\text{-}Et}$I*)$ZrCl_2$] catalyst.

Al/Zr	Activity ($kg_{PE}/mol_{Complex}/h/bar$)	Productivity ($kg_{PE}/g_{Catalyst}/h/bar$)	M_w (g/mol)	M_w/M_n
100	2309 ± 49	0.320 ± 0.007	324700	3.0
150	3404 ± 160	0.325 ± 0.015	375200	3.1
200	4533 ± 81	0.329 ± 0.006	356100	3.1
300	5421 ± 75	0.267 ± 0.004	372000	3.0

Polymerisation conditions: 50 mL_{Hexane}, 2 $bar_{Ethylene}$, 10.0 $mg_{Catalyst}$, 1000 eq_{TIBA}, 60 °C, 30 minutes.

6.8 References

1 B. J. Cosier and A. M. Glazer, *J. Appl. Crystallogr.*, 1986, **19**, 105–107.
2 Z. Otwinowski and W. Minor, *Methods Enzymol.*, 1997, **276**, 307–326.
3 R. H. Blessing, *Acta Crystallogr. Sect. A*, 1995, **51**, 33–38.
4 CrysAlisPRO, Oxford Diffraction/Agilent Technologies UK Ltd., Yarnton, England.
5 G. M. Sheldrick, *Acta Crystallogr. Sect. A Found. Crystallogr.*, 2008, **64**, 112–122.
6 L. Palatinus and G. Chapuis, *J. Appl. Crystallogr.*, 2007, **40**, 786–790.
7 P. W. Betteridge, J. R. Carruthers, R. I. Cooper, K. Prout and D. J. Watkin, *J. Appl. Crystallogr.*, 2003, **36**, 1487.
8 R. I. Cooper, A. L. Thompson and D. J. Watkin, *J. Appl. Crystallogr.*, 2010, **43**, 1100–1107.
9 L. J. Farrugia, *J. Appl. Crystallogr.*, 2012, **45**, 849–854.
10 C. F. Macrae, I. J. Bruno, J. A. Chisholm, P. R. Edgington, P. McCabe, E. Pidcock, L. Rodriguez-Monge, R. Taylor, J. van de Streek and P. A. Wood, *J. Appl. Crystallogr.*, 2008, **41**, 466–470.
11 A. L. Spek, *J. Appl. Crystallogr.*, 2003, **36**, 7–13.
12 T. A. Q. Arnold, J.-C. Buffet, Z. R. Turner and D. O'Hare, *J. Organomet. Chem.*, 2015, **792**, 55–65.
13 X. Zhang, Q. Zhu, I. A. Guzei and R. F. Jordan, *J. Am. Chem. Soc.*, 2000, **122**, 8093–8094.
14 M. D. LoCoco and R. F. Jordan, *Organometallics*, 2003, **22**, 5498–5503.
15 M. D. LoCoco, X. Zhang and R. F. Jordan, *J. Am. Chem. Soc.*, 2004, **126**, 15231–15244.
16 P. J. Bailey, R. A. Coxall, C. M. Dick, S. Fabre, L. C. Henderson, C. Herber, S. T. Liddle, D. Loroño-González, A. Parkin and S. Parsons, *Chem. - A Eur. J.*, 2003, **9**, 4820–4828.
17 J.-C. Buffet, T. A. Q. Arnold, Z. R. Turner, P. Angpanitcharoen and D. O'Hare, *RSC Adv.*, 2015, **5**, 87456–87464.
18 Q. Wang and D. O'Hare, *Chem. Commun.*, 2013, **49**, 6301–6303.
19 C. Chen, M. Yang, Q. Wang, J.-C. Buffet and D. O'Hare, *J. Mater. Chem. A*, 2014, **2**, 15102–15110.

Conclusions

The aim of the thesis is to synthesise novel substituted indenyl complexes inspired by the very active ^{Me2}SBI*ZrCl$_2$. By looking to improve on the ethylene polymerisation activity and the racemo-selectivity, different alkyl and aryl groups are introduced on the silyl bridge and at the 3- position of the indenyl rings. The synthesised complexes are then tested for homogeneous and heterogeneous ethylene polymerisation activity and evaluated for their potential industrial applications, including polyethylene waxes by using hydrogen as a chain transfer agent, and linear low-density polyethylene (LLDPE) by copolymerisation of ethylene and 1-hexene.

Chapter Two describes the modifications of ^{Me2}SBI* ligand by introducing various alkyl groups on the silyl bridge and at the 3- position of the indenyl rings. ^{Et2}SBI*H$_2$, $^{n\text{Pr,Me}}$SBI*H$_2$ and ^{All,Me}SBI*H$_2$ pro-ligands were successfully synthesised and fully characterised. However, attempts to introduce larger alkyl groups, including isopropyl and phenyl groups, were unsuccessful due to high steric demand. Ethyl and phenyl groups were successfully introduced at the 3- position of the indenyl rings of the ligand. The synthesis of ^{Me2}SB($^{3\text{-Et}}$I*)H$_2$ pro-ligand was accomplished. The pro-ligand and its synthetic intermediates were fully characterised. However, ^{Me2}SB($^{3\text{-Ph}}$I*)H$_2$ pro-ligand, despite being successfully synthesised, was unable to be isolated for further use.

Chapter Three describes the syntheses of novel substituted indenyl group 4 complexes using the pro-ligands synthesised in Chapter Two. All complexes were fully characterised by NMR spectroscopy, mass spectrometry, elemental analysis and, when possible, single crystal X-ray diffraction. Unbridged ($^{3\text{-R}}$Ind$^{\#}$)$_2$MCl$_2$ (R = Et, Ph; M = Zr, Hf) were successfully synthesised as 50:50 mixtures of the corresponding *rac* and *meso* isomers. The synthesis of ($^{3\text{-R}}$Ind$^{\#}$)$_2$ZrBr$_2$ (R = Me, Et) was accomplished but undesirably favoured the formation of the *meso* isomers. Jordan's reagent was also used but only formed the monosubstituted product. Silyl bridged substituted indenyl zirconocenes, including ^{Et2}SBI*ZrCl$_2$ and ^{Me2}SB($^{3\text{-Et}}$I*)ZrX$_2$ (X = Cl, Br), were synthesised and no selectivity towards the formation of the *rac* isomers was observed. Dibenzylation of the synthesised dichloro and dibromo zirconocenes were successfully carried out.

Chapter Four describes homogeneous and heterogeneous ethylene polymerisation using the synthesised substituted indenyl group 4 complexes. The complexes were immobilised onto a highly unique sMAO support. The sMAO-[^{Me2}SB($^{3\text{-Et}}$I*)ZrCl$_2$] catalyst was

characterised by solid state NMR spectroscopy and SEM showing that the complex ligand framework and support morphology are retained after the immobilisation. The ethylene polymerisation results show that the silyl bridged complexes are substantially more active compared to their unbridged relatives with *rac*-^{Et_2}SBI*$ZrCl_2$ being the most active. Interestingly, *rac*- and *meso*-^{Me_2}SB($^{3\text{-}Et}$I*)$ZrCl_2$ display similar activities. Dibenzylation of the dichloro complexes increases the ethylene polymerisation activity. The resulting polyethylenes were characterised by GPC, XRD and SEM.

Chapter Five describes ethylene polymerisation studies of supported ^{Me_2}SB($^{3\text{-}Et}$I*)$ZrCl_2$ catalysts. The complex was immobilised onto SSMAO, LDHMAO and sMAO supports and the resulting catalysts were tested for ethylene polymerisation activity. Polymerisation conditions, including scavenger type and loading, complex loading, catalyst loading and reaction volume, were optimised for sMAO-[^{Me_2}SB($^{3\text{-}Et}$I*)$ZrCl_2$] catalyst. sMAO-[*rac*-^{Me_2}SB($^{3\text{-}Et}$I*)$ZrCl_2$] catalyst was subjected to high throughput screening process and found to be responsive to hydrogen but not suitable for copolymerisation of ethylene and 1-hexene. The resulting polyethylenes were characterised by GPC and SEM.